INFLUENCE OF GLUCOSE AND OXYGEN ON HUMAN EMBRYOS AND EMBRYONIC STEM CELLS

A thesis submitted to the University of Manchester

for the degree of Doctor of Philosophy

in the Faculty of Biology, Medicine and Health

2021

Maribel Montufar Martinez

School of Biological Sciences

Division of Cell Matrix Biology & Regenerative Medicine

	Page
LIST OF TABLES	5
LIST OF FIGURES	6
ABBREVIATIONS	9
ABSTRACT	11
DECLARATION	13
COPYRIGT STATEMENT	14
ACKNOWLEDGEMENTS	14
1. Introduction	
1.1. Human preimplantation development	16
1.2. Embryo metabolism	18
1.2.1. Mitochondria and energy metabolism	21
1.2.2. Mitochondrial membrane potential	22
1.3. The Developmental Origins of Health and Disease (DOHaD)	24
1.3.1 Assisted reproductive technologies and DOHaD	25
1.4. Assisted reproductive technologies (ART)	25
1.4.1. In vitro fertilization and embryo transfer (IVF-ET)	26
1.4.2. Embryo monitoring and grading	27
1.4.3. Embryo Freezing and thawing	30
1.4.3.1. Slow freezing	30
1.4.3.2 Vitrification	30
1.4.4. Embryo Culture	32
1.4.4.1. Key components of embryo culture media	33
1.4.4.2. Oxygen tension	34
1.5. DNA methylation mechanisms in preimplantation development	35
1.6. Human embryonic stem cells (HESCs)	38
1.6.1. HESCs as a model for studying human embryo development	38
1.6.2. Characterization of HESCs	39
1.7. HESCs metabolism	39
1.8. Aims and objectives	41
2. Materials and methods	42
2.1. Human Embryo handling, culture and analysis.	42
2.1.1. Cryopreservation and thawing protocols	42
2.2. Double stranded cDNA synthesis from Embryos (PolyA PCR)	44
2.2.1. cDNA synthesis	45
2.2.2. Quantification of double stranded cDNA	47
2.3. Isolation of ICM and TE from human embryo	48
2.4. DNA methylation analysis	50
2.4.1. Library preparation PBAT	50
2.5. Routine culture of HESCs	55
2.5.1. Culture and passaging of HESCs	55
2.5.2. Cryopreservation of HESCs	56

2.5.3. Cell thawing 56
2.5.4. Cell counting 56
2.6. HESCs Characterization 57
2.6.1. Immunofluorescence staining 57
2.6.2. Flow cytometry analysis 58
2.7. Gene expression analysis for hESCs 60
2.7.1. RNA isolation 60
2.7.2. RNA quantification 61
2.7.3. cDNA synthesis 62
2.7.4. Real time qPCR 62
2.7.5. Real time qPCR analysis 63
2.7.6. Primer design for RT-qPCR 64
2.8. Mitochondrial membrane potential 68
2.8.1. Mitochondrial membrane potential in hESCs 68
2.8.2. Mitochondrial membrane potential in human embryos 69
2.9. Mitochondrial respiration 69
2.9.1. Cell seeding 69
2.9.2. Cartridge preparation and measurement 70
2.9.3. Blastocyst seeding cartridge preparation and measurement 72

3. Effect of glucose concentration and oxygen on human preimplantation embryos
3.1. Introduction 73
3.2. Study design 74
3.3. Effect of glucose on gene expression 75
3.4. Effect of oxygen on gene expression 76
3.5. Effect of embryo culture conditions on mitochondria membrane potential 83
3.5.1. Thawed embryos vs Fresh embryos 83
3.6. Effect of glucose and oxygen on mitochondrial respiration in human embryos 87
3.7. Effect of glucose on DNA methylation in human embryos 96
3.7.1. Global methylation 99
3.7.2. Low glucose ICM vs High glucose ICM 102
3.7.3. Low glucose TE vs High glucose TE 108
3.7.4. High glucose ICM vs High glucose TE 113
3.7.5. Low glucose ICM vs Low glucose TE 115
3.7.6. Comparison between low glucose and high glucose blastocysts (ICM+TE) 117
3.7.7. Differential methylation on H3K4me3 sites 125
3.7.8. Differential methylation on H3K27me3 sites 129
3.7.9. Differential methylation on CpG islands 132
3.7.10. Differential methylation on Imprinted genes 136
3.8. Discussion 139

4. Effect of glucose concentration and oxygen on HESCs
4.1. Introduction 149
4.2. Study design 151
4.3. Characterization of pluripotency HESCs 151

4.4. Effect of glucose and oxygen on gene expression 156
4.5. Effect of glucose and oxygen on mitochondrial membrane potential 163
4.6. Effect of glucose and oxygen Mitochondrial DNA 167
4.7. Mitochondrial respiration 168
4.8. Discussion 175
5. General Discussion 183
6. General conclusions 190
7. Future work 191
8. References 192

Total word Count: 49450

LIST OF TABLES

	Page
Table 1.1 Principal components in embryo culture media, a comparison between manufacturers	33
Table 2.1 Cycle profile for first strand cDNA synthesis and polyA tailing	46
Table 2.2 Cycle profile for Primary amplification of cDNA	46
Table 2.3 Cycle profile for Secondary amplification of cDNA	47
Table 2.4 Preparation of dsDNA Standards.	48
Table 2.5 EZ-DNA Methylation Lysis mix	50
Table 2.6 Conversion reagent preparation	51
Table 2.7. Second strand synthesis master mix	52
Table 2.8. Library amplification master mix	53
Table 2.9. Library amplification protocol	53
Table 2.10. Antibody list for immunocytochemistry analysis	58
Table 2.11. Number of hESCs seeded per experimental condition in each well of a 6-well plate	59
Table 2.12. List of antibodies used in Flow cytometry analysis	60
Table 2.13. DNAse master mix for treatment of 1 µg of RNA	62
Table 2.14. RT Mastermix for the synthesis of 1 µg of RNA to cDNA single stranded	62
Table 2.15. QPCR master mix for hESCs	63
Table 2.16 Primers sequences used for gene expression analysis	64
Table 2.17. Compound preparation for loading to XFe96 sensor cartridges.	71
Table 3.1. List of embryos used to evaluate the effects of oxygen on gene expression.	77
Table 3.2. List of embryos used to evaluate the effects of glucose on gene expression.	79
Table 3.3. Blastocysts evaluated through the Cell Mito Stress Test.	88
Table 3.4. Mean Oxigen consumption Rate (OCR) in embryos.	92
Table 3.5. Mean Extracellular Acidification Rate (ECAR) in embryos	93
Table 3.6. Multiple comparison tests by respiration parameters.	95
Table 3.7. Sample groups for DNA methylation analysis.	100
Table 3.8. Signalling pathways resulted from hypermethylated H3K27me3 sites in high glucose.	131
Table 3.9. Imprinted genes.	137
Table 4.1. Statistics for gene expression.	161

LIST OF FIGURES

	Page
Figure 1.1. Representation of events during human preimplantation development.	17
Figure 1.2. Metabolism of cleavage-stage embryo	19
Figure 1.3. Metabolism of the blastocyst.	20
Figure 1.4. High potential mitochondria (HPM) allocation on early developed embryos.	23
Figure 1.5. Oocyte insemination by in vitro fertilization (IVF)	27
Figure 1.6. Monitored stages of human embryo in vitro	27
Figure 1.7. The Gardner scale for blastocyst grading	29
Figure 1.8. The alpha/ ESHRE consensus grading system for blastocysts	29
Figure 1.9. Schematic comparison of slow freezing and vitrification.	31
Figure 1.10. Life cycle of genomic imprinting and assisted reproductive technologies	37
Figure 2.1. Consensus scoring system for blastocysts	43
Figure 2.2. PolyA PCR workflow.	44
Figure 2.3. Composition of master mixes used in polyA PCR method	45
Figure 2.4. Post-bisulfite adaptor tagging (PBAT).	54
Figure 2.5. Representative diagram of sequencing method.	54
Figure 2.6. Mito Stress test measurement protocol	71
Figure 3.1. Effect of oxygen concentration on embryos gene expression.	78
Figure 3.2. Effect of glucose concentration on blastocysts gene expression 1.	80
Figure 3.3. Effect of glucose concentration on blastocysts gene expression 2	82
Figure 3.4. Fundamentals of JC-1 and mitochondria membrane potential.	84
Figure 3.5. Mitochondrial membrane potential (ΔΨm) in fresh embryos.	85
Figure 3.6. Mitochondrial membrane potential (ΔΨm) in frozen embryos.	86
Figure 3.7. ΔΨm comparison between fresh and frozen embryos.	86
Figure 3.8. Cell Mito Stress Test Kit parameter calculation.	89
Figure 3.9. Schematic of mitochondrial stress test in human blastocysts.	90
Figure 3.10. Metabolic phenogram contrasting basal OCR and ECAR in embryos.	91
Figure 3.11. Mitochondrial respiration parameters calculated for embryos.	94
Figure 3.12. Schematic representation of DNA Methylation analysis in human embryos.	97
Figure 3.13. Quality control of PBAT libraries.	98

Figure 3.14. Representative image of methylation landscape on SeqMonk. 101
Figure 3.15. PCA plot of DNA methylation profiles of high and low glucose samples 101
Figure 3.16. PCA plot showing DNA methylation profiles of grouped samples. 102
Figure 3.17. Correlation between Low glucose ICM and High glucose ICM. 104
Figure 3.18. Mean Methylation levels in ICM 104
Figure 3.19. Gene set analyses for ICM 1. 105
Figure 3.20. Gene set analyses for ICM 2. 106
Figure 3.21. Gene set analyses for ICM 3. 107
Figure 3.22. Correlation between Low glucose TE and High glucose TE. 109
Figure 3.23. Mean Methylation levels in TE. 109
Figure 3.24. Gene set analyses for TE 1. 110
Figure 3.25. Gene set analyses for TE 2. 111
Figure 3.26. Gene set analyses for TE 3. 112
Figure 3.27. Correlation between High glucose ICM and High glucose TE 113
Figure 3.28 Results High glucose ICM vs High glucose TE 114
Figure 3.29. Correlation between Low glucose ICM and Low glucose. 115
Figure 3.30. Results Low glucose ICM vs Low glucose. 115
Figure 3.31. Correlation between Low glucose ICM+TE and High glucose ICM+TE 119
Figure 3.32. Distribution of methylation levels of human blastocysts in low and high glucose. 119
Figure 3.33. Mean Methylation levels in blastocysts. 120
Figure 3.34. Mean Methylation levels in blastocysts after EdgeR. 120
Figure 3.35. Quantitation trend plot for blastocyst. 121
Figure 3.36. Gene set analyses for blastocysts 1. 122
Figure 3.37. Gene set analyses for blastocysts 2. 123
Figure 3.38. Gene set analyses for blastocysts 3. 124
Figure 3.39. Methylated H3K43me sites 126
Figure 3.40. Gene set analysis for H3K43me sites 1. 127
Figure 3.41. Gene set analysis for H3K43me sites 2 127
Figure 3.42. Gene set analysis for H3K43me sites 3. 128
Figure 3.43. Distribution of methylation levels from H3k27me3 sites. 130
Figure 3.44. Gene set analysis for H3K27me3 sites 1**.** 130
Figure 3.45. Gene set analysis for H3K27me3 sites 2 131
Figure 3.46. Distribution of methylation levels in CpGi. 133
Figure 3.47. Methylation levels on CpG islands. 133
Figure 3.48. Gene set analysis for CpG islands 1. 134
Figure 3.49. Gene set analysis for CpG islands 2. 134
Figure 3.50. Gene set analysis for CpG islands 3. 135

Figure 3.51. Endocrine resistance pathway (KEGG:01522) 135
Figure 3.52. Quantitative trend plots of imprinted genes. 138
Figure 4.1. Immunostaining of HESCs for pluripotency markers. 154
Figure 4.2. Expression of nuclear and cell surface markers in hESCs. 155
Figure 4.3. Comparative analysis of nuclear and cell surface markers in hESCs. 156
Figure 4.4. Analysis of transcript levels relative to ACTB (2-ΔCT) in hESCs. 161
Figure 4.5. Analysis of mitochondrial membrane potential (ΔΨm) in hESC 165
Figure 4.6. Analysis of mitochondrial membrane potential (ΔΨm), FACS. 166
Figure 4.7. Comparison of mitochondrial membrane potential (ΔΨm) 167
Figure 4.8. Analysis of mitochondrial DNA (mtDNA) in hESC (N=3). 168
Figure 4.9. Cell Mito Stress test profile. 170
Figure 4.10. Cell Mito Stress Test Kit parameter calculation. 171
Figure 4.11. Analysis of mitochondrial respiration on hESC (MAN7 and MAN13). 172
Figure 4.12. Cell Mito Stress Test parameters**.** 173
Figure 4.13. Metabolic phenogram contrasting basal OCR and ECAR. 174

ABBREVIATIONS

ART	Assisted reproductive technologies
ATP	Adenosine triphosphate
B-ACTIN	Actin beta
Bp	Base pair
CCCP	Carbonyl cyanide m-chlorophenyl hydrazone
cDNA	Complementary DNA
CpG	CG site
CpGi	CG islands
CpGi	CG island
DAPI	4',6-diamidino-2-phenylindole
DMEM	Dulbecco's Modified Eagle Medium
DMG	Differentially Methylated Gene
DMR	Differentially methylated Region
DOHAD	Developmental Origen of Health and Disease
ECAR	Extracellular acidification Rate
ESHRE	European Society of Human Reproduction and Embryology
FDR	False Discovery Rate
HESC	Human Embryonic Stem Cells
HPM	High potential mitochondria
ICM	Inner Cell Mass
iPSC	Induced Pluripotent Stem Cells
IVF	In-vitro fertilization
JC-1	Tetraethylbenzimidazolylcarbocyanine iodide
KEGG	Kyoto Encyclopaedia of Genes and Genomes
mg/mL	Milligram per millilitre
mM	Mill molar
MP	Methylated point
mRNA	Messenger RNA
mtDNA	Mitochondrial DNA
ng/µL	Nano gram per microliter
nm	Nano meter
OCR	Oxygen Consumption Rate
OMIM	Online Mendelian Inheritance in Man
ORA	Over Representation Analysis
OXPHOS	Oxidative Phosphorylation
P	Probability value
PBAT	Post-bisulfite adaptor tagging
PBS	Phosphate buffered saline
PCA	Principal Component analysis
PFA	Paraformaldehyde
PN	Pronuclear
PolyA-PCR	Poly A tail, Polymerase chain reaction
PSC	Pluripotent Stem Cell
ROCKi	Rho-associated protein kinase inhibitor

RT-qPCR	Reverse transcription quantitative polymerase chain reaction
SAM	S-Adenosyl methionine
SD	Standard deviation
SEM	Standard error of the mean
TE	Thophectoderm
VTN	Vitronectin
ΔΨm	Membrane potential

ABSTRACT

INFLUENCE OF GLUCOSE AND OXYGEN ON HUMAN EMBRYOS

AND EMBRYONIC STEM CELLS

A thesis submitted to the University of Manchester for the degree of PhD in the Faculty of Biology, Medicine and Health

Maribel Montufar Martinez

Despite the significant improvements in Assisted Reproductive Technologies (ART) there is an extensive area that remains unknown in regards to effect of embryo culture on the long-term health of the offspring. The preimplantation embryo has specific requirements depending on developmental stage; however, it remains unclear how the different compositions of commercial culture media can affect embryo development. The in vitro factors that most influence the embryo health include cryopreservation methods, culture media components, and oxygen levels. Several studies have reported alterations of birth weight, and higher risk of congenital anomalies when comparing between assisted and naturally conceived babies. Others have reported effects on epigenetic regulation, gene expression and imprinting, suggesting that embryo culture medium may have a potential impact on further development of the new born. Nevertheless, the most commonly reported alterations in offspring health outcomes include foetal growth, birthweight, childhood growth and long-term diseases such as metabolic, cardiovascular, and neurological. Due to the number of reports indicating the possible effect of the environment on embryo development, it is crucial to be aware of the mechanisms involved in order to prevent embryo alterations and long-term diseases. Therefore, the objective of this thesis was to determine whether specific components of embryo culture such as glucose and oxygen had any effect on the epigenetic patterns, at transcript levels, as well as on mitochondrial function.

The analysis of transcripts was assessed to determine differential expression of genes related to pluripotency, mitochondrial function, apoptosis, oxidative stress, DNA methylation, glucose transporters, among others. The epigenome analysis (Bisulfite Sequencing) was carried out to determine differential DNA methylation levels on human blastocyst cultured in high or low glucose (0.9mM or 3.5mM). Finally, mitochondrial

function was evaluated through the measurement of mitochondrial membrane potential (MitoProbe™ JC-1 assay) and through the analysis of mitochondrial respiration (Seahorse XF Cell Mito Stress Test) by directly measuring the oxygen consumption rate (OCR). In order to accomplish the objectives of this project and to obtain the most relevant clinical data, this research was conducted using preimplantation human embryos at blastocyst stage (day 6) and a model of human embryonic stem cells (HESCs). HESCs are pluripotent stem cells derived from the inner cell mass (ICM) of human blastocysts. The combination of the analysis on human embryos and HESCs allowed the validation of initial protocols, set up experimental conditions and the evaluation of different culture conditions. Firstly, I evaluated combined oxygen levels (5% and 20%) and glucose concentration (5mM and 17.5mM) on HESCs to determine their effect on transcript levels and mitochondrial function. Findings revealed altered transcript levels and mitochondrial function when cells were exposed to different concentrations of either oxygen or glucose, as well as to the combinations of both. However, the most significant effects were observed with changes in glucose concentration. Secondly, oxygen levels (5% and 20%), glucose concentration (0.9mM and 3.5mM) and the effect of cryoprotectants were evaluated on human blastocysts to determine their effect on transcript levels, mitochondrial function and DNA methylation. Findings revealed altered gene expression due to changes in oxygen but more significantly due to changes in glucose. Also, the analysis of DNA methylation showed significant differences as a result of glucose concentration. Furthermore, for the evaluation of mitochondrial function, the analysis of membrane potential was only carried out on blastocysts, treated/untreated with cryoprotectant. On the other hand, the measurement of OCR for mitochondrial respiration was only possible to determine the baseline on fresh blastocyst but not to make comparison between culture conditions due to technical limitations.

Overall, these findings suggest that altered culture conditions during early embryo development have the potential to affect several pathways that could be linked to the development of diseases. This project provides the first evidence about specific components of the embryo culture that could alter embryo development. Therefore, the conditions evaluated in this project are worth further investigation to elucidate the altered mechanisms and their direct association with the development of diseases.

DECLARATION

No portion of the work referred to in the thesis has been submitted in support of an application for another degree or qualification of this or any other university or other institute of learning.

COPYRIGHT STATEMENT

ACKNOWLEDGEMENTS

First of all, I would like to express my sincere acknowledgments to my supervisors Professor Susan Kimber and Professor Daniel Brison for giving me an opportunity to work on this project. For their support, encouragement, patience, empathy, their invaluable advice throughout my Ph.D. journey.

This thesis has been completed thanks to the support from all present and past members in Kimber lab including Steven, Alan, Edina, Phil, Jila, Helen Ioannis Rosie, Paweena, Paul, Mark, Qi Wang, Faris, Erum Miguel, Julieta, Fabrizio, Kirsty, Leona, Sophia and Samira. I am grateful for their friendship and their contribution in making this experience much more pleasant. My sincere gratitude to Nicola Bates, Dr Sara Cuvertino and Dr Christopher Smith for their invaluable technical advice, friendship and for always been supportive personally and professionally.

Acknowledgements to my colleagues at the Manchester Children's hospital and Old Saint Mary's hospital; Tope Adeniyi, Peter Ruane, and Anna Burdina for their support on the collection of clinical samples and their great advice on Reproductive Medicine.

Acknowledgements to Kelsey's group at the Babraham Institute, especially to Dr Hannah Demond and Dr Gavin Kelsey for their great support on the DNA methylation analysis.

Thanks to my Mexican friends in the UK; Karen, Ricardo, Arturo, Julio, Marco, Ruben and Rodrigo for their friendship and support.

The most especial gratitude to my family; Paco, Coca, Lore and Francisco, for their unconditional support at all times despite the distance.

Finally, thanks to my sponsor the Nacional Council for Science and Technology of Mexico (CONACyT) for the financial support during my Ph.D. studies at the University of Manchester.

CHAPTER 1

Introduction

1.1. Human preimplantation development

Human embryogenesis is a critical process that depends on a highly coordinated cascade of genetically encoded events through a process known as the maternal-to-zygotic transition (MZT). Here, maternal transcription factors initially control development, while the zygotic nuclear genome is quiescent. Subsequently, the embryo genome is activated, gene products are mobilized and maternal factors are cleared (Figure 1.1) [1].

Human embryo development begins after fusion of the egg and sperm in relative transcriptional silence with an oocyte to embryo transition. Here the molecular programs of the oocyte are degraded and those of the embryo are activated (days 0-3). The zygote passes thought epigenetic reprogramming and a series of cleavage divisions that culminate with a major wave of embryonic genome activation (EGA), between the 4- and 8-cell stages [2]. Here the mitotic divisions occurred during cleavage lead to the development of a multicellular embryo by producing smaller embryonic cells, called blastomeres [3].

Subsequently, the embryo undergo the first major morphological change to form the morula as consequence of the blastomeres compaction at 8- to 16-cell stage Here, blastomeres transform into a compact, ball-like structure, in which individual cells cannot be easily distinguished [4]. Compaction and polarization are fundamental events that leads cell differentiation and linage specification [5]. The formation of the blastocyst culminates by the formation and expansion of the fluid-filled cavity (blastocoele) and an inner cell mass (ICM) surrounded by trophectoderm (TE) cells due to a process known as cavitation [6] [7]. Just before implantation, the ICM further diverges into early epiblast (pluripotent cells) and primitive endoderm (extra-embryonic endoderm cells that will form the yolk sac) [8]. At this point, the embryo is ready to be implanted into the uterine wall, which concludes the preimplantation development at approximately day 7 [9].

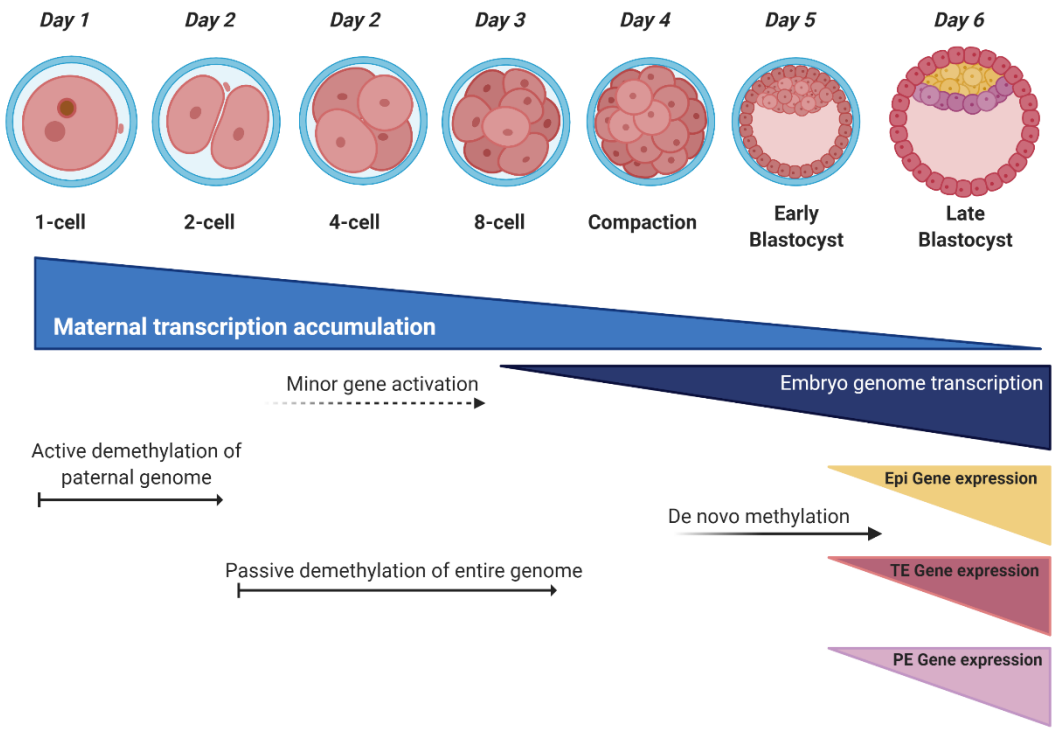

Figure 1.1. Representation of events during human preimplantation development. Fertilization occurs and the two pronuclei (2PN) zygote is formed at day one, then the cleavage process begins. At day 2 after first cleavage, zygote becomes into 2-cell embryo, 4-cell embryo and 8-cell embryo by day 3. Then compaction process begins at day 4, first cell fate decisions begin as well as cell polarization and the embryo is now called morula. At day five the embryo has become in an early blastocyst and there are two groups of cells, the inner cell mas (ICM) and Trophectoderm (TE). Subsequently, second fate decisions occur for the specification of primitive endoderm (PE) or hypoblast and epiblast (Epi) by day 6, just before implantation. Figure created with BioRender.com

1.2. Embryo metabolism

The mammalian embryo undergoes qualitative and quantitative changes in energy substrate utilization during the preimplantation period. The human embryo exhibits a characteristic switch in substrate preference; from pyruvate during the early cleavage stages, to glucose after compaction [10].

The preferred energy source for early preimplantation human embryos is pyruvate as the embryo relies on oxidative metabolism to obtain ATP [11]. Cleavage embryos have sub-optimal glycolytic metabolism via the Embden–Meyerhof pathway (Figure 1.2) [12]. At the morula stage, there is a switch to glucose uptake due to increased hexokinase activity, coincident with an increase in oxygen consumption. Although glycolysis is not the preferential metabolic pathway during the cleavage stage, glucose is still required at the zygote stage [3]. Zygotes have displayed reduced proliferative capacity and increased apoptosis in the absence of glucose [13]. Substantial perturbations in metabolic pathways culminate in compromised embryo development in culture and a reduction of viability post-transfer [14].

A relationship between carbohydrate utilisation by embryos and resultant viability has been established both in animal models and in the human. In fact, glucose consumption after compaction has been positively correlated with subsequent embryo viability [15]. However, an excessive glycolytic activity by the blastocyst, has been associated with a significantly compromised viability in the mouse model [16].

Regarding the glucose metabolism, there is strong evidence that shows that preimplanted embryos at blastocyst stage have the ability to convert glucose in lactate (Figure 1.3) [17]. However, there is also evidence showing that mouse blastocysts with a high glycolytic rate are less viable post-transfer than their low glycolytic counterparts (Lane & Gardner 1996). Nevertheless, preimplantation embryos require at least a brief exposure to glucose to develop from morula to the blastocyst stage. In addition, at morula stage, the expression of the glucose transporter GLUT3 is essential for blastocyst formation [12] and it is regulated by oxygen [18]. It has been demonstrated that the ICM display a relatively quiescent metabolism in comparison with that of the

TE. The TE consumed significantly more oxygen, produced more ATP and contained a greater number of mitochondria than the ICM [19].

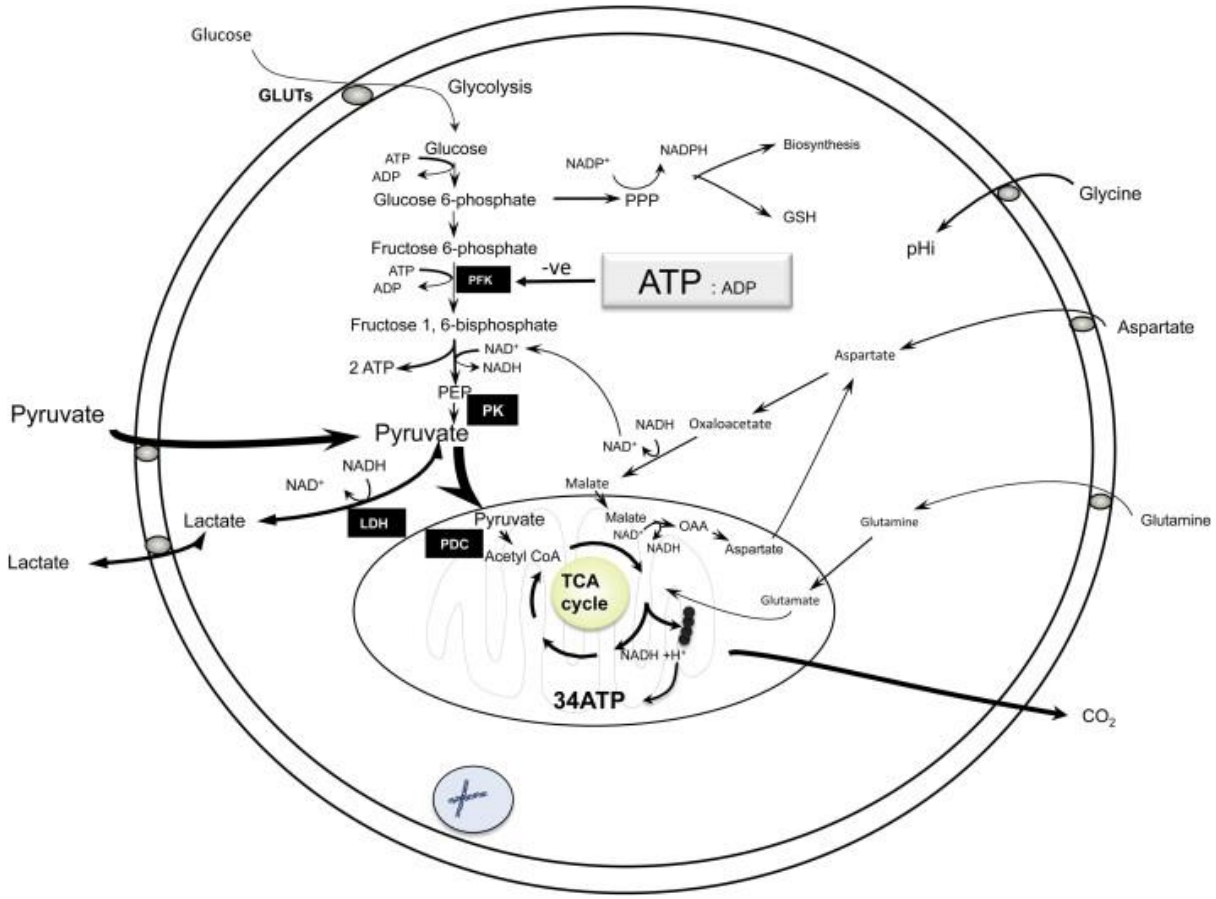

Figure 1.2. Metabolism of cleavage-stage embryo. The surrounding cumulus cells create a high concentration of pyruvate and lactate and a low concentration of glucose around the embryo. Before compaction, the embryo has a metabolism based on low levels of oxidation of pyruvate, lactate, and specific amino acids. The high ATP:ADP level inhibits phosphofructokinase (PFK), thereby limiting the flux of glucose through the glycolytic pathway before compaction. The pyruvate:lactate ratio in the environment directly affects the NADH:NAD+ ratio, which controls the redox state and thus the flux of other nutrients. The thickness of the lines in the figures represents the relative flux of metabolites through that pathway. GLUTs: glucose transporters; GSH: reduced glutathione; OAA: oxaloacetate; PDC: pyruvate dehydrogenase complex; PK: pyruvate kinase; PPP: pentose phosphate pathway [20].

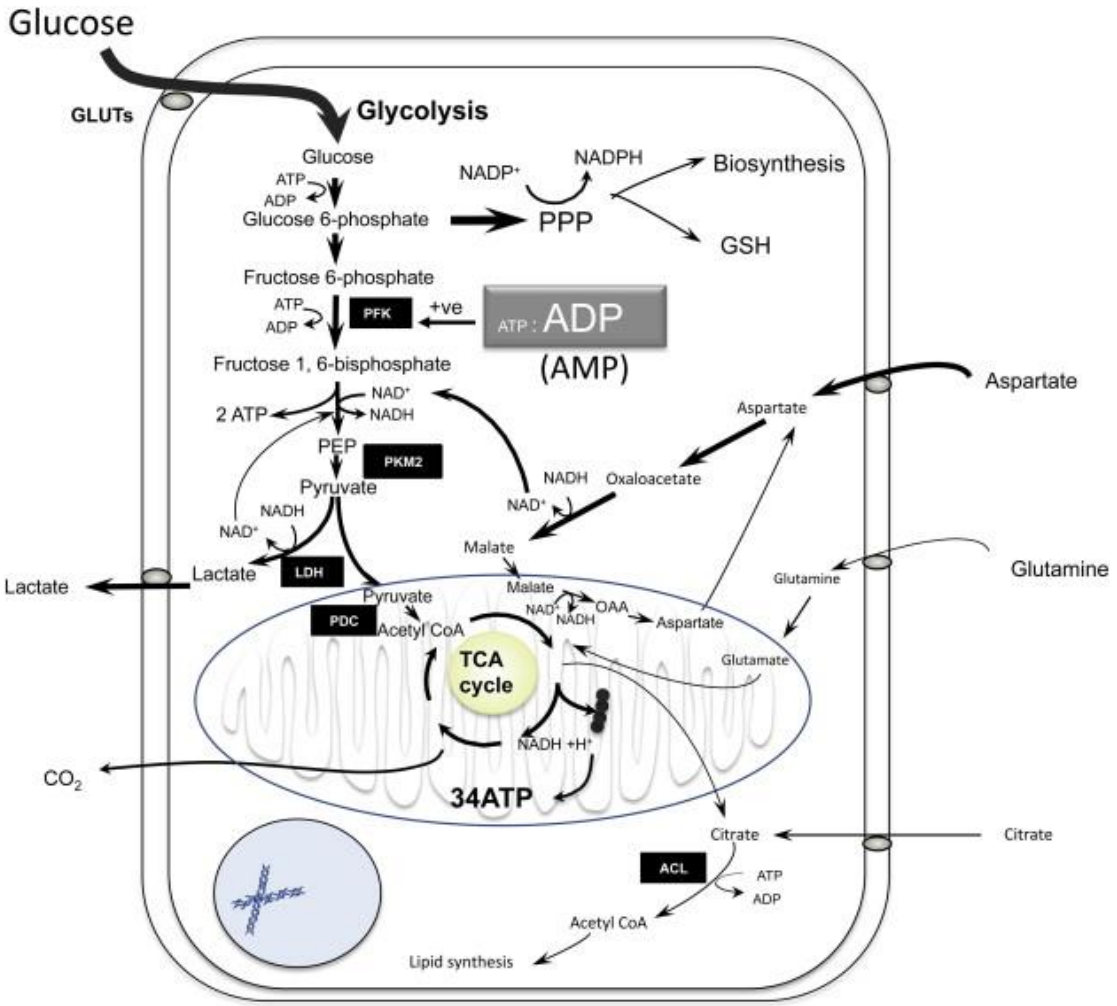

Figure 1.3. Metabolism of the blastocyst. After compaction, the embryo increases oxygen consumption and the capacity to use glucose as an energy source. In fact, the blastocyst exhibits high levels of aerobic glycolysis. There is a reduction in the ATP:ADP ratio, and a increase in AMP, which positively affects phosphofructokinase (PFK), thereby facilitating a higher flux of glucose through glycolysis. Blastocyst metabolism is combination of the relative activity of two cell types, the TE and ICM. It has been determined that TE exhibits higher levels of glucose oxidation in comparison to the ICM, which is almost exclusively glycolytic. The thickness of the lines in the figure represents the relative flux of metabolites through the pathway. ACL: acetyl-citrate lyase; GLUTs: glucose transporters; LDH: lactate dehydrogenase; OAA: oxaloacetate; PDC: pyruvate dehydrogenase complex; pHi: intracellular pH [20].

1.2.1. Mitochondria and energy metabolism

Mitochondria are maternally inherited organelles that use high efficiency oxidative phosphorylation pathways to supply ATP for cellular energy demand [21]. They are produced during oogenesis and the number of mitochondria remains static during preimplantation development until the time of implantation [22].

Mitochondria in fertilized oocytes, are numerous and are spread in the ooplasm. The principal change in distribution occurs at the pronuclear stage, when mitochondria allocate around the pronuclei. Also in 2-16-cell embryos mitochondria remain in perinuclear aggregation [23]. Elongated mitochondria with inner mitochondrial membranes arranged into transverse cristae begin to appear in expanding blastocysts, in the trophoblast, embryoblast, and endodermal cells. These mitochondria seem to play a role in blastocyst differentiation, expansion, and hatching, with their morphological changes reflecting increased cellular activity [24] [25].

Mitochondria play a fundamental role in the mammalian early embryo, contributing to many different aspects of early development principally in energy production and intracellular redox metabolism [26]. As mitochondria produce ATP, they release reactive oxygen species (ROS) locally that must be detoxified as they can induce oxidative damage on mtDNA, which can result in mutations and deletions [27].

Mammalian early embryos are very sensitive to oxidative stress, which can cause permanent developmental arrest before ZGA and apoptosis in the blastocyst. As mitochondria is crucial to balance ROS, they play an important role in maintaining embryo viability [25].

Embryos have shown low oxygen consumption at the early stages of development, which has been associated with small and sparse cristae in the mitochondria of early embryos, thereby maintaining a low level energy metabolism [28]. The low oxygen consumption of embryos correlate with loss cristae content and the low electro-density in the mitochondria [27], therefore it has been suggested that mitochondria also serve for the production of NADPH and metabolic intermediates by the TCA cycle. This is another important function of mitochondria that does not require developed cristae but rather a large matrix space [25] [26].

The mitochondria have a separate genome, which is a double stranded, circular DNA of approximately 16.7 kb. Human mitochondrial DNA (mtDNA) contains no introns and it replicates independently of the cell cycle. Mitochondrial DNA encodes enzymes involved in (aerobic) oxidative phosphorylation, which provides a more efficient method for the production of ATP compared with the (anaerobic) glycolytic pathway [21]. It is still unclear whether the total amount of mtDNA remains the same during human preimplantation development, as in other mammals is variable [26].

The mitochondrial genome encodes 13 proteins (part of the oxidative phosphorylation pathway), 22 transfer RNAs, and two ribosomal RNAs [29].

The expression of these gene products is controlled, in large part, by regulatory factors produced in the nucleus [30]. As cellular demand increases, proteins encoded by nuclear DNA are imported into the mitochondria to initiate and regulate the replication and transcription of mtDNA [31].

1.2.2. Mitochondrial membrane potential

Changes on the mitochondrial membrane potential (Δψm) has been found to be a key factor in determining whether or not mitochondria are healthy. The pattern of mitochondrial membrane potential progressively changes throughout preimplantation development, and an aberrant shift in Δψm could contribute to a decreased on developmental potential [32].

The membrane potential is created as a result of hydrogen pumping from matrix to the intermembrane space through Complexes I, III and IV. The ATP synthase utilizes these hydrogen ions to produce ATP. Thus, the membrane potential decreases as the protons are used to produce energy. However, the membrane potential is maintained by pumping more protons across the membrane. A balanced Δψm is requires to maintain cell viability. A long-lasting drop or rise of Δψm normal levels may induce unwanted loss of cell viability and be a cause of various pathologies [33].

Intracellular distinction between high and low potential mitochondria only occurs until the blastocyst stage. Mitochondria in trophectoderm cells usually exhibits a high potential, reflective of high activity whereas mitochondrial bioenergetics activity in the inner cell mass is lower (Figure 1.4) [23]. This is consistent with measurement of ATP generation in the inner cell mass showing lower levels of ATP production than in trophectoderm [16]. The mitochondrial membrane potential is a good indicator of mitochondrial activity and cellular health [33]. It is known to be affected by ROS production and other disrupter molecules such as carbonyl cyanide 3-chlorophenyl hydrazine (CCCP) that causes an uncoupling of the proton gradient in the electron transport chain and reduces the ATP synthase function, which causes cell damage. Mitochondria depolarization can indicate low metabolic activity, mitochondrial dysfunction or apoptosis. Whereas mitochondria polarization is an indicator of healthy mitochondria. [24]

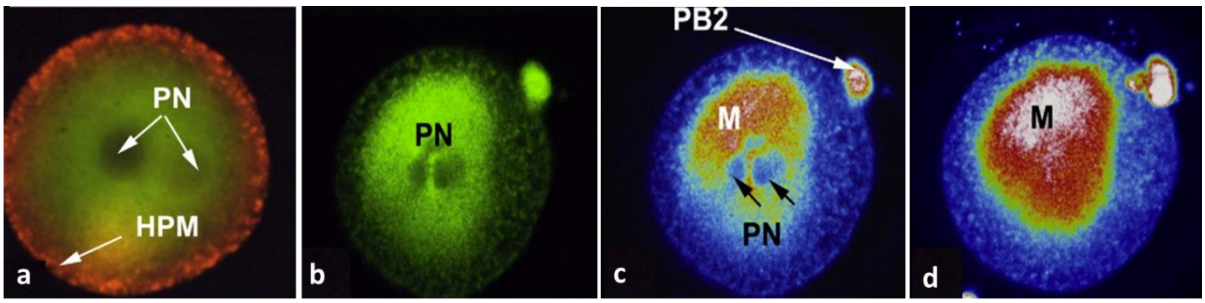

Figure 1.4. High potential mitochondria (HPM) allocation on early developed embryos. a. Human embryo at pronuclear stages, the HPM are located at the periphery of the cell (red); b. Low potential mitochondria (LPM) are located in the central cytoplasm (green); c. As development continues, HPM begin to accumulate around the pronuclei; d. Once pronuclei have disappeared, a dense and transient perinuclear accumulation of mitochondria can be observed. Modified image from [24].

1.3. Developmental Origins of Health and Disease

Patterns of health, illness and disease are influenced at different stages of the life course by a combination of genetic, epigenetic and environmental factors. In fact, substantial research has demonstrated that during early development, responses to a range of stimuli are likely to 'programme' the risk of certain disorders [34].

An important example of this phenomena was reported in the study of famine during the Dutch hunger winter. Here, foetal growth, and mortality, and mental and physical health in early adult life were explored in addition to the hypothesis that prenatal undernutrition can retard brain growth and impair mental performance [35] [36].

The Developmental Origins of Health and Disease (DOHaD) hypothesis postulates that during early development cells present certain phenotypic plasticity which enables them to reprogram gene expression patterns in order to adapt to the environmental conditions [37]. This adaptive process can increase the risk for developing diseases later in the adult life [38]. In fact, there is a close association between early embryonic development and the processes that lead to adverse programing of postnatal phenotype and the risks of adult diseases [39] [40].

More recently, studies have shown that environmental factors can induce epigenetic alterations in gametes that can potentially be transmitted transgenerationally. The heritable transmission of environmentally induce phenotypes is of particular interest as it may transmit risk of disease across generation in the absence of continued exposures [41], [42].

Currently, major concerns focussed on critical stages during early development, including how suboptimal exposures restricted specifically to gamete maturation or the preimplantation period can affect postnatal growth, glucose metabolism, fat deposition, and vascular function. Today, some evidences of the effects of assisted reproduction in diverse mammal's models have begun to emerge but it remains unclear whether or not in vitro embryo manipulation in humans will have lasting health consequences in the offspring [43].

1.3.1. Assisted reproductive technologies and DOHaD

Despite the huge advances on the assisted reproduction technologies, it remains unclear how exactly the embryo culture media affects the IVF outcome. Several studies have reported lower on the birth weight and higher risk of congenital anomalies when reported IVF compared to than natural conceived babies [44], [45] [46]. However, others have not found any significant differences [47]–[49].

On the other hand, other studies have also demonstrated that adverse culture conditions have effects on epigenetic, gene expression, imprinting or reprogramming events, suggesting that embryo culture medium may have a potential impact on further development of the new-born [38], [42], [43], [50][40]. In fact, these changes have been associated with low birth weight, congenital abnormalities, childhood growth [51] rare genetic diseases, and increased cardio metabolic and behavioural diseases in adulthood [52].

The impact of embryo culture systems is now a subject of focus due to recent increases in understanding of preimplantation human development since the first successful IVF treatment in 1978 [53]. The relative concentrations of nutrients present in culture media directly affects embryo metabolism. However, other variations in the culture system such as the concentration of oxygen used in the incubator can affect metabolic function [54].

1.4. Assisted reproductive technologies

Since 1987, more than 7 million individuals have been conceived by Assisted Reproductive Technologies (ART), which has significantly contributed to the infertility treatments around the globe [55], [56]. The main objective of human Assisted Reproductive Technologies (ART) is for the woman to give birth of a healthy singleton conceived through a Single-embryo transfer (SET) [55]. The most common male factors of infertility are the low sperm concentration, motility and morphology, whereas female factors are, tubal disease, ovulatory dysfunction, reduced ovarian reserve, endometriosis, and uterine factors [57].

Several procedures for infertility treatment are described in the literature. Some of them require little manipulation, for instance Artificial Insemination (AI) and Intrauterine Insemination (IUI) [58]. Others require broader manipulation of either gametes or embryos, such as In vitro fertilization (IVF) and Intracytoplasmic sperm injection (ICSI). Both IVF and ICSI are extensively used in ART, although they imply a high exposure of the gametes to the environment, they achieve good pregnancy rates [59][60].

1.4.1. In vitro fertilization and embryo transfer (IVF-ET)

IVF is the best treatment option for female infertility patients with partners with normal semen parameters. It consists in a series of controlled procedures that leads to the fertilization of the oocyte by the spermatozoa on a culture dish in the laboratory instead of in the woman's fallopian tube. It involves ovarian stimulation to obtain multiple oocytes, besides sperm collection and capacitation. The male and female gametes are mixed together and left to undergo the fertilization process in a culture system that mimics the fallopian tubes environment (Figure 1.5). This process has to be appropriately monitored. If fertilization occurs, the embryo development will begin (Figure 2) and the embryo might be transferred [61].

ICSI is intended to overcome male infertility, is the best treatment option for severe oligozoospermia, asthenozoospermia, and/or severe teratozoospermia. This procedure allows the absolute in vitro manipulation of the two gametes to achieve fertilization [62]. It is performed with the aid of an inverted microscope, and a pair of glass pipettes that allows the embryologist to hold the oocyte while the chosen spermatozoon is injected into the ooplasm (Figure 1.5). It can be carried out with fresh or frozen-thawed oocytes in addition to ejaculate or epididymal / testicular motile (live) spermatozoa [63]. However, a good selection of the spermatozoon is crucial in order to achieve insemination [61].

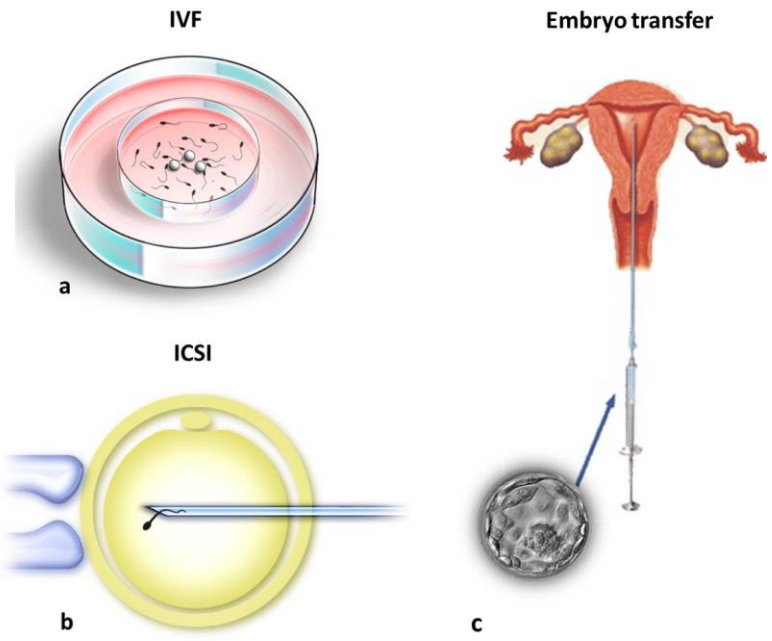

Figure 1.5. Oocyte insemination by in vitro fertilization (IVF) and Intracytoplasmic sperm injection (ICSI) followed by embryo transfer. a) IVF involves oocytes and sperm that are incubated together to achieve fertilization and the formation of a zygote. b) ICSI involves the microinjection of one sperm cell into the ooplasm. c) Embryo transfer can be performed up to 6 days after fertilization.

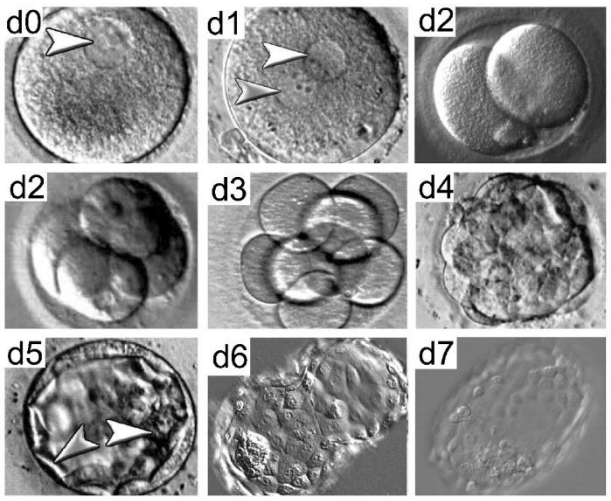

Figure 1.6. Monitored stages of human embryo during in vitro pre-implantation development, from day (d) 0 to day 7. Arrowheads in d0 and d1 indicate pronuclei. From d1 to d4 changes in the number of embryonic cells are noticeable, as a result of cleavage process. On d4, the embryo forms a morula that consists of cells (blastomeres) in a compact cluster contained within the zona pellucida. On d5, the early blastocyst is formed; a fluid- filled structure composed of an inner cell mass (white arrowhead) and trophectoderm (grey arrowhead). On d6, the blastocyst 'hatches' from the zona pellucida and it is ready to implant into the uterine wall on d7 [8].

1.4.2. Embryo Monitoring and Grading

Non-invasive methods for evaluation of the quality and prediction of developmental competence of in vitro-produced preimplantation-stage embryos are of crucial importance in human-assisted reproduction. Ensuring the quality of the culture process to maintain the viability of embryos is crucial to achieve the highest pregnancy (and live birth) rates and to keep the proportion of multiple pregnancies at a minimum level [64]. The most feasible approach to meet these requirements is using the single-embryo transfer (SET) technique This involves extended culture and decreased number of transferred embryos to increase survival of the best embryos, while decreasing the chance of multiple implantation [65].

At present, the only routine and gold standard method for prediction and selection of high quality embryos is the bi-daily light microscopic evaluation of the morphology (Figure 1.6) [64]. Due to its simplicity and cost-effectiveness, allows the evaluation of morphological features and the developmental rate through in a non-invasive manner [66][67]. Morphological evaluation has currently been extended to include continuous surveillance, enabled by the introduction of time-lapse incubators developed specifically for IVF treatment. Unlike embryo culture in standard incubators, time-lapse monitoring offers uninterrupted culture, a flexible workflow in the laboratory, and improved embryo selection. This is based on the assumption that more frequent observations will provide substantially more information on the relationship between development, timing, and embryo viability. [68]

Different scoring systems for blastocysts have been described worldwide. The most commonly used is the Gardner scale (Figure 1.7), which is based on an alphanumeric scoring system [65]. It has been defined based on the degree of blastocyst expansion-hatching status (EH), the development of the inner cell mass (ICM grade) and the development of the trophectoderm (TE grade) [69]. Initially, blastocysts are given a numeric score from 1–6 based on their degree of expansion and hatching status: 1) early blastocyst, the blastocoel being less than half the volume of the embryo; 2) blastocyst, the blastocoel being greater than half the volume of the embryo; 3) full blastocyst, the blastocoel completely filling the embryo; 4) expanded blastocyst, the blastocoel volume now being larger than that of the early embryo and the zona

starting to thin; 5) hatching blastocyst, the trophectoderm starting to herniate though the zona; and 6) hatched blastocyst, the blastocyst having completely escaped from the zona [70]. Currently, there is a newer grading system (Figure 1.8) that has been created with the propose of harmonization between IVF clinics worldwide [71] [67].

Gardner scale	
EH stage	1. Early blastocyst, blastocoele being less than half volume of that of the embryo. 2. Blastocyst with blastocoele whose volume is half of, or greater than half of that of the embryo. 3. Full blastocyst with a blastocoele completely filling the embryo. 4. Expanded blastocyst with a blastocoele volume larger than that of the full blastocyst, with a thinning zona. 5. Hatching blastocyst with the TE starting to herniate through the zona. 6. Hatched blastocyst, in which the blastocyst has completely escaped from the zona.
ICM	A. Tightly packed, many cells. B. Loosely grouped, several cells. C. Very few cells.
TE	A. Many cells forming a cohesive epithelium. B. Few cells forming a loose epithelium, C. Very few, large cells.

Figure 1.7. The Gardner scale for blastocyst grading [70]

Alpha/ ESHRE Consensus Grading for balstocytes			
	Grade	**Rating**	**Description**
Stage of development	1 2 3 4		Early Blastocyst Expanded Hatched/hatching
ICM	1	Good	Prominent, easily discernible, with many cells that are compacted and tightly adhered together.
	2	Fair	Easily discernible, with many cells that are loosely grouped together.
	3	Poor	Difficult to discern, with few cells.
TE	1	Good	Many cells forming a cohesive epithelium
	2	Fair	Few cells forming a loose epithelium
	3	Poor	Very few cells

Figure 1.8. The alpha/ ESHRE consensus grading system for blastocysts [72]

1.4.3. Embryo Freezing and Thawing

Cryopreservation is widely used in assisted reproduction. It relies on preserving cellular viability of gametes and embryos in an arrested state, without compromising cell function, in order to be used posteriorly [73]. Although it is extensively used, is well known that there is a risk of two principal types of injuries that can cause cell damage, ice crystal formation and high salt concentrations (Figure 1.9) [74].

During slow freezing, the destruction of a cell is caused by dehydration (exosmosis), which results in the growth of the intracellular concentration of solutes and the shrinking of the cell [75]. On the other hand, during fast freezing the water might not have enough time to leave the cell which can lead to the formation of the intracellular ice causing the cell destruction by mechanically disrupting the cell membrane and the cytoskeleton [76]. In order to prevent cell damage, cryoprotectant agents (CPAs) can be used during cryopreservation protocols [77].

1.4.3.1. Slow freezing

Slow freezing is currently the most widely used method for cryopreserving human embryos. During slow freezing, embryos are exposed to low concentrations of CPAs in addition to controlled cooling rates using a programmed freezer [78]. Unlikely Vitrification, slow freezing has the advantage of using low concentrations of CPAs, which are associated with chemical toxicity and osmotic shock [79]. On the other hand, the controlled rates of temperature during slow freezing in combination with the low concentration of CPAs, provoke the extracellular or intracellular ice formation, which can cause cell damage [75] [80].

1.4.3.2. Vitrification

Vitrification is an effective method that prevents the primary cause of cell injury, which is the intracellular ice formation. It allows the cryopreservation of cells by a simple and rapid method without a programmed freezer, which reduces costs, time besides the chilling sensitivity and crystallization damage caused to cells (Figure 1.9). It involves rapid cooling and liquid solidification as a result of the increment in viscosity provided by the chosen CPAs and their high concentrations [79]. In consequence, a

solid and amorphous structure like glass is obtained, therefore it can readjust and take the shape of the cell, hence enabling the cell to maintain its structure and remain intact, unlike in slow freezing, where the formation of ice crystals during cooling prevents the cell from maintaining its structure (Figure 1.9) [80]. Several studies have suggested that Vitrification results in significantly higher survival and developmental rates than slow freezing [73][75][80]. However, there are many concerns regarding the toxicity caused by the high concentration of CPAs during Vitrification [79] [78].

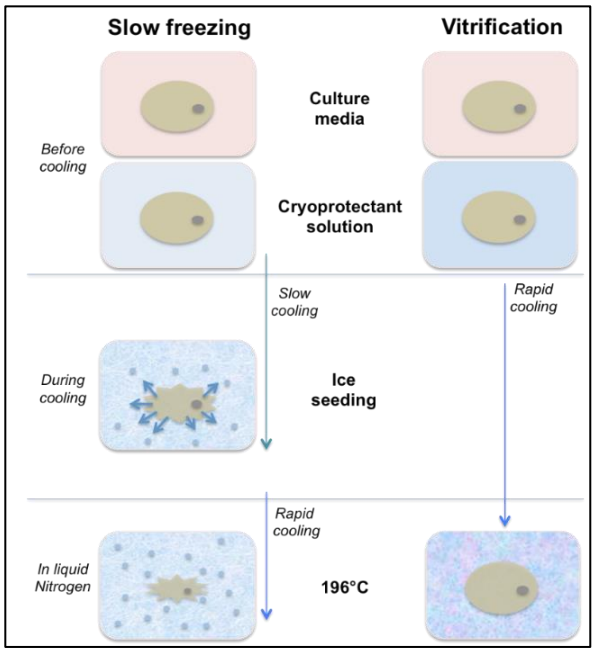

Figure 1.9. Schematic comparison of slow freezing and vitrification. The figures illustrate and embryo (circle) under both methods of cryopreservation. During slow freezing, cells suffer dehydration due to extracellular ice crystal formation, causing mechanical damage to the cell structure. During vitrification, cells are inserted into vitrification medium of high viscosity, which prevents extracellular ice crystallization and hence, cells remain intact.

1.4.4. Embryo Culture

Since the establishment of ART worldwide, several media formulations and culture systems have been used for the in vitro development of the human embryo. Media formulation is focussed on the maintenance of healthy embryos in order to achieve implantation after transfer and subsequently a successful pregnancy [13].

It is important to understand the role of each medium component and to identify possible sources of cellular stress to the embryo that will ultimately affect the function and viability of the embryo, besides the health of the offspring [81], [82]. There are specific requirements for the embryo depending its developmental stage; therefore, the main objective for each system is to meet these natural requirements [83].

Currently, there are two types of culture systems:

a) Single-step, also called monoculture. This system follows the principle ¨let the embryo choose¨. It is designed for the simultaneous use of all the media components in a balanced mixture, made with tolerable ranges of concentration for each component. This system would lead the embryo itself to adapt and utilize whatever it requires. With single-step culture system, it is no need for a media change, so there is not perturbation for the embryo during the entire period of in-vitro culture from fertilization until blastocyst stage [84].
b) Sequential system. This system follows the principle “back to nature”. It is designed to try to mimic the natural changes of the environment in order to provide the specific requirements for every embryo stage, from the oviduct and the uterus. This system requires media changing; it utilizes one type of media for the early stages of the embryo (before compaction) and another for late stages (after compaction). One of the principal reasons of these changes is the energy source required for embryo development, which are pyruvate in the early stages and glucose in late stages [85] [86].

1.4.5. Key components of embryo culture media.

The oviduct and uterus provide the environments for the earliest stages of mammalian embryo development. In humans, pyruvate concentration is ~0.25 mM, lactate varies from 4.8 – 10.5 mM, and glucose from 0.5 – 3.11 mM [87]. In vivo, the composition of the early embryo's environment (oviductal and uterine fluids) is largely determined by the composition of the maternal diet [88]. Although several companies have worked on the development of the optimal culture media, the identification of the best and safest conditions in vitro for embryo culture to support optimal embryo development remains elusive [84]. In fact most of the efforts to improve media formulation focussed on increasing the pregnancy success rate and minimising cellular stress to prevent undesired long-term effects on the late embryo. However, details of the long-term effects of culture media on assisted reproductive technology are limited by a lack of data [86] Basic components in culture media include carbohydrates, essential amino acids, non- essential amino acids pH buffers, antioxidant [82] [89]. However, media composition varies widely (Table 1.1) with notable differences in glucose, pyruvate, lactate, and amino acids between commercial brands [84].

	Sequential										Single-step			
Brand	Vitrolife		Sage		Cook		In Vitro Care		Origio		IVF Online	Irvine	Vitrolife	Origio
Name	G1	G2	QACM	QABM	SICM	SIBM	IVC1	IVC3	ISM1	BA	Global	CSC	G-TL	1-Step
Glucose (mM)	0.5	3.4	0.1	2.8	0.3	3.1	0	2.7	1	1	0.18	0.47	0.97	0.19
Citrate (mM)	0.08	0.08	0	0.16	0	0	0	0.16	0.02	0.003	0	0.02	0.01	0
Lactate (mM)	10.8	6	3.9	3.9	1.8	1.8	10.1	9.4	3.2	2.4	4.9	5.71	10.01	4.35
Pyruvate (mM)	0.3	0.07	0.52	0.07	0.36	0.31	0.08	0.09	2	0.17	0.24	0.28	0.55	0.22
L:P ratio	36	86	7.5	56	5	5.9	126	105	18.5	1.2	20	21	18	20
Met (uM)	0	63	0	56	4	43	0	100	89	54	44	50	54	54
Gln (uM)	0	0	0	0	30	26	0	0	778	0	0	0	10	36
Tau (uM)	131	0	122	120	6489	6380	0	0	296	0	0	0	48	0

Table 1.1 Principal components in embryo culture media, a partial comparison between manufacturers [86], [84].

1.4.6. Oxygen tension

Cellular respiration (aerobic and anaerobic) can be defined generally as the process by which chemical energy is released during the oxidation of organic molecules [90]. Molecular oxygen (O_2) is an essential nutrient in aerobic respiration that works as a key substrate for mitochondrial ATP production and numerous intracellular biochemical reactions. The maintenance of oxygen homeostasis is, therefore, essential for cell survival. Oxygen deprivation (hypoxia) activates complex and adaptive responses at cellular, tissue, and organismal levels to cover the metabolic and bioenergetics demand [91].

The concentration of oxygen to which embryos are exposed in vivo varies between 2 and 8% in the oviduct and uterus, depending on the species. In other words, gametes and embryos are never exposed to atmospheric oxygen (~20%) under physiological conditions [92]. However, embryos obtained in vitro through insemination or ICSI are routinely cultured at such elevated concentrations of oxygen in many IVF laboratories around the globe [93].

Early embryos benefit from being cultured under conditions which tend to limit reactive oxidative species (ROS) formation, for example, low oxygen concentration (5%), similar to that in the oviduct [94] [95]. Most of the evidence indicates that atmospheric oxygen affects the utilisation of both carbohydrates and amino acids [16], which has a significant impact on gene expression at blastocyst stage, the embryonic proteome and embryo metabolism [3]. In addition, embryo culture can have a significant impact in the embryo survival as formulation could promote cell arrest or cell death [96], [97]. Furthermore, other embryonic mechanisms may also be affected by the culture systems causing stress, which might be more relevant for the future health of the offspring [98]. Moreover, atmospheric oxygen has been associated with the alteration of global DNA methylation in human embryos [99].

Although most of the studies suggest that physiological concentration of oxygen is beneficial during preimplantation development, there is not conclusive evidence [100]. Overall, the influence of oxygen and nutrient availability on the metabolism and

cell survival should be considered, as well as other metabolic adaptations regulated by oxygen that may impact the embryo epigenome.

1.5. DNA methylation mechanisms in preimplantation development

Although DNA methylation mechanisms have been investigated for years, the effect of ART on preimplantation development has not been fully understood. Nevertheless, several studies now agreed that ART might impair DNA methylation reprogramming. Recently, the investigation of the effect of culture media, ovarian stimulation or embryo transfer on the epigenetic mechanisms has been emphasised in order to search for strategies to mitigate adverse effects on the health of ART-derived children [101].

The establishment of the correct epigenetic state during preimplantation development may be crucial to avoid immediate or future alterations in the offspring's health. According to the DOHaD hypothesis, the epigenetic marks that are rewritten during early embryonic development of an individual may serve to predict predisposition to certain diseases in adult life. Therefore, it is important to establish the normal patterns and to identify aberrant patterns [41]. Preimplantation embryos experience profound resetting of epigenetic information inherited from the gametes. Changes in epigenetic information, associated with states of gene activity, are at least one order of magnitude more frequent than genetic changes and more susceptible to environmental conditions [102]. In fact, there is evidence of differential methylation levels in imprinted genes when comparing siblings that were prenatally unexposed and exposed to famine during the Dutch Hunger Winter in 1944 [103].

Epigenetic mechanisms such as DNA methylation and histone modifications play crucial roles during embryo development (Figure 1.10). These mechanisms are active during the preimplantation phase and can restrict cells to a particular fate [104]. Hence there is a potential risk for permanent alterations in the epigenome as epigenetic mechanism are involved in several processes including, gene regulation, establishing of imprinting patterns, maintaining the genome stability and inactivating

X chromosome in females [52]. The main epigenetic mechanisms are covalent modifications of the DNA (methylation) and post-translational modifications of histone proteins (histone code). DNA methylation occurs by addition of a methyl group to the carbon-5 position of the pyrimidine ring of cytosine, producing 5-methyl cytosine (5mC) [105]. CpG methylation is one of the most commonly studied, and it refers to the methylation of a cytosine preceding a guanine. Along the genome, there are regions of high CpG density, termed CpG islands (CpGi), which frequently overlap promoter regions. High CpG methylation at the promoters is related to repression, while in gene bodies methylation it favours transcriptional fidelity by suppressing cryptic intragenic initiation [106]. The regulation of 5mC in the CpG sequence context is the result of the relative contribution of three interconnected pathways: (1) De novo methylation (DNMT3 a/b/l); (2) maintenance of existing methylation patterns (UHRF1and *DNMT1*); and (3) active demethylation (TET) [107].

Genomic imprinting is an epigenetic mechanism that determines expression or repression of genes according to their parental origin [108]. Some imprinted genes are involved in regulating proper embryo development and cell proliferation [109] [110]. DNA methylation is a key epigenetic regulator of embryogenesis and stem cell differentiation in mammals, critically involved in cell-type-specific transcriptional regulation. It is predominantly restricted to CpG dinucleotides and it is stably distributed across the genome [111]. DNA methylation is a great concern in developmental biology, as it is involved in processes that includes regulating gene expression, establishing imprinting patterns, genome stability and inactivating one X chromosome in females among others [112]. The embryo undergoes dramatic reprogramming during early development, therefore is critical to regulate the mechanisms involved in DNA methylation [38].

Interestingly, the number of studies reporting association between epigenetic disorders and ART have recently increased. Some studies report increased frequency of imprinting syndromes such as Beckwith-Wiedemann (BWS) and Silver-Russell (SRS) associated with ART [113] [114]. Others have studied the association of ART with neurological disorders such as autism spectrum disorders (ASDs), Attention deficit/hyperactivity disorders, sleep disorders, Cerebral Palsy (CP) [115].

In addition, a few reports have now confirmed the potential impact of embryo culture systems on the new-born's birth weight [44] [46]. Human gametes are characterised by differential average levels of DNA methylation, from intermediate (oocyte) to high (sperm). However, they undergo global demethylation following different mechanisms and dynamics after fertilization [116] [117]. DNA methylation is highly active after fertilisation and can restrict cells to a particular fate, which can potentially lead to embryo arrest, but more importantly, there exists a potential risk of permanent alterations that can only be noticeable after birth.

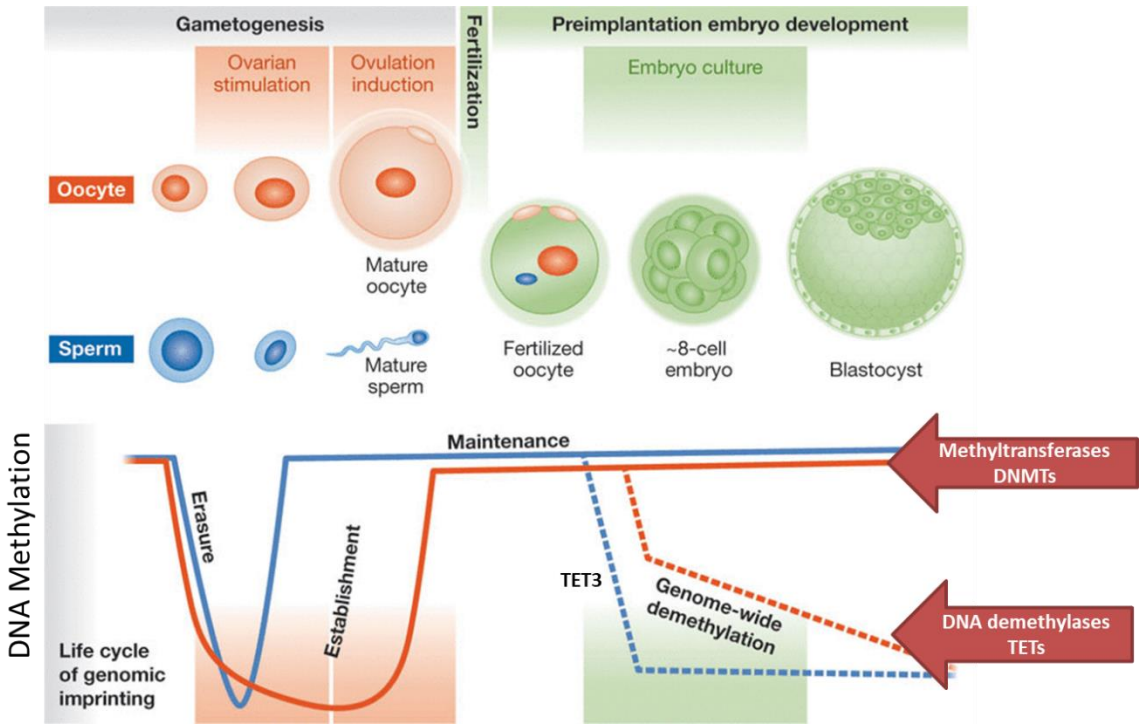

Figure 1.10. Life cycle of genomic imprinting and assisted reproductive technology. Erasure, re-establishment and maintenance of genomic imprinting occur during gametogenesis and preimplantation embryo development. Paternal and maternal methylation through gametogenesis and early stages of preimplantation development (blue and red solid lines). Imprinting marks are erased at early stages of gametogenesis. Re-establishment of imprinting occurs throughout gametogenesis, but finishes much later in oocytes compared with sperm. During preimplantation development, both maternal and paternal imprinting marks are maintained whilst the rest of the genome is demethylated. The paternal genome is demethylated rapidly and actively (dashed blue line) whilst the maternal genome is demethylated at a slower rate passively through cell division (dashed red line). Preimplantation development in vitro could alter the establishment of imprinting marks in embryos. Adapted from Grafodatskaya et. al [118].

1.6. Human Embryonic Stem Cells (HESCs)

HESCs are derived from the inner cell mass (ICM) of the human embryo at blastocyst stage [119], they can be maintained undifferentiated *in vitro* under defined medium conditions and still maintaining the developmental potential to form trophoblast and derivatives of all three embryonic germ layers [122]. They can generate all somatic cell types including gut epithelium (endoderm); cartilage, bone, smooth muscle, and striated muscle (mesoderm); and neural epithelium, embryonic ganglia, and stratified squamous epithelium (ectoderm) [120].

HESCs have normal karyotype and express high levels of telomerase activity, cell markers, and key transcription factors that are crucial for the maintenance of pluripotency [121]. HESCs can be a valuable and versatile tool for understanding mechanisms in human development as well as in the establishment of organ structures [123].

1.6.1. HESCs as a model for studying human embryo development

The indefinite self-renewal ability, developmental potential and plasticity of HESCs to generate unlimited distinct cell types in vitro, has now opened new avenues for regenerative medicine and for modelling of human diseases [124]. Those features make HESC extremely important in basic and applied research and therefore they are a promising model for studying human development [125]. Despite the limitations that HESCs may present, they are a powerful tool to study mechanisms that occur in human embryogenesis. Moreover, they can be used to analyse the effect of specific mutations on particular developmental events and may enable us to identify critical factors that play a role in the processes of cell commitment, differentiation, and adult cell reprogramming [126].

1.6.2. Characterization of HESCs

Characterization is crucial on studies with embryonic stem cells. Following the International Stem Cell Initiative, characterization can be performed by measuring the expression of a broad list of proteins or genes. Despite diverse genotypes and different techniques used for derivation and maintenance, all lines exhibited similar expression patterns for several markers of human embryonic stem cells. They expressed the glycolipid antigens SSEA3 and SSEA4, the keratan sulfate antigens TRA-1-60, TRA-1-81, GCTM2 and GCT343, and the protein antigens CD9, Thy1 (also known as CD90), tissue-nonspecific alkaline phosphatase and class 1 HLA, as well as the strongly developmentally regulated genes *NANOG* and *OCT4* [127] [128] [129]

1.7. HESCs metabolism

Similar to ICM cells in the human blastocyst, HESCs rely mostly on glycolysis as an energy supply [130]. In addition, mitochondria in HESCs are rather immature and they become mature as cells differentiate and undergo a metabolic switch from glycolysis to oxidative phosphorylation (OXPHOS) [131] [132].

Glucose and oxygen are crucial in mammalian cell culture; however, the impact of their availability or concentration on the glycolysis pathway and how this may alter the regulation of the pluripotent state, is not yet well understood [133].

Recent studies link changes in energy metabolism with the fate of pluripotent stem cells. Shifts in metabolism from pluripotent stem cells to differentiated cells represent variable demands on mitochondrial function as different cell types have distinct energetic and biosynthetic requirements [130]. In this context, mitochondrial function has the potential to influence reprogramming and differentiation outcomes. Changes in cellular metabolism also affect enzymes that control epigenetic configuration, which affects chromatin reorganization and gene expression changes during reprogramming and differentiation [134]. The importance of DNA methylation in regulating pluripotency is evidenced by the fact that perturbations of the expression level or function of different epigenetic enzymes can impair stem cell self-renewal and

lead to the loss of pluripotency, events that are followed by differentiation. Enzymes such as acetylases, methylases and demethylases necessary for specific chromatin structural and functional states [135].

1.8. Aims and objectives

The aim of this project is to investigate the effect glucose concentration and oxygen tension on human embryos and human embryonic stem cells determine mechanism that may be affected during preimplantation development as result of assisted reproduction technologies (ART).

This project has been accomplished using donated human embryos at blastocyst stage and HESCs as model of study.

Objectives

1. To evaluate the effects of oxygen in human preimplantation embryos
    a. Evaluation mitochondrial function and gene expression of embryos cultured in GTL medium at 5% and 20% oxygen.
2. To evaluate the effects of glucose in human preimplantation embryos.
    a. Evaluation mitochondrial function, gene expression, and DNA methylation in embryos cultured in GTL medium at 0.9 Mm and 3.5 mM glucose.
3. To evaluate the effect of oxygen on HESCs
    a. Evaluate pluripotency markers, mitochondrial function and gene expression in HESC cultured in E8 media in physiological (5%) and atmospheric (20%) oxygen.
4. To evaluate the effect of glucose on HESCs
    a. Evaluate of pluripotency markers, mitochondrial function and gene expression in HESC cultured in E8 media with 5 mM glucose and 17.5 mM

Chapter 2

Materials and Methods

2.1 Human Embryo handling, culture and analysis.

All Human embryos used in this project were donated to research after fully informed patient consent in writing, with approval from Central Manchester Research Ethics Committee and the Human Fertility and Embryology Authority (HFEA, www.hfea.gov.uk) licence R0026.

Fresh and frozen human embryos at blastocyst stage (day 6), as well as frozen human embryos at 2PN stage (day 1) were donated by couples undergoing IVF treatment at St Mary's Hospital, Manchester. All embryos were graded by a qualified Clinical Embryologist from St Mary's Hospital according to the Consensus scoring system for blastocysts (Figure 2. 1) from the Alpha/ESHRE 2011 guidelines [71].

Embryos were either graded and lysed the same day or kept in culture in GTL medium (Vitrolife, Sweden) at 37°C/5% oxygen up to Day 6. Blastocysts then were graded and lysed for cDNA synthesis.

2.1.1 Cryopreservation and thawing protocols

Slow frozen embryos donated at cleavage stage were thawed using the THAWKIT™ CLEAVE (Vitrolife, Sweden) following the manufacturer's instructions and clinical standard operating procedures. Briefly, embryos frozen in straws were removed from liquid nitrogen, left for 30 sec at room temperature (RT), transferred into water at 37°C for 45 sec and opened. Immediately after, the contents were placed in TS1 solution for 5 min/RT, transferred to TS2 for 5 min/RT followed by 5 min/RT in ES solution. Embryos were then placed in 0.5 ml of pre-equilibrated GTL medium overlaid with OVOIL™ (Vitrolife, Sweden) and incubated at 37°C /5% oxygen in air for recovery and blastocyst formation up to Day 7 before being graded and lysed for cDNA.

Vitrified embryos donated at blastocyst stage were thawed using the MediCult Vitrification Warming Kit™ (Origio, Fr) following the manufacturer's instructions. Briefly, Cryopettes™ containing embryos were removed from liquid nitrogen and were warmed at 37°C for 1 min. The Cryopettes™ were cut and the contents were ejected into Warming Solution (Origio, Fr) for incubation at 37°C/3 min. The contents were then transferred to the different solutions included in the MediCult Vitrification Warming Kit™ (Origio, Fr) for incubation at RT/3 min (Dilution solution 1, Dilution solution 2, Washing solution 1, and Washing solution 2). Subsequently, embryos were placed in 0.5 ml GTL medium overlaid with OVOIL™ (Vitrolife, Sweden), incubated at 37°C in 5% oxygen in air for recovery and kept up to Day 7 to be graded (Figure 2.1) and lysed for cDNA synthesis.

	Grade	*Rating*	*Description*
Stage of development	1		Early
	2		Blastocyst
	3		Expanded
	4		Hatched/hatching
Inner cell mass	1	Good	Prominent, easily discernible, with many cells that are compacted and tightly adhered together
	2	Fair	Easily discernible, with many cells that are loosely grouped together
	3	Poor	Difficult to discern, with few cells
Trophectoderm	1	Good	Many cells forming a cohesive epithelium
	2	Fair	Few cells forming a loose epithelium
	3	Poor	Very few cells

Figure 2.1. Consensus scoring system for blastocysts. The s scoring system for blastocysts is a numerical interpretation of the Gardner scale (Gardner and Schoolcraft, 1999a, b) that combines the stage of development, the grade of the inner cell mass and the trophectoderm. For instance, a hatched blastocyst with a good inner cell mass and a good trophectoderm would be scored as 411 [71].

2.2 Double stranded cDNA synthesis from Embryos (PolyA PCR)

Double stranded cDNA was synthesized from all embryo samples using the PolyA PCR method as shown in Figure 2.2 [136].

For the LYSIS mix preparation of Primer mix (Figure 2.3) and 4 µl of RNasin Ribonuclease Inhibitor (Promega, USA) were added to 192 µl of First Lysis Buffer (Figure 2.3), and then 10 µl of this lysis mix was added to UV irradiated tubes. Embryos were removed from culture drops in a minimal amount of medium and one embryo was carefully placed in each tube containing lysis mix. The tubes were then heated for 1 min at 65°C followed by 3 min at 25°C and held at 4°C or on ice for a minimum of 5 min. Subsequently first strand synthesis of cDNA was completed by adding 0.5 µl of reverse transcriptase M-MLV (Promega) to each tube, then placed in a thermocycler to allow the activation of the reverse transcriptase at 37°C. This process included a restricted cycle length of 15 minutes to limit the extension of the first strand to between 100 and 700 base pairs. Deactivation of the reverse transcriptase was performed at 65°C just before the samples were kept at 4°C in order to prevent degradation of the newly synthesised cDNA.

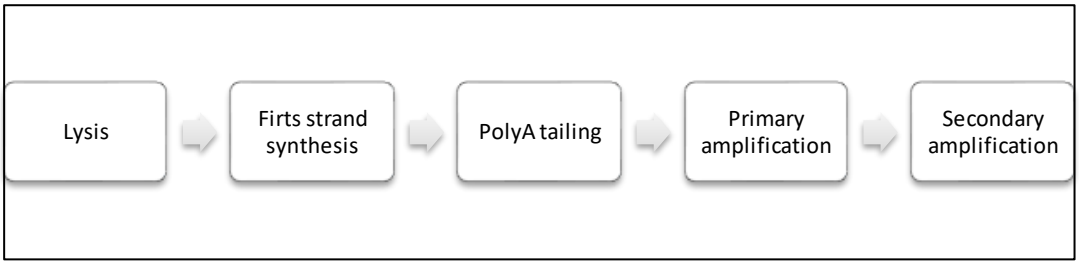

Figure 2.2 PolyA PCR workflow. This diagram show an overview of the processes involved in PolyA PCR protocol that is used to synthesise cDNA from low input samples

2.2.1 cDNA synthesis

PolyA tailing was prepared by adding 10 µl of 2x tailing buffer (Figure 2.3) and 0.5 µl of Terminal transferase (TdT) (Invitrogen, UK) to each tube containing newly synthesised cDNA. Sample tubes were then placed in the thermo cycler following the same cycle as for the first strand synthesis (Table 2.1). Heating to 37°C activates the enzyme terminal transferase which synthesises the polyA tail in the presence of dATP to the 3'end of the first strand of cDNA. The enzyme is deactivated by heating to 65°C and the holding of samples at 4°C or on ice prevents the degradation of the polyA tailed cDNA and if primary amplification was not done straight after, samples were stored at -80°C. For primary amplification, 10 µl of primary amplification master mix (Figure 2.3) was added to UV irradiated PCR tubes plus 5 µl of the poly A tailed first strand synthesis. Tubes were placed in the thermal cycler following the program in Table 2.2. Primary amplified samples were stored at -80°C. For secondary amplification 49 µl of secondary amplification master mix (Figure 2.3) was added to UV irradiated PCR tubes plus 1 µl of PCR product from the primary amplification. Tubes were placed in a thermal cycler and run at the settings described in Table 2.3 Secondary amplified samples were stored at -20°C for further quantification and dilution at 1 ng/µl.

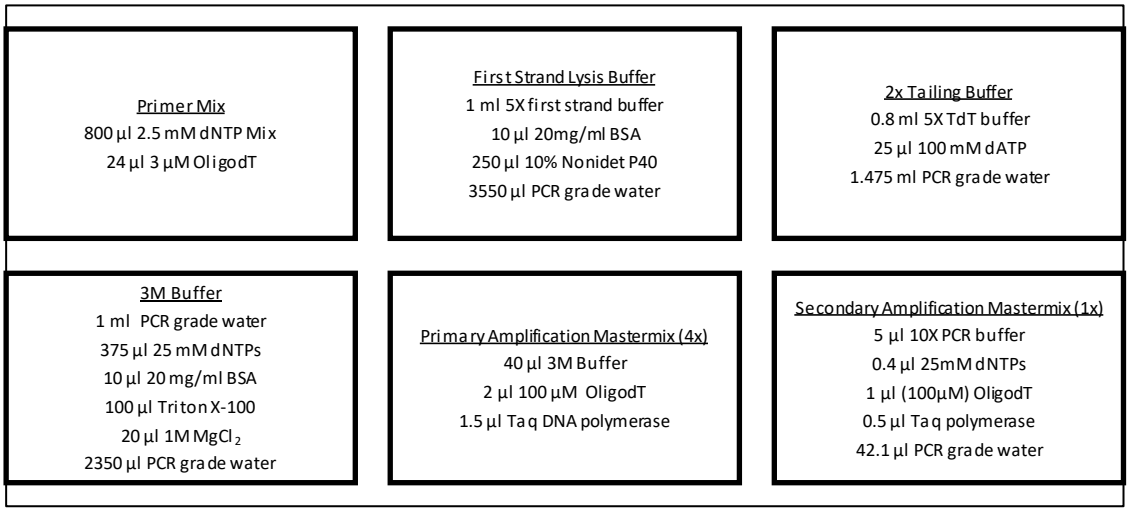

Figure 2.3 Composition of master mixes used in polyA PCR method

Step No.	Temperature (^{O}C)	Time (min)
1	37	15
2	65	10
3	4	Hold

Table 2.1 Cycle profile for first strand cDNA synthesis and polyA tailing.

Step No.	Temperature (^{O}C)	Time (min)
1	95	1
2	42	2
3	72	6
4	Repeat steps 1-3 for 29 cycles	
5	94	1
6	42	2
7	72	2
8	Repeat steps 5-7 for 29 cycles	
9	4	Hold

Table 2.2 Cycle profile for Primary amplification of cDNA.

Step No.	Temperature (^{O}C)	Time (sec)
1	94	60
2	94	30
3	54	30
4	72	30
5	Repeat steps 2-4 for 70 cycles	
6	4	Hold

Table 2.3 Cycle profile for Secondary amplification of cDNA

2.2.2 Quantification of double stranded cDNA from PolyA PCR

Quantitation of dsDNA was done using the QuantiFluor® dsDNA System (Promega, USA) according to manufacturers' instructions. Briefly, Tris-EDTA (TE) buffer (10mM Tris HCL, 1mM EDTA, pH 7.5) was used to prepare DNA standards (in triplicate), samples, and the QuantiFluor® reagent. Firstly, QuantiFluor® dsDNA Dye was diluted 400-fold with TE buffer 1X to make the QuantiFluor working solution. Lambda DNA Standard, 100µg/ml was used to prepare the standard curve as described in Table 2.4

The assay was prepared in a black 96-well plate (200 µL/well) at room temperature and the QuantiFluor® reagent was always protected from light to avoid degradation. All standards or PolyA-cDNA samples were added in triplicated to the 96-well plate as follows: 1 µL sample or Standard + 199 µL of QuantiFluor working solution. After 30 min incubation at room temperature, fluorescence was measured in a Glomax Multi+ plate reader (Promega, USA) using the Blue filter (Ex: 490nm, Em: 510–570nm). For the standards, the mean fluorescence was plotted in a typical standard curve to obtain a line equation ($y = mx + b$) and R^2 value for further calculations of concentration. Sample (cDNA) concentration was then calculated using their mean fluorescence values on the obtained line equation from the standard curve. All samples were diluted at 1 ng/µL for further qPCR analysis.

Standard	Volume of 1X TE (µL)	Lambda DNA Standard (100µg/ml)	Final DNA Concentration (ng/µL)
A	10	10 µL	50
B	20	5 µL of A	10
C	20	5 µL of B	2
D	20	5 µL of C	0.4
E	20	5 µL of D	0.08
Blank	20	N/A	0

Table 2.4 Preparation of dsDNA Standards. Standard solutions were diluted according to the manufacturer's recommendations in order to get appropriate concentrations for this study.

2.3. Isolation of ICM and TE cells from human blastocyst

Human embryos were kept in culture for up to six days in GTL medium supplemented with 1mM or 3.5mM glucose. After the incubation, embryos were graded according to the consensus scoring system and only good quality embryos were selected for immuno-surgery.

Isolation of ICM and TE was assessed as follows:

Three 3.5 cm dishes with microdrops were prepared for each embryo. One dish was prepared with 50 µL drops of 1:3 Rabbit anti-human serum antibody (Sigma-Aldrich H8765), another with 50 µL drops of Guinea pig complement (Sigma-Aldrich S1639) and the last one with 50 µL drops of EmbryoMax acidic tyrode's solution (Millipore). Drops were allocated in the centre of the dish surrounded by three 30 µL drops of GTL medium that were used to rinse the sample. All dishes were overlaid with oil and incubated prior to use.

1. Individual blastocysts were transferred into a 50 µL drop of EmbryoMax acidic tyrode's solution using a 290 µM Flexipet® Pipette (Cook) and kept until the zona degradation was observed (30-60sec). Subsequently, they were washed through 3x 30 µL drops of GTL medium to remove the acidic tyrode's solution.

2. Zona-free blastocysts were transferred to a 50 µL drop of pre-warmed Rabbit anti-human serum diluted 1:3 in PBS and kept for 30 min. at 37˚C / 5% oxygen. After incubation, blastocysts were washed through 3x 30 µL drops of GTL medium

3. Labelled blastocyst were transferred to a 50 µL drop of pre-warmed Guinea pig complement diluted 1:10 in PBS and kept for 30 min. at 37˚C / 5% oxygen. After the incubation, "blebbing" of the outer trophectoderm cells was evident. Blastocysts were washed through 3x 30 µL drops of GTL medium and transferred to a new 50 µL drop of GTL medium.

4. Using a glass pipette, the trophectoderm cells were removed from around the ICM and carefully aspirated. These TE cells with a minimal volume of GTL carry over was placed in a new labelled micro tube and stored at -80˚C for further analysis. The ICM was also transferred into a new labelled micro tube and stored at -80˚C for further analysis.

2.4 DNA methylation analysis for human blastocyst

Isolated ICM or TE cells from human blastocyst samples were sodium bisulphite treated using the EZ DNA Methylation Kit (D5001, Zymo Research) for conversion of methylated bases. DNA methylation analysis was assessed using WGBS according to the single-cell adaptation (scBS-seq) of the Post-Bisulphite Adaptor Tagging (PBAT) method [137]. Single-cell embryo libraries were amplified for 14 cycles and quantified by qPCR to assess library quality. Libraries were then sequenced in the Illumina NextSeq platform for 75bp pair-end.

2.4.1 Library preparation (PBAT protocol)

In order to complete library amplification samples went through several processes that include DNA extraction, bisulphite conversion, desulfunation, first and second strand synthesis as well as several purifications (Figure 2.4).

DNA extraction was completed using an adaptation for the EZ-DNA Methylation kit (D5001, Zymo Research). Total sample volume from immune-surgery process (~5 µL) was mixed in a PCR tube with 19 µL master mix (Table 2.5) and incubated for 60 min at 37˚C.

Bisulphite conversion was completed by adding 125 µL of conversion reagent (Table 2.6) to each sample and incubating them at 98˚C for 8 min followed by 64˚C for 3.5h

Component	Volume per reaction
Cell Lysis buffer (fresh)	12 µL
EB Buffer:	6 µL
Proteinase K:	1 µL
Final Volume:	24 µL

Table 2.5 EZ-DNA Methylation Lysis mix

Bisulphite converted samples were desulphonated and purified using Zymo-spin IC columns previously treated with 300 µL of M-Binding buffer. Converted samples were transferred to the column followed by extra 100 µL of M-Binding buffer that were used to wash and collect residuals from the previous reaction tube. Columns were centrifuged for 30 sec at 13000 rpm. 100 µL M-Wash buffer were added to the column followed by centrifugation 30 sec/13000 rpm. 100 µL M-Desulphonation buffer were added and incubated for 20min at RT. After incubation the column was centrifuged 30 sec/13000 rpm and flow through was discarded. The column was then washed twice with 200 µL of M-Wash buffer and then transferred into a new clean 1.5 mL tube. 40 µL of Nuclease free water were added to the column, incubated at RT for 5 min and centrifuged at 13000 rpm/ 1 min.

Reagent	**Volume**
M-Solubilization Buffer	790 µL
M-Dilution Buffer	300 µL
Mixing 10 min/RT	N/A
M- Reaction Buffer	160 µL
Mixing 1 min / RT	N/A

Table 2.6 Conversion reagent preparation

The eluted flow-through was transferred to clean PCR tubes and mixed with first strand master mix composed by 5 µL of NEB Buffer 2 (10X), 2 µL dNTP mix (10 µM) and 2 µL of 10 µM 6N-F primer (5'-CTA CAC GAC GCT CTT CCG ATC TNN NNN N-3'). Samples were then incubated at 65˚C for 2 min and immediately cooled down on ice where1 µL of Klenow-exo enzyme (50 U) was added. Once the enzyme was added, tubes were incubated for 5 min at 4˚C, 37˚C for 90 min (rampage 1˚C/ 15 sec) followed by 4˚C hold.

First strand synthesis was purified using AMPure XP beads (Beckman Coulter, US) at 1:0.8 ratio. 40 µL AMPure XP beads were added, mixed and incubated for 10 min at RT. After incubation, the reaction tubes were place on a magnet and samples were washed twice with 100 µL 80% Ethanol. Tubes were left open for 7-10 min until the beads were dry and the 48 µL of Second strand master mix (Table 2.7) were added to proceed with second strand synthesis.

Reagent	**Volume**
H2O	39.0 µL
NEBuffer 2 (10x)	5.0 µL
dNTPs (10 mM)	2.0 µL
6N-R primer (10uM) 5'-TGC TGA ACC GCT CTT CCG ATC TNN NNN N-3'	2.0 µL
Total volume	48.0 µL
Incubate 3 min / RT	N/A

Table 2.7. Second strand synthesis master mix

Second strand synthesis mix was incubated at 98˚C for 1 min and immediately cooled to 4˚C on ice. Two microliters of Klenow exo- (50 U) were added to each sample, mixed, briefly spin down and immediately transferred to the thermocycler where they incubated as follows: 5 min at 4˚C,then raised 37˚C with 1˚C per 15 sec (33x ramp steps), followed by for 90 min at 37˚C. Samples were vortexed every 20-30 min to re-suspend beads and were keep at 4˚C after finishing the incubation.

Second strand synthesis was purified by adding 50 µL of nuclease free water and 80 µL of AMPure XP buffer. Samples were mixed thoroughly and incubated for 10 min at RT. After incubation, samples were placed on a magnet and washed twice with 180 µL of 80% ethanol. Samples were then incubated at RT for 10 min until the beads were dry and they were eluted with 49 µL of Library amplification master mix (Table 2.8). Finally, 1 µL of specific iTAG was added to each sample and they were then transferred to a termociclyer to proceed with the library amplification (Table 2.9).

Finally, amplified libraries were purified by adding 35 µL of AMPure XP buffer to each product. They were well mixed by pipetting up and down, and then incuvated for 10 min at RT. After incubation, libraries were placed on a magnet and washed twice with 100 µL of 80% ethanol. Libraries were then incubated at RT for 7-10 min until the beads were dry and then eluted in 15 µL of Nuclease-free water, where they were incubated for 2 min at RT. Tubes were then placed on a magnet and carefully 13-14 µL of supernatant were transferred to clean tubes, without taking any beads. Purified libraries were stored at -20˚C for further paired-end sequencing analysis (Figure 2.5).

Reagent	**Volume**
H2O	36.µL
KAPA HiFi or HF Phusion buffer (5x)	10 µL
dNTPs (10 mM)	1.0 µL
PE1.0 primer (10uM)	1.0 µL
KAPA HiFi or Phusion HF DNA polymerase	1.0 µL
Total volume	49 µL

Table 2.8. Library amplification master mix

Temperature	**Duration**	**Cycles**
95 ˚C	2 min	
95 ˚C 65 ˚C 72 ˚C	80 sec 30 sec 30 sec	10-14x
72 ˚C	3 min	
4 ˚C	hold	

Table 2.9. Library amplification protocol

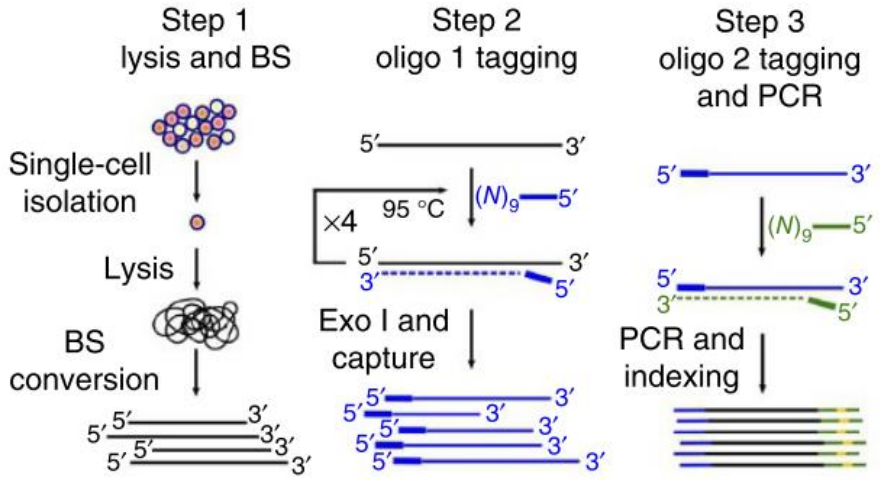

Figure 2.4. Post-bisulfite adaptor tagging (PBAT). scBS-Seq library preparation is performed in three stages: (1) Single cells are isolated and lysed before bisulfite conversion is performed. (2) Five rounds of random priming and extension are performed using oligo1 (which carries the first sequencing adaptor) and newly synthesized fragments are purified. (3) A second random priming and extension step is performed using oligoxygen (which carries the second sequencing adaptor) and the resulting fragments are amplified by PCR. [137]

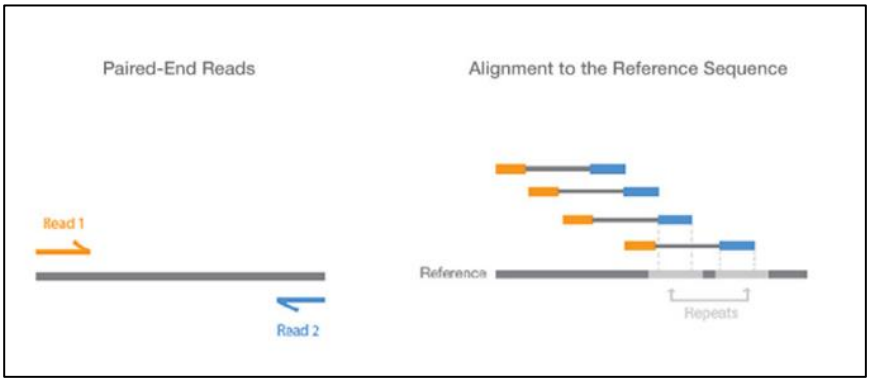

Figure 2.5. Representative diagram of sequencing method. Paired-end sequencing enables both ends of the DNA fragment to be sequenced. Because the distance between each paired read is known, alignment algorithms can use this information to map the reads over repetitive regions more precisely. This results in much better alignment of the reads, especially across difficult-to-sequence repetitive regions of the genome.

2.5 Routine culture of HESCs

2.5.1 Culture and passaging of HESCs

Human embryonic stem cell lines Man7 and Man13 were derived in the North West Embryonic Stem Cell Centre (NWESCC) University of Manchester [129] and they were cultured through a feeder-free system. Prior to cell culture, tissue-culture grade plastic dishes were coated with 5 µg/ml solution of Truncated N-terminal Vitronectin (Life Technologies A14700) diluted with PBS (0.5 µg/cm^2). Plates were incubated overnight at 4ºC or for a minimum of 30 mins to 2 hours at 37ºC. Cells were thawed and seeded into Vitronectin coated 6-well plates using TeSR™-E8™ medium (Stem Cell Technologies, US) additionated with 10 µM Rho-associated kinase (ROCK) inhibitor (Y27632). Cells were incubated at 37°C / 5% oxygen /20% oxygen and left undisturbed for 24 h and the medium was replaced every 24h until the cells reached 80% confluency. Cells were routinely visualized with an inverted microscope Leica MD IL LED (Leica) and images were taken with a DFC295 camera using the Application Suite software (Leica). At 80-90% of confluency, HESCs were washed once with 1X PBS without Ca^{+2} / Mg^{+2} and 1 mL of 0.5mM EDTA was added; then incubated at room temperature for 5 min. EDTA solution was carefully removed and discarded. Cells were harvested by pipetting and resuspended in TeSR™-E8™ medium to be split as required.

Preparation of modified TeSR-E8 medium

For the purpose of this project, culture media for HESCs was prepared according to Chen *et at* 2011 [138]. Briefly, media was prepared using DMEM/F12 as basal media (without glucose), then it was supplemented with TGFß1 (2 ng/ml), FGF2 (0.1 mg/L), LAA, sodium selenium (14 ng/ml), NaHCO3 (543 mg/L), Transferrin (10.7 mg/L), Insulin (19.4 mg/L), ascorbic acid (64 mg/L), and D-glucose (5 mM or 17.5 mM). Osmolarity of all media was adjusted to 340 mOsm at pH 7.4.

2.5.2 Cryopreservation of hESCs

For cell freezing, appropriate number of cells (0.5 - 2 x 10^6 cells/ml) were resuspended in 1 ml of ice cold PSC Cryopreservation medium (Thermo Fisher, US). Cryovials were immediately wrapped in three layers of blue roll paper to allow slow freezing overnight at -80°C . Vials were transferred to a liquid nitrogen container for long-term storage within a period no longer than 48 hours.

2.5.3 Cell thawing

Liquid nitrogen frozen cryovials containing HESCs (Man1 and Man13) were immediately placed into a 37°C water bath for thawing. Cells in PSC Cryopreservation medium (Thermo Fisher, UK) were transferred into a 15 ml tubes with 5 ml of E8 stem cell maintenance medium (Stem Cell Technologies) and centrifuged for 3 min at 700 x *g* (Sigma 3-16K), then the cell pellet was resuspended in E8 medium supplemented with 1X RevitaCell Supplement (Thermo Fisher, UK) for counting and seeding.

2.5.4 Cell counting

Cells number, viability percentage and cell diameter were determined using the automatic cell counter NucleoCounter® NC-200™ (ChemoMetec, DK). The automatic counter uses disposable cassettes for sample loading, which contains immobilized fluorescent dyes such as Acridine orange and DAPI (4', 6-diaminido-2-phenylindole). Briefly, sample was taken by inserting the tip of the Via1-Cassette™ (ChemoMetec, DK) into the homogeneous cell suspension and pressing the piston. Immediately, the loaded Via1-Cassette™ was inserted on the tray of the NucleoCounter® where the measurement was completed within one minute.

2.6 HESC characterization

2.6.1 Immunofluorescence staining

Immunofluorescence for cell surface, cytoplasmic and nuclear antigen expression was done to verify pluripotency of Man7 and Man13 cell lines [129]. Cells plated in 24-well dishes were washed once with PBS washing solution (PBS 1X, 5% BSA, 0.05% Tween 20) and fixed with 500 µl/well 4% paraformaldehyde (PFA) solution in PBS for 10-15 min at room temperature. Subsequently, cells were washed three times with PBS washing solution to remove PFA and blocked for 30 min with 100 µl /well of 10% serum solution of the same species as the secondary antibody (Goat, Sheep or Donkey). For nuclear or cytoplasmic staining 0.1% of Triton X-100 was added to the serum solution and primary antibody solution. The cells were then incubated either for 2 hours at room temperature or overnight at 4°C with 100 µl/well of primary antibody solution or isotype control antibodies (Table 2.10). Cells were then washed three times with PBS washing solution and incubated 2 hours at room temperature with 100µl/well of the corresponding secondary antibody (Table 2.10) conjugated with Alexafluor^{488} or Alexafluor^{594} (Invitrogen). Cells were washed three times to remove the secondary antibody excess and stained with 50-100 µl/well of DAPI solution 1:100000 (Invitrogen). Finally, cells were washed twice with PBS washing solution and left in 500 µl PBS/well at 4°C for microscopy. Cell images were subsequentely collected through a fluorescence microscope with a Retiga-SRV Fast 13394 camera (Olimpus IX71, Japan) and processed using the Q-Capture Pro image software 6.0.

Antibody	Supplier	Isotype	Ab. Dilution	Triton-X	2° Antibody	Supplier	2° Ab Dilution
OCT3/4	BD Biosciences	Mouse IgG	1:100	YES	Goat Anti-Mouse IgG	Invitrogen	1:200
NANOG	Cell Signaling	Rabbit IgG	1:400	YES	Goat Anti-Rabbit IgG	Invitrogen	1:200
SOX2	Cell Signaling	Rabbit IgG	1:400	YES	Goat Anti-Rabbit IgG	Invitrogen	1:200
SSEA1	Millipore	Mouse IgM	1:200	NO	Goat Anti-Mouse IgM	Invitrogen	1:200
SSEA3	Millipore	Rat IgM	1:200	NO	Goat Anti-Rat IgM	Invitrogen	1:200
SSEA4	Millipore	Mouse IgG	1:200	NO	Goat Anti-Mouse IgG	Invitrogen	1:200
TRA-160	Abcam	Mouse IgM	1:200	NO	Goat Anti-Mouse IgM	Invitrogen	1:200
TRA-181	Abcam	Mouse IgM	1:200	NO	Goat Anti-Mouse IgM	Invitrogen	1:200
Rabbit IgG	Santa Cruz	Rabbit IgG	1:400	YES	Goat Anti-Rabbit IgG	Invitrogen	1:200
Mouse IgG	Santa Cruz	Mouse IgG	1:200	YES	Goat Anti-Mouse IgG	Invitrogen	1:200
Mouse IgM	Santa Cruz	Mouse IgM	1:200	NO	Goat Anti-Mouse IgM	Invitrogen	1:200
Rat IgM	Santa Cruz	Rat IgM	1:200	NO	Goat Anti- Rat IgM	Invitrogen	1:200

Table 2.10. Antibody list for immunocytochemistry analysis

2.6.2 Flow cytometry analysis of cell surface and nuclear antigen expression

Flow cytometry analysis was done to evaluate pluripotency status of cells after the different conditions of culture. Cells were seeded in a 6-well Vitronectin coated plate using E8 medium with 10µM ROCKi (Table 2.11), then feeded with E8 medium (Stem Cell Technologies) for up to 6 days.

Cells were harvested after a specific time of culture using 500 µl/well of TrypLE and incubated for 3min at 37°C. TrypLE was inactivated with 2 ml of E8 medium; cells were dissociated by pipetting, then counted to get a cell solution of $1x10^6$ to $3 x10^6$ and placed in a 15 ml tube for centrifugation for 3 min at 700 x g to form a cell pellet. The

cell pellet was washed once with 2 ml PBS 1X (Sigma) and then fixed with 1 ml 4% PFA 7 min at room temperature. After incubation, cells were centrifuged for 3 min at 700 x g, PFA was removed and cells were washed once with 2 ml 1X PBS. Cells were then blocked with 2 ml 10% FBS in 1X PBS for 30 min at room temperature plus overnight at 4°C. Subsequently, 5ml 1X PBS was added to give 7 ml of cell suspension, and then this was split in 7 Eppendorf tubes (1 ml / tube). All tubes were centrifuged for 3 min at 700 x g and resuspended in 100 µl PBS. For extracellular staining cells were incubated with appropriated antibodies according Table 2.12 for 30 min at room temperature protected from light. For nuclear staining, cells were first permeabilised with 1 ml ice cold 70% Methanol /PBS for 7 min at 4°C, then cells were washed once and resuspended 100 µl 1X PBS, to proceed with nuclear staining according Table 2.12. After incubation for 30 min at room temperature protected from light, cells were washed once, resuspended in 400 µl 1X PBS and kept on ice for further analysis.

Flow cytometry analysis using a BD FACSFortessa™ (BD) was done immediately after staining. Unstained cell controls for each sample were used to determine the light scattering parameter of the cell population measured as forward scatter (FSC) and side scatter at 90° of the light source (SSC). Unstained cells plotted as FSC-A vs FSC-H were gate as Singlets, subsequently this gated population was plotted as SSC-A vs FSC-A to gate a population of live cells. Unstained cells were also plotted in the fluorescence detection channels (AF488-B-530/30, PE-Y-580/15 and AF647-R-670/14) to determine auto-fluorescence of cells and set the positive and negative gates. Subsequently, fluorescence parameters for the markers of interest *NANOG*, *SOX2*, Tra181, SSEA3 and their correspondent isotype controls mouse IgG1, mouse IgG, mouse IgM-PE, rat IgM-PE (Table 5.2.2) were evaluated and used to set the compensation values that would be applied in all the analyses. Histogram plots showing the marker of interest, its isotype control and percentage positive population were generated for all the analysis.

Condition	Cells per cm^2	Number of wells	Volume/ well
12 hours	4×10^4	4	2 ml
2 Days	2×10^4	4	2 ml
4 Days	1×10^4	4	2 ml
6 Days	5×10^3	4	2 ml

Table 2.11. Number of HESCs seeded per experimental condition in each well of a 6-well plate.

Tube	Permeabilised	Antibodies	Dilution	Supplier
1	No	None	N/A	N/A
2	No	Anti-Human Tra181-PE	1:30	eBioscience
3	No	Anti-Human SSEA3-PE	1:20	BD Pharmingen
4	No	mouse IgM-PE	1:30	Santa Cruz
5	No	rat IgM-PE	1:80	BD Pharmingen
6	Yes	Anti-Human *NANOG*-AF488 Anti-Human *SOX2*-AF647	1:10 1:80	BD Pharmingen
7	Yes	mouse IgG1-AF488 mouse IgG1-AF647	1:100 1:300	BD Pharmingen

Table 2.12. List of antibodies used in Flow cytometry analysis

2.7 Gene Expression analysis for hESCs

2.7.1 RNA isolation

RNA was isolated from HESCs (Man1 and Man13) using the RNeasy Mini Kit (Qiagen, UK) according to the manufacturers protocol. Briefly, cells were harvested from culture using TrypLE express protocol (Appendix 3). A pellet of maximum 5×10^6 cells was formed followed by the addition of 350 µl of RLT buffer and mixing on vortex for 15 seconds until the pellet was lysed. 1 volume of 70% Ethanol was added to the lysate and this was mixed well by pipetting. 700 µl of the lysate were transferred to an RNeasy Mini spin column placed in a 2 ml collection tube and centrifuged for 15 s at 8000 x *g*. The flow-through was discarded; 700 µl of Buffer RW1 were added to the

column and centrifuged for 15 s at 8000 x *g.* The flow-through was discarded; 500 µl of Buffer RPE were added to the column and centrifuged for 15 s at 8000 x *g.* The flow-through was discarded; 500 µl of Buffer RPE were added to the column and centrifuged for 2 min at 8000 x *g.* The column was placed into a new 1.5 collection tube; 50 µl of RNAse-free water were added directly to the spin column membrane and centrifuged for 1 min at 8000 x *g.*

2.7.2 RNA Quantification

The quantity and purity of all RNA samples was verified by measuring the absorbance (A260/A280) using the Spectrophotometer NanoDrop ND-100 (Thermo Scientific, USA) according to the manufacturers instructions. Briefly, the instrument was blanked with 1 µl of RNase/DNAse free water, and then 1 µl of each sample was measured to obtain the concentration in ng/µl.

2.7.3 cDNA synthesis

cDNA was synthesized from HESCs (Man1 and Man13) cells . To avoid the presence of contaminating DNAses, all surfaces were cleaned with 70% IMS followed by RNase-ZAP solution (Ambion, US). All plastic consumables and pipettes were UV irradiated for 10 min prior to setting up the RT-PCR reaction.

All RNA samples were treated to eliminate DNAses prior to cDNA synthesis using the RQ1 RNase-Free DNAse (Promega, UK) according to the manufacturer's instructions. Briefly, 1 µg of sample was placed into a thin wall 0.5 ml tube, mixed with the DNAse Master Mix (Table 2.13) and incubated for 30 min at 37 °C followed by 10 min at 65 °C. Subsequently, 1 µl of 0.5 µg Random Hexamers (Promega, USA) was added to the tube, which was incubated for 5 min at 70°C and placed on ice immediately after incubation. RT Master Mix (Table 2.14) was added to the tube, mixed, centrifuged and incubated for 60 min at 37 °C. Finally, the synthesized cDNA (42.55 ng/µl) was aliquoted and diluted at 1 ng/µl to be stored at -20°C.

DNAse Master Mix	Volume
RNA sample at 125 ng/µl	8 µL
RQ1 DNAse Buffer	1 µL
RQ1 DNAse	1 µL
RQ1 DNAse Stop Solution	1 µL

Table 2.13. DNAse master mix for treatment of 1 µg of RNA

RT Master Mix	Volume
5X MMLV RT Buffer	5 µL
10Mm dNTP mix	5 µL
RNAse Inhibitor (40 U/µl)	0.5 µL
MMLV RT (200 U/µl)	1 µL

Table 2.14. RT Mastermix for the synthesis of 1 µg of RNA to cDNA single stranded.

2.7.4 Real Time qPCR

Real time qPCR was used to measure and compare the relative expression of thirty genes (Table 2.15). All cDNAs where diluted to 1 ng/µl prior to setting up the qPCR reactions. Ten microliter reactions were prepared on ice using the Power SYBR Green System (Applied Biosystems, U.S) as detailed in Table 5.3. The reactions were loaded in triplicate into a 384 well plate (BioRad, U.S), closed with optical quality film (BioRad, U.S) and placed into a thermal cycler Real-Time PCR CFX384 (BioRad, U.S) programmed as follows: Initial activation 10 min at 95°C, 40 cycles of amplification including: Denaturation at 95°C for 30 secs, annealing at 60 °C for 30 secs and extension at 72°C for 35 secs followed by the acquisition of fluorescent signal). To ensure the specificity of every reaction a melting analysis step was added after the amplification step as follows: (denaturation at 95°C for 15 secs, dissociation from 60°C to 95°C with an increment of 0.5°C/0.05 sec and a continuous acquisition of fluorescent signal).

qPCR Master Mix	Volume
SYBR Green Mix	5 µl
Nuclease-Free water	2 µl
Primer Mix (3µM)	1 µl
cDNA (1 ng/µl)	2 µl

Table 2.15. QPCR master mix for HESCs

2.7.5 Real Time qPCR Analysis

Data was analysed with the Bio-Rad CFX Manager 3.1 Software (BioRad). The baseline level was set between 3 and 8 and threshold value was set according to standard dilutions of cDNA and a Non Template Control (NTC). The threshold cycle (C_T) which determines the cycle number at which the fluorescence level meets the threshold was calculated using a series of dilutions in triplicate of cDNA from Man13 cell line amplifying all genes mentioned in Table 5.3.8. Subsequently a standard curve was plotted using C_T values and the standards concentrations in logarithmic values to obtain a correlation coefficient (R^2) > 0.99 and efficiency between 90% and 110% for each reaction.

For all samples C_T values were expected between 8 and 35 since the baseline was set between cycles 3 and 8, therefore C_T values <8 indicated that the reaction was over saturated whereas CT values >35 indicated a very low amount of target in the reaction which produces a higher standard deviation. A Non Template Control (NTC) was added for every run resulted in no detectable signal after 40 cycles of amplification. The Melting curve analysis ensured the amplification of one specific fragment by the presence of a unique peak per reaction and no peaks in the NTC.

Gene expression of genes of interest was determined in comparison to reference gene actin beta (*ACTB*) by the method $2^{-\Delta CT}$ [139]. Statistical differences between samples were determined using T-Test.

2.7.6 Primer design for RT-qPCR

All primers were designed for targeting the mRNA sequence present within 600bp from the 3' polyA tail. They were carefully designed using PrimerBlast design tool (NCBI) and oligoAnalyser tool (Integrated DNA Technologies, US) to avoid dimer formation, secondary structures or unspecific binding with other targets and they were supplied by Sigma (Sigma, UK). All sequences are listed in Table 2.16.

Gene symbol	Sequence	Description
ACTB-F	GAACGGTGAAGGTGACAGCA	Actins are highly conserved proteins that are involved in cell motility, structure, and integrity. This actin is a major constituent of the contractile apparatus.
ACTB-R	CCTCGGCCACATTGTGAACT	
ARNT-F	TGTGTGATCTTGATTGCGGC	This protein is a co-factor for transcriptional regulation by hypoxia-inducible factor 1.
ARNT-R	ATTCCTCTGGTTGTGGGTGC	
ASNS-F	GCTTAGGTGGTCTTTATGCTGTA	The protein encoded by this gene is involved in the synthesis of asparagine. It is involved in the Amino Acid Response (AAR) pathway, triggered by protein and/or amino acid deprivation.
ASNS-R	GCCTGAGTTGACTCTCATTGT	
ATP5F1-F	GCTGAGGTCTTCACAGGTCA	This gene encodes a subunit of mitochondrial ATP synthase. Mitochondrial ATP synthase catalyzes ATP synthesis, utilizing an electrochemical gradient of protons across the inner membrane during oxidative phosphorylation.
ATP5F1-R	GGACAAAGACCCCTCACGAT	
BAX-F	ACAACACAAACAAAGTGC CATT	This protein forms a heterodimer with BCL2, and functions as an apoptotic activator. This protein is reported to interact with, and increase the opening of, the mitochondrial voltage-dependent anion channel (VDAC), which leads to the loss in membrane potential and the release of cytochrome c.
BAX-R	ACCCCCTCAAGACCACTC	
BCL2-F	CATGGTTAAGGTAAA GTA AGTCTC CA	This gene encodes an integral outer mitochondrial membrane protein that blocks the apoptotic death of some cells. Regulates cell death by controlling the mitochondrial membrane permeability.
BCL2-R	ACA ACA CAA ACA AAG TGC CAT T	
BCL2L1-F	TTGTTAAGCGTGTCTGTATTTATGTG	Potent inhibitor of cell death. Inhibits activation of caspases. Appears to regulate cell death by blocking the voltage-dependent anion channel (VDAC) by binding to it and preventing the release of the caspase activator, CYC1, from the mitochondrial membrane.
BCL2L1-R	CATCAGGCCGTCCAATCT	
CBL-F	CTTTCTCCAGAATGAAGAGTCC	This gene is a proto-oncogene that encodes a RING finger E3 ubiquitin ligase. The encoded protein is one of the enzymes required for targeting substrates for degradation by the proteasome.
CBL-R	CAGGTGAGAATGATTAAATACTGC	
CDX2-F	TTCGTTTCGATCTTCCCACCA	The encoded protein is a major regulator of intestine-specific genes involved in cell growth an differentiation. This protein also plays a role in early embryonic development of the intestinal tract.
CDX2-R	TCTGCTCATCTTCCCCAACTG	
COX11: F	ATGTGCATGCAAGTCTCCAGT	Cytochrome c oxidase (COX), the terminal component of the mitochondrial respiratory chain, catalyzes the electron transfer from reduced cytochrome c to oxygen.
COX11: R	GAAGCCTGGAAGACAATACCTGT	
DAP3-F	CCTCTTGTTGCAGGTCAGAAG	This gene encodes a mammalian mitochondrial ribosomal 28S subunit protein that participates in apoptotic pathways which are initiated by tumour necrosis factor-alpha, Fas ligand, and gamma interferon.
DAP3-R	TAAAGCCTCAACAGAACCACTG	
DNMT1-F	GTGCAGTACTTTGTGCATTCTG	This gene encodes an enzyme that transfers methyl groups to cytosine nucleotides of genomic DNA. This protein is the major enzyme responsible for maintaining methylation patterns following DNA replication and shows a preference for hemi-methylated DNA. Methylation of DNA is an important component of mammalian epigenetic gene regulation.
DNMT1-R	CCACTCATACAGTGGTAGATTTGA	

DNMT3A-F	CAAGGATGGAGAAAGGGAGAC	This gene encodes a DNA methyltransferase that is thought to function in de novo methylation, rather than maintenance methylation. The protein localizes to the cytoplasm and nucleus and its expression is developmentally regulated
DNMT3A-R	CTCCTCCTTCACTTCGTTACAA	
DNMT3B-F	GGTGCTCCCTTTGGAGATTT	This gene encodes a DNA methyltransferase which is thought to function in de novo methylation, rather than maintenance methylation. The protein localizes primarily to the nucleus and its expression is developmentally regulated.
DNMT3B-R	GCTTGTCTGAATTCCCGTTCT	
EGFR-F	CACCTCAGGACATGCAGAAATA	The protein encoded by this gene is a transmembrane glycoprotein that is a member of the protein kinase superfamily. It is a cell surface protein that binds to epidermal growth factor, thus inducing receptor dimerization and tyrosine autophosphorylation leading to cell proliferation.
EGFR-R	CTTACAACTGACCTGCCTCATC	
EIF1AX-F	GCAGAATTGTTGGGAGGATTG	This gene encodes an essential eukaryotic translation initiation factor.
EIF1AX-R	AGACATGCACCTTCTATCTTACA	
EIF2S2-F	GGTGATGGGTAAAGCAGTAGAG	Eukaryotic Translation Initiation Factor 2 Subunit Beta is a Protein Coding gene. Among its related pathways are Activation of the mRNA upon binding of the cap-binding complex and eIFs, and subsequent binding to 43S and Nanog in Mammalian ESC Pluripotency.
EIF2S2-R	GCATAAACAGCAGTTGGGTTC	
EOMES-F	GTCTACATAGGTGTCTGGGATAATG	Functions as a transcriptional activator playing a crucial role during development. Functions in trophoblast differentiation and later in gastrulation, regulating both mesoderm delamination and endoderm specification. Plays a role in brain development being required for the specification and the proliferation of the intermediate progenitor cells and their progeny in the cerebral cortex.
EOMES-R	CCTGCAGCTGTTAAGTGATTTG	
EP300-F	AGAGGGTAAGAAACGATTCCG	It functions as histone acetyltransferase that regulates transcription via chromatin remodeling and is important in the processes of cell proliferation and differentiation.
EP300-R	GGAGGAAGAAAGCAAGCAAAG	
FGF4-F	TTCGAGGTTCCTGTATGTGC	Member of the fibroblast growth factor (FGF) family. Plays an important role in the regulation of embryonic development, cell proliferation, and cell differentiation.
FGF4-R	ATTGTCGGTCAGCATGTCAA	
GAPDH-F	CAAGCTCATTTCCTGGTATGACA	The product of this gene catalyzes an important energy-yielding step in carbohydrate metabolism, the reversible oxidative phosphorylation of glyceraldehyde-3-phosphate in the presence of inorganic phosphate and nicotinamide adenine dinucleotide (NAD).
GAPDH-R	GGGTCTTACTCCTTGGAGGC	
GPX2-F	GCACCTTCCCAACCATCAAC	The protein encoded by this gene belongs to the glutathione peroxidase family, members of which catalyze the reduction of organic hydroperoxides and hydrogen peroxide (H2O2) by glutathione, and thereby protect cells against oxidative damage.
GPX2-R	AAGGCTCCTCAGGACTGGAT	
HIF1A-F	ATAGTCACTTTGCCAGCTCAAAA	This gene encodes the alpha subunit of transcription factor hypoxia-inducible factor-1 (HIF-1), which is a heterodimer composed of an alpha and a beta subunit. HIF-1 functions as a master regulator of cellular and systemic homeostatic response to hypoxia by activating transcription of many genes, including those involved in energy metabolism, angiogenesis, apoptosis, and other genes whose protein products increase oxygen delivery or facilitate metabolic adaptation to hypoxia. HIF-1 thus plays an essential role in embryonic vascularization, tumor angiogenesis and pathophysiology of ischemic disease.
HIF1A-R	TATACCAACAGGGTAGGCAGAA	
HIF2A-F	ATAGTCACTTTGCCAGCTCAAAA	This gene encodes a transcription factor involved in the induction of genes regulated by oxygen, which is induced as oxygen levels fall. The encoded protein contains a basic-helix-loop-helix domain protein dimerization domain as well as a domain found in proteins in signal transduction pathways which respond to oxygen levels.
HIF2A-R	TATACCAACAGGGTAGGCAGAA	
MAT2A-F	TGTTGCCCTGGCATTAAGGG	Catalyzes the formation of S-adenosylmethionine from methionine and ATP. The reaction comprises two steps that are both catalyzed by the same enzyme: formation of S-adenosylmethionine (AdoMet) and triphosphate, and subsequent hydrolysis of the triphosphate.
MAT2A-R	TCGTTACGTTGACAGGTAGGG	
MTOR-F	AGCAGGGTTCTGGGATGTTT	

MTOR-F	TTCAGCACCTCCATGACAGT	The protein encoded by this gene belongs to a family of phosphatidylinositol kinase-related kinases. These kinases mediate cellular responses to stresses such as DNA damage and nutrient deprivation.
NANOG-F	CGTATTTGCTGCATCGTAATG	DNA binding homeobox transcription factor involved in embryonic stem (ES) cell proliferation, renewal, and pluripotency. The encoded protein can block ES cell differentiation and can also autorepress its own expression in differentiating cells.
NANOG-R	CTCGGTGAAATCAGGGTAAA	
OCT4-F	GTTTGTGCCAGGGTTTTTGG	This gene encodes a transcription factor containing a POU homeodomain that plays a key role in embryonic development and stem cell pluripotency.
OCT4-R	TGAACTTCACCTTCCCTCCA	
PPARA-F	CAGGCTTCGCAAACTTGGAC	Ligand-activated transcription factor. Key regulator of lipid metabolism.
PPARA-R	GCTACCAGCATCCCGTCTTT	
PPARG-F	TATTCTCAGTGGAGACCGCC	Nuclear receptor that binds peroxisome proliferators such as hypolipidemic drugs and fatty acids.
PPARG-R	AGGGCTTGTAGCAGGTTGTC	
SDHB-F	GGAAGGCAAGCAGCAGTATC	Complex II of the respiratory chain, which is specifically involved in the oxidation of succinate, carries electrons from FADH to CoQ. The complex is composed of four nuclear-encoded subunits and is localized in the mitochondrial inner membrane.
SDHB-R	AGAATGCACTCGTAGAGCCC	
SLC2A1-F	ACTTCATCTGCTCCTTCATCAC	Facilitative glucose transporter, which is responsible for constitutive or basal glucose uptake
SLC2A1-R	GGACCCACAGGAACCAAAT	
SLC2A3-F	TGCAACTTCATGTCAACTTCTGG	Facilitative glucose transporter that can also mediate the uptake of various other monosaccharides across the cell membrane
SLC2A3-R	TCAGTGAGAAATGGGACCCTG	
SLC7A3-F	CGATTTGGGGTCTGGATGCT	Transport of glucose and other sugars, bile salts and organic acids, metal ions and amine compounds and Amino acid transport across the plasma membrane.
SLC7A3-R	TTGCGTGAGGGTTGGTTACT	
SLC16A1-F	ACTGAGAGCATCCAGAGCAG	The protein encoded by this gene is a proton-linked monocarboxylate transporter that catalyzes the movement of many monocarboxylates, such as lactate and pyruvate, across the plasma membrane.
SLC16A1-R	GCCAAGCCTGCCAATACTCT	
SOD1-F	GATGACTTGGGCAAAGGTGG	The protein encoded by this gene binds copper and zinc ions and is one of two isozymes responsible for destroying free superoxide radicals in the body.
SOD1-R	CACAAGCCAAACGACTTCCA	

SOD2-F	ACCCTATAAGGTCCTGGATAAT	It encodes a mitochondrial protein that binds to the superoxide byproducts of oxidative phosphorylation and converts them to hydrogen peroxide and diatomic oxygen. Destroys superoxide anion radicals which are normally produced within the cells and which are toxic to biological systems.
SOD2-R	CCTCTTTGATGGTTGACAGAT	
SOD3-F	AGACCCACCATCCTTCCATC	This gene encodes a member of the superoxide dismutase (SOD) protein family. SODs are antioxidant enzymes that catalyze the conversion of superoxide radicals into hydrogen peroxide and oxygen, which may protect the brain, lungs, and other tissues from oxidative stress.
SOD3-R	CGGGGTGTTTCGGTACAAAT	
SOX2-F	GAACCATCTCTGTGGTCTTG	This intronless gene encodes a member of the SRY-related HMG-box (SOX) family of transcription factors involved in the regulation of embryonic development and in the determination of cell fate.
SOX2-R	ATTACCAACGGTGTCAACC	
TET1-F	CATCCCATTCTCTGCCCTGTG	Dioxygenase that catalyzes the conversion of the modified genomic base 5-methylcytosine (5mC) into 5-hydroxymethylcytosine (5hmC) and plays a key role in active DNA demethylation. Also mediates subsequent conversion of 5hmC into 5-formylcytosine (5fC), and conversion of 5fC to 5-carboxylcytosine (5caC).
TET1-R	TCTAAAAGCAGTGTAGCCAGC	
TET2-F	ATGCTTCTGAGTGGTGTCAACT	Dioxygenase that catalyzes the conversion of the modified genomic base 5-methylcytosine (5mC) into 5-hydroxymethylcytosine (5hmC) and plays a key role in active DNA demethylation. Has a preference for 5-hydroxymethylcytosine in CpG motifs.
TET2-R	ACTGTACATCACTGTGCGTCA	
TET3-F	GGCTTCCAATGGAGGTGAACT	Dioxygenase that catalyzes the conversion of the modified genomic base 5-methylcytosine (5mC) into 5-hydroxymethylcytosine (5hmC) and plays a key role in epigenetic chromatin reprogramming in the zygote following fertilization
TET3-R	ACCATTCATCCATCAACCCCAG	
TFAM: F	CCACCAGGTTGTGCTAAAACAG	Binds to the mitochondrial light strand promoter and functions in mitochondrial transcription regulation. Component of the mitochondrial transcription initiation complex, composed at least of TFB2M, TFAM and POLRMT that is required for basal transcription of mitochondrial DNA
TFAM: R	GGAGAATGGCTGTGAGTGGA	
TIMM23-F	GGTGGTCTGACAGGACTAACA	The protein encoded by this gene is part of a complex located in the inner mitochondrial membrane that mediates the transport of transit peptide-containing proteins across the membrane.
TIMM23-R	GAGTGACTGTTGGAGCAAGG	
TP53 -F	AAA AGG AAA TCT CAC CCC ATC	This gene encodes a tumor suppressor protein containing transcriptional activation, DNA binding, and oligomerization domains. The encoded protein responds to diverse cellular stresses to regulate expression of target genes, thereby inducing cell cycle arrest, apoptosis, senescence, DNA repair, or changes in metabolism.
TP53-R	AGT CTT GGT GGA TCC AGA TCA	
TRIM28-F	GAA GTT GTC ACC TCC CTA CAG	Required to maintain a transcriptionally repressive state of genes in undifferentiated embryonic stem cells
TRIM28-R	GTCTGCCTTGTCCTCAGTTA	
TRMT10C-F	GAGGCTCTGCAATTCGTTCC	This gene encodes the precursor of a subunit of the mitochondrial ribonuclease P, which is involved in 5' processing of mitochondrial tRNAs. The encoded protein may confer RNA-binding capacity to mitochondrial ribonuclease P and may be essential for transcript processing, RNA modification, translation and mitochondrial respiration.
TRMT10C-R	AGTCTTTGCCTTCTTTAGTCTGTT	
ZSCAN4-F	GAG AGA ATC CAC ACA GGA GAA A	The ZSCAN4 gene encodes a protein involved in telomere maintenance and with a key role in the critical feature of mouse embryonic stem (ES) cells, namely, defying cellular senescence and maintaining normal karyotype for many cell divisions in culture
ZSCAN4-R	CTCATATGGCGGTGGTATGT	

Table 2.16 Primers sequences used for gene expression analysis (https://www.ncbi.nlm.nih.gov).

2.8 Mitochondrial membrane potential

Mitochondrial membrane potential (Δψm) was evaluated by staining HESCs or human blastocysts with the MitoProbe™ JC-1 (5',6,6'-tetrachloro-1,1',3,3'-tetraethylbenzimidazolylcarbocyanine iodide, Thermofisher) cationic dye. JC-1 fluorescence is excited at 590nm and detected at 514/529nm therefore it can be detected through flow cytometry and fluorescence microscopy.

The efficiency of the JC-1 probe was verified for every experiment using a depolarized control that was used as reference and as baseline. This control was prepared with 1 x 10^5 cells/mL (Man 7 or Man 13) or a single blastocyst incubated in culture medium with 50µM Carbonyl cyanide m-chlorophenylhydrazone (CCCP) and 2µM JC-1. The protonphore CCCP is a widely used uncoupler of mitochondrial oxidative phosphorylation and reduces Δψm to 0 due to proton gradient disruption.

2.8.1 Mitochondrial membrane potential in hESCs

Cells were harvested by adding 0.5 mL TrypLE™ Express Enzyme 1X (Gibco) and incubating 2 min at 37°C, 5% oxygen. Cells were the washed with 2 ml TeSR™-E8™ medium to inactivate trypsin, they were centrifuged for 5 min at 400*g* and media was discarded. Subsequently, the cell pellet was suspended and incubated 30min at 37°C, 5% oxygen in TeSR™-E8™ medium with 2µM JC-1 and 0.01 µg/mL TRA-1-81/ APC (eBioscience, 17-8883-42). After incubation, cells were washed twice with 1X PBS and were taken to the flow cytometer protected from light. DAPI (4,6-diamindino-2-phenylindole) Solution (Thermo Scientific) was added prior cytometer injection at 1 µg/mL. Cell viability was evaluated through DAPI staining (355 450/50), pluripotency through TRA-1-81 staining (640 670/30) and mitochondrial membrane potential through JC-1 staining (488 530/30 vs 488 575/26).

2.8.2 Mitochondrial membrane potential in human blastocysts

Blastocysts were incubated for 30min at 37°C, 5% oxygen in GTL medium (Vitrolife, Sweden) with 2µM JC-1 for further analysis in the fluorescence microscope. They were washed two times after incubation to remove JC-1 excess and stained with 1 µg/mL DAPI solution (Thermo Scientific). Samples were then protected from light and transferred to the fluorescence microscope were DAPI, FITC and TRITC filters were employed. Cell images were subsequently collected using a Retiga-SRV Fast 13394 camera (Olimpus IX71, Japan) and processed using the Q-Capture Pro image software 6.0.

2.9 Mitochondrial respiration

Cellular Metabolic Analyser Seahorse XFe96 (Agilent Technologies) was used to evaluate mitochondrial respiration in HESCs that were cultured in different concentrations of oxygen (5% or 20%) or glucose (5mM or 17.5mM). The Seahorse XF Cell Mito Stress Test Kit (Agilent Technologies, 103015-100) was used to determine changes in mitochondrial and glycolytic activity by measuring the oxygen consumption rate (OCR) and the extracellular acidification rate (ECAR) in real time. This metabolic analyser works at a physiological temperature 37°C and contains highly sensitive optic probes that sit in a cartridge sleeve placed just above the cellular monolayer creating a chamber where the measurements take place. A set of drugs was is loaded into the cartridge ports and they were injected at a defined (FIGURE X) time to perform the OCA and ECAR measurements.

2.9.1 Cell lines seeding, cartridge preparation and measurement.

HESCs were first optimized for the optimal cell density between 10K-100K cells in the Seahorse 96-well cell culture plate (Agilent Technologies). Cells were plated into 84/96 wells in a 96-well plate, leaving 12 wells free of cells but with medium to correct for background noise. HESCs were passaged and plated as previously described in section 5.2.4 with fresh TeSR E8 medium (5mM or 17.5mM glucose). Cells were plated by

calculating the desired cell count per well and then adding 100 µL of suspended cells to each well. HESCs were incubated for 12 hours at 20% or 5% oxygen and then medium was replaced in each well with fresh E8 medium Vitronectin-free. Cells then were incubated for up to six days.

2.9.2 Cartridge preparation and measurement.

On the day prior to assay, 250 µL of distillate sterile water were added to each well of the XFe96 sensor cartridges(Agilent Technologies, 102416-100) for probes/sensor hydration.

One hour prior to assay, water was replaced for 250 µL of Calibrant Solution (Agilent Technologies, 102340-100) and XFe96 sensor cartridge was incubated for 1 hour / 37°C in a non-gassed incubator. Seahorse XF base medium (Agilent Technologies, 102353-100) was freshly supplemented with 2.5mM L-glutamine, 0.5mM sodium pyruvate and D-glucose 17.5mM or 5mM and warmed up at 37°C in a non-gassed incubator. During this time, the XF Cell Mito Stress drugs were prepared using the supplemented Seahorse XF medium and subsequently added to the cartridge as indicated in Table 2.17. The loaded XFe96 sensor cartridge was placed into the Seahorse XFe96 Analyzer to calibrate background noise and to verify that both OCR and ECAR optic probes were working properly.

After 12 or 144 hours of incubation, cells were rinsed twice with supplemented Seahorse XF medium. Then they were kept in 180µL of fresh supplemented Seahorse XF medium. Subsequently the cell culture plate was incubated in a non-gassed incubator for maximum 15 min / 37°C while the Seahorse XFe96 was calibrated.

Port designation	10X [Port] (µM)	[Final Well] (µM)	Add to port volume (µL)
Port A Oligomycin	10 µM	1 µM	20 µL
Port B FCCP	10 µM	1 µM	22 µL
Port C Rot/AA	5 µM	0.5 µM	25 µL

Table 2.17. Compound preparation for loading to XFe96 sensor cartridges. Starting assay medium volume for cell plate is 180 µL per well.

After calibration, the XF96 cell culture microplate was placed into the Seahorse XFe96 Analyzer for the completion of the OCR and ECAR measurements using the pre-loaded Mito Stress Test protocol (Figure 2.6). The Seahorse measured the effect of each drug in 3 cycles. Each cycle included a waiting period, drug injection, mixing and 10 measures of OCR and ECAR. Following the basal reading, Oligomycin was the first compound injected into the well from port A followed by FCCP (port B) and finally Rotenone/Antimycin A (port C).

Once the Mito stress test was completed, cells were immediately removed from the Seahorse analyser and washed carefully with XF medium. Cells were then incubated 30min at 37°C with 10% PrestoBlue™ Cell Viability Reagent (Thermofisher, A13261) for cell counting as this data was required for further normalization.

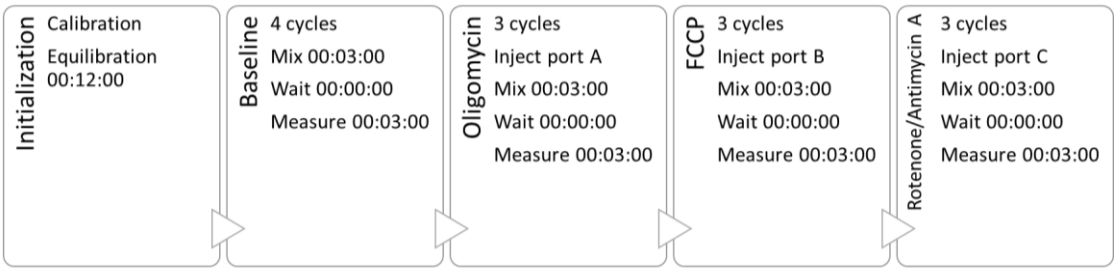

Figure 2.6. Mito Stress test measurement protocol. The protocol includes an initial calibration/equilibration, basal respiration (baseline) and three serial injections of test compounds (oligomycin, FCCP, and rotenone/antimycin A). The instrument performs ten readings per cycle (10 reads / 3 min) for each step so final data are expressed as means ± SEM.

2.9.3 Blastocyst seeding cartridge preparation and measurement

Seahorse XFp Cell Culture Miniplates (Agilent technologies, 103721-100) were coated with 20 µL of 100 µg/mL Poly-D-lysine (Sigma, UK) and incubated for 3 hours at RT or overnight at 4 °C . They were then carefully rinsed with sterile PBS (Sigma, UK) prior blastocysts seeding. XFp sensor cartridges (Agilent technologies, 103721-100) were hydrated overnight prior to assay 250 µL of distillate sterile water to each well. One hour prior assay, water was replaced for 250 µL of Calibrant Solution (Agilent Technologies, 102340-100) and XFp sensor cartridge was incubated for 1 hour / 37°C in a non-gassed incubator.During this time, the XF Cell Mito Stress drugs were prepared using the supplemented Seahorse XF medium and subsequently added to the cartridge as indicated in Table 2.17. The loaded XFp sensor cartridge was placed into the ahorse XF HS Mini Analyzer for background noise calibration.

Donated fresh blastocyst at day 6 were graded and transferred to a coated XFp miniplate with 180 µL of supplemented Seahorse XF medium and kept for maximum 15 min / 37°C in a non-gassed incubator while the Seahorse XF HS Mini Analyzer was calibrated. Seahorse XF base medium (Agilent Technologies, 102353-100) was supplemented with 10 µM XF Glutamine Solution (Agilent Technologies 103579-100), 0.55 mM XF Pyruvate Solution (Agilent Technologies 103578-100) and XF Glucose Solution 1 mM (Agilent Technologies 103577-100).

CHAPTER 3

Effect of glucose concentration and oxygen on human preimplantation embryos

3.1 Introduction

Early embryos should benefit from being cultured under conditions which prevent stress or the formation of harmful molecules such as reactive oxidative species (ROS), as the embryo is unable to respond to environmental stress [96], [97]. Historically, atmospheric oxygen (20 %) has been used in IVF laboratories for embryo culture. However, the physiological concentration of oxygen within the female reproductive tract has been reported to be below 10 % in mammals. Currently most of IVF clinics worldwide have improved embryo culture by reducing oxygen levels similar to that in the oviduct (5% oxygen) but there are still clinics that conduct embryo culture in atmospheric conditions (20% oxygen) [3], [94], [95]. Most of the evidence indicates that atmospheric oxygen has a significant negative impact on blastocyst gene expression, the embryonic proteome and embryo metabolism, affecting the utilisation of both carbohydrates and amino acids [16]. In addition, culture media formulation can have a significant impact in the embryo survival or other embryonic mechanisms that might be relevant for the future health of the offspring [98].

Epigenetic marks may serve to predict predisposition to certain diseases in adult life. Therefore, it is important to establish the normal patterns and to identify aberrant patterns [41]. Preimplantation embryos experience profound resetting of epigenetic marks, which are very susceptible to environmental conditions [102]. Although DNA methylation mechanisms have been investigated for years, the effect of ART on preimplantation development has not been fully understood. Nevertheless, several studies now coincide that ART might impair DNA methylation reprogramming. Recently, the investigation of the effect of culture media, ovarian stimulation or embryo transfer on the epigenetic mechanisms has been emphasised in order to search for strategies to mitigate adverse effects on the health of ART-derived children [101]. DNA methylation is a key epigenetic regulator of embryogenesis and stem cell differentiation

in mammals, critically involved in cell-type-specific transcriptional regulation. It occurs at cytosines, therefore it is predominantly restricted to CpG dinucleotides and stably distributed across the genome [111]. The establishment of the correct epigenetic state during preimplantation development may be crucial to avoid immediate or future alterations in the offspring's health as DNA methylation is involved in processes that includes regulating gene expression, establishing imprinting patterns, maintaining genome stability and inactivating one X chromosome, among others [112] [38].

3.2 Study design

This project was accomplished using fresh and frozen human embryos (from PN to day 6 stage) donated by couples undergoing IVF treatment at St Mary's Hospital. All embryos were graded by a qualified Clinical Embryologist following the Alpha/ESHRE 2011 guidelines [71].

Evaluation of gene expression was completed for human embryos that were cultured in GTL medium (Vitrolife) either at 0.9 mM or 3.5 mM glucose and under 20% or 5% oxygen. These embryos were cultured until blastocyst-stage and the processed through the PolyA-PCR protocol (section 2.2). This analysis contributed to the investigation of the effects of oxygen and glucose concentration on preimplantation embryos. This evaluation included markers of apoptosis, pluripotency, metabolism, mitochondrial activity, hypoxia, oxidative stress, methylation, among others. Gene list fully described in Table 2.16. Gene expression analysis was assessed by the comparative CT method for quantitative real-time PCR data (Section 2.9), also known as the $2^{-\Delta\Delta CT}$ method [140].

Mitochondrial function was evaluated through the comparative analysis of mitochondrial membrane potential ($\Delta\Psi m$) and mitochondrial respiration (Methods described in sections 2.10 and 2.11Z). Mitochondrial membrane potential analyses were carried out using human embryos that were cultured in GTL medium (Vitrolife) at 0.9 mM in 5% oxygen. This analysis allowed determination of the allocation of mitochondria and therefore the relative energetic level of the cell populations in the blastocyst. Embryos were graded at day 6 and stained with JC-1 probe according to

section 2.10.2. Moreover, mitochondrial respiration analysis was only performed as a pilot study to evaluate the sensitivity of the technology Mito Stress test (Seahorse, Agilent). Fourteen fresh blastocysts (day 6 stage) in separated runs. All blastocysts were fresh and were cultured in GTL medium (Vitrolife) at 0.9 mM glucose and 5% oxygen according to Section 2.11.

Finally, DNA methylation analysis was performed to evaluate only the effect of glucose concentration on the embryo epigenome. Two groups of embryos grown in GTL medium (Vitrolife) at glucose concentration of 0.9 mM (Low glucose) or 3.5 mM (High glucose) were evaluated (briefly explained in Figure 3.14 and detailed in Section 2.5). Four groups of samples were evaluated in total as embryos were dissected into ICM and TE for a more comprehensive analysis.

3.3 Effect of glucose and oxygen on blastocyst's gene expression.

Using the PolyA-PCR method [136], the expression of 48 genes (Table 2.16) was examined in human preimplantation embryos These included markers for: Cell survival (*BAX, BCL2, BCL2L1, CBL, DAP3, TP53*); Cell growth and differentiation (*CDX2, EGFR*, *EOMES, EP300, FGF4, ZSCAN4*); Pluripotency (*NANOG*, *OCT4*, *SOX2*); Transcription factors (*EIF1AX, EIF2S2, TRIM28);* DNA methylation (*DNMT1*, *DNMT3A*, *DNMT3B*, *TET1*, *TET2*, *TET3*, MAT2A); Mitochondrial activity (ATP5F1, COX11, SDHB, TFAM *TIMM23*, *TRMT10C*); Metabolism (*SLC2A1*, *SLC2A3*, *SLC7A3*, SLC16A1, GAPDH, ASNS, MTOR, PPARA, PPARG); Oxidative stress (SOD1, SOD2, SOD3, GPX2) and Hypoxia (HIF1A, HIF2A, ARNT).

Significant differences were only found for *SLC2A1*, EOMES due to oxygen concentration, whereas *OCT4*, *SOX2*, *TIMM23*, *DNMT3A*, *SLC7A3*, *TET1* and *TET2* shown significant differences due to glucose concentration. Unpaired t-test and Mann-Whitney test were applied to determine statistical significances for every gene on each condition. Data are presented as the mean ± SD. Overall, blastocysts have shown high heterogeneity for the majority of the transcripts independently of their quality grade and the oxygen concentration used in culture. Nevertheless, some genes evaluated shown significant differences between experimental conditions.

3.4 Effect of oxygen concentration on blastocysts' gene expression.

Two groups of embryos (Table 3.1) were culture in r GTL medium (0.9 mM) at either physiological (5%) or atmospheric oxygen (20%). Detailed results areshown in Figure 3.1.

The expression of the maintenance methylase *DNMT1* and the de novo methylases *DNMT3A* and *DNMT3B* did not show any significant differences between the physiological and atmospheric oxygen groups. However, *DNMT1* and *DNMT3A* tend to be upregulated in 20% oxygen. The demethylase *TET3* did not show any significant differences between the two oxygen groups.

The expression of glucose transporter 3 (*SLC2A3*) was not significantly different between the two oxygen groups, although there is a clear tendency for this marker to be upregulated in 5% oxygen. On the other hand, glucose transporter 1 (*SLC2A1*) was significantly upregulated at physiological oxygen (5%). The mitochondrial markers, TRCT10C and *TIMM23* did not show significant differences between the two oxygen groups.

Finally, the transcription factor POU5F1 (*OCT4*), also did not show significant differences in expression but it tends to be upregulated in 20% oxygen. Whereas, the transcription factor EOMES, was significantly upregulated in the atmospheric oxygen group (20%). The rest of transcripts mentioned in this section were analysed through the same method but they did not show differences between the two groups (data not shown).

#	Research code	Stage	Grade	Oxygen
1	281	Day 6	4CB	5%
2	282	Day 7	4DC	5%
3	295	Day 8	4DD	5%
4	296	Day 9	4DC	5%
5	301	Day 10	5DC	5%
6	303	Day 11	5CB	5%
7	304	Day 12	5BC	5%
8	305	Day 13	4BC	5%
9	327	Day 14	4CC	5%
10	328	Day 15	5DB	5%
11	329	Day 16	GCD	5%
12	330	Day 17	5DD	5%
13	331	Day 18	3DD	5%
14	332	Day 19	5BA	5%
15	333	Day 20	5CC	5%
16	334	Day 21	4CD	5%
17	335	Day 22	5DD	5%
18	336	Day 23	5CC	5%
19	337	Day 24	2BC	5%
20	338	Day 25	3DC	5%
21	339	Day 26	5CC	5%
22	340	Day 27	5CB	5%
23	341	Day 28	5CC	5%
24	342	Day 29	3CC	5%
25	343	Day 30	5CC	5%
26	344	Day 31	4CB	5%
27	345	Day 32	4CC	5%
28	346	Day 33	5DC	5%
29	347	Day 34	4DD	5%
30	348	Day 35	4DC	5%
31	WOK-001	Day 36	3BB	20%
32	WOK-005	Day 37	4BB	20%
33	WOK-006	Day 38	5BC	20%
34	WOK-009	Day 39	5BB	20%
35	WOK-022	Day 40	3BB	20%
36	WOK-023	Day 41	3CB	20%
37	WOK-024	Day 42	3BB	20%
38	WOK-025	Day 43	4BB	20%
39	WOK-032	Day 44	3CB	20%
40	WOK-033	Day 45	4BB	20%
41	WOK-034	Day 46	5AB	20%
42	LWH11-176	Day 47	3DC	20%
43	LWH11-184	Day 48	5BB	20%
44	Liv-001	Day 49	4CC	20%
45	Liv-077	Day 50	5BB	20%

Table 3.1. List of embryos used to evaluate the effects of oxygen on gene expression. Only high-grade blastocysts were selected for this comparison to reduce heterogeneity due to sample quality. All embryos were cultured in GTL medium at 0.9mM glucose until day 6.

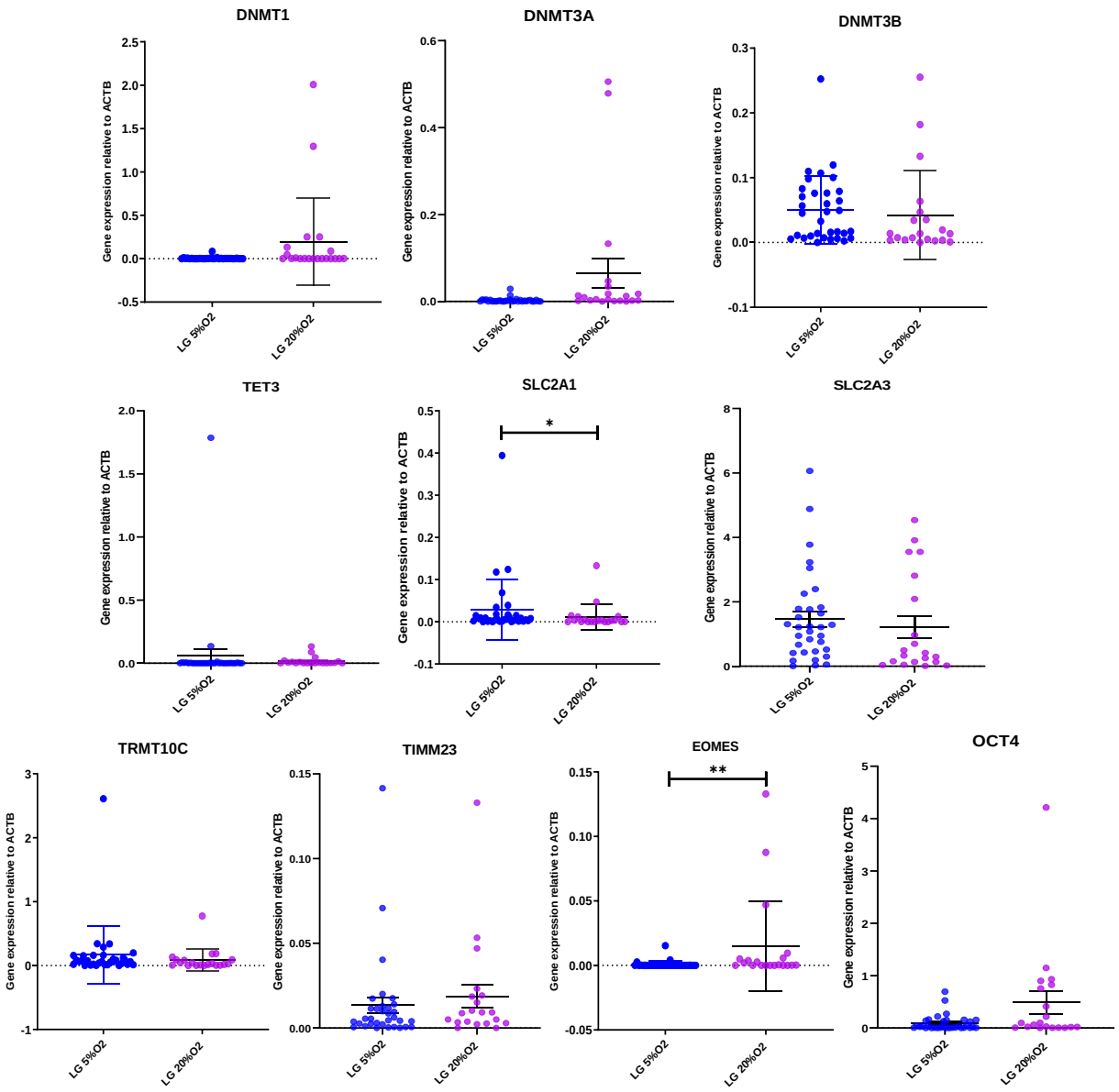

Figure 3.1. Effect of oxygen concentration on embryos gene expression. Analysis of gene expression ($2^{-\Delta CT}$) relative to Beta- actin (*ACTB) was performed on* day-6 blastocysts. Dot plots represent gene expression levels of Glucose transporter 3 (*SLC2A3),* Tet Methylcytosine Dioxygenase 3*(TET3),* DNA methyltransferase 1 *(DNMT1)*, DNA methyltransferase 3-alpha *(DNMT3A)* DNA methyltransferase 3-beta *(DNMT3B),* Mitochondrial RNase P Protein 1 *(TRMT10C),* Translocase of Inner Mitochondrial Membrane *(TIMM23)* and POU Domain Class 5 Transcription Factor (*OCT4).* The analyses were performed in single embryos cultured in 0.9mM glucose (GTL medium, Vitrolife) at 20% or 5% oxygen. Blue dots represent single embryos cultured at 5% oxygen (n=33); Purple dots represent single embryos cultured at 20% oxygen (n=20). The data plots show the mean relative expression and error bars represent standard deviation (SD). Three technical replicates were run per sample. Significance *(p<0.05), ** (p<0.01).

3.4.1 Effect of glucose concentration on blastocysts' gene expression.

This study was conducted to investigate the effects of glucose concentration on preimplantation embryos at transcriptomic levels.

Human embryos were cultured for up to six days in low or high glucose concentrations (0.9mM or 3.5mM) from PN to Blastocyst-stage (Table 3.2). At day 6, they were analysed to evaluate gene expression through the PolyA-PCR method (Section 2.2).

#	Research code	Stage	Grade	Glucose
1	281	Day 6	4CB	0.9 mM
2	282	Day 6	4DC	0.9 mM
3	295	Day 6	4DD	0.9 mM
4	296	Day 6	4DC	0.9 mM
5	301	Day 6	5DC	0.9 mM
6	303	Day 6	5CB	0.9 mM
7	304	Day 6	5BC	0.9 mM
8	305	Day 6	4BC	0.9 mM
9	327	Day 6	4CC	0.9 mM
10	SAL-7	Day 6	4BC	**3.5 mM**
11	SM-001	Day 6	4BA	**3.5 mM**
12	MID/14-19	Day 6	4BB	**3.5 mM**
13	MID/14-20	Day 6	5BA	**3.5 mM**
14	MID/14-22	Day 6	4CB	**3.5 mM**
15	MID/14-26	Day 6	5BC	**3.5 mM**
16	MID/15-08	Day 6	4BB	**3.5 mM**
17	MID/15-10	Day 6	5AB	**3.5 mM**
18	MID/15-11	Day 6	4BA	**3.5 mM**

Table 3.2. List of embryos used to evaluate the effects of glucose on gene expression. Eighteen embryos divided in two groups were analysed to evaluate the effects of glucose on gene expression. Only high-grade blastocysts were selected for this comparison to reduce heterogeneity due to sample quality. Embryos 1-7 were maintained in 0.9mM glucose medium whereas embryos 8-16 were maintained in 3.5 mM glucose.

Key pluripotency-associated transcription factors POU5F1 (*OCT4*) and *SOX2* showed differential expression when comparing between the high and low glucose groups (Figure 3.2). Both markers were significantly downregulated at low glucose (0.9mM) relative to the high glucose group (3.5 mM). These results suggest that high glucose concentration supports the expression of pluripotency markers, in this case, transcription factors.

Mitochondrial RNase P (TRCT10C) did not show a significant difference between the two groups whereas the mitochondrial importer (*TIMM23*) showed significantly higher expression in the high glucose group (3.5mM).

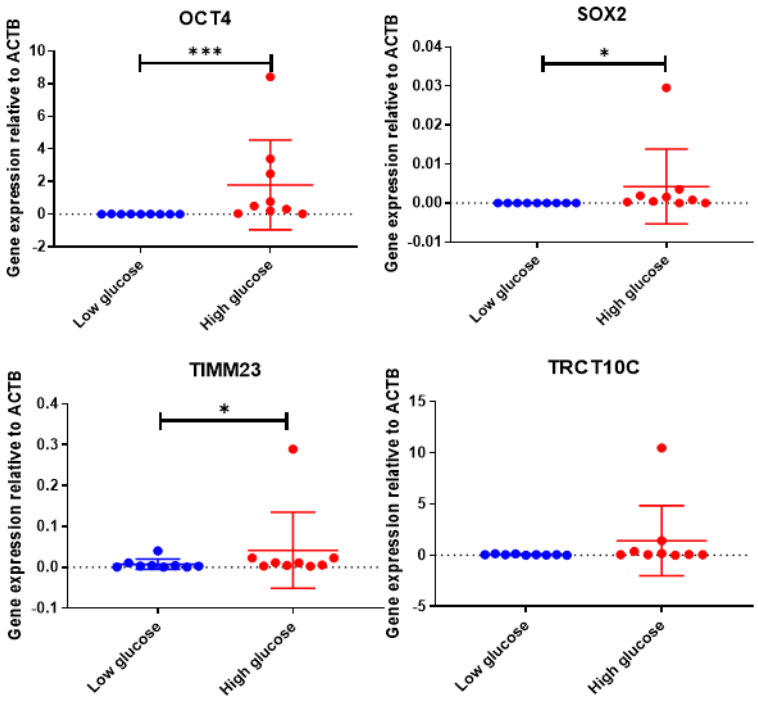

Figure 3.2. Effect of glucose concentration on blastocysts gene expression 1. Expression of pluripotency-associated genes (*OCT4, SOX2*), mitochondrial importer (*TIMM23*) and mitochondrial RNase P (*TRMT10C*) in human embryos undergoing 6-day culture at 5% oxygen in 0.9 mM glucose (Low glucose) or 3.5 mM glucose (High glucose). The data plots show the mean expression and error bars represent standard deviation (mean ±SD) of three technical replicates per sample. Significance *($p<0.05$).

DNA methyltransferase showed different response in expression (Figure 3.3). The maintenance methyltransferase *DNMT1* and the de novo methyltransferase *DNMT3B*, DNMT3L did not show any significant differences between groups. On the other hand, the de novo methyltransferase *DNMT3A* that plays an essential role in paternal and maternal imprinting showed higher expression in the high glucose group. Increased activity of de novo methyltransferases are associated with a hypermethylated promoter phenotype.

Demethylases *TET1* and *TET2* also showed increased expression in high glucose, whereas *TET3* did not show any significant difference.

Glucose transporters *SLC2A1* and *SLC2A3* were not differentially expressed but amino acid transporter *SLC7A3* was significantly upregulated in high glucose.

Moreover, the transcription factors ZSCAN4, EIF2S2 and EOMES did not show significant differences between the high and low glucose groups (data not shown).

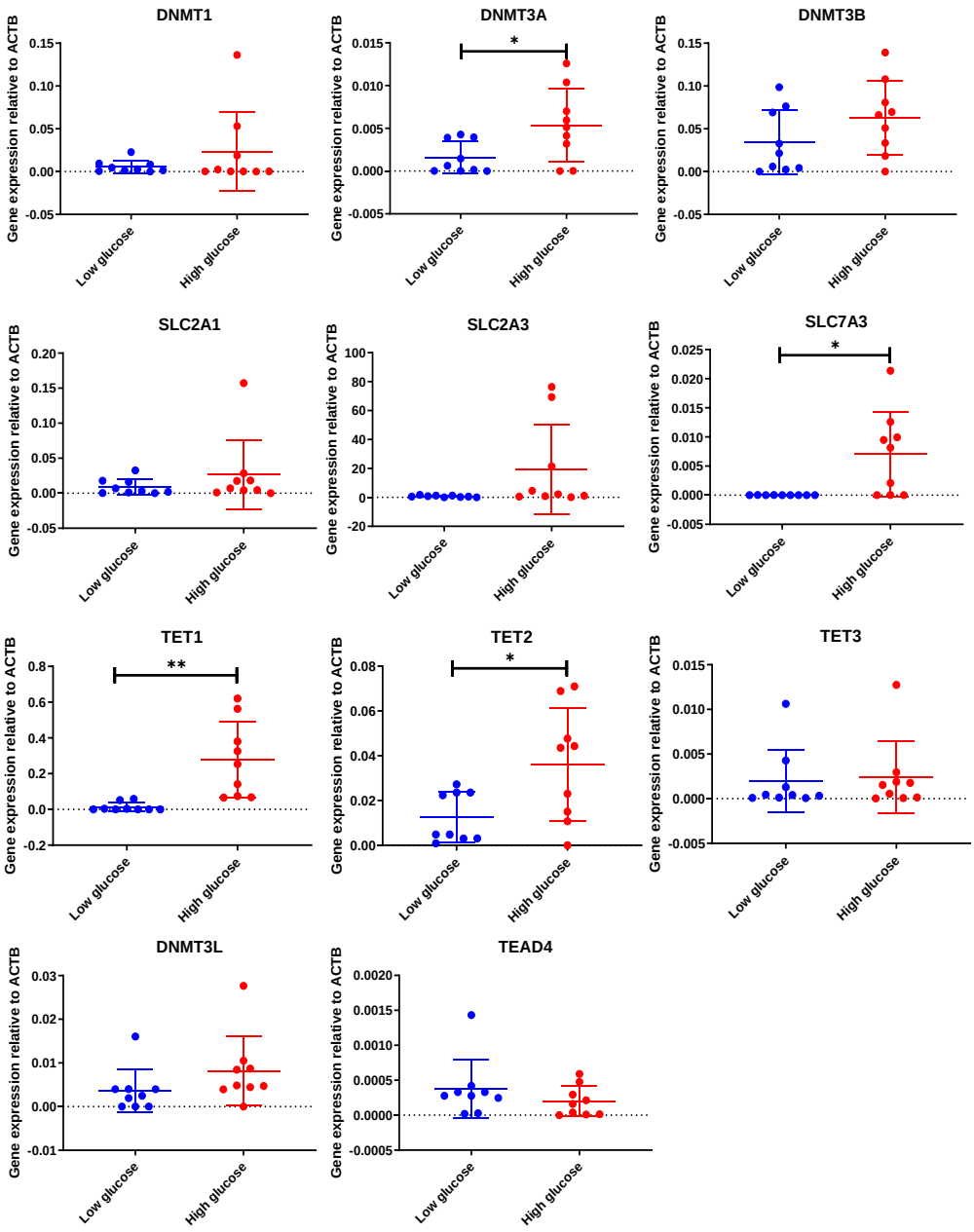

Figure 3.3. Effect of glucose concentration on blastocysts gene expression 2. Gene expression of glucose transporters (*SLC2A1, SLC2A3*), amino acids transporter (*SLC7A3*), DNA demethylases (*TET1, TET2, TET3*), DNA methyl-transferase genes (*DNMT1, DNMT3A, DNMT3B, DNMT3L*) in human embryos undergoing 6-day in culture at 5% oxygen in 0.9 mM glucose (Low glucose) or 3.5 mM glucose (High glucose). Gene expression was normalized to Actin-beta gene (*ACTB)*. The error bars represent standard deviation (SD) (n=3 separate experiments per sample). Data were analysed by unpaired t test and Mann-Whitney test for comparison between the Low glucose and High glucose groups. * $p< 0.05$, ** $p< 0.01$, ***$p<0.001$

3.5 Effect of cryopreservation on mitochondria membrane potential.

Mitochondria depolarization can be used as an indicator of low metabolic activity or mitochondrial dysfunction, whereas mitochondria polarization is an indicator of a healthy mitochondria. As mentioned in section 1.4.3, cryopreservation methods are widely used in assisted reproduction. However, they can have a detrimental impact on the embryo. Mitochondria depolarization was determined by the cationic JC-1 dye, which exhibits potential-dependent accumulation in the mitochondria, resulting in a fluorescence emission shift from red to green as the mitochondrial membrane loses its potential due to damage (Figure 3.4). This analysis contributed to determine the allocation of embryonic mitochondria and to estimate the mitochondrial energy state that could be correlated to the metabolic state.

3.5.1 Thawed embryos vs Fresh embryos

Fresh and thawed blastocyst were evaluated in this objective. Frozen blastocyst at day-5 stage were thawed and cultured for 24 hours as described in section 2.10. All day-6 blastocysts were stained with JC-1 probe to determine the state of mitochondrial membrane potential.

Firstly, intracellular distinction can be observed a clear heterogeneity can be observed in the group of fresh embryos (Figure 3.5). Besides, a pattern of perinuclear clustering of high-polarized mitochondria can be observed for some of the embryos (572, 572, 627, and 628).

The low energy dye (green fluorescence, monomer-form) is observed in a different location to the high-energy dye (red fluorescence, aggregated-form). On the other hand, the group of thawed embryos did not show energetic distinction as they showed uniform distribution of polarized and depolarized mitochondria across the TE and ICM cells (Figure 3.6).

Although the differences observed between the two groups were not significant, there is a clear trend of lower membrane potential in the group of frozen embryos compared with fresh embryos (Figure 3.7).

These results suggest that treatments such as cryopreservation in the early embryo might directly affects mitochondrial membrane potential as well as the distribution of the differentially polarized mitochondria. However, further investigation with higher number of samples is required to confirm this observation.

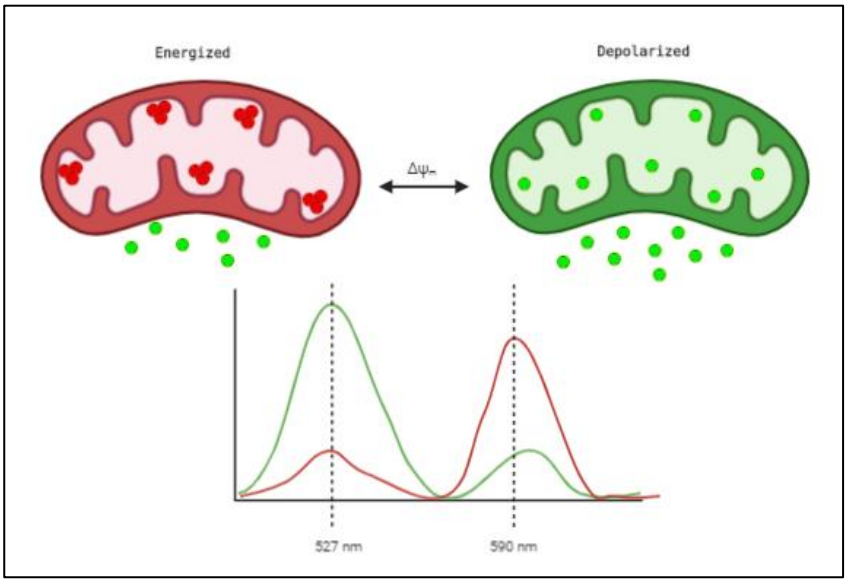

Figure 3.4. Fundamentals of JC-1 and mitochondria membrane potential. JC-1 exhibits potential-dependent accumulation in mitochondria, indicated by a fluorescence emission. Monomeric JC-1 shift from green (~527 nm) to red aggregates (~590 nm) depending on the energetic levels. A polarized membrane is indicative of energized or active mitochondria, whereas depolarized membranes indicates non-mitochondrial activity. The potential-sensitive colour shift is due to concentration-dependent formation of red fluorescent J-aggregates. The ratio of green to red fluorescence is dependent only on the membrane potential and not on other factors such as mitochondrial size, shape, and density.

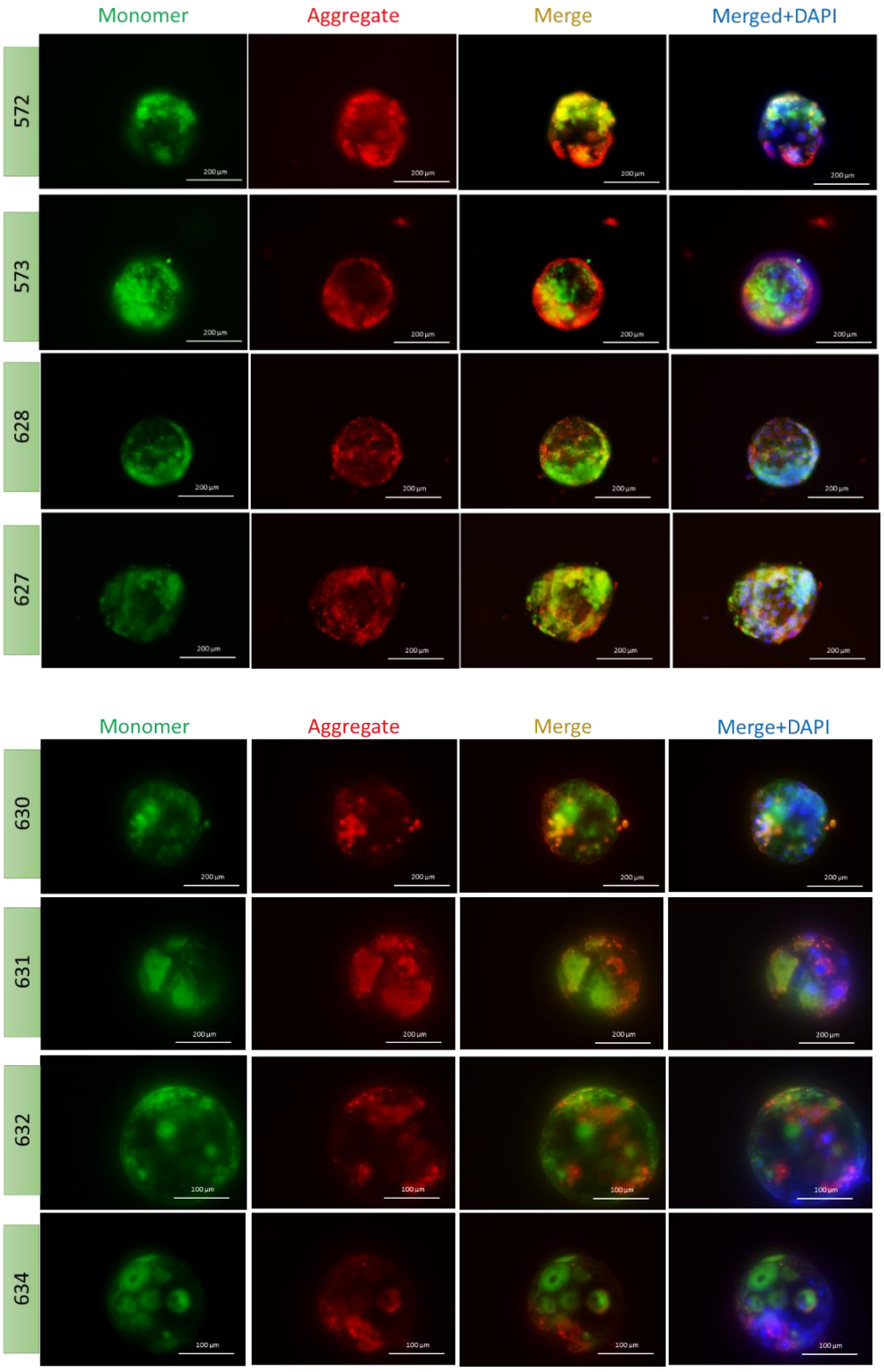

Figure 3.5. Mitochondrial membrane potential (ΔΨm) in fresh embryos. ΔΨm measured by JC-1 dye in fresh embryos (on Day6 in 5% Oxygen, 0.9mM Glucose). Monomer (529 nm) indicates depolarized mitochondria and aggregate (590 nm) indicates energized mitochondria. The third panel (merge) shows the combination of green and red fluorescence whereas the fourth panel indicates merged fluorescence plus DAPI staining (blue).

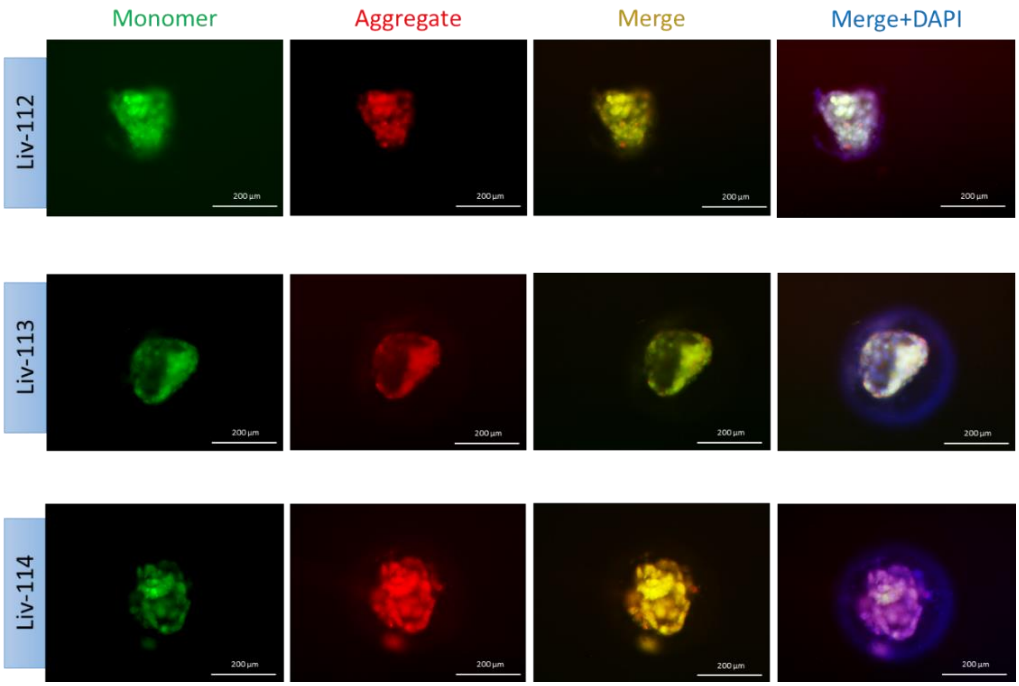

Figure 3.6. Mitochondrial membrane potential (ΔΨm) in frozen embryos. (ΔΨm) measured by JC1 dye in three cryopreserved day-6 blastocyst (Liv-112, Liv-113 and Liv-114). Green fluorescence (529 nm) indicates depolarized mitochondria and red fluorescence (590 nm) indicates energized mitochondria. The third column (merged) shows the combination of green and red fluorescence whereas the fourth panel indicates merged fluorescence plus DAPI staining.

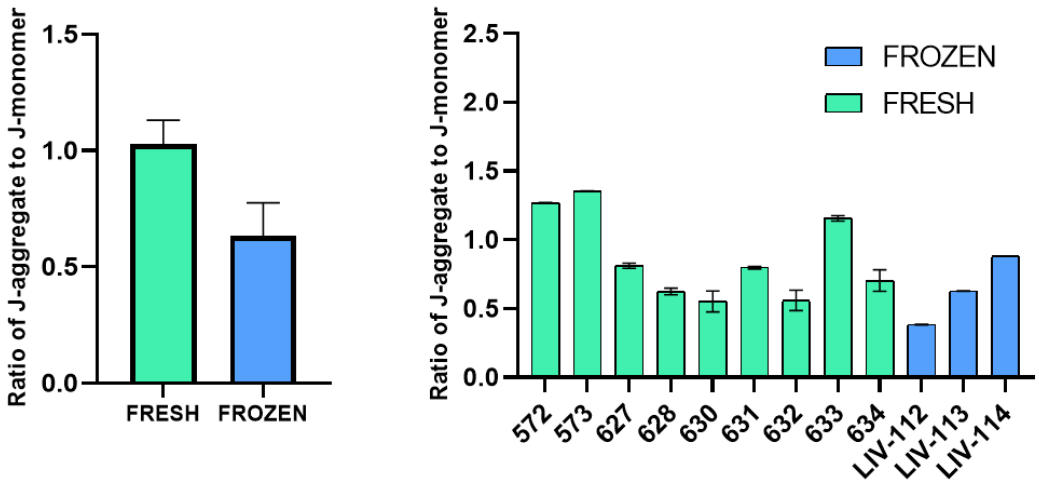

Figure 3.7. ΔΨm comparison between fresh and frozen embryos. Mitochondrial membrane potential measurement by JC1 dye. Comparison between fresh and thawed blastocysts grown in low glucose (0.9mM) and 5% Oxygen. Non-significant differences were observed. Error bar represent SEM.

3.6 Effect of glucose and oxygen on mitochondrial respiration in human embryos.

A pilot study was performed to evaluate the sensitivity of the technology (Seahorse, Agilent) for measurements in low input samples (1-3 blastocysts). To complete this evaluation, a total of 14 day-six blastocysts were used. All blastocysts were fresh and were cultured in GTL medium (Vitrolife) at 0.9 mM glucose and 5% oxygen.

Data shown in this study are representative of eight independent groups and indicated as mean ±SD, and were analysed on GraphPad Prism v. 8.1.2. Since data were not normally distributed, it was analysed using the Kruskal-Wallis non-parametric ANOVA and groups were individually analysed using the Dunn's test for multiple comparisons. Groups were considered to be significantly different if $p<0.05$. Detailed information about the groups is in Table 3.3.

Mitochondrial respiration profiles were evaluated for eight groups of embryos (Table 3.3). For every group, an OCR profile similar to the one shown in Figure 3.8 was expected. However, despite embryos were carefully grouped according to embryo grading, we could not observed a clear pattern that shows any similarities (Figure 3.9). In fact, the heterogeneity of the results was confirmed through non-parametric ANOVA test ($p>0.0001$). Detailed statistical results shown in Table 3.4 for OCR and in Table 3.5 for ECAR. Mean OCR and mean ECAR were plotted on an energy map (Figure 3.10), which is a simplified phenogram representing the mean energetic state of each group.

Furthermore, individual parameters were calculated according to formulas described in Figure 3.8 and these were compared between groups (Figure 3.11 and Table 3.6). All individual parameters resulted in significant differences when assessing by multiple comparison ANOVA ($p = 0.0017$), even when they were cultured under the same conditions. We were not able to identify differences in regards the embryo grading or quality.

In this experiment, the magnitude of the response was almost undetectable by the Seahorse system, and the measurements did not change as expected after the addition of the mitochondrial inhibitors. Due to limited availability of embryos, the sensitivity limits of the system, and the heterogeneity of the results is difficult to make accurate quantitative comparisons. Especially because we were not comparing treatments, so

we were not expecting as many differences between the groups. Therefore, data represented in this pilot study can be used to demonstrate proof of principle only and it would requires further optimization to be used with single embryos

Group	N	Grade	Mean ECAR	Mean OCR
Group 1	1	4CC	0.25	4.06
Group 2	2	4DD 4CD	0.36	4.66
Group 3	2	4DC 5CC	5.4	6.56
Group 4	1	2CD	-0.08	10.5
Group 5	3	3CD 3CC 3CD	-0.46	10.13
Group 6	1	5CD	-0.81	9.99
Group 7	1	3CD	-2.02	-6.69
Group 8	2	5CD 4DC	1.01	11.27

Table 3.3. Blastocysts evaluated through the Cell Mito Stress Test. Descriptive table showing the number of blastocysts (N) and their quality grade used per well (group) to obtain independent measurements.

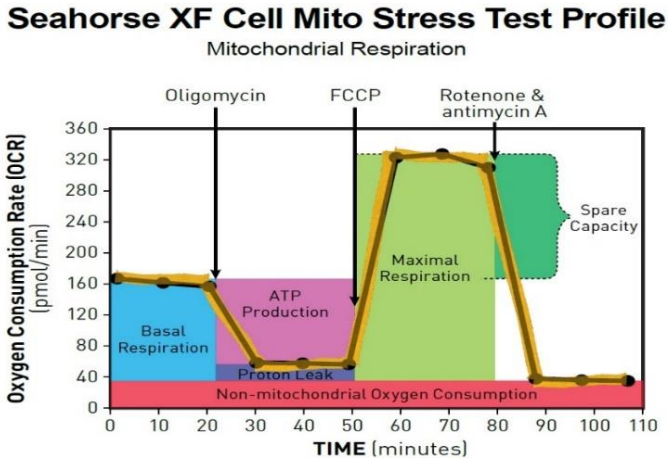

Parameter Value	Equation
Non-mitochondrial Oxygen Consumption	Minimum rate measurement after Rotenone/antimycin A injection
Basal Respiration	(Last rate measurement before first injection) – (Non-Mitochondrial Respiration Rate)
Maximal Respiration	(Maximum rate measurement after FCCP injection) – (Non-Mitochondrial Respiration)
H+ (Proton) Leak	(Minimum rate measurement after Oligomycin injection) – (Non-Mitochondrial Respiration
ATP Production	(Last rate measurement before Oligomycin injection) – (Minimum rate measurement after Oligomycin injection)
Spare Respiratory Capacity	(Maximal Respiration) – (Basal Respiration)
Spare Respiratory Capacity as a %	(Maximal Respiration) / (Basal Respiration) × 100
Acute Response	(Last rate measurement before oligomycin Injection) – (Last rate measurement before acute injection)
Coupling Efficiency	ATP Production Rate) / (Basal Respiration Rate) × 100

Figure 3.8. Cell Mito Stress Test Kit parameter calculation. This table explains the calculations applied to obtain every parameter (Agilent Seahorse XFp, Cell Mito Stress Test Kit, User Guide, Kit 103010-100).

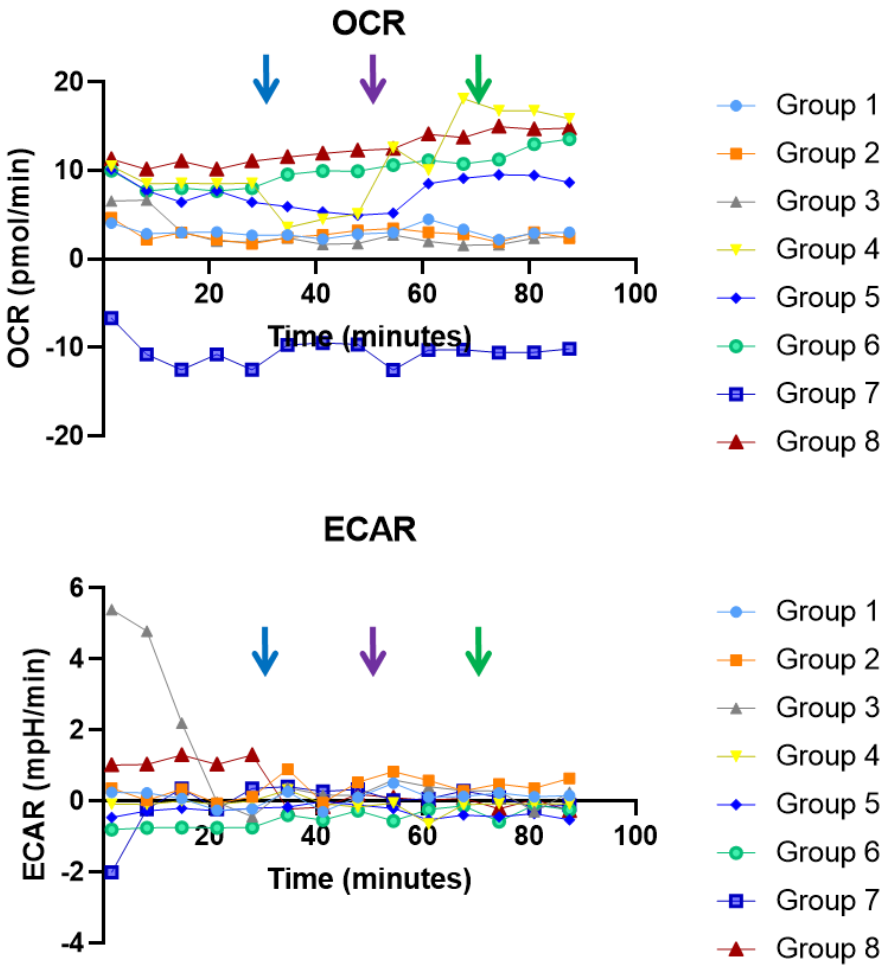

Figure 3.9. Schematic of mitochondrial stress test in human blastocysts. Oxygen Consumption rate (OCR) and Extracellular acidification Rate (ECAR) were measured from day-6 blastocysts grown in 5% oxygen and 0.9mM glucose. Followed by the sequential addition of drugs Oligomycin (1 µM), FCCP (1 µM), Rotenone/Antimycin A (0.5 µM), indicated by coloured arrow drug blue, purple and green respectively. Each data point represents an OCR measurement.

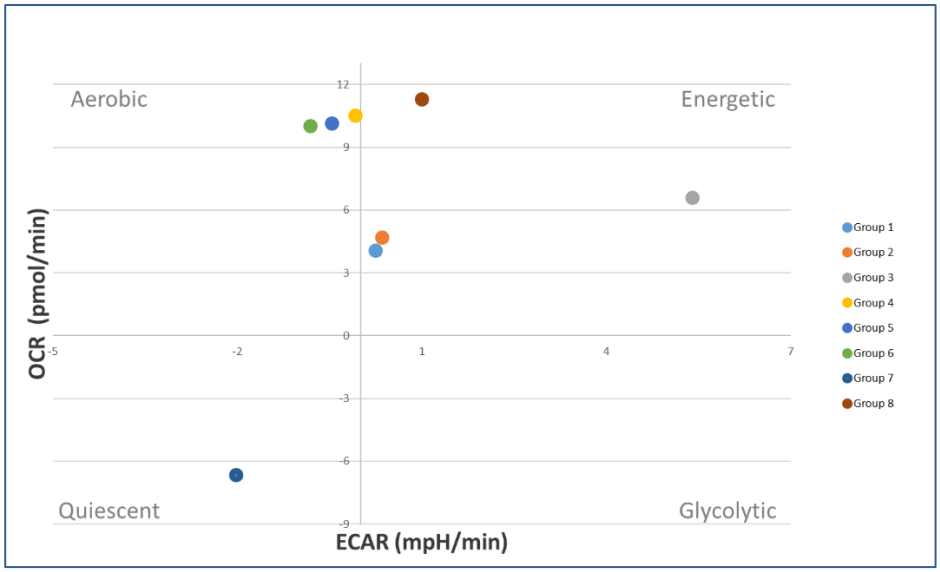

Figure 3.10. Metabolic phenogram contrasting basal OCR and ECAR in embryos. This energy map allow us make a relative comparison in a simplified manner of the energetic status for each sample. We were expected one single cluster near the quiescent or glycolytic area however; we can appreciate here the heterogeneity of the groups. Groups 1 and 2 show very similar energy levels Groups 4, 5 and 6 cluster together on the top left side of the plot, showing a more aerobic metabolism. Group 7 showed the lowest basal energy level. Finally, group 3 with the most energetic level.

Kruskal-Wallis test	*Number of Groups*	*Summary*	*Adjusted P Value*
Mean OCR Group 1 – Group 8	8	****	<0.0001
Dunn's multiple comparisons test	**Mean rank diff.**	**Summary**	**Adjusted P Value**
Group 1 vs. Group 2	4.500	ns	>0.9999
Group 1 vs. Group 3	9.714	ns	>0.9999
Group 1 vs. Group 4	-43.29	*	0.0118
Group 1 vs. Group 5	-28.71	ns	0.5409
Group 1 vs. Group 6	-43.43	*	0.0113
Group 1 vs. Group 7	33.29	ns	0.1874
Group 1 vs. Group 8	-57.79	****	<0.0001
Group 2 vs. Group 3	5.214	ns	>0.9999
Group 2 vs. Group 4	-47.79	**	0.0028
Group 2 vs. Group 5	-33.21	ns	0.1907
Group 2 vs. Group 6	-47.93	**	0.0026
Group 2 vs. Group 7	28.79	ns	0.5325
Group 2 vs. Group 8	-62.29	****	<0.0001
Group 3 vs. Group 4	-53.00	***	0.0004
Group 3 vs. Group 5	-38.43	*	0.0488
Group 3 vs. Group 6	-53.14	***	0.0004
Group 3 vs. Group 7	23.57	ns	>0.9999
Group 3 vs. Group 8	-67.50	****	<0.0001
Group 4 vs. Group 5	14.57	ns	>0.9999
Group 4 vs. Group 6	-0.1429	ns	>0.9999
Group 4 vs. Group 7	76.57	****	<0.0001
Group 4 vs. Group 8	-14.50	ns	>0.9999
Group 5 vs. Group 6	-14.71	ns	>0.9999
Group 5 vs. Group 7	62.00	****	<0.0001
Group 5 vs. Group 8	-29.07	ns	0.5001
Group 6 vs. Group 7	76.71	****	<0.0001
Group 6 vs. Group 8	-14.36	ns	>0.9999
Group 7 vs. Group 8	-91.07	****	<0.0001

Table 3.4. Mean Oxygen consumption Rate (OCR) in embryos. Kruskal-Wallis non-parametric ANOVA was performed to evaluate the sample (8 groups) which resulted significant with a P value <0.0001. Dunn's test was also performed for multiple individual comparisons between each group.

Kruskal-Wallis test	***Number of Groups***	***Summary***	***Adjusted P Value***
Mean ECAR Group 1 – Group 8	8	****	<0.0001
Dunn's multiple comparisons test	**Mean rank diff.**	**Summary**	**Adjusted P Value**
Group 1 vs. Group 2	-20.86	ns	>0.9999
Group 1 vs. Group 3	-14.43	ns	>0.9999
Group 1 vs. Group 4	16.21	ns	>0.9999
Group 1 vs. Group 5	38.86	*	0.0433
Group 1 vs. Group 6	48.79	**	0.0020
Group 1 vs. Group 7	3.214	ns	>0.9999
Group 1 vs. Group 8	-5.500	ns	>0.9999
Group 2 vs. Group 3	6.429	ns	>0.9999
Group 2 vs. Group 4	37.07	ns	0.0707
Group 2 vs. Group 5	59.71	****	<0.0001
Group 2 vs. Group 6	69.64	****	<0.0001
Group 2 vs. Group 7	24.07	ns	>0.9999
Group 2 vs. Group 8	15.36	ns	>0.9999
Group 3 vs. Group 4	30.64	ns	0.3512
Group 3 vs. Group 5	53.29	***	0.0004
Group 3 vs. Group 6	63.21	****	<0.0001
Group 3 vs. Group 7	17.64	ns	>0.9999
Group 3 vs. Group 8	8.929	ns	>0.9999
Group 4 vs. Group 5	22.64	ns	>0.9999
Group 4 vs. Group 6	32.57	ns	0.2230
Group 4 vs. Group 7	-13.00	ns	>0.9999
Group 4 vs. Group 8	-21.71	ns	>0.9999
Group 5 vs. Group 6	9.929	ns	>0.9999
Group 5 vs. Group 7	-35.64	ns	0.1032
Group 5 vs. Group 8	-44.36	**	0.0084
Group 6 vs. Group 7	-45.57	**	0.0057
Group 6 vs. Group 8	-54.29	***	0.0003
Group 7 vs. Group 8	-8.714	ns	>0.9999

Table 3.5. Mean Extracellular Acidification Rate (ECAR) in embryos. Kruskal-Wallis non-parametric ANOVA was performed to evaluate the sample (8 groups) which resulted significant with a P value <0.0001. Dunn's test was also performed for multiple individual comparisons for each group.

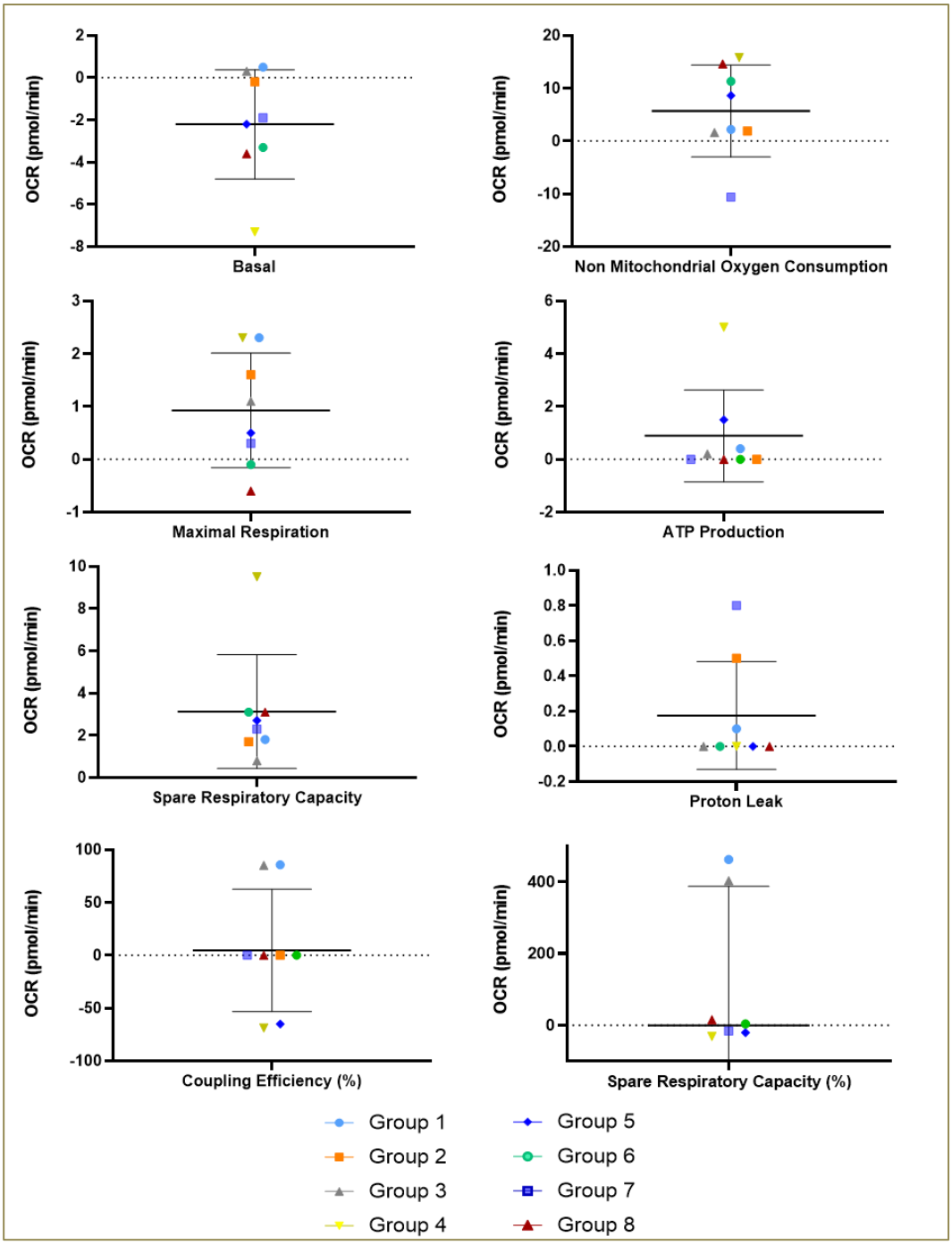

Figure 3.11. Mitochondrial respiration parameters calculated for embryos. This individual plots allow us to visualize the heterogeneity of the groups. Individual parameters for basal respiration (-2.2125 ± 2.58), proton leak (0.175 ±0.305), maximal respiration (0.92 ±1.08), spare respiratory capacity (3.125 ±2.69), non-mitochondrial respiration (5.67 ±8.70), ATP production (0.8875 ±1.73), coupling efficiency percentage (4.6125 ±57.80) and Spare respiratory capacity percentage (-0.575 ±388.26). Data are expressed as mean ± SD, *n* = 8 independent experiments.

Dunn's comparison test	*Mean diff.*	*Parameter*	*Adjusted P Value*
Group1 vs. Group4	21.00	Basal	0.0070
Group1 vs. Group8	18.00	Basal	0.0474
Group3 vs. Group4	18.00	Basal	0.0474
Group1 vs. Group8	19.50	Maximal Respiration	0.0174
Group4 vs. Group8	19.50	Maximal Respiration	0.0174
Group2 vs. Group4	-18.00	Spare Respiratory Capacity	0.0444
Group3 vs. Group4	-21.00	Spare Respiratory Capacity	0.0064
Group3 vs. Group4	-18.00	Non-Mitochondrial Oxygen C.	0.0474
Group4 vs. Group7	21.00	Non-Mitochondrial Oxygen C.	0.0070
Group7 vs. Group8	-18.00	Non-Mitochondrial Oxygen C.	0.0474
Group1 vs. Group4	21.00	Coupling Efficiency %	0.0027
Group1 vs. Group5	18.00	Coupling Efficiency %	0.0230
Group3 vs. Group4	18.00	Coupling Efficiency %	0.0230
Group1 vs. Group2	21.00	Spare Respiratory Capacity %	0.0070
Group1 vs. Group4	18.00	Spare Respiratory Capacity %	0.0474
Group2 vs. Group3	-18.00	Spare Respiratory Capacity %	0.0474

Table 3.6. Multiple comparison tests by respiration parameters. Representative table showing only the comparisons that resulted significantly different. Full results are plotted in Figure 3.11.

3.7 Effect of glucose on DNA methylation in human preimplantation embryos.

This study was performed in order to investigate the impact of glucose concentration on the embryo epigenome and its correlation with altered signalling pathways that could affect embryo development. In order to obtain relevant clinical results out of this study, embryos were treated with same conditions as in the IVF clinic. Normal culture conditions in clinic are at 5% oxygen in GTL medium (0.9mM glucose), besides the modified GTL supplemented with 3.5 mM glucose. The selection of glucose concentrations was based the Morbeck's studies, which reports the composition of commercial media used for human embryo culture [86], [84]. In this case, 0.9 mM glucose was an average concentration and 3.5 mM was one of the highest concentrations used for human embryo culture.

Donated human embryos at PN stage were collected and divided into two groups, low glucose and high glucose. The low glucose group was composed of five embryos, which were kept six days at 5% oxygen in GTL medium/0.9mM glucose. The high glucose group also composed by five embryos were kept three days at 5% oxygen in GTL medium/0.9mM glucose and then it was moved into modified GTL medium/3.5Mm glucose for the completion of six days. At day six blastocysts were graded and dissected by immunosurgery for the isolation of the Inner Cell Mass (ICM) and Trophectoderm (TE). The experimental procedure was performed on TE and ICM samples but samples were paired and treated as single embryos during data analysis. The schematic representation of this study can be observed on Figure 3.12.

As mentioned on Figure 3.12, once libraries were synthesised and purified, they were analysed through capillary electrophoresis to determine the mean fragment sized. Once the size was determine (Figure 3.13), all samples were normalized and quantified right before the sequencing analysis.

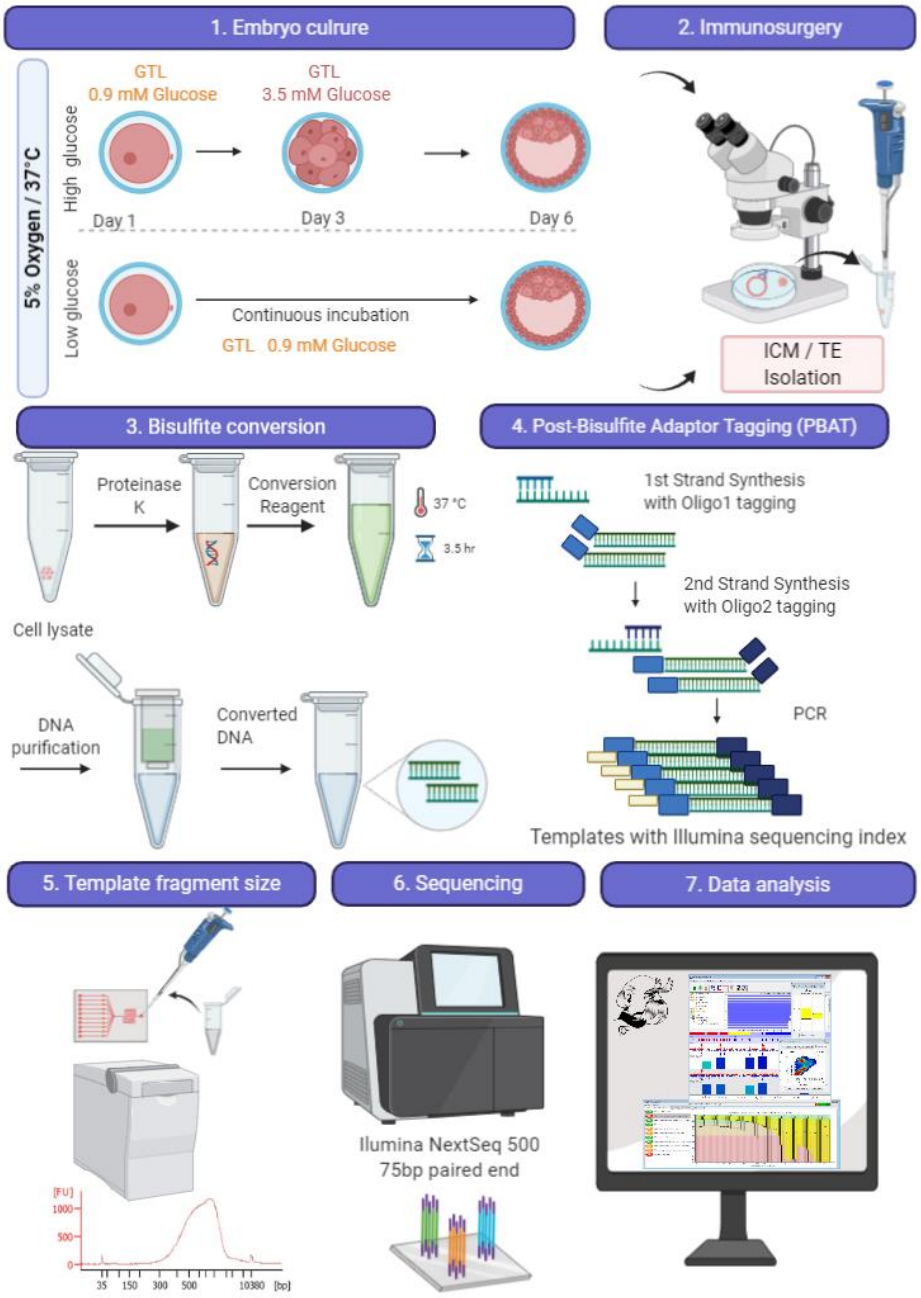

Figure 3.12. Schematic representation of the protocol for DNA Methylation analysis in preimplantation human embryos. 1) Embryos in the high glucose group were cultured in 0.9mMglucose from day 1 to day 3 and in 3.5mM glucose from day 3 to day 6. Embryos in the low glucose group were kept in GTL 0.9mM glucose from day1 to day 6. 2) ICM and TE was isolated from day 6 blastocysts 3) DNA was isolated and treated with Bisulphite 4) BS-seq libraries were prepared through the post-bisulfite adapter tagging method. 5) Library quantification was assessed using High-Sensitivity DNA chips on the Agilent Bio- analyser 6) Pools of 10 libraries were prepared for 75bp paired-end sequencing on a NextSeq500 and run in duplicate 7) Unbiased analysis was performed in SeqMonk.

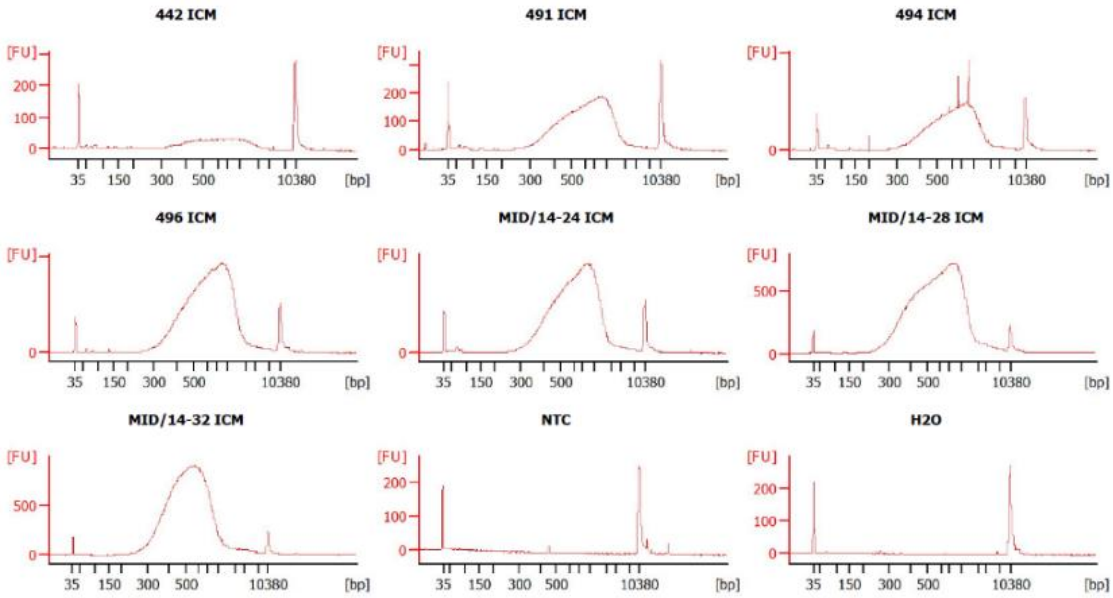

Sample ID	iTAG	(pmol/l)	Sample ID	iTAG	(pmol/l)
Glucose-low_543_ICM	1	7048.1	Glucose-high_14-24_TE	14	12735.5
Glucose-low_543_TE	2	23078.9	Glucose-high_14-28_TE	15	4875.2
Glucose-low_442_ICM	3	875.6	Glucose-high_14-32_TE	16	12412.1
Glucose-low_491_ICM	4	3504.9	Glucose-low_465_ICM	17	25035.6
Glucose-low_494_ICM	5	4261.8	Glucose-low_465_TE	18	30842.6
Glucose-low_496_ICM	6	9660.8	Glucose-high_SM-002_ICM	19	907.0
Glucose-high_14-24_ICM	7	9146.2	Glucose-high_SM-002_TE	20	14905.8
Glucose-high_14-28_ICM	8	22103.1	Glucose-high_019_ICM	21	25591.9
Glucose-high_14-32_ICM	9	25003.8	Glucose-high_019_TE	22	21888.9
Glucose-low_442_TE	10	1668.5	Glucose-high_14-25_ICM	23	7574.2
Glucose-low_491_TE	11	6490.7	Glucose-high_14-25_TE	24	2925.0
Glucose-low_494_TE	12	21832.6	Glucose-low_490_ICM	25	18278.6
Glucose-low_496_TE	13	50,150.4	Glucose-low_490_TE	26	7764.0

Figure 3.13. Quality control of PBAT libraries. Amplified libraries were evaluated for quality and quantity using High-Sensitivity DNA chips on the Agilent Bioanalyser, and the KAPA Library Quantification Kit for Illumina (KAPA Biosystems). Plots represent electropherogams obtained from Bionalyser that indicates quality and mean fragment size. Table indicates absolute quantification of libraries obtained per sample.

3.7.1 Global methylation

The identification of differentially methylated regions (DMRs) from each glucose conditions is useful, but a more powerful use of this information is to identify genes and biological processes that may be affected in preimplantation development. I hypothesized that glucose may directly affect methylation within gene bodies. Therefore, I first identified genes that were overlapped by probes defining differentially methylated regions.

To identify candidate loci I searched for regions that were differentially methylated in high glucose samples compared to low glucose. Data analysis and visualization were performed using the SeqMonk software (RRID:SCR_001913), which relies on R and Java scripts to create plots. Cytosine and Guanine (CpG) methylation was calculated as the average of methylation for each CpG position. Comparisons to obtain hypermethylated and hypomethylated regions were set as those with minimum difference of 10% in the methylation level and with p value <0.05 using EdgeR statistical analysis.

For the first global methylation analysis, methylated points (MPs) were mapped according to the CG_occurrences_GRCh38.txt.gz database. Subsequently, methylated regions (MRs) were defined by grouping 100 continuous methylated points within a probe for further analysis. These created probes were able to overlap any region on the genome as long as they were grouping 100 continuous MPs (Figures 3.14).

Firstly, all samples (Table 3.7) were individually compared on a PCA plot so a broad image of their methylation levels was obtained (Figure 3.15). Roughly, the PCA plot shows that the low and high glucose samples cluster apart independently of the cell type, suggesting that glucose may be affecting the methylation patterns.

Grouped samples were also compared on a PCA plot so a broad image of their methylation levels was obtained (Figure 3.16). The PCA plot resulted into two main clusters, high glucose and low glucose. The samples cluster apart in concordance with the glucose level but independently of the cell population type (ICM or TE).

Methylated regions across the genome were compared as follows:

- Low glucose ICM vs High glucose ICM
- Low glucose TE vs High glucose TE
- High glucose ICM vs High glucose TE
- Low glucose ICM vs Low glucose TE
- Low glucose blastocysts (ICM+TE) vs High glucose blastocysts (ICM+TE)

Low glucose	High glucose
Glucose-low_465_ICM	Glucose-high_1424_ICM
Glucose-low_465_TE	Glucose-high_1424_TE
Glucose-low_490_ICM	Glucose-high_1425_ICM
Glucose-low_490_TE	Glucose-high_1425_TE
Glucose-low_491_ICM	Glucose-high_1428_ICM
Glucose-low_491_TE	Glucose-high_1428_TE
Glucose-low_494_ICM	Glucose-high_1432_ICM
Glucose-low_494_TE	Glucose-high_1432_TE
Glucose-low_496_ICM	Glucose-high_019_ICM
Glucose-low_496_TE	Glucose-high_019_TE

Table 3.7. Sample groups for DNA methylation analysis. This table shows the distribution of sequenced samples across the two groups. This distribution was maintained for all DNA methylation data analysis.

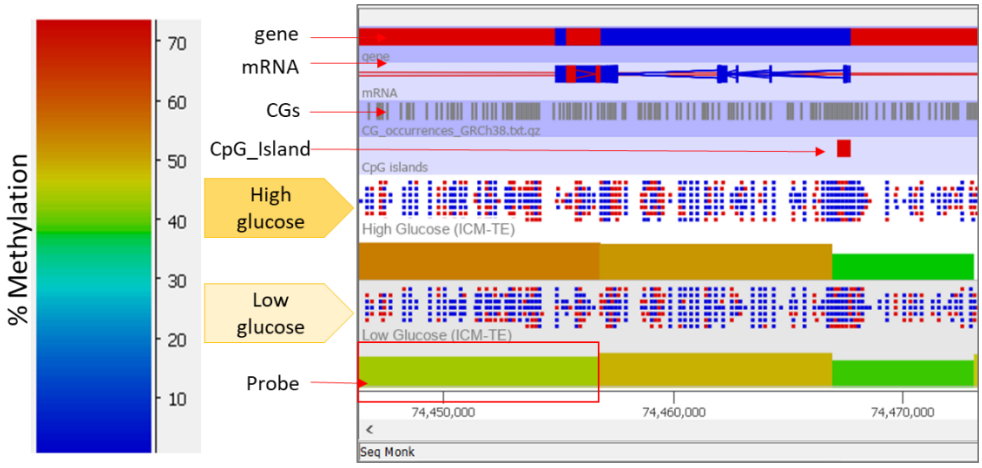

Figure 3.14. Representative image of methylation landscape on SeqMonk. The first four rows represent the genes, mRNA, CG-occurrences (CG_oc) or methylated points and CpG-Islands annotated in the human genome (Homo sapiens GRCh38). Colour bars along the groups represent probes or methylated regions. Colour scale on the left represents methylation levels from red (> 70% methylation) to blue (0% methylation).

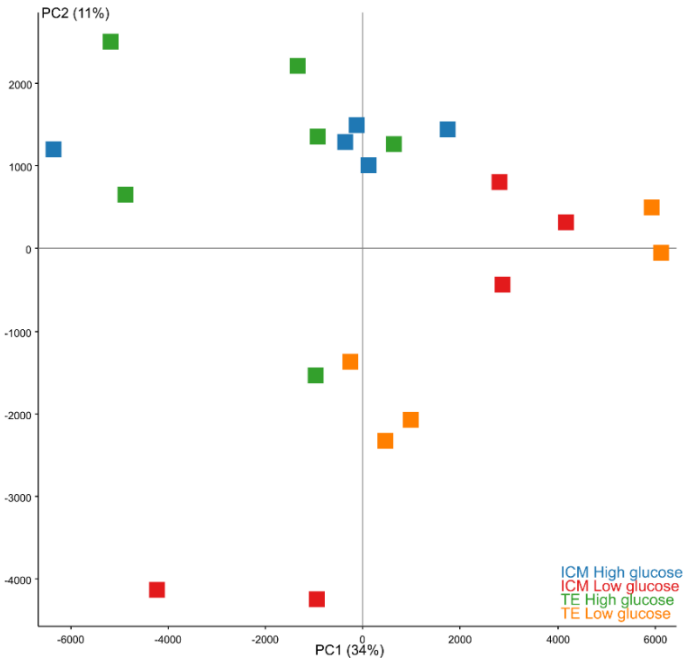

Figure 3.15. PCA plot of DNA methylation profiles of high and low glucose samples (isolated ICM and TE). Each coloured dot represents an individual DNA sample from High Glucose ICM (blue), Low Glucose ICM (red), High Glucose TE (green), or Low Glucose TE (orange) groups.

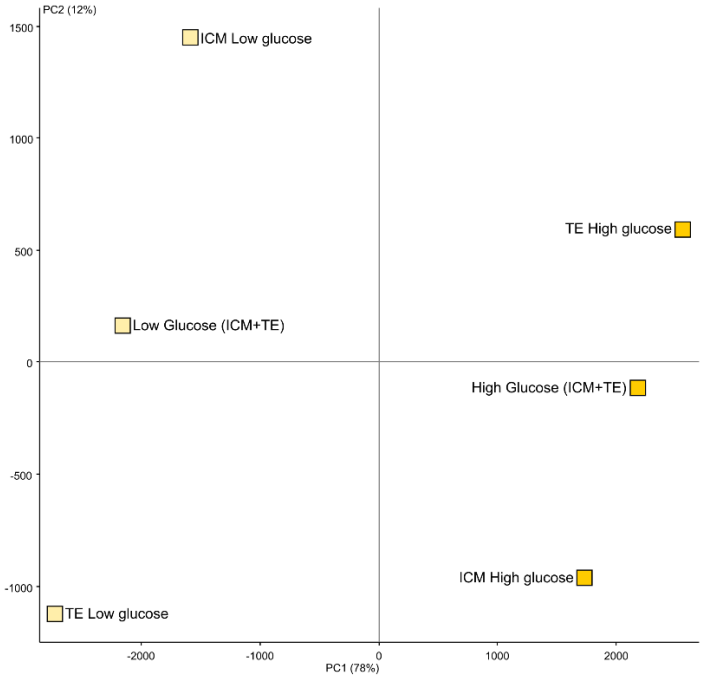

Figure 3.16. PCA plot showing DNA methylation profiles of grouped samples. Samples separated by glucose are clustered in opposite quadrants, low glucose on the left and high glucose on the right. When samples are plotted by cell population, they are clustered in opposite sides of the plot (TE vs ICM). When samples are plotted as a whole embryo, in other words as a paired combination of ICM+TE, they cluster in the middle of the plot but significantly separated to be differentiated from low and high glucose.

3.7.2 Low glucose ICM vs High glucose ICM

Samples were analysed by the EdgeR test to obtain regions that were differentially methylated between the two groups where ICM Glucose high vs ICM Glucose low had a significance below 0.05 after Benjamimi and Hochberg correction with a minimum difference of 10.0. This test resulted in 5023 DMRs, which were overlapping 2755 genes. Methylated regions from the low glucose group were plotted against methylated regions from the high glucose groups in Figure 3.17 with a correlation of 0.872. Differentially methylated regions, their abundance and their methylation levels for the two groups are shown in Figure 3.18.

Differentially methylated genes (2755) were evaluated through Over-Representation Analysis (ORA) using the WEB-based Gene Set Analysis Toolkit (WebGestalt.org)

where gene ontology was obtained for biological processes and diseases. Results from this analysis are represented in Figure 3.19. Here, the most enriched gene sets were related to regulation of biosynthetic processes in the cell and regulation of gene expression, besides gene sets related to neurogenesis. In regards to diseases form the OMIM database, cancer was the most common, followed by heart malformation, mitochondrial deficiency and obesity. From the GLAD4U database, the most enriched diseases were related to Cell adhesion.

Hypermethylated genes in high glucose ICM (151) were evaluated through Over-Representation Analysis (ORA) where gene ontology was obtained for biological processes and diseases (Figure 3.20). Although p values on gene ontology were significant, false discovery rate was not, therefore the results obtained. Therefore, the gene ontology and diseases reported may not be accurate unless the gene number increased in the list. Interesting metabolic and rare genetic disorders came our through the OMIM database. As well as through the GLAD4U data base, that also reported the Bardet-Bield syndrome, child development disorders as well as mental and neurodegenerative disorders

Hypermethylated genes in Low glucose ICM (2604) were evaluated through Over-Representation Analysis (ORA) where gene ontology was obtained for biological processes and diseases (Figure 3.21). These results were significant in p value and FDR. Here, the most enriched gene sets were related to regulation of biosynthetic processes and gene expression, besides gene sets related to neurogenesis. In regards to diseases form the OMIM database, cancer was the most common, followed by heart malformation, mitochondrial deficiency and obesity. From the GLAD4U database, the most enriched diseases was related to cell adhesion stress and cancer.

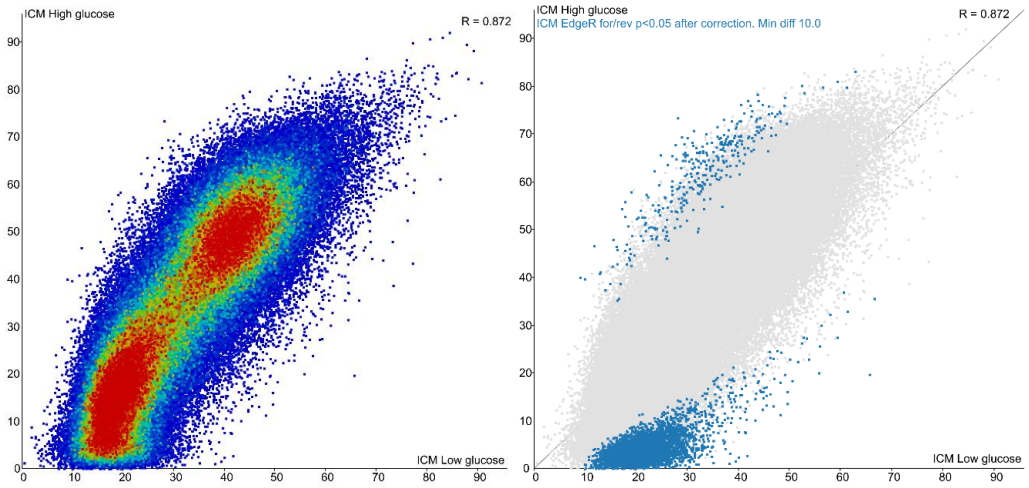

Figure 3.17. Correlation between Low glucose ICM and High glucose ICM. Scatter plots show a common scale for methylation levels (0-90%) in both data sets and a Pearson correlation value R=0.872. Each dot represents a Methylated Region (MR) spanning 100 methylated points (CpGs). A) Overall correlation of methylation levels for 285517 MRs in ICM samples. B) Correlation of methylation levels for 5023 MRs resulted after EdgeR statistical test (blue dots).

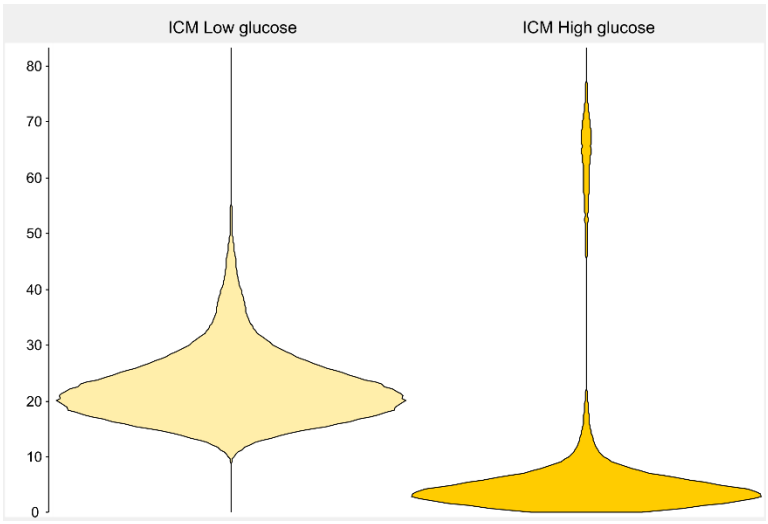

Figure 3.18. Mean Methylation levels in ICM. Bean plot showing DNA methylation average levels (0-100%) of grouped samples after EdgeR statistical test. Samples grouped were in two: Low glucose ICM and High glucose ICM, each group contains five individual samples.

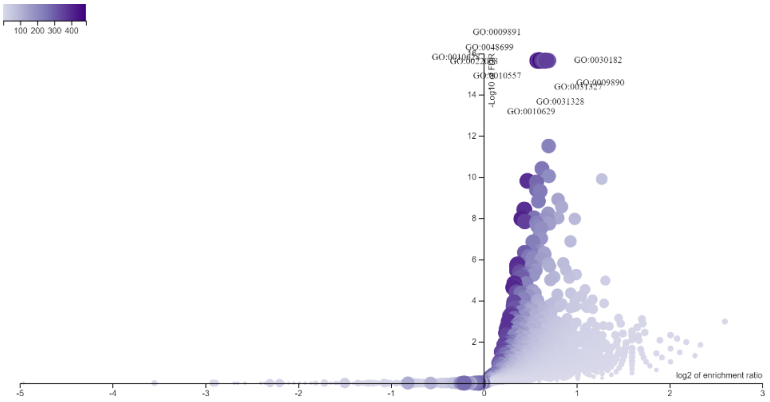

Gene Set	Description	P Value	FDR
GO:0009891	positive regulation of biosynthetic process	0	0
GO:0031328	positive regulation of cellular biosynthetic process	0	0
GO:0010628	positive regulation of gene expression	0	0
GO:0010557	positive regulation of macromolecule biosynthetic process	0	0
GO:0010629	negative regulation of gene expression	0	0
GO:0022008	neurogenesis	0	0
GO:0009890	negative regulation of biosynthetic process	0	0
GO:0031327	negative regulation of cellular biosynthetic process	0	0
GO:0048699	generation of neurons	0	0
GO:0030182	neuron differentiation	0	0

Gene Set	Description	P Value	FDR
187500	TETRALOGY OF FALLOT	3.2563e-11	2.1492e-9
217095	CONOTRUNCAL HEART MALFORMATIONS	1.5775e-7	0.0000052058
176807	PROSTATE CANCER	2.7040e-7	0.0000059488
601626	LEUKEMIA, ACUTE MYELOID	5.2436e-7	0.0000086519
114480	BREAST CANCER	0.0000010224	0.000013495
252010	MITOCHONDRIAL COMPLEX I DEFICIENCY	0.0000053166	0.000058483
189960	TRACHEOESOPHAGEAL FISTULA WITH OR WITHOUT ESOPHAGEAL ATRESIA	0.0000072974	0.000068804
114500	COLORECTAL CANCER	0.000013123	0.00010826
608089	ENDOMETRIAL CANCER	0.00013594	0.00099688
601665	OBESITYLEANNESS, INCLUDED	0.00036989	0.0024413

Gene Set	Description	P Value	FDR
PA443275	Adhesion	4.3299e-15	1.1773e-11
PA445752	Stress	1.2885e-12	1.5402e-9
PA446836	Craniofacial Abnormalities	1.6994e-12	1.5402e-9
PA165108622	Drug interaction with drug	2.5425e-11	1.7283e-8
PA445000	Musculoskeletal Abnormalities	7.0423e-11	3.8296e-8
PA443653	Cell Transformation, Neoplastic	2.7466e-10	1.2447e-7
PA444898	Medulloblastoma	2.6974e-9	0.0000010477
PA446668	Neoplasms, Basal Cell	5.0757e-9	0.0000017251
PA443559	Breast Diseases	1.1030e-8	0.0000033323
PA445538	Retinoblastoma	1.8954e-8	0.0000051535

Figure 3.19. Gene set analyses for ICM 1. Gene ontology analysis of differentially methylated genes (2755) from DRMs between Low glucose ICM and High glucose ICM groups. Volcano plot showing Enrichment ratio vs False Discovery Rate (-Log10 FDR). Blue table showing top biological functions, orange table showing top biological diseases (OMIM) and green table showing top biological diseases (GLAD4U) obtained from Over Representation analysis (ORA). Enrichment were significant in all cases (FDR≤0.05).

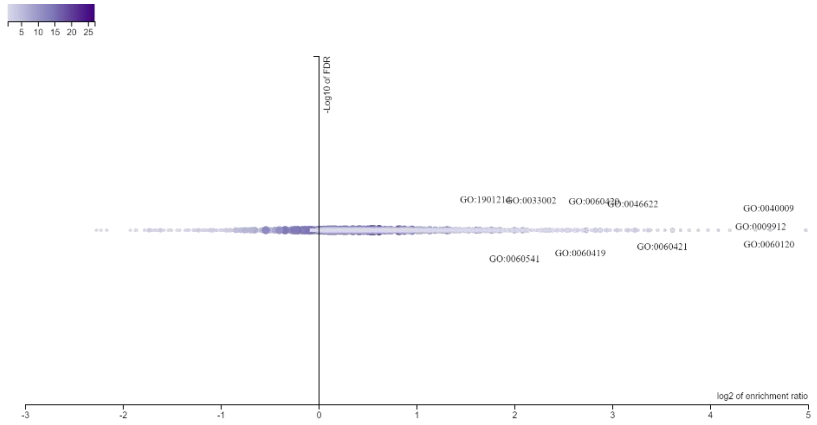

Gene Set	Description	P Value	FDR
GO:0060421	positive regulation of heart growth	0.00030440	1
GO:0046622	positive regulation of organ growth	0.00085328	1
GO:0060419	heart growth	0.00094012	1
GO:0033002	muscle cell proliferation	0.0013602	1
GO:1901214	regulation of neuron death	0.0013879	1
GO:0009912	auditory receptor cell fate commitment	0.0016622	1
GO:0060120	inner ear receptor cell fate commitment	0.0016622	1
GO:0040009	regulation of growth rate	0.0016622	1
GO:0060541	respiratory system development	0.0019021	1
GO:0060420	regulation of heart growth	0.0021301	1

Gene Set	Description	P Value	FDR
609135	APLASTIC ANEMIAAPLASTIC ANEMIA, SUSCEPTIBILITY TO, INCLUDED	0.0099230	0.20903
178500	PULMONARY FIBROSIS, IDIOPATHIC	0.0099230	0.20903
143890	HYPERCHOLESTEROLEMIA, FAMILIAL	0.013868	0.20903
209900	BARDET-BIEDL SYNDROME 1	0.013868	0.20903
187500	TETRALOGY OF FALLOT	0.015835	0.20903
176270	PRADER-WILLI SYNDROME	0.021717	0.23889
176807	PROSTATE CANCER	0.025621	0.24157
256000	LEIGH SYNDROME	0.033388	0.27545
252010	MITOCHONDRIAL COMPLEX I DEFICIENCY	0.039177	0.28393
601626	LEUKEMIA, ACUTE MYELOID	0.043020	0.28393

Gene Set	Description	P Value	FDR
PA447082	Bardet-Biedl Syndrome	0.00039128	0.46705
PA166048756	Child Development Disorders, Pervasive	0.00044759	0.46705
PA446227	Retinal Dysplasia	0.00051532	0.46705
PA165108839	Psychomotor epilepsy	0.0010173	0.56118
PA447199	Bipolar Disorder	0.0012244	0.56118
PA447208	Mental Disorders	0.0012767	0.56118
PA444066	Epilepsies, Partial	0.0014447	0.56118
PA444065	Epilepsy	0.0019442	0.66077
PA443659	Cerebellar Ataxia	0.0024306	0.66659
PA445538	Retinoblastoma	0.0024516	0.66659

Figure 3.20. Gene set analyses for ICM 2. Gene ontology analysis of Hypermethylated genes in High glucose ICM (151). Volcano plot showing Enrichment ratio vs False Discovery Rate (-Log10 FDR). Blue table showing top biological functions, orange table showing top biological diseases (OMIM) and green table showing top biological diseases (GLAD4U) obtained from Over Representation analysis (ORA). Enrichment were not significant as FDR was greater than 0.05 in all cases.

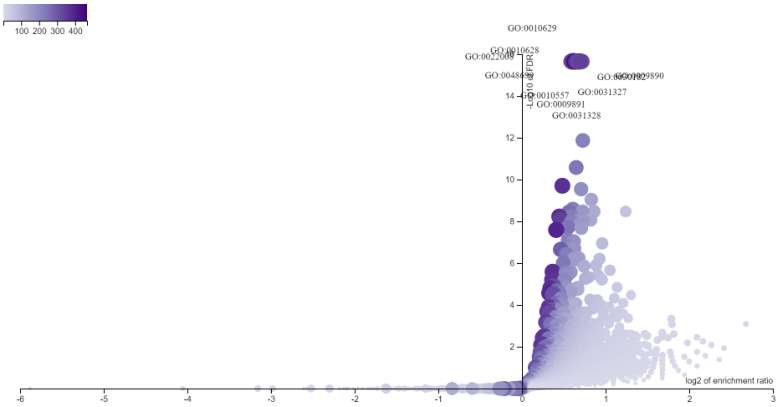

Gene Set	Description	P Value	FDR
GO:0009891	positive regulation of biosynthetic process	0	0
GO:0031328	positive regulation of cellular biosynthetic process	0	0
GO:0010628	positive regulation of gene expression	0	0
GO:0010557	positive regulation of macromolecule biosynthetic process	0	0
GO:0010629	negative regulation of gene expression	0	0
GO:0022008	neurogenesis	0	0
GO:0009890	negative regulation of biosynthetic process	0	0
GO:0031327	negative regulation of cellular biosynthetic process	0	0
GO:0048699	generation of neurons	0	0
GO:0030182	neuron differentiation	0	0

Gene Set	Description	P Value	FDR
187500	TETRALOGY OF FALLOT	2.8919e-9	1.9087e-7
217095	CONOTRUNCAL HEART MALFORMATIONS	1.0244e-7	0.0000033804
114480	BREAST CANCER	5.6904e-7	0.000012519
189960	TRACHEOESOPHAGEAL FISTULA WITH OR WITHOUT ESOPHAGEAL ATRESIA	0.0000044301	0.000065806
176807	PROSTATE CANCER	0.0000056424	0.000065806
601626	LEUKEMIA, ACUTE MYELOID	0.0000059824	0.000065806
114500	COLORECTAL CANCER	0.0000086224	0.000081297
252010	MITOCHONDRIAL COMPLEX I DEFICIENCY	0.000060029	0.00049524
608089	ENDOMETRIAL CANCER	0.00010532	0.00077234
601665	OBESITYLEANNESS, INCLUDED	0.00026633	0.0017578

Gene Set	Description	P Value	FDR
PA443275	Adhesion	7.9936e-15	2.1735e-11
PA445752	Stress	2.6754e-12	3.6372e-9
PA165108622	Drug interaction with drug	6.5761e-12	5.9601e-9
PA446836	Craniofacial Abnormalities	1.1890e-11	8.0824e-9
PA445000	Musculoskeletal Abnormalities	5.7354e-11	3.1189e-8
PA443653	Cell Transformation, Neoplastic	9.8092e-10	4.4452e-7
PA443559	Breast Diseases	2.1853e-9	8.4884e-7
PA446668	Neoplasms, Basal Cell	7.0457e-9	0.0000023947
PA444898	Medulloblastoma	9.6853e-9	0.0000029260
PA443560	Breast Neoplasms	1.7608e-8	0.0000047875

Figure 3.21. Gene set analyses for ICM 3. Gene ontology analysis of Hypermethylated genes in Low glucose ICM (2604). Volcano plot showing Enrichment ratio vs False Discovery Rate (-Log10 FDR). Blue table showing top biological functions, orange table showing top biological diseases (OMIM) and green table showing top biological diseases (GLAD4U) obtained from Over Representation analysis (ORA). Enrichment were significant in all cases (FDR≤0.05).

3.7.3 Low glucose TE vs High glucose TE

Samples were analysed by the EdgeR test to obtain regions that were differentially methylated between the TE Glucose high and TE Glucose low groups, obtained results had a significance below 0.05 after Benjamimi and Hochberg correction with a minimum difference of 10.0. This test resulted in 25234 DMRs, which were overlapping 5079 differentially methylated genes (DMGs). DMRs were plotted in Figure 3.22 for correlation analysis and in Figure 3.23 to visualize abundance and mean methylation levels. Differentially methylated genes (5079) were evaluated through Over-Representation Analysis (ORA) using the WEB-based Gene Set Analysis Toolkit (WebGestalt.org) where gene ontology was obtained for biological processes and diseases. Results from this analysis are represented in Figure 3.24. Here, the most enriched gene sets were related to neurogenesis and morphogenesis. In regards to diseases form the OMIM database, cancer was the most common, followed by hypercholesterolemia, diabetes and Leigh syndrome. From the GLAD4U database, the most enriched diseases were related to cell adhesion and mental disorders.

Hypermethylated genes in high glucose TE (4265) were evaluated through Over-Representation Analysis (ORA) where gene ontology was obtained for biological processes and diseases (Figure 3.25). P values and false discovery rate were significant (<0.05). Here, the most enriched gene sets for gene ontology were neuron development, cell organization, and regulation of plasma membrane. In regards to diseases form the OMIM database, cancer was the most common, followed by hypercholesterolemia, diabetes, and hypertension and Leigh syndrome. From the GLAD4U database, the most enriched diseases were also related to cell adhesion and mental disorders. Hypermethylated genes in Low glucose TE (814) were evaluated through Over-Representation Analysis (ORA) where gene ontology was obtained for biological processes and diseases (Figure 3.26). P values and false discovery rate were significant (<0.05). Here, the most enriched gene sets for gene ontology regulation of transcription and regulation biosynthetic processes. The enriched diseases form the OMIM database were Leukaemia, Wilms tumour and Myocardial infarction. From the GLAD4U database, the most enriched diseases were also related to cell adhesion, Carcinoma and Neoplasms.

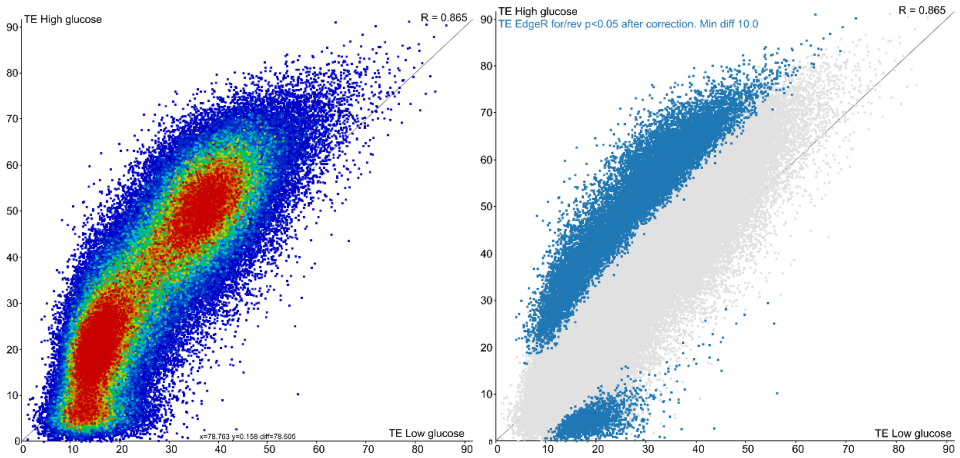

Figure 3.22. Correlation between Low glucose TE and High glucose TE. Scatter plots showing the correlation between the groups Low glucose TE (x-axes) and High glucose TE (y-axes). The plots show a common scale for methylation levels (0-90%) in both data sets and a Pearson correlation value R=0.865. Each dot represents a Methylated Region (MR) spanning 100 methylated points (CpGs). A) Overall correlation of methylation levels for 285517 MRs in TE samples. B) Correlation of methylation levels for 25234 MRs resulted after EdgeR statistical test (blue dots).

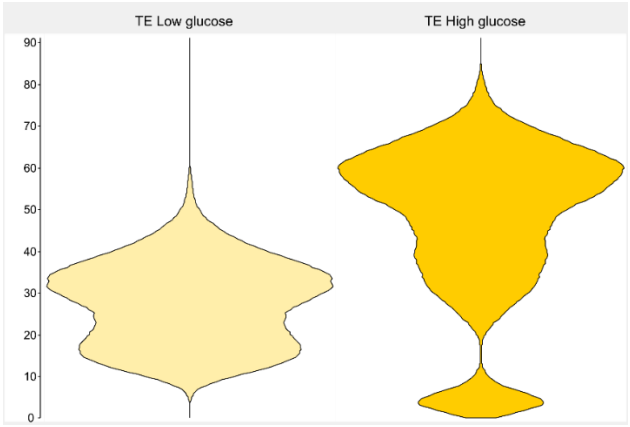

Figure 3.23. Mean Methylation levels in TE. Bean plot showing DNA methylation average levels (0-100%) of grouped samples after EdgeR statistical test. Samples grouped were in two: Low glucose TE and High glucose TE, each group was formed by five individual samples.

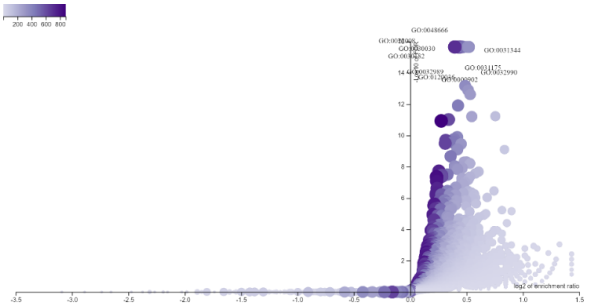

Gene Set	Description	P Value	FDR
GO:0022008	neurogenesis	0	0
GO:0030030	cell projection organization	0	0
GO:0120036	plasma membrane bounded cell projection organization	0	0
GO:0030182	neuron differentiation	0	0
GO:0032989	cellular component morphogenesis	0	0
GO:0048666	neuron development	0	0
GO:0000902	cell morphogenesis	0	0
GO:0031175	neuron projection development	0	0
GO:0031344	regulation of cell projection organization	0	0
GO:0032990	cell part morphogenesis	0	0

Gene Set	Description	P Value	FDR
601626	LEUKEMIA, ACUTE MYELOID	9.5257e-14	6.2870e-12
114480	BREAST CANCER	5.3435e-13	1.7634e-11
189960	TRACHEOESOPHAGEAL FISTULA WITH OR WITHOUT ESOPHAGEAL ATRESIA	1.2848e-12	2.8265e-11
176807	PROSTATE CANCER	3.6969e-8	6.0999e-7
133239	ESOPHAGEAL CANCERESOPHAGEAL SQUAMOUS CELL CARCINOMA, SUSCEPTIBILITY TO, INCLUDED	3.0667e-7	0.0000040480
143890	HYPERCHOLESTEROLEMIA, FAMILIAL	0.0000059240	0.000055855
613065	LEUKEMIA, ACUTE LYMPHOBLASTIC	0.0000059240	0.000055855
125853	DIABETES MELLITUS, NONINSULIN-DEPENDENT	0.0000071647	0.000059109
256000	LEIGH SYNDROME	0.0000092736	0.000068006
607785	JUVENILE MYELOMONOCYTIC LEUKEMIA	0.000029851	0.00016484

Gene Set	Description	P Value	FDR
PA443275	Adhesion	0	0
PA447208	Mental Disorders	0	0
PA153906318	Autism Spectrum Disorder	0	0
PA447199	Bipolar Disorder	3.5560e-13	2.4172e-10
PA444929	Mental Retardation	1.9273e-12	1.0481e-9
PA443919	Disease Susceptibility	2.4790e-10	1.1234e-7
PA165108317	Developmental disorder NOS	3.5859e-10	1.3929e-7
PA447216	Schizophrenia	4.1701e-10	1.4173e-7
PA447198	Autistic Disorder	4.4147e-9	0.0000013337
PA165108622	Drug interaction with drug	6.4903e-9	0.0000017647

Figure 3.24. Gene set analyses for TE 1. Gene ontology analysis of differentially methylated genes (5079) genes from DRMs between Low glucose TE and High glucose TE groups. Volcano plot showing Enrichment ratio vs False Discovery Rate (-Log10 FDR). Blue table showing top biological functions obtained from ORA. Orange table showing top biological diseases (OMIM). Obtained from ORA. Green table showing top biological diseases (GLAD4U) obtained from ORA. Enrichment method: Over Representation analysis (ORA), (FDR≤0.05).

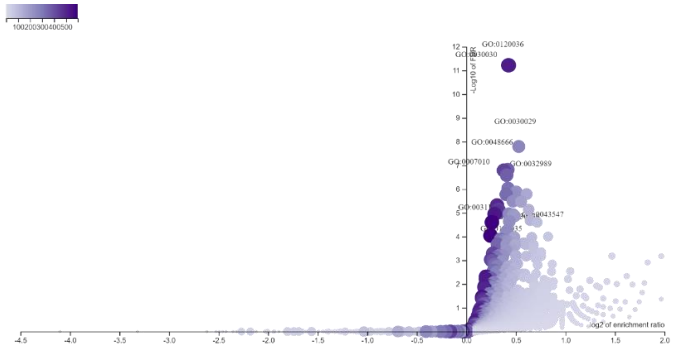

Gene Set	Description	P Value	FDR
GO:0120036	plasma membrane bounded cell projection organization	8.8818e-16	6.0558e-12
GO:0030030	cell projection organization	1.3323e-15	6.0558e-12
GO:0030029	actin filament-based process	5.2804e-12	1.6002e-8
GO:0048666	neuron development	6.6205e-11	1.5047e-7
GO:0007010	cytoskeleton organization	8.9776e-11	1.6323e-7
GO:0032989	cellular component morphogenesis	1.6961e-10	2.5698e-7
GO:0031175	neuron projection development	7.1803e-10	9.3252e-7
GO:0030036	actin cytoskeleton organization	1.1390e-9	0.0000012944
GO:0043547	positive regulation of GTPase activity	1.7626e-9	0.0000016191
GO:0120035	regulation of plasma membrane bounded cell projection organization	1.7810e-9	0.0000016191

Gene Set	Description	P Value	FDR
189960	TRACHEOESOPHAGEAL FISTULA WITH OR WITHOUT ESOPHAGEAL ATRESIA	9.9777e-9	6.5853e-7
114480	BREAST CANCER	4.0670e-8	9.4525e-7
133239	ESOPHAGEAL CANCERESOPHAGEAL SQUAMOUS CELL CARCINOMA, SUSCEPTIBILITY TO, INCLUDED	4.2966e-8	9.4525e-7
252010	MITOCHONDRIAL COMPLEX I DEFICIENCY	0.0000024635	0.000040647
114500	COLORECTAL CANCER	0.0000033836	0.000044663
256000	LEIGH SYNDROME	0.000012810	0.00014091
145500	HYPERTENSION, ESSENTIAL	0.000028021	0.00026420
125853	DIABETES MELLITUS, NONINSULIN-DEPENDENT	0.000038328	0.00029232
143890	HYPERCHOLESTEROLEMIA, FAMILIAL	0.000041863	0.00029232
176807	PROSTATE CANCER	0.000044291	0.00029232

Gene Set	Description	P Value	FDR
PA443275	Adhesion	3.4195e-14	9.2976e-11
PA153906318	Autism Spectrum Disorder	1.4329e-10	1.9481e-7
PA447199	Bipolar Disorder	4.2935e-10	3.8913e-7
PA447208	Mental Disorders	1.5510e-9	8.4386e-7
PA443919	Disease Susceptibility	1.5518e-9	8.4386e-7
PA447216	Schizophrenia	2.2554e-8	0.000010220
PA443687	Chagas Cardiomyopathy	8.3251e-8	0.000028295
PA446743	Parasitemia	8.3251e-8	0.000028295
PA444065	Epilepsy	1.0097e-7	0.000030503
PA447198	Autistic Disorder	1.7332e-7	0.000045323

Figure 3.25. Gene set analyses for TE 2. Gene ontology analysis of Hypermethylated genes in TE High glucose (4265). Volcano plot showing Enrichment ratio vs False Discovery Rate (-Log10 FDR). Blue table showing top biological functions obtained from ORA. Orange table showing top biological diseases (OMIM) obtained from ORA. Green table showing top biological diseases (GLAD4U) obtained from ORA. Enrichment method: Over Representation analysis (ORA), (FDR≤0.05).

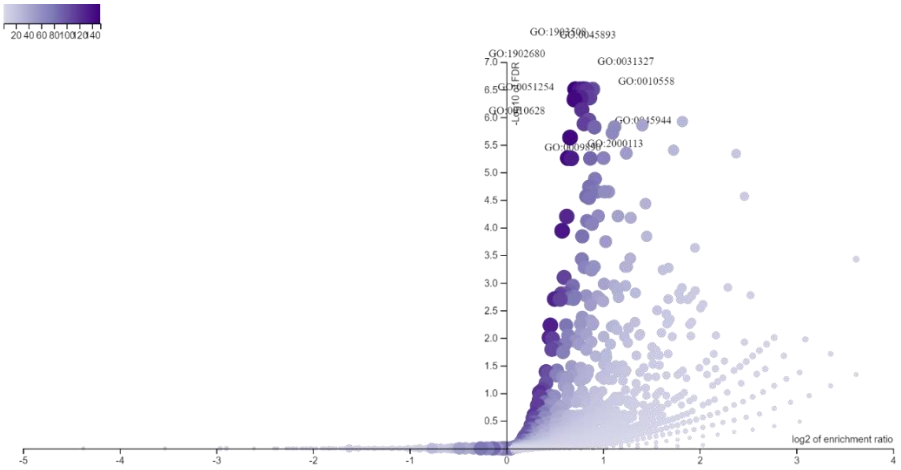

Gene Set	Description	P Value	FDR
GO:0045893	positive regulation of transcription, DNA-templated	8.4763e-11	3.1234e-7
GO:1903508	positive regulation of nucleic acid-templated transcription	1.0493e-10	3.1234e-7
GO:1902680	positive regulation of RNA biosynthetic process	1.0954e-10	3.1234e-7
GO:0010558	negative regulation of macromolecule biosynthetic process	1.5542e-10	3.1234e-7
GO:0010628	positive regulation of gene expression	2.4111e-10	3.1234e-7
GO:0031327	negative regulation of cellular biosynthetic process	2.4956e-10	3.1234e-7
GO:0051254	positive regulation of RNA metabolic process	2.5312e-10	3.1234e-7
GO:0045944	positive regulation of transcription by RNA polymerase II	2.7486e-10	3.1234e-7
GO:0009890	negative regulation of biosynthetic process	3.5418e-10	3.3077e-7
GO:2000113	negative regulation of cellular macromolecule biosynthetic process	3.6384e-10	3.3077e-7

Gene Set	Description	P Value	FDR
194070	WILMS TUMOR 1	0.0000047551	0.00030779
601626	LEUKEMIA, ACUTE MYELOID	0.0000093270	0.00030779
613065	LEUKEMIA, ACUTE LYMPHOBLASTIC	0.00082941	0.018247
608446	MYOCARDIAL INFARCTION, SUSCEPTIBILITY TOMYOCARDIAL INFARCTION, SUSCEPTIBILITY TO, 1, INCLUDED	0.0030079	0.049631

Gene Set	Description	P Value	FDR
PA443275	Adhesion	0.0000060621	0.016483
PA443623	Carcinoma, Papillary	0.000021766	0.029591
PA446668	Neoplasms, Basal Cell	0.000051089	0.046304

Figure 3.26. Gene set analyses for TE 3. Gene ontology analysis of Hypermethylated genes in Low glucose TE (814). Volcano plot showing Enrichment ratio vs False Discovery Rate (-Log10 FDR). Blue table showing top biological functions obtained from ORA. Orange table showing top biological diseases (OMIM) obtained from ORA. Green table showing top biological diseases (GLAD4U) obtained from ORA. Enrichment method: Over Representation analysis (ORA), (FDR≤0.05).

3.7.4 High glucose ICM vs High glucose TE

Samples were analysed by the EdgeR test to obtain regions that were differentially methylated between the ICM Glucose high and TE Glucose high groups, obtained results had a significance below 0.05 after Benjamimi and Hochberg correction with a minimum difference of 10.0. This test resulted in 7 DMRs, which were overlapping 4 genes (UBE2D3, PIP5K1B, FAM122A and PLXNC1). Correlation analysis resulted in 0.945 (Figure 3.27) and methylation levels are between 10-45% (Figure 3.28)

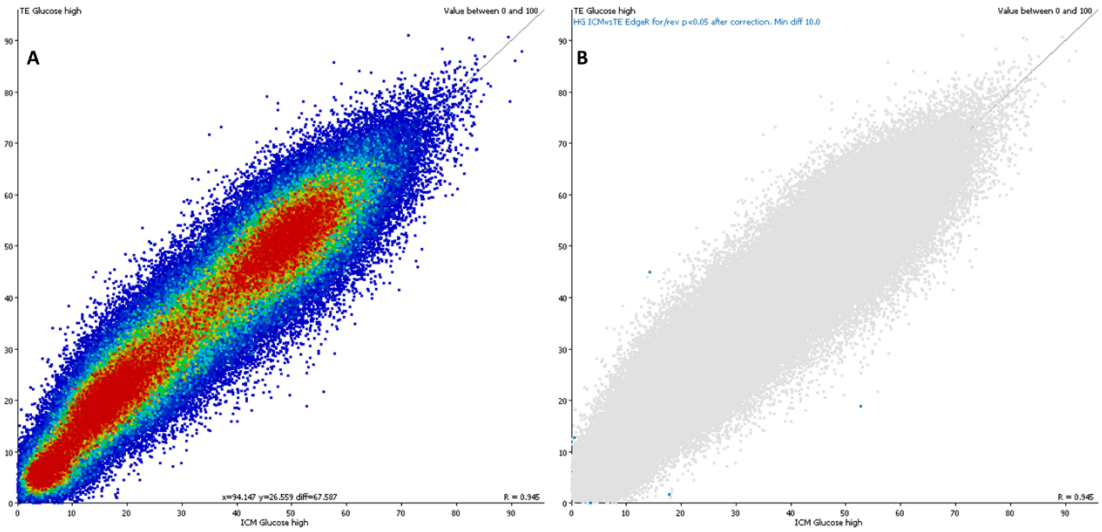

Figure 3.27. Correlation between High glucose ICM and High glucose TE. Scatter plots showing the correlation between the groups High glucose TE (x-axes) and High glucose ICM (y-axes). The plots show a common scale for methylation levels (0-90%) in both data sets and a Pearson correlation value R=0.945. Each dot represents a Methylated Region (MR) spanning 100 methylated points (CpGs). A) Overall correlation of methylation levels for 285517 MRs in TE samples. B) Correlation of methylation levels for 4 MRs resulted after EdgeR statistical test (blue dots).

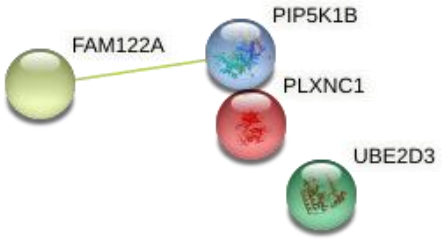

UBE2D3	Ubiquitin conjugating enzyme E2 D3; Belongs to the ubiquitin-conjugating enzyme family (149 aa). Chr9
PIP5K1B	Phosphatidylinositol 4-phosphate 5-kinase type-1 beta; Participates in the biosynthesis of phosphatidylinositol 4,5-bisphosphate. Mediates RAC1-dependent reorganization of actin filaments. Contributes to the activation of PLD2. Together with PIP5K1A is required after stimulation of G-protein coupled receptors for stable platelet adhesion (By similarity) (540 aa). Chr4
FAM122A	Protein FAM122A; Family with sequence similarity 122A (287 aa) is a Protein Coding gene.Chr12
PLXNC1	Plexin-C1; Receptor for SEMA7A, for smallpox semaphorin A39R, vaccinia virus semaphorin A39R and for herpesvirus Sema protein. Binding of semaphorins triggers cellular responses leading to the rearrangement of the cytoskeleton and to secretion of IL6 and IL8 (By similarity); Belongs to the plexin family (1568 aa). Chr19

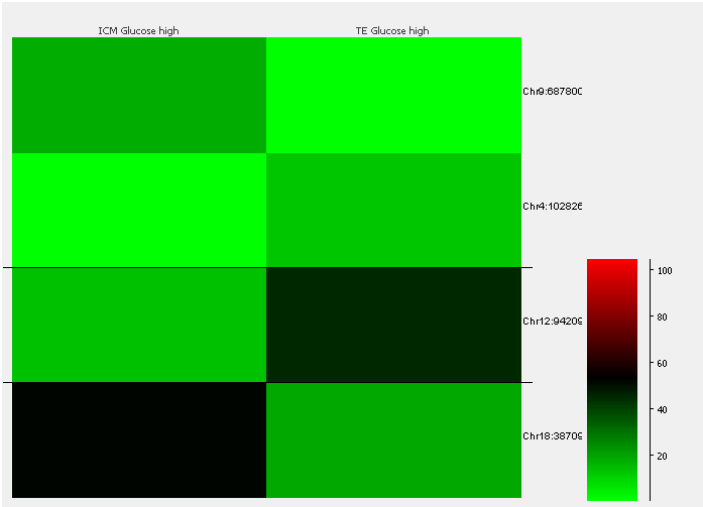

Figure 3.28 Results High glucose ICM vs High glucose TE. Differentially methylated genes from high glucose ICM vs TE samples. The heat map (0-100%) represents methylation levels and the gene description is indicated in the table on top.

3.7.5 Low glucose ICM vs Low glucose TE

Samples were analysed by the EdgeR test to obtain regions that were differentially methylated between the ICM Glucose low and TE Glucose low groups, obtained results had a significance below 0.05 after Benjamimi and Hochberg correction with a minimum difference of 10.0. This test resulted in 2 DMRs, which were overlapping 1 gene (DHX9). Correlation analysis is resulted in 0.885 (Figure 3.29) and methylation levels are between 10-45% (Figure 3.30)

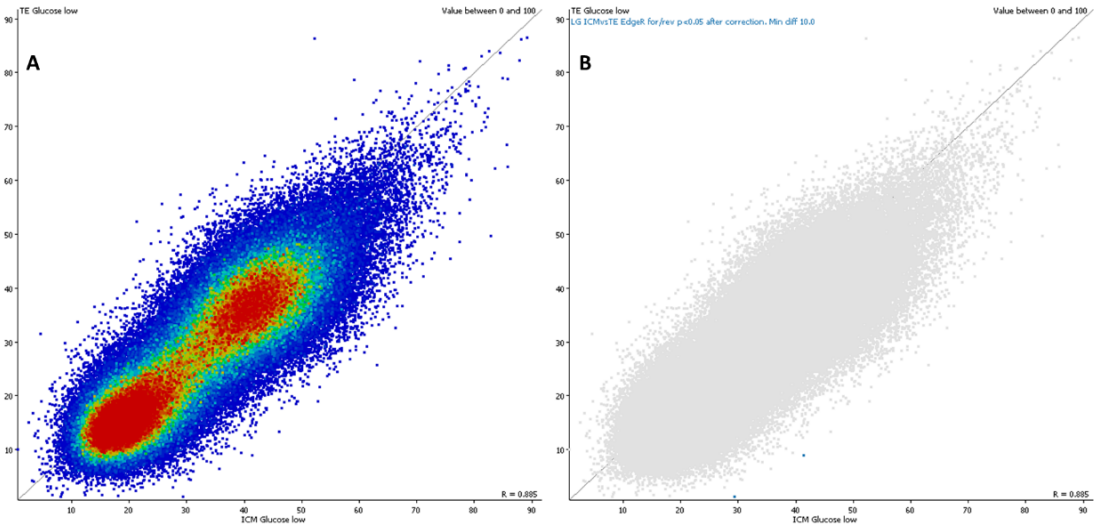

Figure 3.29. Correlation between Low glucose ICM and Low glucose. TE Scatter plots showing the correlation between the data group's Low glucose ICM (x-axes) and Low glucose TE (y-axes). The plots show a common scale for methylation levels (0-90%) in both data sets and a Pearson correlation value R=0.885. Each dot represents a Methylated Region (MR) spanning 100 methylated points (CpGs). A) Overall correlation of methylation levels for 285517 MRs in Low glucose samples. B) Correlation of methylation levels for 2 MRs resulted after EdgeR statistical test (blue dots).

DHX9	*ATP-dependent RNA helicase A; Multifunctional ATP-dependent nucleic acid helicase that unwinds DNA and RNA in a 3' to 5' direction and that plays important roles in many processes, such as DNA replication, transcriptional activation, post-transcriptional RNA regulation, mRNA translation and RNA-mediated gene silencing. Requires a 3'-single-stranded tail as entry site for acid nuclei unwinding activities as well as the binding and hydrolyzing of any of the four ribo- or deoxyribo- nucleotide triphosphates (NTPs).*

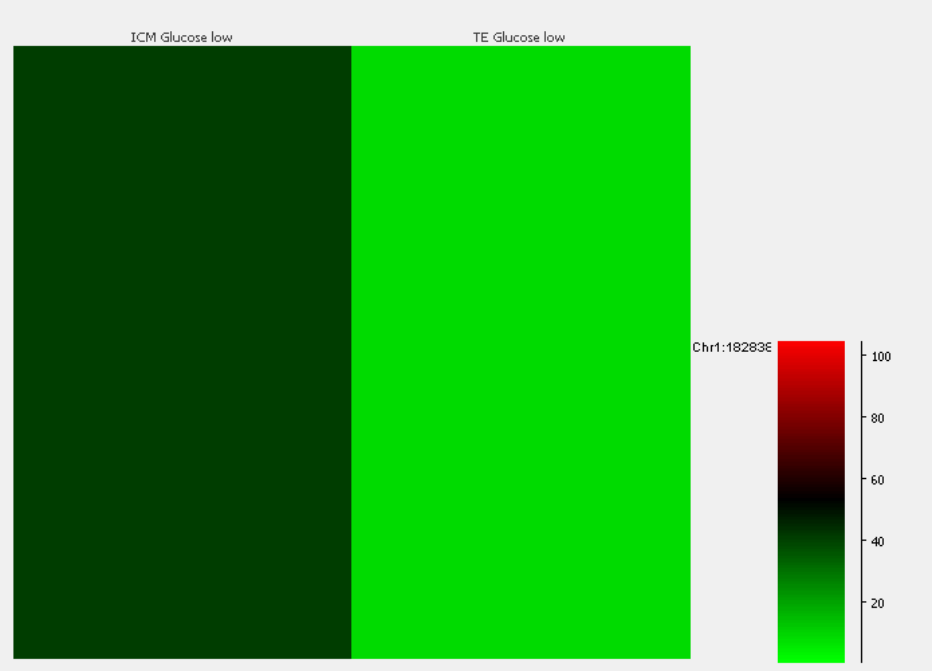

Figure 3.30. Results Low glucose ICM vs Low glucose. Differentially methylated gene from low glucose ICM vs TE samples. The heat map (0-100%) represents methylation levels and the gene description is indicated in the table on top.

3.7.6 Comparison between low glucose and high glucose blastocysts

Global methylation analysis was assessed by comparing high glucose and low glucose paired samples (ICM+TE). Methylated regions (MRs) were defined through all the genome by spanning probes over 100 CpGs, which resulted 288,333 probes as described in Figure 3.14.

Unbiased measures of methylation were performed over a fixed window size of 100 methylated points (CpGs) as this was found to give at least 100 reads per methylated region (Figure 3.31). This can be appreciated in a scatter plot where data form both groups low glucose and high glucose was correlated. The average levels of methylation (0-100%) and percentage of abundance in the two groups can be appreciated in Figure 3.32. An interesting observation is that the high glucose group has the more methylated genes relative to the low glucose group as 23% of the genome present from 50-75% methylation. This distribution is also represented in a bean plot (Figure 3.33).

Groups were compared using EdgeR test with the filtering criterion of adjusted p value ($p < 0.05$) and difference in methylation greater than 10% ($\Delta\beta \geq 10\%$). This resulted in 57,737 probes identified as being differentially methylated, of which 18.1% were hypomethylated and 81.9% hypermethylated in High glucose vs Low glucose (Figure 3.34). Finally, the mean methylation of gene bodies form both groups can be compared by a quantitation trend plot showing the relative methylation levels of gene bodies ±5000bp in low glucose and high glucose groups (Figure 3.35). Here we could confirm that the high glucose group show higher mean methylation levels relative to the low glucose samples.

8654 genes were defined as being differentially methylated (DM) when overlapped at least by one probe containing 100 CpGs (Figure 3.36). Then, a subset of genes whose methylation levels decreased in high glucose or increased in low glucose were identified (Figure 3.37) in addition to a subset of genes whose methylation levels increased in high glucose or decreased in low glucose (Figure 3.38). Gene lists were

analysed on the WEB-based Gene Set Analysis Toolkit (WebGestalt.org) through Over-Representation Analysis (ORA). Gene ontology analysis resulted in the identification of biological processes and diseases that are related to these gene sets. Results from ORA from 8654 differentially methylated genes are represented in Figure 3.38. Here, the most enriched gene sets were related to cell cycle, embryo development regulation of gene expression and intracellular transport. Diseases resulted from the OMIM database include leukaemia, breast cancer, diabetes, mitochondrial deficiency, cancer and Leigh syndrome.

Results from ORA from hypermethylated genes in low glucose TE (4317) are represented in Figure 3.37. P values and false discovery rate were significant (<0.05) for all analysis. Here, the most enriched gene sets for gene ontology include cell cycle, regulation of gene expression, embryo development, head and brain development. Enriched diseases resulted from the OMIM database include leukaemia, myocardial infarction, cancer, diabetes, Wilms tumour and mitochondrial deficiency. From the GLAD4U database, the most enriched diseases were also related to cell adhesion, cell transformation, meduloblastoma, neoplasm and craniofacial abnormalities.

Hypermethylated genes in Low glucose TE (4337) ORA where gene ontology was obtained for biological processes and diseases (Figure 3.38). P values and false discovery rate were significant (<0.05). Here, the most enriched gene sets for gene ontology include macromolecule localization, intracellular transport, cytoskeleton organization and cell cycle. The enriched diseases form the OMIM database include cancer, leukaemia, diabetes, mitochondria deficiency and Leigh syndrome. From the GLAD4U database, the most enriched diseases were ataxia, protein deficiency, anaemia, metabolism inborn errors and genetic translocation.

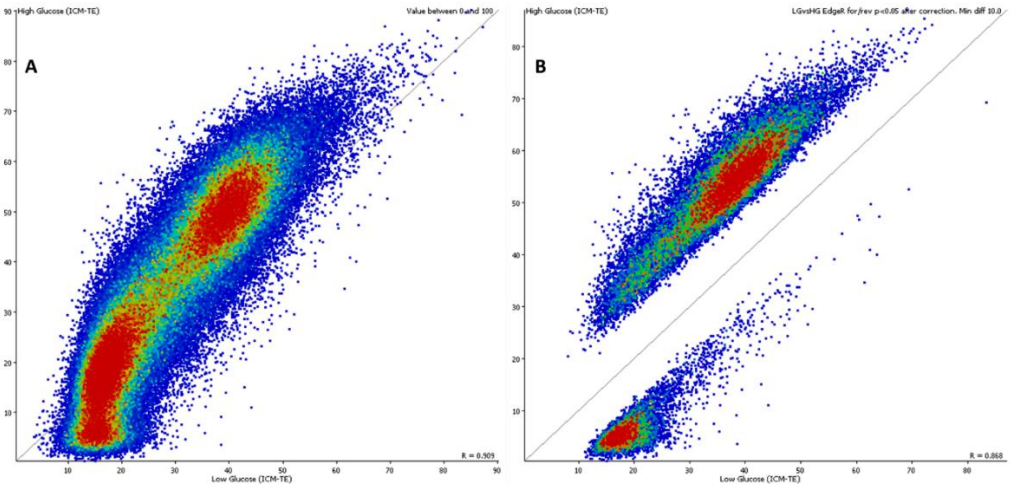

Figure 3.31. Correlation between Low glucose ICM+TE and High glucose ICM+TE. (Y-axis). Scatter plots showing the correlation between data groups of merged samples Low glucose ICM+TE (x-axis) and High glucose ICM+TE (y-axis). Each dot represents a Methylated Region (MR) spanning 100 methylated points (CpGs). A) Overall correlation of methylation levels for 285517 MRs in merged ICM+TE samples. The plots show a common scale for methylation levels (0-90%) in both data sets and a Pearson correlation value R=0.909. B) Correlation of 57737 DMRs resulted after EdgeR statistical test ($p < 0.05$, $\Delta\beta \geq 10\%$). The plots show a common scale for methylation levels (0-80%) in both data sets and a Pearson correlation value R=0.868.

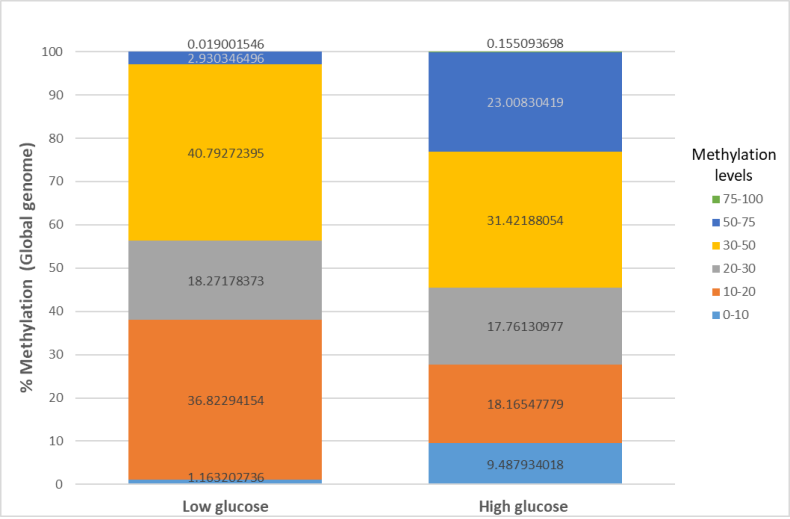

Figure 3.32. Distribution of methylation levels of human blastocysts in low and high glucose. The y-axis is indicating the percentage of abundance from 0-100 (Y-axis). Bars are representing the total (288,333 = 100%) of methylated regions per group. Each colour indicates a range of methylation levels and the numbers within the bars/colour are indicated the abundance of methylated regions.

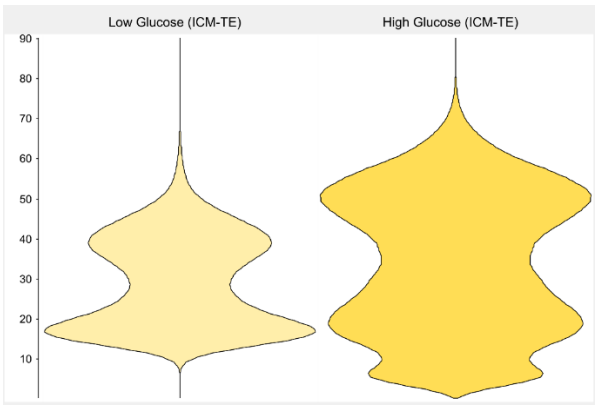

Figure 3.33 Mean Methylation levels in blastocysts. Bean plots showing the mean distribution of the global methylation levels (0-90%) in the Low glucose (left) and High glucose (right) groups. Each group is formed by five paired samples (5* ICM-TE) as per patient. Value above zero

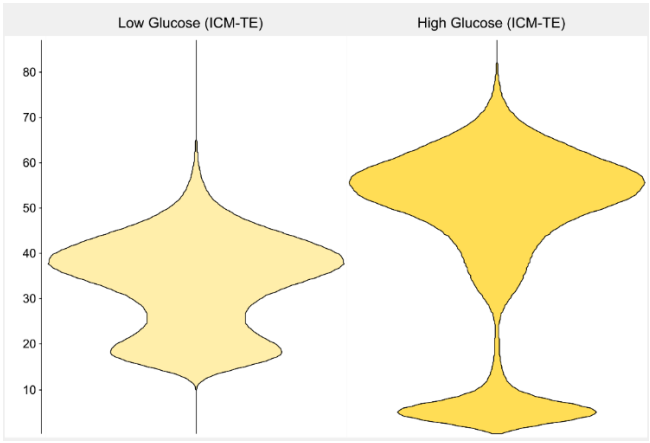

Figure 3.34 Mean Methylation levels in blastocysts after EdgeR. Bean plots showing the mean distribution of DMRs in the Low glucose (left) and High glucose (right) groups. DMRs were identified after applying the adjusted EdgeR test ($p < 0.05$, $\Delta\beta \geq 10\%$), 18.1% were hypomethylated and 81.9% hypermethylated when comparing High glucose vs Low glucose groups.

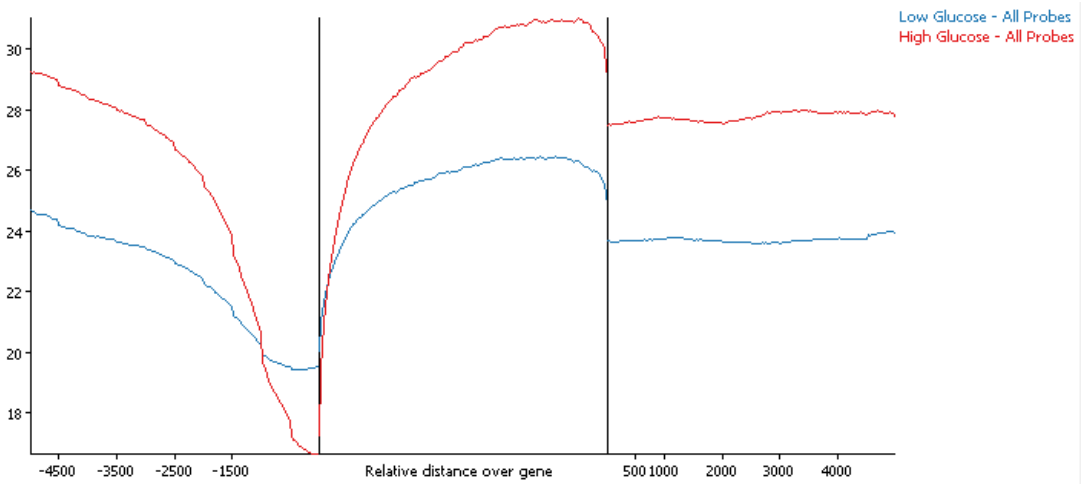

Figure 3.35 Quantitation trend plot for blastocyst. Showing the relative methylation levels of gene bodies ±5000bp in Low glucose (blue) and High glucose (red) groups. This representative plot shows the mean distribution of a gen body including its upstream and downstream regions (±5000 bp). Overall, low glucose samples are hypomethylated in the upstream region, gene body and downstream region in comparison with the high glucose samples. Interestingly, there is a small region about -500 to -1500 bp where the high glucose samples become hypomethylated.

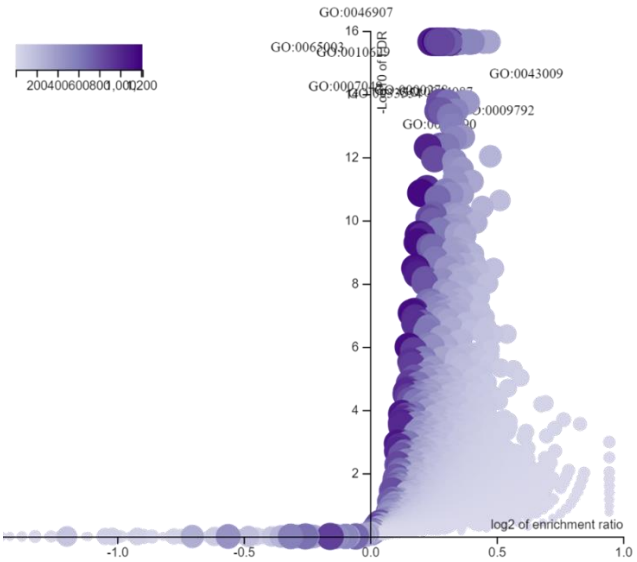

Gene Set	Description	Size	Expect	Ratio	P Value	FDR
GO:0000278	mitotic cell cycle	927	481.35	1.3130	0	0
GO:0007049	cell cycle	1739	902.99	1.2470	0	0
GO:0009790	embryo development	980	508.88	1.2813	0	0
GO:0009792	embryo development ending in birth or egg hatching	622	322.98	1.3283	0	0
GO:0010629	negative regulation of gene expression	1734	900.40	1.1839	0	0
GO:0033554	cellular response to stress	1867	969.46	1.1883	0	0
GO:0043009	chordate embryonic development	603	313.11	1.3286	0	0
GO:0044087	regulation of cellular component biogenesis	940	488.11	1.2559	0	0
GO:0046907	intracellular transport	1803	936.23	1.2016	0	0
GO:0065003	protein-containing complex assembly	1836	953.36	1.1832	0	0

Gene Set	Description	Size	Expect	Ratio	P Value	FDR
189960	TRACHEOESOPHAGEAL FISTULA WITH OR WITHOUT ESOPHAGEAL ATRESIA	21	1.4220	12.659	0	0
601626	LEUKEMIA, ACUTE MYELOID	22	1.4897	11.412	2.2204e-16	7.3275e-15
114480	BREAST CANCER	24	1.6251	10.461	1.7764e-15	3.9080e-14
125853	DIABETES MELLITUS, NONINSULIN-DEPENDENT	29	1.9637	9.1666	9.1038e-15	1.5021e-13
252010	MITOCHONDRIAL COMPLEX I DEFICIENCY	20	1.3542	10.338	8.2823e-13	1.0933e-11
114500	COLORECTAL CANCER	14	0.94797	11.604	3.4293e-11	3.7722e-10
176807	PROSTATE CANCER	13	0.88026	10.224	1.4806e-8	1.3960e-7
256000	LEIGH SYNDROME	17	1.1511	8.6873	2.1958e-8	1.8115e-7
171300	PHEOCHROMOCYTOMA	8	0.54170	12.922	4.5747e-8	3.0193e-7
187500	TETRALOGY OF FALLOT	8	0.54170	12.922	4.5747e-8	3.0193e-7

Figure 3.36. Gene set analyses for blastocysts 1. Gene ontology analysis obtained from DMRs overlapping genes in Low glucose vs High glucose groups (8654). Over Representation analysis (ORA) resulted in a volcano plot showing Enrichment ratio vs False Discovery Rate (-Log10 FDR), top biological functions obtained (blue table) and top biological diseases from OMIM database (orange table). False discover rate (FDR≤0.05).

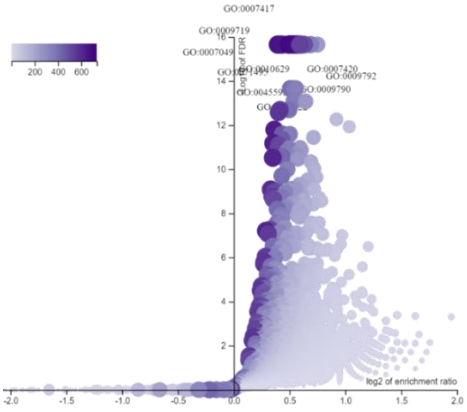

Gene Set	Description	Size	Expect	Ratio	P Value	FDR
GO:0007049	cell cycle	1739	450.45	1.3342	0	0
GO:0010629	negative regulation of gene expression	1734	449.16	1.4494	0	0
GO:0045595	regulation of cell differentiation	1699	440.09	1.3565	0	0
GO:0009719	response to endogenous stimulus	1595	413.15	1.3530	0	0
GO:0071495	cellular response to endogenous stimulus	1347	348.91	1.3958	0	0
GO:0009790	embryo development	980	253.85	1.6112	0	0
GO:0007417	central nervous system development	949	245.82	1.5133	0	0
GO:0060322	head development	758	196.35	1.5432	0	0
GO:0007420	brain development	714	184.95	1.5464	0	0
GO:0009792	embryo development ending in birth or egg hatching	622	161.12	1.6820	0	0

Gene Set	Description	Size	Expect	Ratio	P Value	FDR
601626	LEUKEMIA, ACUTE MYELOID	22	0.75031	18.659	4.4409e-16	2.9310e-14
189960	TRACHEOESOPHAGEAL FISTULA WITH OR WITHOUT ESOPHAGEAL ATRESIA	21	0.71621	12.566	9.9777e-9	3.2926e-7
608446	MYOCARDIAL INFARCTION, SUSCEPTIBILITY TOMYOCARDIAL INFARCTION, SUSCEPTIBILITY TO, 1, INCLUDED	13	0.44337	15.788	6.6670e-8	0.0000014667
114480	BREAST CANCER	24	0.81852	9.7737	6.9232e-7	0.000011423
176807	PROSTATE CANCER	13	0.44337	13.533	0.0000019890	0.000024350
187500	TETRALOGY OF FALLOT	8	0.27284	18.326	0.0000022137	0.000024350
125853	DIABETES MELLITUS, NONINSULIN-DEPENDENT	29	0.98905	8.0886	0.0000034961	0.000032964
211980	LUNG CANCERALVEOLAR CELL CARCINOMA, INCLUDED	17	0.57979	10.349	0.000012810	0.00010568
194070	WILMS TUMOR 1	6	0.20463	19.547	0.000018429	0.00013515
252010	MITOCHONDRIAL COMPLEX I DEFICIENCY	20	0.68210	8.7964	0.000036858	0.00024326

Gene Set	Description	P Value	FDR
PA443275	Adhesion	0	0
PA445752	Stress	0	0
PA165108622	Drug interaction with drug	8.9533e-12	8.1147e-9
PA443653	Cell Transformation, Neoplastic	2.8066e-11	1.8110e-8
PA446522	Neuroectodermal Tumors	3.4075e-11	1.8110e-8
PA444898	Medulloblastoma	3.9963e-11	1.8110e-8
PA447230	HIV	9.7995e-11	3.8064e-8
PA446668	Neoplasms, Basal Cell	1.9176e-10	6.5173e-8
PA446836	Craniofacial Abnormalities	3.7575e-10	1.1065e-7
PA166123207	overall survival	4.0694e-10	1.1065e-7

Figure 3.37. Gene set analyses for blastocysts 2. Gene ontology analysis of hypermethylated regions in low glucose overlapping genes (4317). Over Representation analysis (ORA) resulted in a volcano plot showing Enrichment ratio vs False Discovery Rate (-Log10 FDR), top biological functions obtained (blue table) and top biological diseases from OMIM database (orange table). False discover rate (FDR≤0.05).

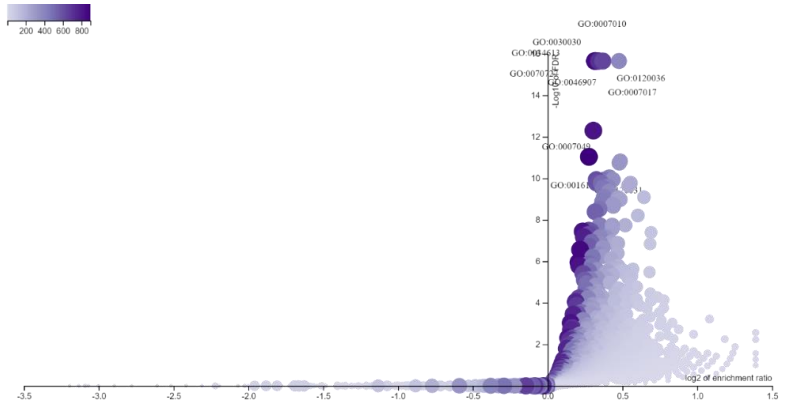

Gene Set	Description	Size	Expect	Ratio	P Value	FDR
GO:0070727	cellular macromolecule localization	1825	696.23	1.2453	0	0
GO:0034613	cellular protein localization	1815	692.41	1.2449	0	0
GO:0046907	intracellular transport	1803	687.84	1.2503	0	0
GO:0030030	cell projection organization	1522	580.64	1.2659	0	0
GO:0120036	plasma membrane bounded cell projection organization	1488	567.66	1.2684	0	0
GO:0007010	cytoskeleton organization	1300	495.94	1.2905	0	0
GO:0007017	microtubule-based process	729	278.11	1.3915	0	0
GO:0007049	cell cycle	1739	663.42	1.2360	4.4409e-16	5.0465e-13
GO:0016192	vesicle-mediated transport	1942	740.86	1.2107	9.1038e-15	9.1959e-12
GO:0120031	plasma membrane bounded cell projection assembly	588	224.32	1.3998	1.6431e-14	1.4938e-11

Gene Set	Description	Size	Expect	Ratio	P Value	FDR
114480	BREAST CANCER	24	1.2009	11.658	4.9849e-13	3.2900e-11
189960	TRACHEOESOPHAGEAL FISTULA WITH OR WITHOUT ESOPHAGEAL ATRESIA	21	1.0508	12.372	1.2045e-12	3.9748e-11
125853	DIABETES MELLITUS, NONINSULIN-DEPENDENT	29	1.4511	9.6480	1.5775e-11	3.4704e-10
114500	COLORECTAL CANCER	14	0.70052	14.275	6.6452e-11	1.0965e-9
601626	LEUKEMIA, ACUTE MYELOID	22	1.1008	9.9925	1.6347e-9	2.1578e-8
114550	HEPATOCELLULAR CARCINOMA	9	0.45034	15.544	2.3453e-8	2.5799e-7
252010	MITOCHONDRIAL COMPLEX I DEFICIENCY	20	1.0007	8.9933	1.7122e-7	0.0000016144
608089	ENDOMETRIAL CANCER	5	0.25019	19.985	2.9908e-7	0.0000024674
256000	LEIGH SYNDROME	17	0.85063	9.4047	5.6390e-7	0.0000041352
176807	PROSTATE CANCER	13	0.65049	10.761	9.4061e-7	0.0000062080

Gene Set	Description	P Value	FDR
PA443455	Ataxia Telangiectasia	2.2982e-14	6.2487e-11
PA445428	Protein Deficiency	1.2714e-12	1.7285e-9
PA444146	Fanconi Anemia	5.3083e-11	4.3372e-8
PA445752	Stress	6.3805e-11	4.3372e-8
PA443919	Disease Susceptibility	7.3263e-10	3.9841e-7
PA165108622	Drug interaction with drug	3.4282e-9	0.0000015535
PA444939	Metabolism, Inborn Errors	5.4476e-9	0.0000021134
PA153906318	Autism Spectrum Disorder	6.2182e-9	0.0000021134
PA443454	Ataxia	7.6742e-9	0.0000023185
PA445914	Translocation, Genetic	9.9365e-9	0.0000027017

Figure 3.38. Gene set analyses for blastocysts 3. Gene ontology analysis of hypermethylated regions overlapping genes in high glucose (4337). Over Representation analysis (ORA) resulted in a volcano plot showing Enrichment ratio vs False Discovery Rate (-Log10 FDR), top biological functions obtained (blue table) and top biological diseases from OMIM database (orange table). False discovery rate (FDR≤0.05).

3.7.7 Differential methylation on H3K4me3 sites

Histone modifications are essential for regulating gene expression in development. Different types of histone modifications have diverse functions and define distinct genomic elements [141]. For example, trimethylated histone H3 lysine 4 (H3K4me3) is a conserved hallmark of promoters and transcriptional initiation [142].

Potentially active promoters were mapped using published date sets (accession number GSE124718) for ChIP H3K4me3 on ICM. Called picks on ChIP-seq analyses were used as guide to select regions within the blastocysts (ICM + TE) genome that could evaluate further. From these mapped regions, I have identified those differentially methylated between the low and high glucose groups. Groups were compared using EdgeR test with the filtering criterion of adjusted p value ($p < 0.05$) and difference in methylation greater than 10% ($\Delta\beta \geq 10$percentage). Figure 3.39 clearly shows how DMRs from high glucose are can have very high or very low levels of methylation (0-100%) whereas DMRs from low glucose samples are concentrated at mid-levels of methylation.

762 DMRs were identified in total, from which 338 were hyperactive methylated in low glucose and 424 in high glucose. Differentially methylated genes were analysed by ORA and ten gene sets were enriched for the category of biological function (Figure 3.40) with a significant p-value but non-significant FDR. Interestingly, these gene sets have been related to neurological disorders and cancer according to KEGG and OMIM databases.

Hypermethylated regions in low glucose (338) which resulted in 329 gene IDs were unambiguously mapped by ORA where ten gene sets were enriched for the category of biological function (Figure 3.41) with a significant p-value but non-significant FDR. Moreover, genes CDKN2A, DAPK3, E2F3, MAP2K2, RASSF1 resulted enriched for the Bladder cancer pathway KEGG:05219 with adjusted p-value 0.02840.

Hypermethylated regions in high glucose (424) resulted in 314 gene IDs were unambiguously mapped by ORA where ten gene sets were enriched for the category of biological function (Figure 3.42) with a significant p-value and only four with significant FDR. Moreover, genes CNOT3, CNOT6L (CCR4), DDX6, EDC4, EXOSC10

(RRP6), EXOSC3 (RRP40), LSM4, PFKL, XRN1 resulted enriched for the RNA degradation pathway KEGG:03018 with adjusted p-value 0.007904.

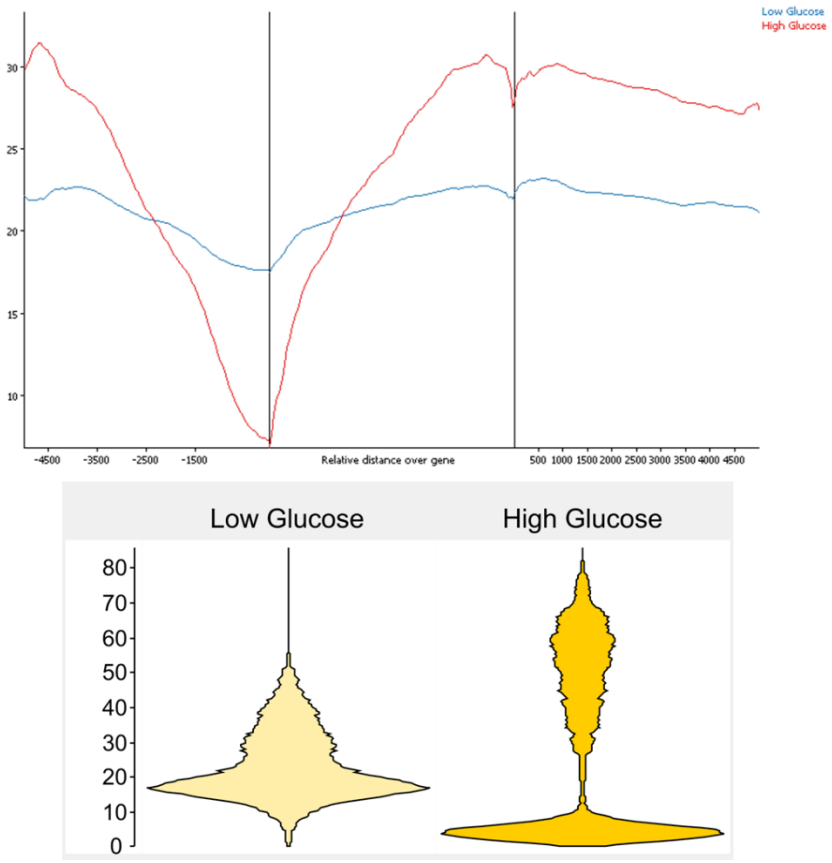

Figure 3.39. Methylated H3K4me3 sites. Representative plots of potentially active promoters from blastocysts cultured in low and high glucose. DMRs were identified by comparing high glucose and low glucose blastocysts. Bean plot is indicating abundance of DMRs distributed by percentage of methylation (Y-axis) and comparing distribution between low glucose and high glucose. Trend plot indicates the mean methylation levels from all mapped regions (H3K4me3) ±5Kb in low glucose (blue) and high glucose (red).

Gene Set	Description	P Value	FDR
GO:0046700	heterocycle catabolic process	0.000037582	0.087579
GO:0007034	vacuolar transport	0.000012358	0.087579
GO:0051276	chromosome organization	0.00049514	0.50015
GO:1990090	cellular response to nerve growth factor stimulus	0.0010945	0.55281
GO:0032801	receptor catabolic process	0.00097896	0.55281
GO:0010629	negative regulation of gene expression	0.00093663	0.55281
GO:0009890	negative regulation of biosynthetic process	0.00084608	0.55281
GO:0007156	homophilic cell adhesion via plasma membrane adhesion molecules	0.00064896	0.55281
GO:0044772	mitotic cell cycle phase transition	0.0013088	0.60263
GO:0006851	mitochondrial calcium ion transmembrane transport	0.0013258	0.60263

Figure 3.40. Gene set analysis for H3K43me sites. Gene ontology analysis of differentially methylated genes overlapping H3K4me3 sites. Over Representation, analysis (ORA) resulted in a table showing Enrichment p-value and False Discovery Rate (FDR).

Gene Set	Description	P Value	FDR
GO:0007156	homophilic cell adhesion via plasma membrane adhesion molecules	0.000079784	0.72532
GO:0007286	spermatid development	0.00049867	1
GO:0048515	spermatid differentiation	0.00067013	1
GO:0007281	germ cell development	0.00070901	1
GO:1900112	regulation of histone H3-K9 trimethylation	0.00078630	1
GO:0032802	low-density lipoprotein particle receptor catabolic process	0.0010102	1
GO:0098742	cell-cell adhesion via plasma-membrane adhesion molecules	0.0013313	1
GO:0008333	endosome to lysosome transport	0.0022560	1
GO:0036124	histone H3-K9 trimethylation	0.0022915	1
GO:1902581	multi-organism cellular localization	0.0024403	1

Figure 3.41. Gene set analysis for H3K43me sites 2. Gene set analysis for H3K43me sites. Gene ontology analysis of hypermethylated genes overlapping H3K4me3 sites in low glucose blastocysts. Over Representation, analysis (ORA) resulted in a table showing Enrichment p-value and False Discovery Rate (FDR).

Gene Set	Description	P Value	FDR
GO:0046700	heterocycle catabolic process	0.0000046103	0.021575
GO:0044270	cellular nitrogen compound catabolic process	0.0000047466	0.021575
GO:0034655	nucleobase-containing compound catabolic process	0.000010942	0.033158
GO:0019439	aromatic compound catabolic process	0.000020718	0.047088
GO:1901361	organic cyclic compound catabolic process	0.000046741	0.084984
GO:0000956	nuclear-transcribed mRNA catabolic process	0.000072592	0.10999
GO:0007264	small GTPase mediated signal transduction	0.00010372	0.13471
GO:0010629	negative regulation of gene expression	0.00041011	0.46604
GO:0007034	vacuolar transport	0.00081319	0.59465
GO:0000082	G1/S transition of mitotic cell cycle	0.00083430	0.59465

Figure 3.42. Gene set analysis for H3K43me sites 3. Gene set analysis for H3K43me sites. Gene ontology analysis of hypermethylated genes overlapping H3K4me3 sites in high glucose blastocysts. Over Representation, analysis (ORA) resulted in a table showing Enrichment p-value and False Discovery Rate (FDR).

3.7.8 Differential methylation on H3K27me3 sites

Histone modifications are essential for regulating gene expression in development. Different types of histone modifications have diverse functions and define distinct genomic elements [141]. H3K27me3 is a repressive histone mark preferentially occupying the promoters of developmental genes ICM [142]

Potential repressor sites were mapped using the published report for ChIP H3K27me3 (accession number GSE124718). Called picks were used as guide to select regions within the blastocysts genome that were further evaluated to obtain differentially methylated regions (DMRs).

Mean methylation levels from all H3K27me3 sites have been represented in a trend plot for low glucose and high glucose blastocysts (Figure 3.43). Besides, from this mapped regions, those differentially methylated between the low and high glucose were represented by bean plot in the same figure. DMRs were identified using EdgeR test with the filtering criterion of adjusted p value ($p < 0.05$) and difference in methylation greater than 10% ($\Delta\beta \geq 10\%$). 4452 DMRs were identified in total, from which 588 were hypermethylated in low glucose and 3864 in high glucose.

Hypermethylated regions in low glucose (588) resulted in 453 gene IDs that were unambiguously mapped for gene ontology analysis (Figure 3.44). Although, these gene sets did not show a significant FDR, they have shown a significant p-value.

On the other hand, hypermethylated regions in high glucose (3864) resulted in 1716 gene IDs that were unambiguously mapped for gene ontology analysis (Figure 3.45). This analysis resulted in 10 gene sets significantly enriched and 15 signalling pathways, which are particularly related to neurological disorders, cardiovascular disorders and cancer (Table 3.8).

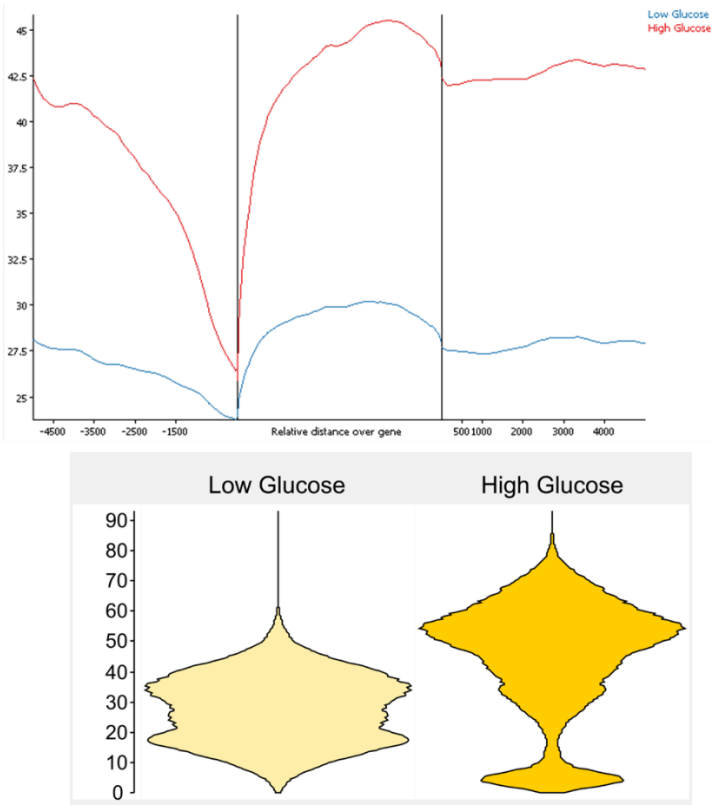

Figure 3.43. Distribution of methylation levels from H3k27me3 sites. DMRs were identified by comparing high glucose and low glucose blastocysts. Bean plot is indicating abundance of DMRs distributed by percentage of methylation (Y-axis). Trend plot indicates the mean methylation levels from all mapped sites (H3K27me3) ±5Kb in low glucose (blue) and high glucose (red).

geneSet	description	pValue	FDR
GO:1903707	negative regulation of hemopoiesis	1.97E-05	0.085827
GO:0051093	negative regulation of developmental process	2.40E-05	0.085827
GO:0022610	biological adhesion	2.83E-05	0.085827
GO:0003006	developmental process involved in reproduction	1.15E-04	0.102922

Figure 3.44. Gene set analysis for H3K27me3 sites 1**.** Hypermethylated H3K27me3 sites in low glucose overlapping genes. Over Representation analysis of 453 genes resulted in four enriched sets with a significant p-value and non-significant false discovery rate (FDR).

Gene Set	Description	P Value	FDR
GO:0051056	regulation of small GTPase mediated signal transduction	3.4993e-10	0.0000031812
GO:0007010	cytoskeleton organization	5.2156e-8	0.00016570
GO:0046578	regulation of Ras protein signal transduction	5.4681e-8	0.00016570
GO:0030029	actin filament-based process	8.7990e-8	0.00019998
GO:0007264	small GTPase mediated signal transduction	3.2675e-7	0.00059409
GO:0030036	actin cytoskeleton organization	5.4472e-7	0.00082534
GO:1902531	regulation of intracellular signal transduction	0.0000019917	0.0020394
GO:0022008	neurogenesis	0.0000020013	0.0020394
GO:0048699	generation of neurons	0.0000020190	0.0020394
GO:0030030	cell projection organization	0.0000023024	0.0020931

Figure 3.45. Gene set analysis for H3K27me3 sites 2. Hypermethylated H3K27me3 sites in high glucose overlapping genes. Over Representation analysis of 1716 genes resulted in 10 enriched sets with a significant p-value and false discovery rate (FDR).

Pathway	**ID**	**p_{adj}**
Dopaminergic synapse	KEGG:04728	1.30179E-05
Cholinergic synapse	KEGG:04725	2.25024E-05
MAPK signalling pathway	KEGG:04010	3.063×10-3
Morphine addiction	KEGG:05032	0.000640067
AMPK signalling pathway	KEGG:04152	0.00078878
Sphingolipid signalling pathway	KEGG:04071	0.002481632
Long-term depression	KEGG:04730	0.005543611
Growth hormone synthesis, secretion and action	KEGG:04935	0.006466461
GABAergic synapse	KEGG:04727	0.007914779
Relaxin signalling pathway	KEGG:04926	0.008596152
Chronic myeloid leukaemia	KEGG:05220	0.010269685
Glutamatergic synapse	KEGG:04724	0.010919087
GnRH secretion	KEGG:04929	0.01516909
Pathways in cancer	KEGG:05200	0.035923367
Human papillomavirus infection	KEGG:05165	0.037538467

Table 3.8. Signalling pathways resulted from hypermethylated H3K27me3 sites in high glucose. Gene profiling analysis was performed over resulted in a table showing Enrichment p-value and False Discovery Rate (FDR).

3.7.9 Differential methylation on CpG islands (CGI)

CpG islands were mapped for Homo sapiens genome GRCh38. Every CpG island was counted as a potentially methylated region independently of the CG occurrences or methylated points contained per island. The mean distribution of methylation levels in CpG islands is represented in a trend plot (Figure 3.46) from all mapped regions (22568 CpG islands) ±1Kb in low glucose and high glucose. Here we can observe that CpG island are hypermethylated in low glucose.

Bisulfite pipeline (Bismark) was used for quantification of methylation levels and EdgeR was used for the statistical analysis with a significance below 0.05 plus Benjamimi and Hochberg correction with a minimum difference of 20.0%. Data represented in Figure 3.47. A total of 858 differentially methylated CpG islands were identified, which are found overlapping 780 genes. These have been identified with a significant increase in mean values of methylation for the low glucose blastocysts group, with a minimum difference of 20% relative to the high glucose group. Gene ontology analysis was performed and we to obtained enriched gene sets in the category of biological processes with p-value and FDR <0.05 (Figure 3.48). Additionally, some of the diseases related to these genes included Aplastic Anaemia, Pulmonary Fibrosis, Idiopathic, Prostate Cancer, Mitochondrial Complex I Deficiency, Leukaemia, Acute Myeloid, Early Infantile Epileptic encephalopathy, Autosomal dominant mental retardation according to OMIM and KEGG.
Hypermethylated regions in low glucose samples resulted in 560 genes overlapped by CpGi sites. These genes went through ORA to determine enriched gene ontology for biological processes (Figure 3.49).

Hypermethylated regions in high glucose samples resulted 220 genes overlapped by CpGi sites. These genes went through ORA to determine enriched gene ontology for biological processes (Figure 3.50). Moreover, it resulted in the enrichment of the Endocrine resistance pathway KEGG:01522 due to the following genes: ADCY6 (AC), CARM1 (CoA), GPER1 (GPR30), JAG2 (Jagged), NOTCH1 (Notch), SHC2 (Shc). (Figure 3.51)

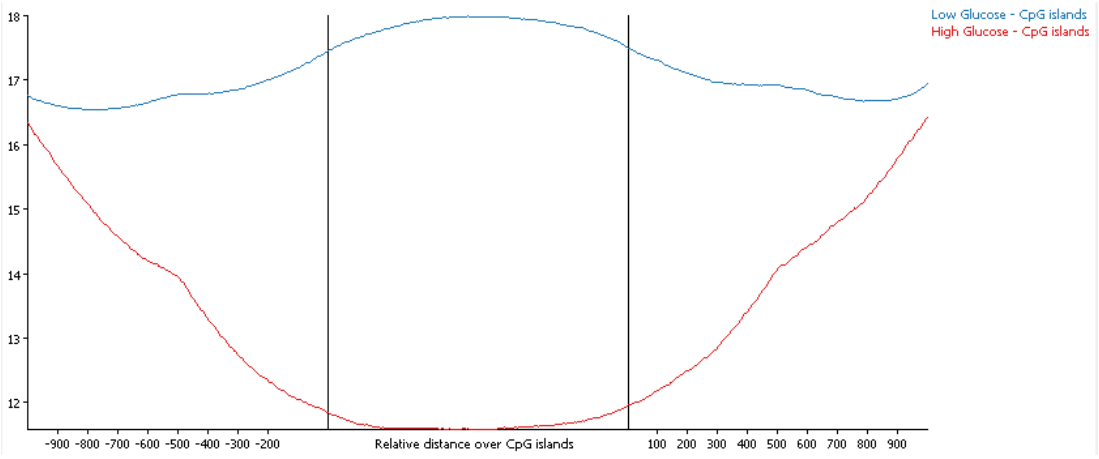

Figure 3.46. Distribution of methylation levels in CpGi. Trend plot indicates the mean methylation levels from all mapped regions (22568 CpG islands) ±1Kb in low glucose (blue) and high glucose (red).

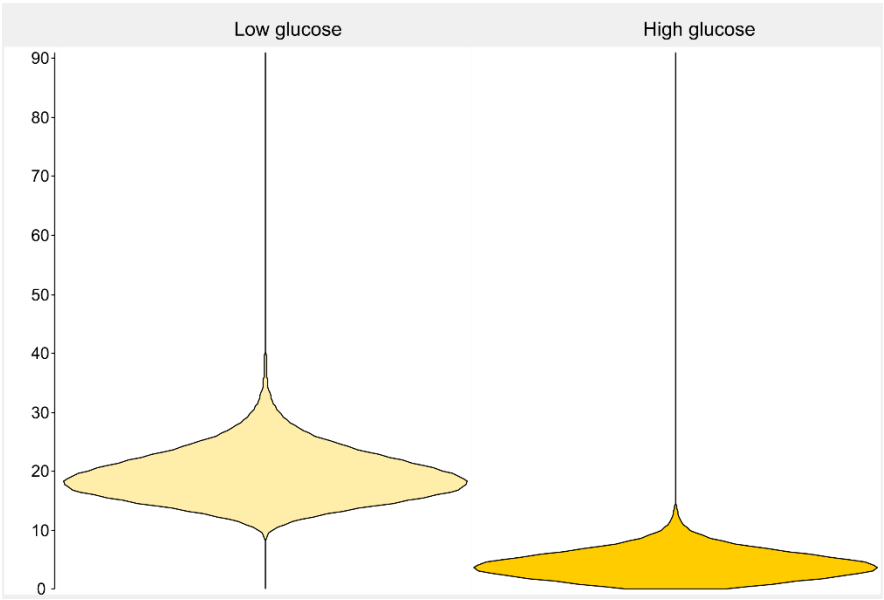

Figure 3.47. Methylation levels on CpG islands. Bean plots indicating percentage of methylation (Y-axis) and sample IDs (X-axis) for DMRs identified in this section, comparing distribution in high glucose vs low glucose. Differentially methylated regions (858) were identified between the two groups after applying Bismark quantification and EdgeR statistical analysis with a significance below 0.05 after Benjamin and Hochberg correction with a minimum difference of 20%.

Gene Set	Description	P Value	FDR
GO:0022008	neurogenesis	0.0000037507	0.018887
GO:0120036	plasma membrane bounded cell projection organization	0.0000049733	0.018887
GO:0007049	cell cycle	0.0000090106	0.018887
GO:0030030	cell projection organization	0.000011368	0.018887
GO:0048699	generation of neurons	0.000013400	0.018887
GO:0071826	ribonucleoprotein complex subunit organization	0.000013865	0.018887
GO:0044770	cell cycle phase transition	0.000016349	0.018887
GO:0022618	ribonucleoprotein complex assembly	0.000017993	0.018887
GO:0044772	mitotic cell cycle phase transition	0.000018698	0.018887
GO:0030182	neuron differentiation	0.000029607	0.026916

Figure 3.48. Gene set analysis for CpG islands 1. Over representation analysis from differentially methylated CpG islands. ORA was performed to obtain gene ontology. The analysis evaluated 780 genes that were found overlapping differentially methylated CpG islands when comparing high and low glucose blastocysts.

Gene Set	Description	P Value	FDR
GO:0009790	embryo development	0.0000059353	0.053958
GO:0071651	positive regulation of chemokine (C-C motif) ligand 5 production	0.00011367	0.22167
GO:0023056	positive regulation of signaling	0.00013726	0.22167
GO:0030509	BMP signaling pathway	0.00014025	0.22167
GO:0010647	positive regulation of cell communication	0.00022081	0.22167
GO:0009792	embryo development ending in birth or egg hatching	0.00022522	0.22167
GO:0048812	neuron projection morphogenesis	0.00022522	0.22167
GO:0032990	cell part morphogenesis	0.00024467	0.22167
GO:0071772	response to BMP	0.00030937	0.22167
GO:0071773	cellular response to BMP stimulus	0.00030937	0.22167

Figure 3.49. Gene set analysis for CpG islands 2. Over representation analysis from hypermethylated, CpGi sites in low glucose. ORA was performed to obtain gene ontology in the biological process category. The analysis evaluated 560 genes that were found overlapping hypermethylated CpG islands in low glucose blastocysts relative to high glucose.

Gene Set	Description	P Value	FDR
GO:0019081	viral translation	0.0000057290	0.031420
GO:0075525	viral translational termination-reinitiation	0.0000069123	0.031420
GO:0000209	protein polyubiquitination	0.000018637	0.056475
GO:0032446	protein modification by small protein conjugation	0.000025164	0.057191
GO:0075522	IRES-dependent viral translational initiation	0.000080262	0.14593
GO:0016567	protein ubiquitination	0.00010602	0.14730
GO:0070647	protein modification by small protein conjugation or removal	0.00012099	0.14730
GO:0070936	protein K48-linked ubiquitination	0.00012962	0.14730
GO:0030812	negative regulation of nucleotide catabolic process	0.00018756	0.17051
GO:0051198	negative regulation of coenzyme metabolic process	0.00018756	0.17051

Figure 3.50. Gene set analysis for CpG islands 3. Over representation analysis from hypermethylated, CpGi sites in high glucose. Functional analysis was performed to obtain gene ontology. The analysis evaluated 220 genes that were hypermethylated in high glucose blastocysts relative to low glucose.

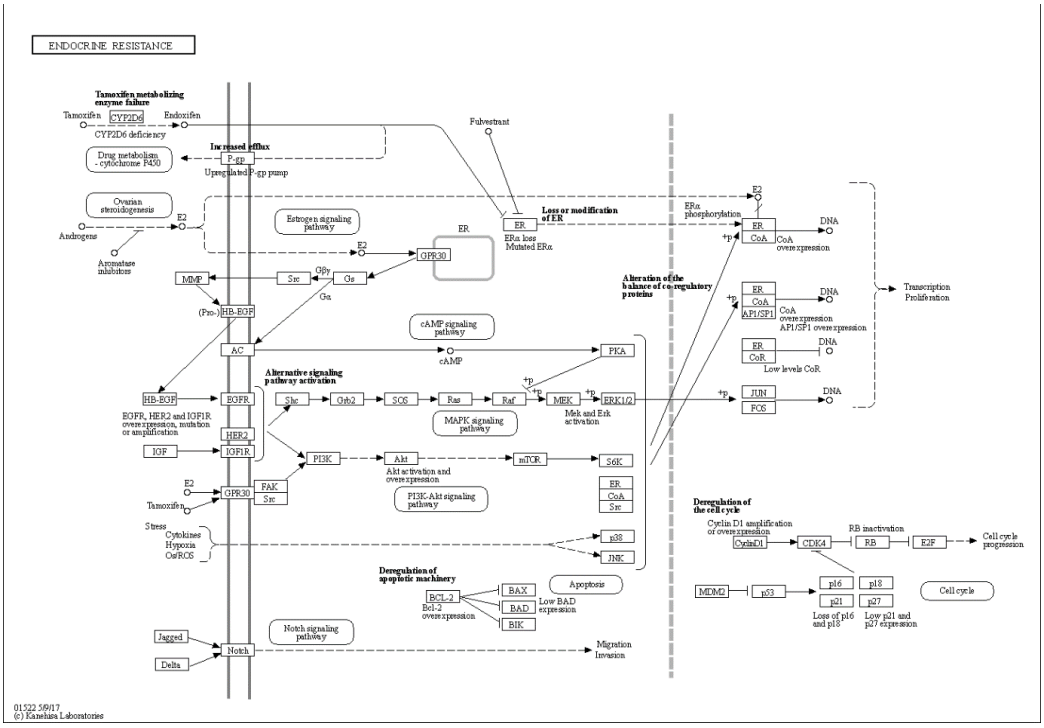

Figure 3.51. Endocrine resistance pathway (KEGG:01522)
Functional gene profiling was performed from 220 genes (overlapping CpGi) that were hypermethylated in high glucose blastocysts. Six genes resulted significant for Endocrine resistance pathway (p=0.019). Genes are named as follows: ADCY6 (AC), CARM1 (CoA), GPER1 (GPR30), JAG2 (Jagged), NOTCH1 (Notch), SHC2 (Shc).

3.7.10 Imprinted genes

Genomic imprinting is a form of epigenetic gene regulation that results in expression from a single allele in a parent-of-origin-dependent manner. This form of mono-allelic expression affects a small number of genes that are essential in mammalian development [143]. In normal development, these genes play important roles in regulating embryonic growth, placental function and neurobehavioral processes [144]. Genomic imprinting is typically regulated by differential DNA methylation inherited from gametes [131].

A descriptive analysis was performed to investigate the effect of glucose concentration on reported imprinted genes in humans. Imprinted genes (Table 3.9) were mapped the SeqMonk software (Homo sapiens genome GRCh38) according to detailed location from the Imprinted library from the University of Otago (https://www.otago.ac.nz). Every imprinted gene was counted as a whole potential methylated region independently of the methylated points (CG occurrences) contained per region. Bisulfite pipeline (Bismark) was used for quantification of methylation levels and EdgeR was used for the statistical analysis with a significance below 0.05 plus Benjamimi and Hochberg correction with a minimum difference of 10.0%.

The mean distribution of methylation levels in each imprinted gene is represented by a trend plot (Figure 3.52) were mapped regions are represented as gene bodies ±1Kb. Trend plots allow comparison of gene body, upstream and downstream region from low glucose and high glucose blastocysts (ICM+TE). Resulted plots are shown only for those genes that presented significant differences between the high and low glucose conditions (Figure 3.52). CDKN1C showed methylation levels from 2 to 20% where the low glucose group was hypermethylated. KCNQ1 showed methylation levels from 30 to 50% where the high glucose group was hypermethylated. ERLIN2 with methylation levels from 20 to 50% where the high glucose group was hypermethylated. TRAPPC9 with methylation levels from 35 to 55% where the low glucose group was hypermethylated from the upstream region to gene body, and hypomethylated in the downstream region. NESP55 presented methylation levels from 10 to 50% where the low glucose group was hypermethylated from the upstream region to gene body, and hypomethylated in the downstream region. Finally, ZFP57 with methylation levels from

5 to 45% where the high glucose group was hypermethylated in the upstream and downstream region, and it was hypomethylated in the gene body.

Chr.	Gene	Allele	Chr.	Gene	Allele
1	p73	M	11	TSSC3	M
1	ARHI	P	11	ZNF215	M
1	PPIEL	M	11	WT1	M/P*(AS)
1	DIRAS3 (DMR3)	M	11	KCNQ1OT1	M
1	DIRAS3 (DMR2)	M	11	H19	M
4	NAP1L5	M	13	HTR2A	M*
6	HYMAI	P	14	MEG3	M
6	PLAGL1	P	15	MKRN3	P(AS)
6	FAM50B	M	15	NDN	P
7	GRB10	M/P*	15	MAGEL2	P
7	COPG2	P*	15	SNRPN	P
7	PEG10/SGCE	M	15	IPW	P
7	MEST/MESTIT1	M	15	UBE3A	M(AS)
7	HTR5A/HTR5A-AS	M	16	ZNF597	P
8	LOC728024/ERLIN2	M	19	ZNF331	M
8	TRAPPC9	M	19	PEG3	M
10	INPP5F	M	20	GNAS	M/P(AS)
11	H19	M	20	PSIMCT1/HM13	M
11	IGF2	P(AS)	20	NNAT	M
11	ASCL2	M	20	L3MBTL1	M
11	MTR1	P	20	NESPAS	M
11	KCNQ1	M(AS)	20	NESP55	P
11	CDKN1C	M	22	NHP2L1	M
11	SLC22A1L	M	X	XIST	P

Table 3.9. Imprinted genes. Updated list obtained from database https://www.otago.ac.nz [144]

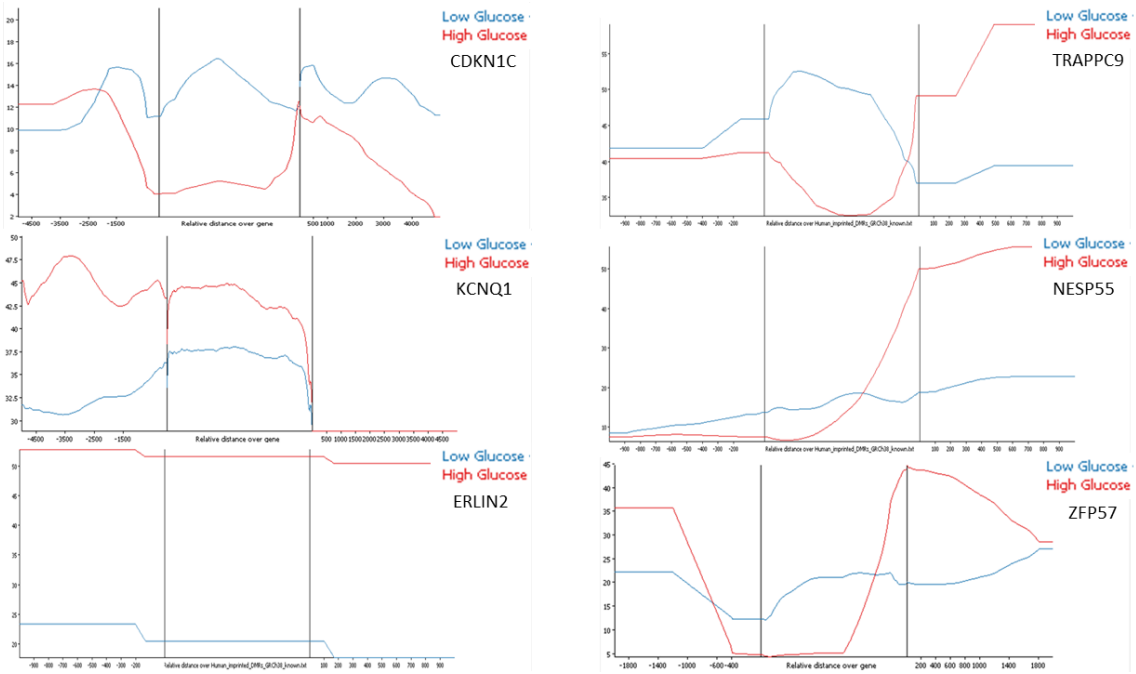

Figure 3.52 Quantitative trend plots of imprinted genes. Levels of methylation are distributed across the gene (upstream, gene body, downstream). Each gene showed different methylation levels (y-axis). CDKN1C from 2 to 20%, KCNQ1 from 30 to 50%, ERLIN2 from 20 to 50%, TRAPPC9 from 35 to 55%, NESP55 from 10 to 50%, ZFP57 from 5 to 45%. EdgeR for/rev Stats Filter on probes where High Glucose vs Low Glucose had a significance below 0.05 after Benjamini-Hochberg correction with a minimum difference of 10.0

3.8 Discussion

Assisted reproduction technologies have provided a unique window into the metabolic processes that drive embryonic development from a fertilized ovum to a competent blastocyst. Although early literature focused on the substrates and culture conditions required for progress through embryonic development, more recent studies suggest that the surrounding environment can alter the epigenome, which can, in turn, impact upon embryonic metabolism and developmental competence [3]. It has been well studied that nutritional perturbations during the preimplantation period can modify development throughout gestation and even affect the physiological, neurological and metabolic health of adult offspring [38] [50].

Of particular interest to this research, previous studies have compared different culture media, demonstrating that embryos on Day 6 after conception can show differential gene expression and differential DNA methylation [145] [115]. Additionally, placentas have shown changes in DNA methylation patterns, specifically when comparing natural versus IVF conceptions [146]. The present study was specifically designed to determine how changes in glucose concentration, oxygen concentration or cryopreservation methods used in assisted reproduction (until Day 6) can influence global methylation, gene expression and mitochondria function in the preimplantation embryo.

Oxygen tension used for embryo culture in IVF clinics varies dramatically between laboratories around the world. Surprisingly, to date around 75% of the world's IVF clinics employ atmospheric oxygen for some or all of the culture process, which makes it more difficult to determine the impact of specific components within the IVF laboratory on embryo phenotype [40].

Although oxygen levels in the human female reproductive tract have not been measured, levels in the oviduct of several mammalian species have been reported to be between 2 and 8% [147]. Whereas the oxygen concentration in the uterus appears to be lower than in the oviduct, ranging from 5% in the hamster and rabbit to 1.5% in the rhesus monkey [92].

There are controversial results about the effect of oxygen at atmospheric tension (20%) on human embryo development. However, most of the studies reported a beneficial effect when lowering atmospheric oxygen tension to 5 % on embryo quality and pregnancy rates, mainly in trials in which embryos were transferred at the blastocyst stage [148] [149]. Oxygen and culture media were of crucial importance for affecting the gene expression of *in vitro* cultured human preimplantation embryos [150].

It has been determined that in mammals, embryo development and implantation post transfer are significantly decreased when embryos are cultured in the presence of atmospheric oxygen. More specifically, exposure to atmospheric oxygen was found to alter embryo developmental kinetics, transcription, histone remodelling and methylation patterns, the proteome and metabolic state [40].

To identify the impact of oxygen on gene expression, mRNAs with a long poly(A) tail were selectively measured using the PolyA-PCR method [151] and qPCR [139]. Forty-eight transcripts were evaluated in this study (Table 2.16) with the aim of determining the impact of oxygen and glucose concentration.

In this study, non-significant differences were found for cell survival markers *(BAX, BCL2, BCL2L1, CBL, DAP3, TP53)* in the oxygen or glucose experiments. From the cell growth and differentiation group of genes (*CDX2, EGFR, EOMES, EP300, FGF4, and ZSCAN4*) only *EOMES* was found upregulated in embryos cultured at 20% oxygen relative to 5% oxygen. However, *EOMES* expression was not affected by glucose concentration. This gene is important to determine trophectoderm (TE) differentiation and its expression has been affected by culture media in other studies, whereas LIF factor has been found to promote *EOMES* expression [152]. *EOMES* has also been affected by cryopreservation methods, as it has been found downregulated in fresh embryos, relative to frozen embryos [153].

Pluripotency makers (*NANOG, OCT4, and SOX2*) did not show significant differences when comparing oxygen concentration. However, *OCT4* showed a tendency to be upregulated in 20% oxygen. On the other hand, *OCT4* and *SOX2* were significantly upregulated in high glucose, relative to low glucose. These three markers have also

been evaluated in other studies, for instance *they* were found downregulated in fresh embryos, relative to frozen embryos [153]. *OCT4* has been found upregulated in embryos grown in ESCM medium relative to KSOM medium [154].

DNA methyltransferases (DNMTs) are primarily responsible for placing methyl groups on CpG dinucleotides, whereas the ten-eleven translocation (TET) family proteins remove methyl groups. *DNMT1* is primarily responsible for maintaining CpG methylation once these marks have been established. *DNMT3A* and *DNMT3B* carry out de novo DNA methylation, which is important in embryo and tissue development as well as differentiation [38]. In this study, DNA methyltransferases *DNMT1*, *DNMT3A*, *DNMT3B*) were not differentially regulated when comparing between 5% and 20% oxygen. However, the expression of *DNMT1* and *DNMT3A* showed a tendency to be upregulated in 20% oxygen. In regards to glucose concentration, *DNMT3A* was significantly upregulated in high glucose, whereas expression of *DNMT1* and *DNMT3B* were not significantly different between high glucose and low glucose groups, although they tend to be upregulated in high glucose. This could suggest that high glucose concentration could be associates with higher levels of de novo methylation. *DNMT3A* has been found differentially regulated due to the media composition but not due to oxygen concentration [149].

The TET enzymes (*TET1*, *TET2*, and *TET3*) oxidize 5mC to 5hmC. Together with passive loss of 5mC during DNA replication, TET enzymes are part of the mechanisms involved in the reprogramming of DNA methylation during early embryo development [106]. Exposure- induced oxidative stress has been shown to alter TET enzyme expression, leading to altered 5hmC levels at numerous imprinted loci, which indicates that environmental toxicants also can alter long-term imprinted gene regulation [104]. In this study, TET enzymes (*TET1*, *TET2*, *TET3*) were not affected by oxygen concentration but *TET1* and *TET2* where upregulated in high glucose, relative to low glucose. This suggests that low glucose concentration in culture media could be associated with higher levels of demethylation during preimplantation development.

Mitochondrial activity marker *TIMM23* was significantly upregulated in high glucose relative to low glucose, whereas *TRMT10C* was not significantly affected by glucose. In addition, both markers were not affected when comparing 5% oxygen and 20%

oxygen. *TIMM23* has been reported upregulated by embryo culture in Whitten's medium relative to KSOM medium [149]. Moreover, the TIMM23 protein has been associated with neurological phenotypes and reduced life span in mice, as it has a critical role of the mitochondrial import machinery for maintaining mitochondrial function (Ahting et al., 2009). This suggest that TIMM23 activity could be dependant of the nutrient availability in culture, specifically to carbohydrates availability.

Glucose transporter 1 (*SLC2A1*) was upregulated in 5% oxygen relative to 20% buy did not show significant differences due to oxygen concentration. Although the expression was tending to be higher in high glucose. This correlates with other reports where hypoxic conditions induced the expression of GLUT1 [155]. Glucose transporter 3 (*SLC2A3*) did not show significant differences either due to glucose or oxygen. However, there was a tendency to be higher in 20% oxygen and in high glucose. *SLC2A3* and *SLC7A3* were reported downregulated by culture in Whitten's medium relative to KSOM medium [156]. Finally, the amino acid transporter *SLC7A3* was not affected by oxygen concentration but it was significantly upregulated in high glucose relative to low glucose. *SLC7A3* has been reported down regulated when culture in Whitten's medium relative to KSOM medium [149] [157]. These results suggest that the activity of glucose transporters may be subjected to the nutrient availability (proteins, amino acids and fatty acids) in culture in combination with oxygen levels.

Glucose transporters, *SLC2A1* and *SLC2A3* appeared to be overexpressed in equine blastocyst in vitro relative to the naturally conceived counterpart [158]. Glucose concentration in the equine oviduct is lower than in other mammals whereas equine IVF uses the highest concentration of glucose routinely, up to 17.5 mmol/L. It has been described in the mouse that hyperglycaemic in vitro culture is associated with downregulation of glucose transporters (GLUT1, GLUT2, GLUT3) in the blastocyst, reducing the glycolytic activity [159]. Besides, high glucose levels during gastrulation in mice due to maternal hyperglycaemia have been associated with an increased rate of ATP production from glycolysis than from oxidative phosphorylation, but with a total reduction of ATP, which implies a reduction in energy production in hyperglycaemic embryos. On the other hand, this does not seem to be the case in

equine embryos, where the in vitro culture conditions increased the expression of *SLC2A1* and *SLC2A3*, regardless of the glucose concentration used [158].

To date, high oxygen tension is considered stressful whereas lower oxygen tension is considered optimal for mouse embryo culture and current IVF clinical practices. In fact, studies have revealed a marked effect of oxygen on transcription, significantly more pronounced than the relative influence culture medium composition [160]. Moreover, exposure to atmospheric oxygen makes the mammalian embryo more susceptible to a second stressor such as ammonium, as oxygen regulates amino acid turnover and carbohydrate uptake during the preimplantation development (Wale and Gardner, 2012).

In other studies the beneficial effect of 5% oxygen has been associated with an increased number of ICM cells in the blastocyst and with a reduced birth weight in singleton pregnancies [161]. Atmospheric oxygen (20%) has been found to mis-regulate genes involved in cell growth and in gastrulation (e.g., Bmp4, Rnf2, Tdgf1, and Trim44) which could compromise developmental competence of blastocysts. Also, the down-regulation of the de novo *DNMT3A* could have implications in loss of imprinting or other consequences that become manifest later in life. Genes involved in the antioxidant response (Abcb6; Hnrph1; Map1lc3a; Pld3; Psmb4; Sqstm1) are abnormally regulated after culture in 20% oxygen [149], [162]. These data are consistent with previous works on the human embryo cultured in atmospheric oxygen, which revealed a decrease in both blastocyst formation and resultant cell number and an altered transcriptome.[163] [164]

Furthermore, a higher incidence of gene mutation in new-borns conceived by IVF was reported, highlighting that IVF may be disruptive to the DNA stability. Although mechanisms remain unclear, studies in mice have demonstrated that the expression and methylation levels of some DNA damage repair genes in the brain tissue were significantly changed at 1.5 years of age, when compared with a naturally conceived control group. In summary, the studies indicated that IVF could bring long- term alterations of gene, protein expression and DNA methylation levels of some DNA damage repair genes in the brain tissue. These alterations might be resulted from the different oxygen concentration of culture environment, providing valuable

perspectives to improve the safety and efficiency of IVF at early embryonic stage and throughout different life stages. [165]. Regarding the long-term effects of oxygen on the preimplantation human embryo, both implantation and pregnancy rates are reduced following embryo culture in atmospheric oxygen, culminating in a decrease in the live birth rate [148][94] [166].

A high glucose concentration in the reproductive tract during early development may result in aberrant embryo or foetal development. In vitro culture in medium with a glucose concentration approximating that of diabetic serum reduces total and trophectoderm cell numbers at the blastocyst stage and conceptus development to term [167].

In equines, the relative mRNA expression of the pro-apoptotic gene *BAX*, was significantly upregulated in high glucose, whereas no differences were found for the anti-apoptotic gene *BCL2* [158]. This effect was previously demonstrated in hyperglycaemic conditions in mouse, rat and bovine embryos where high glucose concentrations during in vitro conception led to a poorer embryo quality [168],[169]. Moreover, the expression of mitochondrial genes *COX2, UQC2, LDHA* was found downregulated for in vivo embryos (low glucose) relative to the in vitro (high glucose) embryos. The glycolysis-related gene LDHA was upregulated high glucose in equine and bovines. In conclusion, hyperglycaemia in bovine and equine embryos enhanced expression of metabolic genes but also and excessive glucose concentration can be non-viable [158]. These finding provide evidence that physiological oxygen promote embryo viability whereas high glucose enhances glycolysis and anaerobic glycolysis pathways in mammals. A hyper activation of these pathways could activate apoptosis pathways and therefore reduced embryo viability. Further studies of the metabolic aspects of human embryo development in vitro conditions are required to provide a deeper knowledge that could be employed to improve culture conditions. However, the clear conclusion is that nutrient availability and oxygen concentration should be balanced in order to preserve embryo viability, and these balanced conditions must be determine per specie.

Mitochondrial function is critical to ensure developmental competence of embryos. Despite the evidence suggesting that mitochondrial metabolism is relatively inactive

during preimplantation embryo development, aerobic (mitochondrial) metabolism contributes a major role in the supply of ATP. Although anaerobic respiration can supplement deficiencies in the energy supply in the short term, this is not sufficient to substitute for aerobic respiration over long periods. Deficiencies in the levels of aerobic respiration can explain variability in the implantation potential of apparently equivalent embryos. Microenvironment changes and nutrient availability have been associated with alterations in blastocyst mitochondrial function [27]. Mitochondrial membrane potential is a key indicator of cellular viability, as it reflects the movement of hydrogen ions across the inner membrane during the process of electron transport and oxidative phosphorylation for ATP production [32].

In the present study, mitochondrial membrane potential evaluated in human embryos showed interesting results when comparing fresh and frozen embryos. JC-1 dye was useful to quantify the ratio of high- to low-polarized mitochondria using fluorescence microscopy. Heterogeneity of ΔΨm within the population of mitochondria in preimplantation stage embryos is in agreement with several studies [32] [24]. Cryopreservation methods in ART may induce mitochondrial depolarization, reduced ATP production, or decreased developmental potential. Increased ΔΨm, if coincident with increased ATP levels, may also be involved in the local regulation of certain enzymatic activities (kinases), signalling pathways, and calcium homeostasis [25]. Although our findings between fresh and frozen embryos were not conclusive, the mean membrane potential ratio was consistently reduced in frozen embryos, which can be an indicator cellular damage or reduced developmental potential. Additional experiments are required in order to test this hypothesis and this could be achieved by increasing the number of samples.

Human embryos were analysed to determine oxygen consumption rate (OCR), which is the measure for mitochondrial oxidative phosphorylation to indicate the ATP production [12], [25]. To accomplish this, a pilot test was executed in order to verify the detection limits of the technology (Mito Stress test, Seahorse, Agilent). Twelve fresh embryos, cultured in similar conditions, were divided in eight groups according their quality grade. Obtained results showed a high level of heterogeneity even between the groups that had the same number of embryos with similar quality. Basal

OCR levels were extremely low for all groups (-2.2125 ± 2.58 pmol/min) which automatically prevented accurate calculation of other parameters. Although this method has been reported as a promising non-invasive method to determine extracellular flux and therefore mitochondrial activity in embryos and oocytes from different species [170], here were have not found favourable results for low input samples. This method could be very helpful for the investigation of mitochondrial activity; however, in the case of work with human embryos, an ultra-sensitive method is required due to the restricted number donated samples, as we would not be able to work with pooled samples. Therefore further optimisation will be required in order to obtain accurate results and being able to compare between culture conditions.

Children conceived by ART have an altered lipid profile, fasting glucose, and body fat distribution and cardiovascular function [171]. Healthy children conceived by ART display generalized vascular dysfunction, which seems to be related to the ART procedure itself and epigenetic changes [172]. In fact, we found differentially methylated gene sets that are associated with several diseases. Gene sets related to Myocardial infarction, Tetralogy of Fallot and Heart malformations were hypermethylated in embryos cultured in low glucose. Global DNA methylation and methylation at specific genes related to adipogenesis, lipid metabolism and inflammation are related to Metabolic syndrome (MetS), which is a cluster of metabolic alterations that altogether increase the risk of suffering diabetes, cardiovascular disease and cancer [173]

The influence of epigenetic modifications has also been reported in other neurological disorders, such as epilepsy or intellectual disability disorders [115]. Epigenetic regulators such as chromatin factors are fundamental in neurodevelopment. Also, there is a correlation between nutrition and epigenetic modifications as ketogenic diet showed a reduction in the frequency of seizures and a change in the DNA methylation levels [50] [115]. Gene sets associated with Autism, Mental disorders and Epilepsy were found hypermethylated in embryos cultured in high glucose. Furthermore, over representation analysis showed enriched get sets related to Embryo development, Brain and Head development and Neurogenesis in embryos cultured in low glucose.

Different conditions during preimplantation embryo culture can act synergistically to modify postnatal phenotype. The synergic act of the microenvironment is sufficient to induce cardio metabolic disorders in adult offspring including relative hypertension, glucose intolerance and insulin resistance, abnormal hepatic and fat metabolomes and behavioural deficits including memory loss [174]. Our findings suggest that glucose concentration could have an effect on the offspring phenotype, as several gene sets were significantly associated with diseases such as Hypertension, Hypercholesterolemia and Diabetes Mellitus noninsulin-dependent. These gene sets were identified as hypermethylated in embryos cultured in high glucose. Furthermore, over representation analysis showed enriched gene ontology sets related to Cytoskeleton, plasma membrane, vesicle-mediated transport and intracellular transport.

Complex I is the first and largest enzyme of the mitochondrial respiratory chain (RC) and oxidative phosphorylation (OXPHOS) system, and plays critical roles in transferring electrons from reduced NADH to coenzyme Q10 (CoQ10, ubiquinone) and in pumping protons to maintain the electrochemical gradient across the inner mitochondrial membrane [175]. The most frequent presentation of complex I deficiency is Leigh syndrome, or subacute necrotising encephalomyelopathy. Affected children typically have normal early development but present in late infancy or early childhood with progressive neurological abnormalities related to brainstem and/or basal ganglia dysfunction [176]. Gene sets associated with Mitochondria Complex I deficiency and Leigh syndrome were hypermethylated in embryos cultured in high glucose.

Additionally, differentially methylated genes were also found on promoter and repressors regions. H3K4me3 sites are located in CpG islands and active promoters, predominantly associated with transcriptional start sites. Whereas H3K27me3 locates in inactive promoters [177]. We found H3K27me3 sites that were hypermethylated in high glucose. After the over representation analysis, signalling pathways related to neurological disorders, cardiovascular disorders and cancer were enriched. Hypermethylated regions were found in H3K4me3 sites in embryos cultured in low glucose. This resulted in gene set enriched for the Bladder cancer pathway

KEGG:05219. Whereas hypermethylated regions in high glucose resulted in the enriched for the RNA degradation pathway KEGG:03018 .

Methylation of imprinted genes can be altered by glucose concentration in embryo culture. Six imprinted genes (CDKN1C, KCNQ1, ERLIN2, TRAPPC9, NESP55, and ZFP57) resulted differentially methylated when comparing high and low glucose concentrations in culture media. Differentially methylated points where distributed through the gene body in a different manner for every gene. Although there is not a clear pattern observed in regards to the differentially methylated regions. This evidence confirms that altered glucose concentration is enough to generate epigenetic changes in imprinted genes, contrary to other reports, where no evidence was found for ART-associated DNA methylation changes at imprinted genes [114], [178]. Further studies would be required to confirm if these changes are maintained through cell divisions or even transgenerationally.

In summary, ART is strongly associated with altered transcriptional regulation, metabolism and epigenetic variation. Minimal variants in embryo culture can cause significant changes on metabolic or energetic pathways that could lead to aberrant cell differentiation. The increase of glucose concentration in culture media caused notable changes in the human embryo transcriptome and epigenome. This is the first study that evaluates individual culture components, such as glucose or oxygen, to determine significant changes in the preimplantation human development. Therefore, it is critical to optimize culture conditions to minimize epigenetic perturbations, with the assumption that these perturbations are responsible for at least some of the adverse phenotypes associated with ART.

CHAPTER 4

Effect of culture glucose and oxygen on human embryonic stem cells

4.1 Introduction

Understanding human embryogenesis is crucial for the field of reproductive medicine. However, apart from the very early stages of preimplantation development, human embryos are not very accessible for research which can be an important limitation for the field. Therefore, some approaches to overcome this obstacle are the use animal models or human cell lines.

In this study, we decided to used Human embryonic stem cells (HESCs) as they are derived from the inner cell mass (ICM) of human embryos at blastocyst-stage. They are great for modelling human diseases and for understanding early development [179].

Characterization is crucial on studies with embryonic stem cells. Following the International Stem Cell Initiative, characterization can be performed by measuring the expression of a broad list of proteins. Nevertheless, the most common panel includes glycolipid antigens SSEA-1, SSEA-3, SSEA-4, TRA-160, TRA-181 and transcription factors *OCT4*, *NANOG*, and *SOX2* [127] [129].

Understanding the metabolic properties of human pluripotent stem cells and the effects of culture conditions on their metabolism is crucial as this will allow us to improve HESC as model of study for human conditions. In fact, since HESCs are derived from the inner cell mass of human embryos, they might be helpful for understanding the effects of culture conditions on preimplantation embryos development in vitro.

Similar to ICM cells in the human blastocyst, HESCs rely mostly on glycolysis as an energy supply. However, as cells differentiate, they undergo a metabolic switch from glycolysis to oxidative phosphorylation (OXPHOS) [131] [132].

The interaction of glucose and oxygen are crucial in mammalian cell culture; however, the impact of their availability or concentration on the glycolysis pathway and how this may alter the regulation of the pluripotent state, is not yet well understood [133].

Changes in cellular metabolism can affect the fate of pluripotent stem cells as well as chromatin reorganization and gene expression changes during reprogramming and differentiation [134] [130]. The importance of DNA methylation in regulating pluripotency is evidenced by the fact that perturbations of the expression level or function of many different epigenetic enzymes can impair stem cell self-renewal and lead to the loss of pluripotency, events that are followed by differentiation. Enzymes such as acetylases, methylases and demethylases necessary for specific chromatin structural and functional states [135].

Several recent studies have identified critical metabolic pathways necessary for cellular reprogramming and/or maintaining pluripotency. Commonly, a high glycolytic flux in HESCs cultures has been associate to the maintenance of pluripotency whereas the oxidative mitochondrial metabolism has been labelled as an ''antagonistic'' to the pluripotent state. However, some evidence suggests that mitochondria are also active in HESCs [133]. Here we have evaluated the impact of different concentrations of oxygen (5% and 20%) and glucose (5 mM and 17.5 mM) in human embryonic stem cell culture.

4.2 Study design

HESCs were cultured in TeSR™-E8™ medium, prepared according Chen *et al.* 2016 [122] at 17.5 mM or 5 mM glucose in physiological (5%) or atmospheric (20%) oxygen.

Cells were cultured for up to 6 days, to try to replicate the same exposure as embryos cultured in vitro. Markers of pluripotency were evaluated through molecular and cellular analysis. Also, mitochondrial function analysis where performed to compare mitochondrial membrane potential, oxygen consumption rates and the extracellular acidification rate between different culture conditions and embryonic stem cell lines. Furthermore, mitochondrial-DNA analysis and gene expression analysis were performed for several genes related to pluripotency, glucose metabolism, mitochondrial function and DNA methylation (Table 4.1). This project was accomplish using the embryonic stem cell lines MAN7 and MAN13, which were derived in the North West Embryonic Stem Cell facility (NWESCC) University of Manchester [129] as described in Section 2.6.

Characterization of HESC was performed by Immunocytochemistry and Flow cytometry using a panel of markers that includes glycolipid antigen, TRA-181 and transcription factors *OCT4*, *NANOG*, and *SOX2* (Section 2.7 and 2.8).

Gene expression analysis was assessed by the comparative CT method for quantitative real-time PCR data (Section 2.9), also known as the $2^{-\Delta\Delta\ CT}$ method [140]. Changes produced at the transcript level as a result of the oxygen and glucose concentrations were identified for genes related to cell survival, pluripotency, cell proliferation, metabolism, mitochondrial activity, hypoxia, oxidative stress, and DNA methylation were analysed and normalized against ACTB (Table 4.1). Mitochondrial function was evaluated through the comparative analysis of mitochondrial DNA (mtDNA), mitochondrial membrane potential (ΔΨm) and mitochondrial respiration (oxygen consumption rate) (Methods described in sections 2.10 and 2.11).

4.3 Characterisation of human embryonic stem cells (hESCs)

Standard characterisation for the HESC lines was performed through immunostaining and flow cytometry analysis. Both cell lines (MAN13 and MAN7) showed at least 80% of cells were positive for expression of pluripotent markers (OCT-4, *SOX2*, *NANOG*, and TRA-1–81) in normal conditions of oxygen (20%) and glucose (17.5 mM).

HESC lines are regularly cultured in medium with 17.5mM glucose and at 20% oxygen under standard laboratory conditions. MAN7 and MAN13 cell lines were evaluated at 12, 48, 96 and 144 hours to determine the combined effects of high glucose (17.5 mM), low glucose (5 mM), atmospheric oxygen (20%) and physiological oxygen (5%).

Immunocytochemistry analysis showed a reduced expression of pluripotency markers by day six (144 hours) in the low glucose group (Figure 4.1). The same reduction was observed by flow cytometry analysis where the effect of glucose concentration was confirmed (Figure 4.2).

Both cell lines showed significant differences due to glucose concentration or due to the combination glucose/oxygen after 144 hours in culture (Figure 4.3). These cell lines tend to express higher expression of pluripotency marker when cultured in high glucose (17.5 mM). Furthermore, no effects were observed due to the oxygen concentration only.

MAN7 cell line showed fewer significant differences in comparison to MAN13 (Figure 4.4). *OCT4* expression tends to be higher in cells cultured at 17.5mM than at 5 Mm glucose. However, the only significant difference was found when comparing the groups High Glucose (17.5 mM) / 20% oxygen vs. Low Glucose (5 mM) / 5% oxygen ($p=0.0301$). *SOX2* expression was higher in high glucose that in low glucose media, when cells where cultured in atmospherically oxygen ($p=0.0055$). In addition, *SOX2* was significantly greater in High Glucose / 20% oxygen than in Low Glucose / 5% oxygen ($p=0.0012$). Similarly to *SOX2*, expression of TRA-181 was significantly higher in the High Glucose / 20% oxygen when compared to Low Glucose / 20% oxygen group ($p=0.02$) and to the Low Glucose / 5% oxygen group ($p=0.0393$).

In the MAN13 cell line, the differences were more evident than in MAN7 (Figure 4.4). Expression of *OCT4* was greater in the High Glucose/20% oxygen group when compared to the Low Glucose/20% oxygen group ($p=0.0006$) and to the Low Glucose/5% oxygen group ($p=0.0035$). *OCT4* expression was also greater in the High Glucose/5% oxygen group when compared to the Low Glucose/20% oxygen group ($p= 0.0018$) and to the Low Glucose/5% oxygen group ($p= 0.0108$). Expression of *SOX2* was greater in the High Glucose/20% oxygen group when compared to the Low Glucose/20% oxygen group ($p <0.0001$) and to the Low Glucose/5% oxygen group ($p= 0.0011$). Also, it was greater in the High Glucose/5% oxygen group when compared to the Low Glucose/20% oxygen group ($p <0.0001$) and to the Low Glucose/5% oxygen group ($p= 0.0062$). The expression of TRA-1-81 was greater in the High Glucose/20% oxygen group when compared to the Low Glucose/20% oxygen group ($p <0.0001$) and to the Low Glucose/5% oxygen group ($p <0.0001$). Besides, its expression was greater in the High Glucose/5% oxygen group when compared to the Low Glucose/20% oxygen group ($p=0.0184$) and to the Low Glucose/5% oxygen group ($p= 0.0287$).

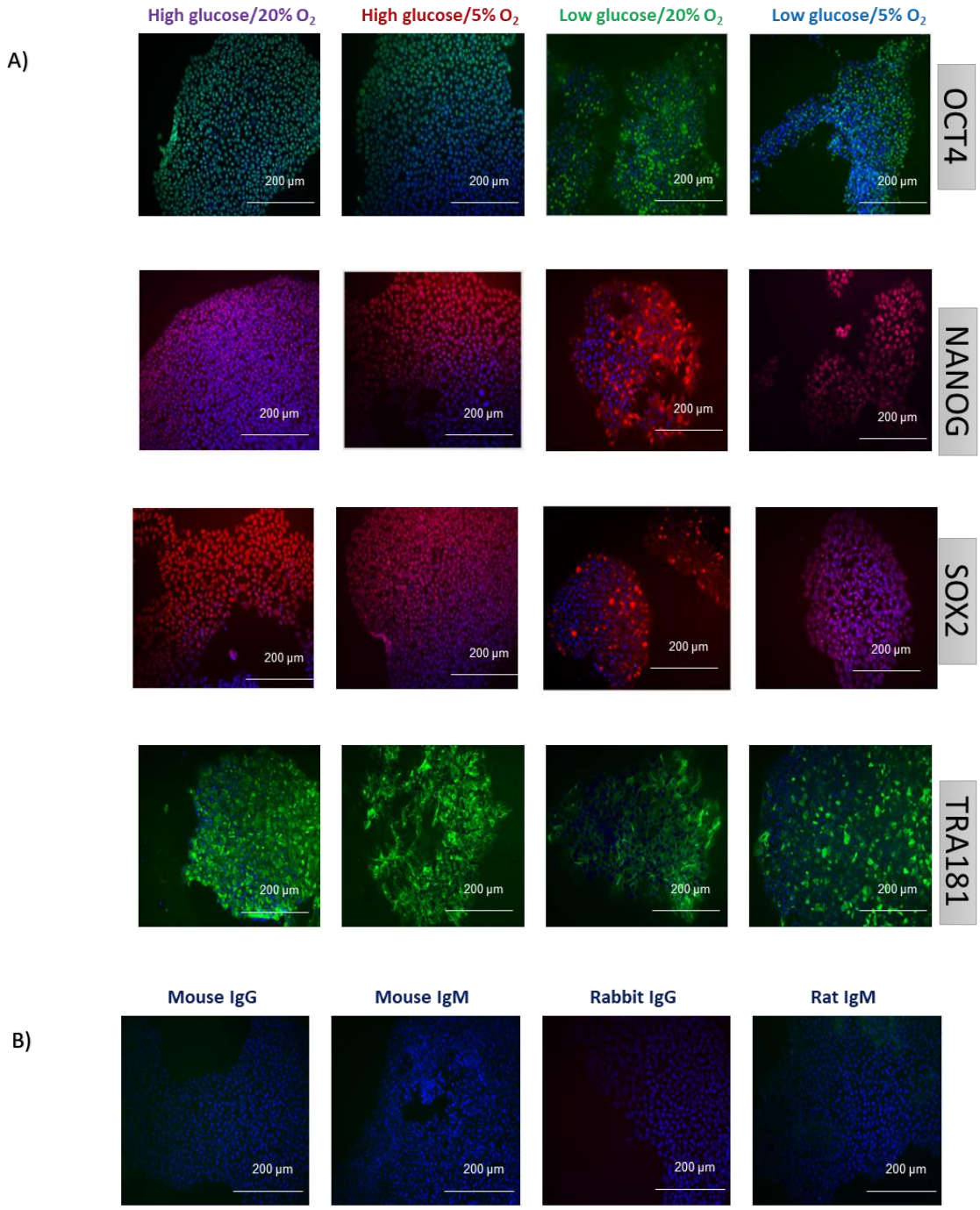

Figure. 4.1. Immunostaining of HESCs for pluripotency markers. A) Representative images of MAN13 cell line after 6 days of culture on different conditions of oxygen and glucose. Nuclear markers were evaluated i.e. *OCT4* (green), *NANOG* (red) and *SOX2* (red) as well as the cell surface marker TRA-1-81 (green). Images are merged showing the antibody staining with their respective DAPI nuclear counterstain (blue). Scale bar 200 µM. B) Isotype controls merged with their respective DAPI nuclear counterstain (blue); they

were negative in all conditions. Isotype control rabbit IgG was used as control for *NANOG* and *SOX2*; Isotype control mouse IgG was used for *OCT4*; Isotype control mouse IgM was used for TRA-1-81. Scale bar 100 µM

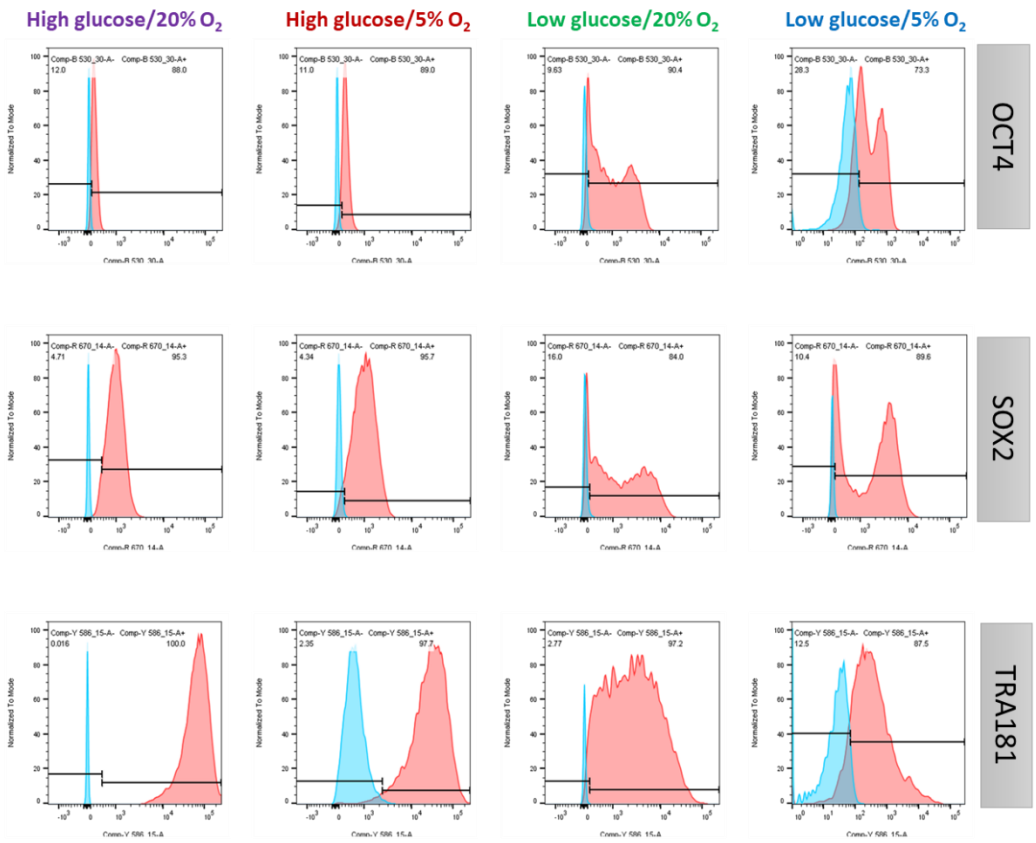

Figure 4.2. Expression of nuclear and cell surface markers in HESCs. Expression of nuclear and cell surface markers of pluripotency in undifferentiated HESC. Representative figure showing flow cytometry plots of MAN13 analysed at day 6 after plating. Stained for nuclear markers (*OCT4*, *SOX2*) and cell surface marker (TRA-1-81). Plots show histograms comparing pluripotency markers (red) and isotype controls (blue).

Tukey's multiple comparisons test Man7	Adjusted P Value
OCT4	
High Glucose / 20% O_2 vs. Low Glucose / 5% O_2	0.0301
SOX2	
High Glucose / 20% O_2 vs. Low Glucose / 20% O_2	0.0055
High Glucose / 20% O_2 vs. Low Glucose / 5% O_2	0.0012
TRA-181	
High Glucose / 20% O_2 vs. Low Glucose / 20% O_2	0.0200
High Glucose / 20% O_2 vs. Low Glucose / 5% O_2	0.0393

Tukey's multiple comparisons test Man13	Adjusted P Value
OCT4	
High Glucose / 20% O_2 vs. Low Glucose / 20% O2	0.0006
High Glucose / 20% O_2 vs. Low Glucose / 5% O2	0.0035
High Glucose / 5% O_2 vs. Low Glucose / 20% O2	0.0018
High Glucose / 5% O_2 vs. Low Glucose / 5% O2	0.0108
SOX2	
High Glucose / 20% O_2 vs. Low Glucose / 20% O2	<0.0001
High Glucose / 20% O_2 vs. Low Glucose / 5% O2	0.0011
High Glucose / 5% O_2 vs. Low Glucose / 20% O2	<0.0001
High Glucose / 5% O_2 vs. Low Glucose / 5% O2	0.0062
TRA-181	
High Glucose / 20% O_2 vs. Low Glucose / 20% O2	<0.0001
High Glucose / 20% O_2 vs. Low Glucose / 5% O2	<0.0001
High Glucose / 5% O_2 vs. Low Glucose / 20% O2	0.0184
High Glucose / 5% O_2 vs. Low Glucose / 5% O2	0.0287

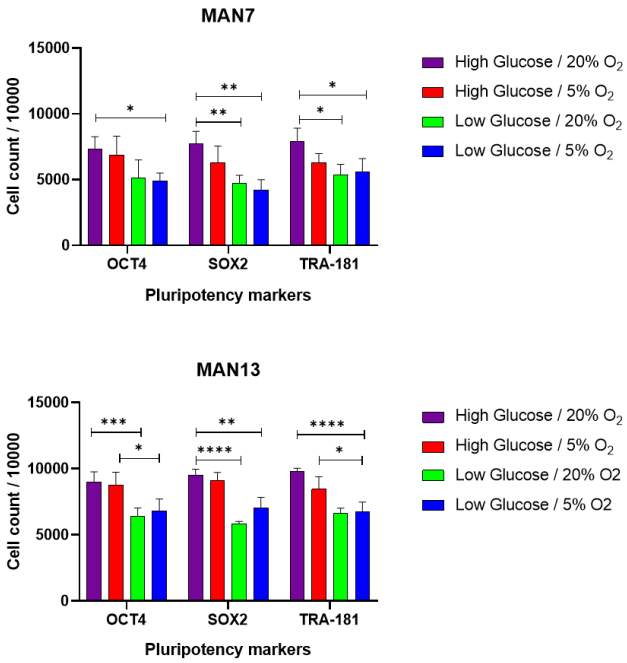

Figure 4.3: Comparative analysis of nuclear and cell surface markers in HESCs. Comparative analysis of nuclear and cell surface markers of pluripotency expressed in MAN7 and MAN13. Comparison was calculated using the total cell count that resulted positive through FACS for each marker. Analyses were performed in triplicates for each condition for each cell line. Statistical significance was calculated through 2-way ANOVA and Tukey's multiple comparison test.

4.4 Effect of glucose and oxygen on gene expression (HESCs)

Using reverse transcription polymerase chain reaction, we examined the expression of 48 genes in HESCs (Table 2.16). These included markers for: Cell survival *(BAX, BCL2, BCL2L1, CBL, DAP3, TP53);* Cell growth and differentiation (*CDX2, EGFR, EOMES, EP300, FGF4, ZSCAN4*); Pluripotency (*NANOG, OCT4, SOX2*); Transcription factors (*EIF1AX, EIF2S2, TRIM28*); DNA methylation (*DNMT1, DNMT3A, DNMT3B, TET1, TET2, TET3, MAT2A*); Mitochondrial activity (*ATP5F1, COX11, SDHB, TFAM TIMM23, TRMT10C*); Metabolism (*SLC2A1, SLC2A3, SLC7A3, SLC16A1, GAPDH, ASNS, MTOR, PPARA, PPARG*); Oxidative stress *(SOD1, SOD2, SOD3, GPX2) and* Hypoxia *(HIF1A, HIF2A, ARNT).*

Significant differences were only found on genes related to Pluripotency (*NANOG, OCT4*), DNA methylation (*DNMT1, DNMT3A, DNMT3B, TET1, TET2, TET3, MAT2A*); Mitochondrial activity (*ATP5F1, SDHB, TIMM23, TRMT10C*); Metabolism (*SLC2A1, SLC2A3)*. Gene expression plots can be found in Figure 4.5. Whereas the rest of the genes were not significantly affected by either glucose or oxygen on any cell line (data not shown). Statistical tests (Two-way ANOVA and Tukey's multiple comparisons tests) were applied to every gene on each condition to determine significant differences due to oxygen or glucose (detailed results shown in Table 4.1).

Pluripotency

In MAN7 the mean expression of *NANOG* was significantly higher in physiological oxygen (5%) and high glucose when compared with the atmospheric oxygen ($p=0.0009$). In addition, at 96 hours and 144 hours a significant increase in expression was observed ($p=0.0216$) in high glucose concentration compared to low glucose. Similarly to *NANOG, OCT4* was significantly upregulated at 144 hours ($p= 0.0435$) high glucose / 5% oxygen when compared to low glucose / 5% oxygen. In MAN13 the mean expression of *NANOG* and *OCT4* were significantly upregulated by high glucose (<0.0001) in atmospheric and physiologic oxygen.

DNA Methylation

In this study, the expression of *DNMT1* was very low in both cell lines. However, significant differences were identified due to glucose concentration. In MAN7 cultured at physiological oxygen *DNMT1* was upregulated in low glucose ($p=0.0387$) compared to the high glucose counterpart. In MAN13, *DNMT1* was upregulated in low glucose at atmospheric oxygen ($p=0.0003$) compared to the high glucose counterpart. *DNMT3A* showed differential patterns of expression due to glucose concentration in both cell lines, although the cell lines behave differently. *DNMT3A* was upregulated in low glucose in MAN7 when cells were maintained at atmospheric oxygen ($p=0.0165$). In MAN13 changes in *DNMT3A* due to glucose concentration were also significant but in this case the upregulation was observed in the high glucose group ($p<0.0001$). On the other hand, the mean expression of *DNMT3B* in MAN7 was not affected, however at day six of culture (144 h) a significant increase was observed in the high glucose at 20% oxygen ($p=0.0085$) compared to the low glucose counterpart and the 5% oxygen . On the other hand, glucose had a significant impact on *DNMT3B* in MAN13 as the expression was upregulated in high glucose 20% oxygen compared to the low glucose counterpart ($p=0.0021$). Interestingly, MAT2A was significantly affected in both cell lines. In MAN7 and MAN13 this gene was upregulated in the low glucose group ($p<0.0001$) when compared to the high glucose counterpart at 5% and 20% oxygen.

Although the mean level of expression of *TET1* was significantly different between in MAN7 and MAN13 ($p= 0.0097$ and $p=0.0092$ respectively), there was not a clear pattern of expression suggesting a defined effect only caused by glucose or oxygen. The expression of *TET2* was extremely low in both cell lines. Nevertheless, there was a significant increase in expression in MAN7 at low glucose 5% oxygen, compared with the high glucose counterpart ($p= 0.0233$) and at low glucose 20% oxygen, compared with the high glucose counterpart ($p= 0.0136$. Moreover, in MAN13 the increased expression was observed in high glucose at 5% and 20% oxygen compared with the low glucose counterpart ($p<0.0001$). *TET3* expression was upregulated in both cell lines as a result of the low glucose concentration independently of the oxygen

concentration. The p value was 0.0461 at 5% oxygen and 0.0394 at 20% oxygen for MAN7, whereas in MAN13 the p value was <0.0001 for both oxygen concentrations.

Glucose transporters

The relative mRNA abundance of *SCL2A1* and *SLC2A3*, which encode for glucose transporters 1 and 3, was investigated in different conditions of oxygen and glucose. *SLC2A1* was upregulated in MAN7 in low glucose at 20% oxygen when compared to the high glucose counterpart (p=0.0373). It also upregulated in high glucose at 5% oxygen when compared to the 20% oxygen counterpart (p= 0.0087). Moreover, this marker was also very sensitive to oxygen in MAN13 as it was upregulated in low glucose at 5% oxygen when compared to the 20% oxygen counterpart (p=0.0062). Also in in high glucose at 5% oxygen when compared to the 20% oxygen counterpart (p=0.0006). Furthermore, *SLC2A3* in MAN7 was only upregulated at day 6 in High Glucose / 5% oxygen when compared to the 20% O_2 counterpart (p=0.0120). *SLC2A3* in MAN13 was significantly upregulated in low glucose at 5% oxygen (p= 0.0020) and at 20% oxygen (p=0.0001) when compared to the high glucose counterpart.

Mitochondrial markers

ATP5F1 was significantly upregulated in MAN7 at Low Glucose / 20% oxygen (p<0.0001) when comparing to Low Glucose / 5% oxygen, High Glucose / 5% oxygen and High Glucose / 20% oxygen. Also, it was upregulated in High Glucose / 20% oxygen compared to its 5% oxygen counterpart (p=0.0012). In MAN13 the effect of glucose and oxygen were more significant. Expression was consistently higher in low glucose at 5% and 20% oxygen when compared to their high glucose counterparts (p<0.0001). The Translocase of Inner Mitochondrial Membrane protein encoded by *TIMM23* gene is part of a complex located in the inner mitochondrial membrane that mediates the transport of transit peptide-containing proteins across the membrane. In MAN7 the mean expression was not significantly different until the last time point 144h where glucose had a significant impact (p=0.0006) increasing the expression in low glucose

medium. On the other hand in MAN13 the expression was significantly increased in high glucose medium at atmospheric oxygen ($p<0.0001$). Similarly to *TIMM23*, the expression of *TRMT10C* in MAN7 was significantly higher in the low glucose groups compared to the high glucose counterparts (5% oxygen $p=0.0112$; 20% oxygen $p=0.0087$). Whereas in MAN13 the effect was opposite *TRMT10C* in MAN13 was upregulated in the High glucose group at 20% oxygen when compared to the low glucose and 5% oxygen counterparts ($p<0.0001$). Although the expression of SDHB in MAN7 was significantly different between 5% and 20% oxygen groups in low glucose concentration ($p=0.0039$), there was not a clear trend indicating an effect of upregulation or downregulation. On the other hand, there is a clear trend in MAN13 where the expression is increased in the low glucose group ($p<0.0001$) in 5% and 20% oxygen when compared to their high glucose counterparts.

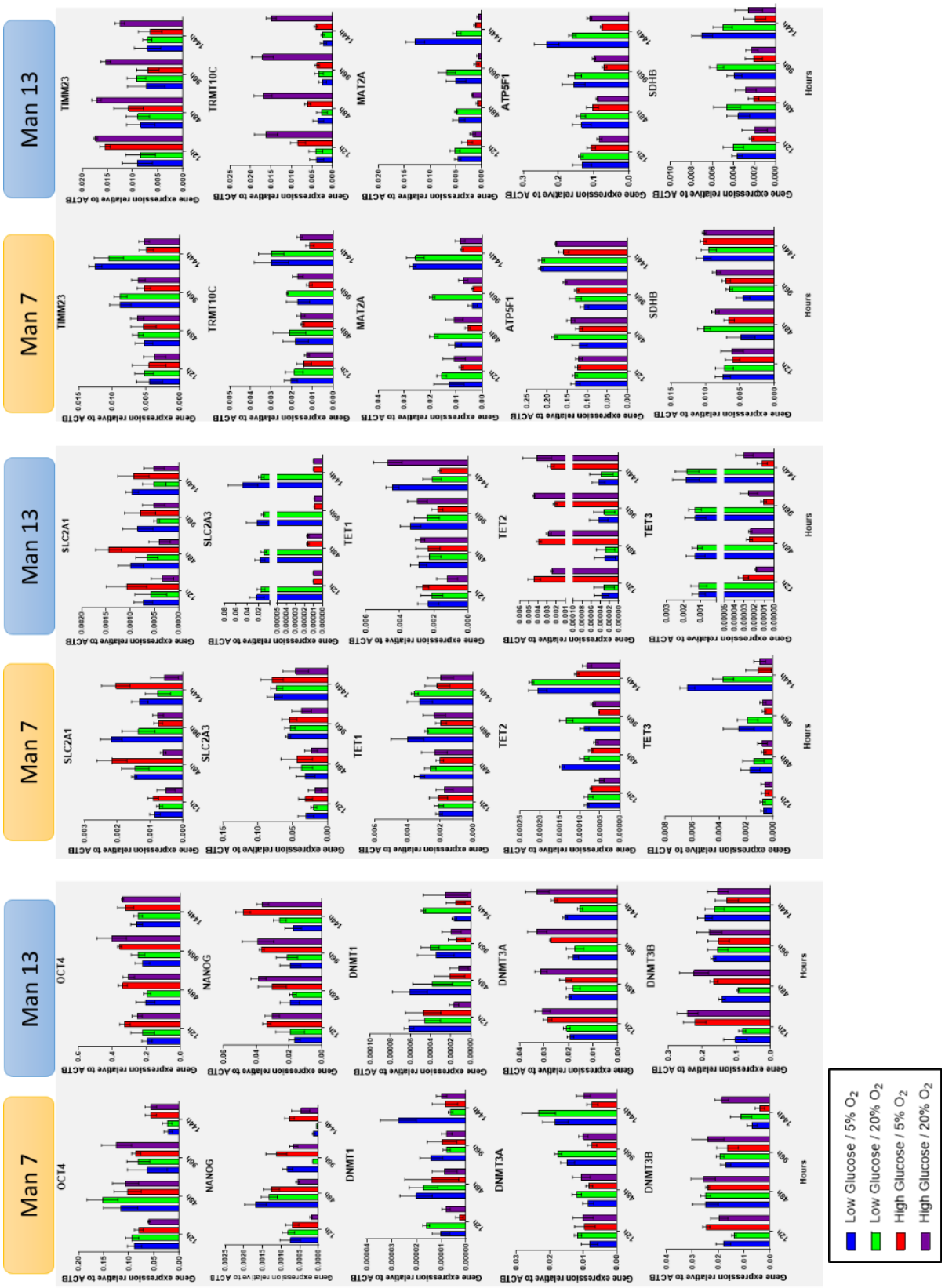

Figure 4.4. Analysis of transcript levels relative to ACTB (2-ΔCT) in HESCs. Representative image show results of RT-qPCR analyses performed at 12h, 48h, 96h and 144h for each both cell lines, MAN7 and MAN13. Comparative results include transcription factors (*NANOG*, *OCT4*), DNA methyltransferases (*DNMT1*,*DNMT3A*, *DNMT3B*), Tetdemethylases (*TET1*, *TET2*, *TET3*, MAT2A), Mitochondrial markers (*TIMM23*, TRT10C, ATP5F1, SDHB) and glucose transporters (*SLC2A1*, *SLC2A3*).

Cell line	Gene	Comparison	P value	Type
MAN7	*NANOG*	**High glucose / 5% O2** vs. High glucose / 20% O2	0.0009	Mean
MAN7	*NANOG*	**Low Glucose / 5% O2** vs. High Glucose / 5% O2	0.0216	144 h
MAN7	*OCT4*	**Low Glucose / 5% O2** vs. High Glucose / 5% O2	0.0435	144 h
MAN13	*NANOG*	**Low Glucose / 5% O2** vs. High Glucose / 5% O2	<0.0001	Mean
MAN13	*NANOG*	**Low Glucose / 5% O2** vs. High Glucose / 20% O2	<0.0001	Mean
MAN13	*NANOG*	**High Glucose / 5% O2** vs. Low Glucose / 20% O2	<0.0001	Mean
MAN13	*NANOG*	**Low Glucose / 20% O2** vs. High Glucose / 20% O2	<0.0001	Mean
MAN13	*OCT4*	**Low Glucose / 5% O2** vs. High Glucose / 5% O2	<0.0001	Mean
MAN13	*OCT4*	**Low Glucose / 5% O2** vs. High Glucose / 20% O2	<0.0001	Mean
MAN13	*OCT4*	**High Glucose / 5% O2** vs. Low Glucose / 20% O2	<0.0001	Mean
MAN13	*OCT4*	**Low Glucose / 20% O2** vs. High Glucose / 20% O2	0.0002	Mean
MAN7	*DNMT1*	**Low Glucose / 5% O2** vs. High Glucose / 5% O2	0.0387	Mean
MAN7	*DNMT1*	**Low Glucose / 5% O2** vs. High Glucose / 20% O2	0.0129	Mean
MAN13	*DNMT1*	**Low Glucose / 5% O2** vs. High Glucose / 20% O2	0.0169	Mean
MAN13	*DNMT1*	**High Glucose / 5% O2** vs. Low Glucose / 20% O2	0.0388	Mean
MAN13	*DNMT1*	**Low Glucose / 20% O2** vs. High Glucose / 20% O2	0.0003	Mean
MAN13	*DNMT1*	**Low Glucose / 5% O2** vs. Low Glucose / 20% O2	0.0358	144 h
MAN13	*DNMT1*	**High Glucose / 5% O2** vs. Low Glucose / 20% O2	0.0267	144 h
MAN7	*DNMT3A*	**High Glucose / 5% O2** vs. Low Glucose / 20% O2	0.0017	Mean
MAN7	*DNMT3A*	**Low Glucose / 20% O2** vs. High Glucose / 20% O2	0.0165	Mean
MAN13	*DNMT3A*	**Low Glucose / 5% O2** vs. High Glucose / 5% O2	0.0001	Mean
MAN13	*DNMT3A*	**Low Glucose / 5% O2** vs. High Glucose / 20% O2	<0.0001	Mean
MAN13	*DNMT3A*	**High Glucose / 5% O2** vs. Low Glucose / 20% O2	<0.0001	Mean
MAN13	*DNMT3A*	**High glucose / 5% O2** vs. High glucose / 20% O2	0.0008	Mean
MAN13	*DNMT3A*	**Low Glucose / 20% O2** vs. High Glucose / 20% O2	<0.0001	Mean
MAN7	*DNMT3B*	**Low Glucose / 5% O2** vs. High Glucose / 20% O2	0.0166	144 h
MAN7	*DNMT3B*	**High Glucose / 5% O2** vs. High Glucose / 20% O2	0.0085	144 h
MAN13	*DNMT3B*	**Low Glucose / 20% O2** vs. High Glucose / 20% O2	0.0021	Mean
MAN7	*MAT2A*	**Low Glucose / 5% O2** vs. High Glucose / 5% O2	<0.0001	Mean
MAN7	*MAT2A*	**Low Glucose / 5% O2** vs. Low Glucose / 20% O2	<0.0001	Mean
MAN7	*MAT2A*	**Low Glucose / 5% O2** vs. High Glucose / 20% O2	0.0021	Mean
MAN7	*MAT2A*	**High Glucose / 5% O2** vs. Low Glucose / 20% O2	<0.0001	Mean
MAN7	*MAT2A*	**High Glucose / 5% O2** vs. High Glucose / 20% O2	0.0282	Mean
MAN7	*MAT2A*	**Low Glucose / 20% O2** vs. High Glucose / 20% O2	<0.0001	Mean
MAN13	*MAT2A*	**Low Glucose / 5% O2** vs. High Glucose / 5% O2	<0.0001	Mean
MAN13	*MAT2A*	**Low Glucose / 5% O2** vs. Low Glucose / 20% O2	0.0142	Mean
MAN13	*MAT2A*	**Low Glucose / 5% O2** vs. High Glucose / 20% O2	<0.0001	Mean
MAN13	*MAT2A*	**High Glucose / 5% O2** vs. Low Glucose / 20% O2	<0.0001	Mean
MAN13	*MAT2A*	**Low Glucose / 20% O2** vs. High Glucose / 20% O2	<0.0001	Mean
MAN7	*TET1*	**Low Glucose / 5% O_2** vs. High Glucose / 5% O_2	0.0097	Mean
MAN7	*TET1*	**Low Glucose / 5% O_2** vs. High Glucose / 20% O_2	0.0222	Mean
MAN7	*TET1*	**High Glucose / 5% O_2** vs. Low Glucose / 20% O_2	0.0177	Mean
MAN13	*TET1*	**Low Glucose / 5% O_2** vs. High Glucose / 5% O_2	0.0092	Mean
MAN13	*TET1*	**Low Glucose / 5% O2** vs. Low Glucose / 20% O2	0.0194	Mean
MAN7	*TET2*	**Low Glucose / 5% O_2** vs. High Glucose / 5% O_2	0.0233	Mean
MAN7	*TET2*	**Low Glucose / 5% O_2** vs. High Glucose / 20% O_2	0.0061	Mean
MAN7	*TET2*	**High Glucose / 5% O_2** vs. Low Glucose / 20% O_2	0.0440	Mean
MAN7	*TET2*	**Low Glucose / 20% O_2** vs. High Glucose / 20% O_2	0.0136	Mean
MAN13	*TET2*	**Low Glucose / 5% O_2** vs. High Glucose / 5% O_2	<0.0001	Mean
MAN13	*TET2*	**Low Glucose / 5% O_2** vs. High Glucose / 20% O_2	<0.0001	Mean
MAN13	*TET2*	**High Glucose / 5% O_2** vs. Low Glucose / 20% O_2	<0.0001	Mean
MAN13	*TET2*	**Low Glucose / 20% O_2** vs. High Glucose / 20% O_2	<0.0001	Mean
MAN7	*TET3*	**Low Glucose / 5% O_2** vs. High Glucose / 5% O_2	0.0461	Mean

MAN7	*TET3*	**Low Glucose / 5% O_2** vs. High Glucose / 20% O_2	0.0474	Mean
MAN7	*TET3*	**High Glucose / 5% O_2** vs. Low Glucose / 20% O_2	0.0392	Mean
MAN7	*TET3*	**Low Glucose / 20% O_2** vs. High Glucose / 20% O_2	0.0394	Mean
MAN13	*TET3*	**Low Glucose / 5% O_2** vs. High Glucose / 5% O_2	<0.0001	Mean
MAN13	*TET3*	**Low Glucose / 5% O_2** vs. High Glucose / 20% O_2	<0.0001	Mean
MAN13	*TET3*	**High Glucose / 5% O_2** vs. Low Glucose / 20% O_2	<0.0001	Mean
MAN13	*TET3*	**Low Glucose / 20% O_2** vs. High Glucose / 20% O_2	<0.0001	Mean
MAN7	*SLC2A1*	**Low Glucose / 5% O2** vs. High Glucose / 20% O_2	0.0008	Mean
MAN7	*SLC2A1*	**High Glucose / 5% O_2** vs. High Glucose / 20% O_2	0.0087	Mean
MAN7	*SLC2A1*	**Low Glucose / 20% O_2** vs. High Glucose / 20% O_2	0.0373	Mean
MAN7	*SLC2A1*	**Low Glucose / 5% O_2** vs. High Glucose / 5% O2	0.0302	144 h
MAN13	*SLC2A1*	**Low Glucose / 5% O2** vs. Low Glucose / 20% O2	0.0062	Mean
MAN13	*SLC2A1*	**Low Glucose / 5% O_2** vs. High Glucose / 20% O_2	0.0003	Mean
MAN13	*SLC2A1*	**High Glucose / 5% O_2** vs. Low Glucose / 20% O_2	0.0038	Mean
MAN13	*SLC2A1*	**High Glucose / 5% O2** vs. High Glucose / 20% O2	0.0006	Mean
MAN7	*SLC2A3*	**Low Glucose / 5% O_2** vs. High Glucose / 20% O_2	0.0284	144 h
MAN7	*SLC2A3*	**High Glucose / 5% O2** vs. High Glucose / 20% O_2	0.0120	144 h
MAN13	*SLC2A3*	**Low Glucose / 5% O_2** vs. High Glucose / 5% O_2	0.0020	Mean
MAN13	*SLC2A3*	**Low Glucose / 5% O_2** vs. High Glucose / 20% O_2	0.0020	Mean
MAN13	*SLC2A3*	**High Glucose / 5% O_2** vs. Low Glucose / 20% O_2	<0.0001	Mean
MAN13	*SLC2A3*	**Low Glucose / 20% O_2** vs. High Glucose / 20% O_2	<0.0001	Mean
MAN7	*ATP5F1*	**Low Glucose / 5% O2** vs. Low Glucose / 20% O2	<0.0001	Mean
MAN7	*ATP5F1*	**High Glucose / 5% O_2** vs. Low Glucose / 20% O_2	<0.0001	Mean
MAN7	*ATP5F1*	**High Glucose / 5% O2** vs. High Glucose / 20% O2	0.0012	Mean
MAN7	*ATP5F1*	**Low Glucose / 20% O_2** vs. High Glucose / 20% O_2	0.0031	Mean
MAN13	*ATP5F1*	**Low Glucose / 5% O_2** vs. High Glucose / 5% O_2	<0.0001	Mean
MAN13	*ATP5F1*	**Low Glucose / 5% O_2** vs. High Glucose / 20% O_2	<0.0001	Mean
MAN13	*ATP5F1*	**High Glucose / 5% O_2** vs. Low Glucose / 20% O_2	<0.0001	Mean
MAN13	*ATP5F1*	**Low Glucose / 20% O_2** vs. High Glucose / 20% O_2	<0.0001	Mean
MAN7	*TIMM23*	**High Glucose / 5% O2** vs. Low Glucose / 20% O2	0.0255	Mean
MAN7	*TIMM23*	**Low Glucose / 20% O2** vs. High Glucose / 20% O2	0.0006	144 h
MAN13	*TIMM23*	**Low Glucose / 5% O_2** vs. High Glucose / 20% O_2	<0.0001	Mean
MAN13	*TIMM23*	**High Glucose / 5% O2** vs. High Glucose / 20% O2	0.0036	Mean
MAN13	*TIMM23*	**Low Glucose / 20% O_2** vs. High Glucose / 20% O_2	<0.0001	Mean
MAN7	*TRMT10C*	**Low Glucose / 5% O_2** vs. High Glucose / 5% O_2	0.0112	Mean
MAN7	*TRMT10C*	**High Glucose / 5% O2** vs. Low Glucose / 20% O_2	0.0008	Mean
MAN7	*TRMT10C*	**Low Glucose / 20% O_2** vs. High Glucose / 20% O_2	0.0087	Mean
MAN13	*TRMT10C*	**Low Glucose / 5% O2** vs. High Glucose / 5% O2	0.0440	Mean
MAN13	*TRMT10C*	**Low Glucose / 5% O_2** vs. High Glucose / 20% O_2	<0.0001	Mean
MAN13	*TRMT10C*	**High Glucose / 5% O2** vs. High Glucose / 20% O2	<0.0001	Mean
MAN13	*TRMT10C*	**Low Glucose / 20% O_2** vs. High Glucose / 20% O_2	<0.0001	Mean
MAN7	*SDHB*	**Low Glucose / 5% O_2** vs. Low Glucose / 20% O_2	0.0039	Mean
MAN13	*SDHB*	**Low Glucose / 5% O_2** vs. High Glucose / 5% O_2	<0.0001	Mean
MAN13	*SDHB*	**Low Glucose / 20% O_2** vs. High Glucose / 20% O_2	<0.0001	Mean

Table 4.1. Statistics for gene expression. This table shows all significant results from gene expression analyses. Results include group comparisons and indicates cell line (MAN7 and MAN13) gene names (*NANOG, OCT4, DNA DNMT1, DNMT3A, DNMT3B, TET1, TET2, TET3, MAT2A, TIMM23, TRT10C, ATP5F1, SDHB, SLC2A1, and SLC2A3*) and p values. Conditions that cause gene upregulation are in bold letters. The TYPE column indicates if the significant differences were calculated from mean values (from 12 hours to 144 hours) or just from one time point (144h).

4.5 Effect of glucose and oxygen on mitochondrial membrane potential (ΔΨm)

ΔΨm is a key indicator of cellular viability, as it reflects the pumping of hydrogen ions across the inner membrane during the process of electron transport and oxidative phosphorylation during ATP production [33]. Therefore, I aimed to quantitatively evaluate the effect of the use of different oxygen and glucose concentrations on ΔΨm in HESCs. ΔΨm was first assessed through the use of the probe tetraethylbenzimidazolylcarbocyanine iodide JC-1 (Thermo Fisher) which works by exhibiting potential-dependent accumulation indicated by a fluorescence emission shift from green for low ΔΨm (~529 nm) to red for high ΔΨm (~590 nm) [180].

Cells stained with JC-1 can be observed in Figure 4.5 where polarized mitochondria (Red) and depolarized mitochondria (green) can be identified HESCs. In addition, these results were quantified in MAN7 and MAN13 cell lines cultured under in glucose and oxygen concentrations. Figure 4.6 is representing the FACS plots results, showing cell population distribution in regards their mitochondrial energy level after JC-1 staining.

Statistical results in Figure 4.7 showed important differences between the two cell lines. Overall, MAN7 has more energized mitochondria than MAN13, with a mean population of 53.25% vs 24.07% respectively. However, no significant patterns or differences were identified in MAN7 as a result of the oxygen or glucose concentration differences.

On the other hand, MAN13 exhibited clear differences due to the glucose concentration at all the time points. Low glucose concentration (5 mM) increased the percentage of population with energized mitochondria in MAN13, independently on the oxygen concentration used during culture ($p<0.0001$).

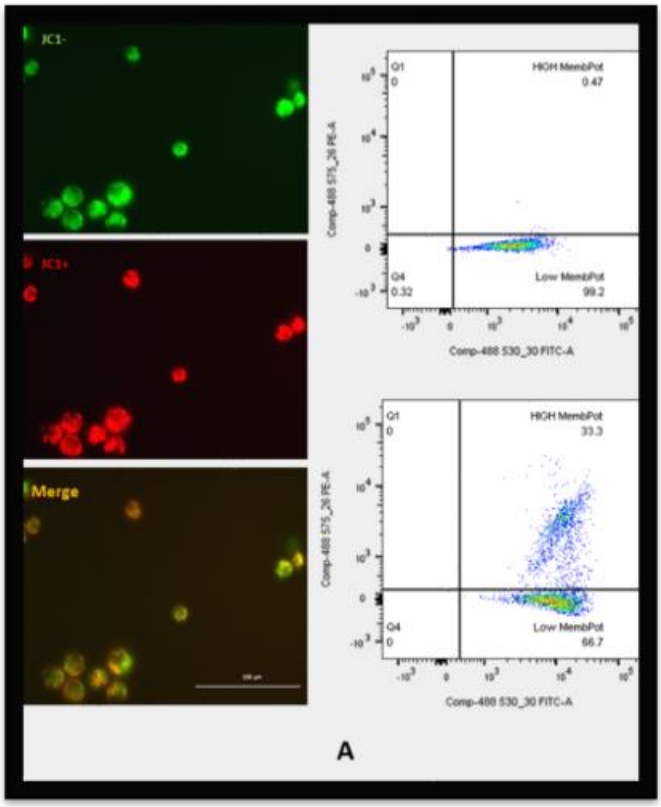

Figure 4.5.: Analysis of mitochondrial membrane potential (ΔΨm) in HESC (N=3). A: Representative images of HESCs after incubation with mitochondria membrane potential fluorescent dye (JC-1), exhibiting potential-dependent accumulation. This is indicated by a fluorescence emission shift from green for low ΔΨm (~529 nm) to red for high ΔΨm (~590 nm). Additionally, flow cytometry plots on the right hand side shows how populations with High/Low ΔΨm can be differentiated (x-axis FITC , y-axis PE). Top plot showing cells treated with FCCP then stained with JC1; this to create a cell population with depolarized or poorly energized mitochondria as control. Bottom plot show cells only stained with JC-1 probe. Cell populations contain both polarized and depolarized mitochondria.

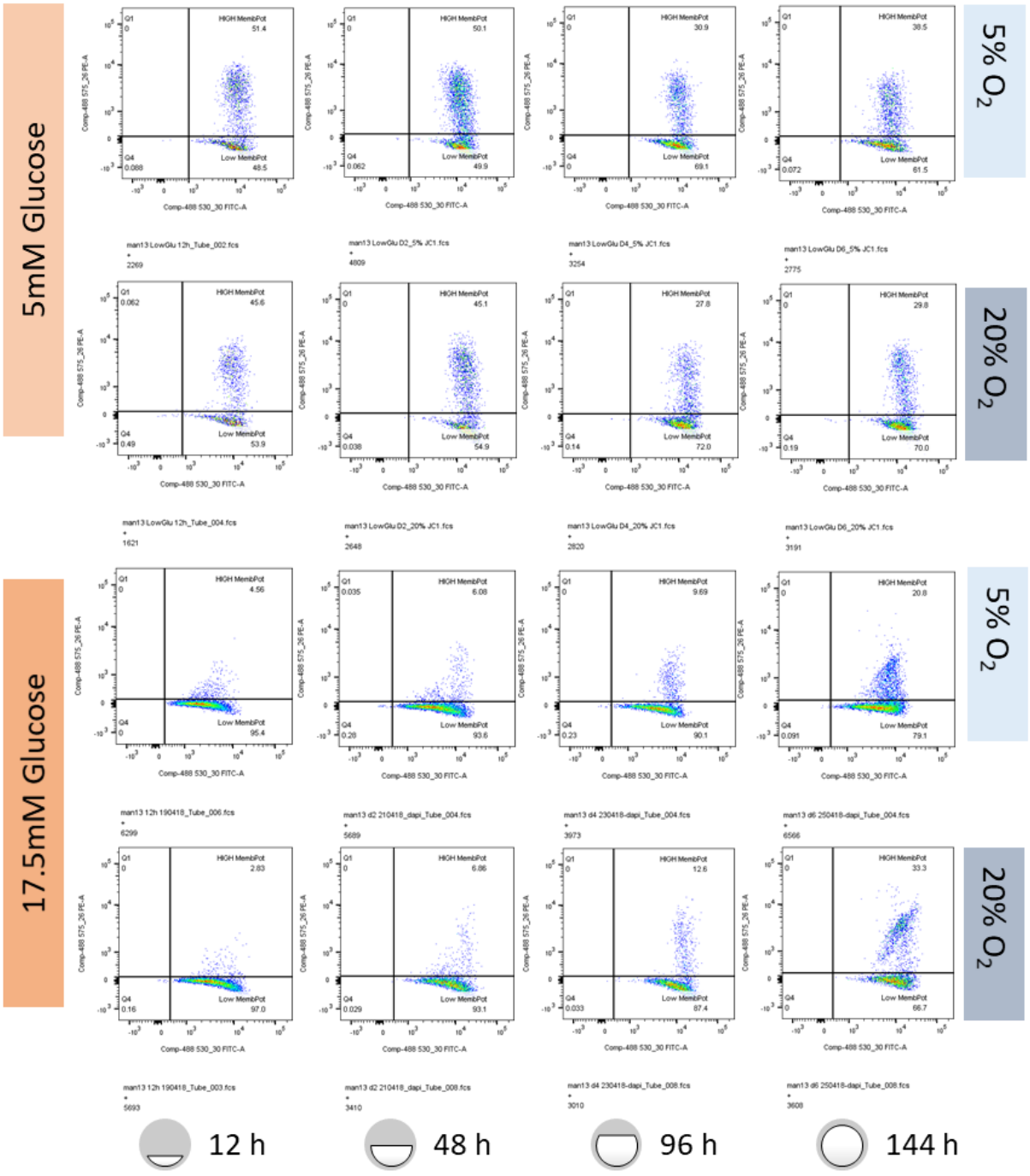

Figure 4.6 Analysis of mitochondrial membrane potential (ΔΨm), FACS.
Mitochondria membrane potential was determined in HESCs through the fluorescence emission shift from green (~529 nm) to red (~590 nm) from 12 hours to day 6. Representative flow cytometry plots shows cell population distribution of the MAN13 cell line according to average mitochondrial membrane potential. Bottom right quadrant of the plot allocates average low ΔΨm cells, whereas the top right allocates average high ΔΨm cells (x-axis FITC, Y-axis PE). Experimental conditions are separated in groups, showing glucose concentration (5 mM and 17.5 mM) and oxygen concentration (5% and 20%).

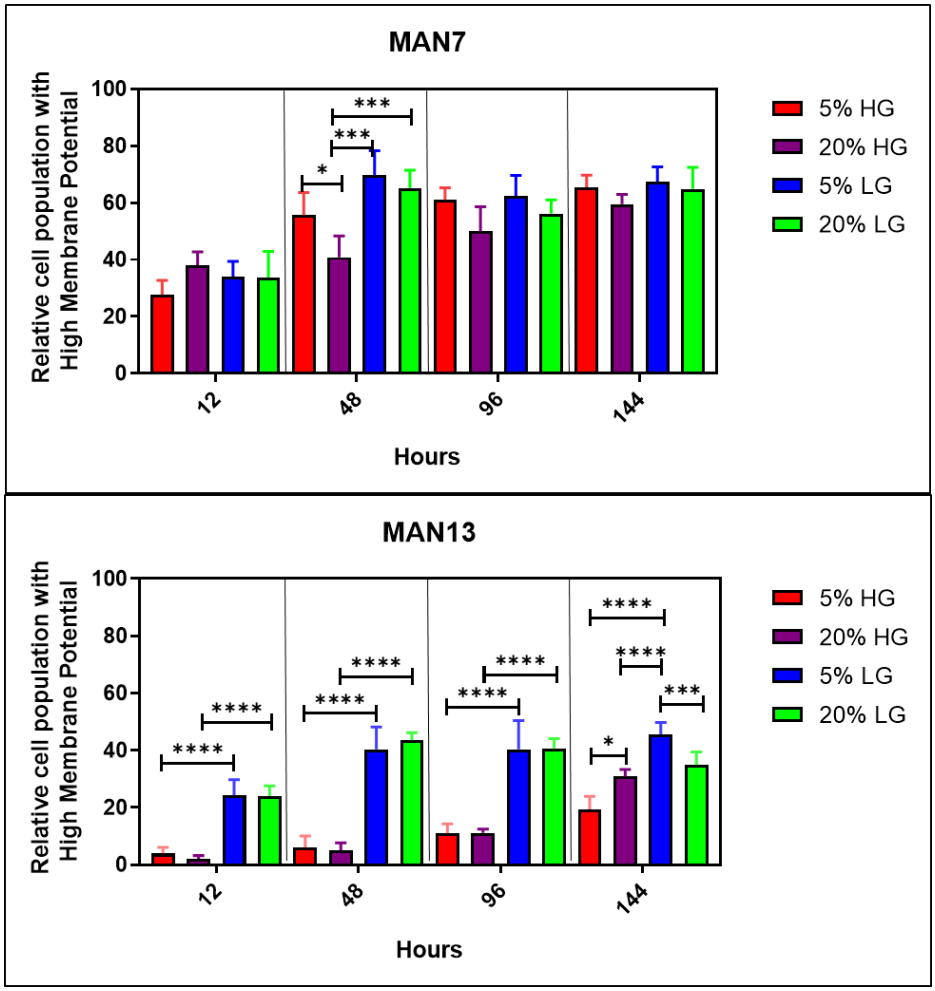

Figure 4.7 Comparison of mitochondrial membrane potential (ΔΨm)
MAN7 and MAN13 human embryonic stem cell lines were evaluated after incubation at 5% or 20% oxygen in combination with 17.5 mM glucose (HG) or 5 mM glucose (LG) and JC-1 dye. Measured by flow cytometry (n=3). Bar plots show cell population percentage (Mean ±SD) that exhibited average red fluorescence (~590 nm), which is indicative of high membrane potential in defined oxygen/glucose conditions.

4.6 Effect of glucose and oxygen on Mitochondrial DNA

Relative quantification of mitochondrial DNA (mtDNA) was determine in relation genomic DNA. To accomplish this objective, the mitochondrial gene MT-ND1 was analysed and compared against the nuclear gene EIF2C1 [181]. Overall, mitochondrial DNA was more abundant than nuclear gene in both cell lines independently of time, oxygen and glucose concentration. Abundance was 30% higher in MAN7 and 40% in MAN13 when comparing nuclear vs mitochondrial DNA (Ratio = gDNA CT/mtDNA CT).

The mean ratio of mitochondrial DNA was significantly higher in MAN13 ($p=0.0376$) compared to MAN7 (Figure 4.8). In MAN7 the mean ratio observed in the condition High glucose / 20% oxygen was significantly higher than in Low glucose / 20% oxygen ($p= 0.0494$). Moreover, the MAN7 showed significant differences at 96 hours, showing greater abundance in high glucose 5% oxygen compared to low glucose 20% oxygen ($p=0.0140$) and greater abundance in high glucose 20% oxygen compared to low glucose 20% oxygen ($p=0.0193$). On the other hand, MAN13 did not show significant differences in the mean ratio. However, it showed significant differences at 144 hours. Greater abundance in high glucose 5% oxygen compared to low glucose 5% oxygen ($p=0.0194$); greater abundance in high glucose 5% oxygen compared to low glucose 20% oxygen ($p=0.0440$) and greater abundance in high glucose 5% oxygen compared to high glucose 5% oxygen ($p=0.0020$).

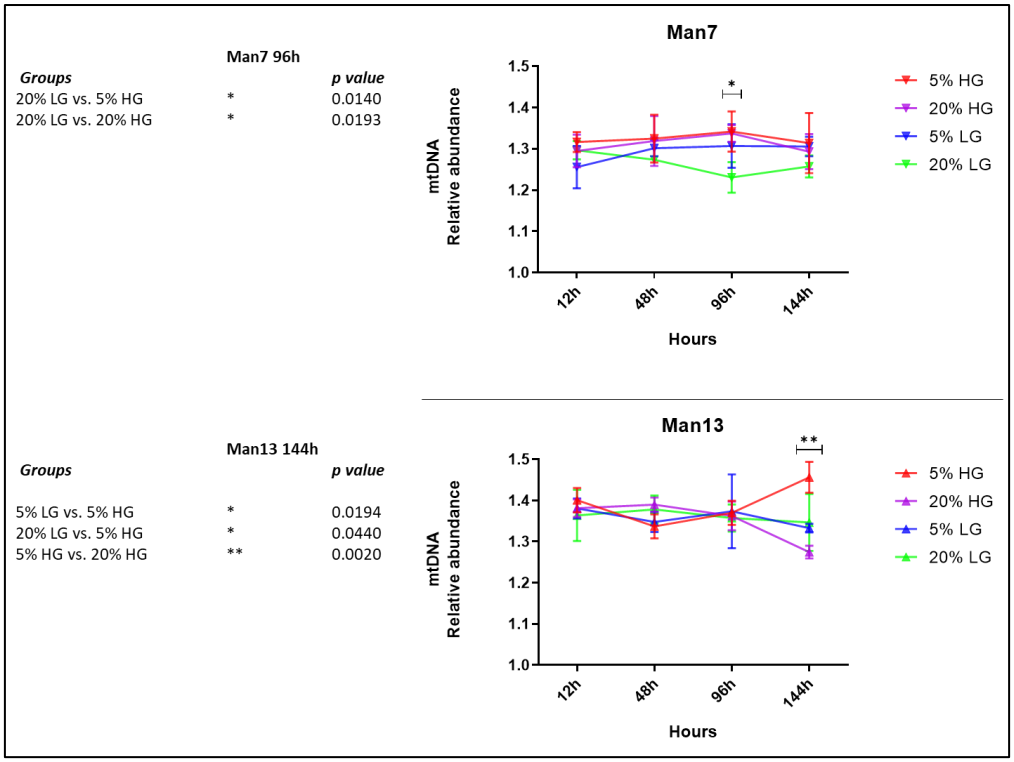

Figure 4.8. Analysis of mitochondrial DNA (mtDNA) in HESC (N=3). Plots showing mtDNA ratio (EIF2C1 / MT-ND1) in MAN7 and MAN13 cell lines. Analyses were performed in triplicates for each condition for each cell line. Statistical significance was calculated through 2-way ANOVA and Tukey's multiple comparison test (Mean ±SD).

4.7 Mitochondrial respiration

In order to determined mitochondrial respiration OCR and ECAR were measured by XF Cell Mito-Stress test kit (#101706-100, Seahorse Biosciences) and as described in Section 2.11. HESCs cultured in high glucose (17.5 mM) or low glucose medium (5 mM) were evaluated using modulator compounds (oligomycin, FCCP, rotenone and antimycin-A) that target the electron transport chain (ETC) in the mitochondria. These modulators were serially injected into the culture plate, which then was read by the Seahorse analyser to obtain OCR AND ECAR values (Figure 4.9). Each modulator targets a specific component of the ETC. Oligomycin inhibits ATP synthase (complex V), and the decrease in OCR following injection of oligomycin correlates with the mitochondrial

respiration associated with cellular ATP production. Carbonyl cyanide-4 (trifluoromethoxy) phenylhydrazone (FCCP) is an uncoupling agent that collapses the proton gradient and disrupts the mitochondrial membrane potential. As a result, electron flow through the ETC is uninhibited and complex IV maximally consumes oxygen. Spare respiratory capacity is a measure of the ability of the cell to respond to increased energy demand. The third injection is a mix of rotenone and antimycin-A, which shuts down mitochondrial respiration and enables the calculation of non-mitochondrial respiration driven by processes outside the mitochondria. Mitochondrial respiration parameters were the calculating according to Figure 4.10.

Mitochondrial respiration patterns can be observed in Figure 4.11 for MAN7 and MAN13 at 12 hours and 144 hours (day 6). Although the OCR levels were significantly different between MAN7 and MAN13, both cell lines showed the same behaviour due to changes in the glucose concentration. MAN13 cells showed higher basal OCR when compared to MAN7 (Fig. 4.11 and 4.12). The lowest basal OCR was observed for MAN7 LG and the highest for MAN13 LG. Both cell lines showed none significant differences due to glucose concentration in most of the parameters evaluated at 12 hours of culture. Except for the Maximal respiration parameter in MAN7 which was higher in low glucose than in high glucose ($p= 0.0133$). Besides the Non- mitochondrial oxygen consumption that were significantly higher in the high glucose group in MAN7 ($p= 0.0285$) in MAN13 ($p= 0.0075$) when compared tit her low glucose counterpart.

Furthermore, at day six more differences were observed in other parameters, in both cell lines. They showed similar behaviour of increased OCR in the low glucose group. Basal respiration in MAN7 was higher in low glucose than in high glucose ($p= 0.0249$), as well as inMAN13 ($p= 0.0010$). Maximal respiration in MAN7 was higher in low glucose than in high glucose ($p=0.0004$), as well as in MAN13 ($p<0.0001$). ATP production in MAN7 was higher in low glucose than in high glucose ($p= 0.0352$), as well as in MAN13 ($p= 0.0025$).

The overall effect of glucose concentration in both cell lines can be categorized using an the energy map where samples are allocated according to the mean OCR and ECAR values (Figure 4.12). This provides a visual indication of the type of metabolism

predominantly used by the cell population. We can observe that samples in high glucose condition (17.5 mM) at atmospheric oxygen were allocated towards a glycolytic metabolism in MAN7 and MAN13. Whereas the use of low glucose (5 mM) medium at atmospheric oxygen allocated samples towards a more energetic or oxidative metabolism (Figure 4.13).

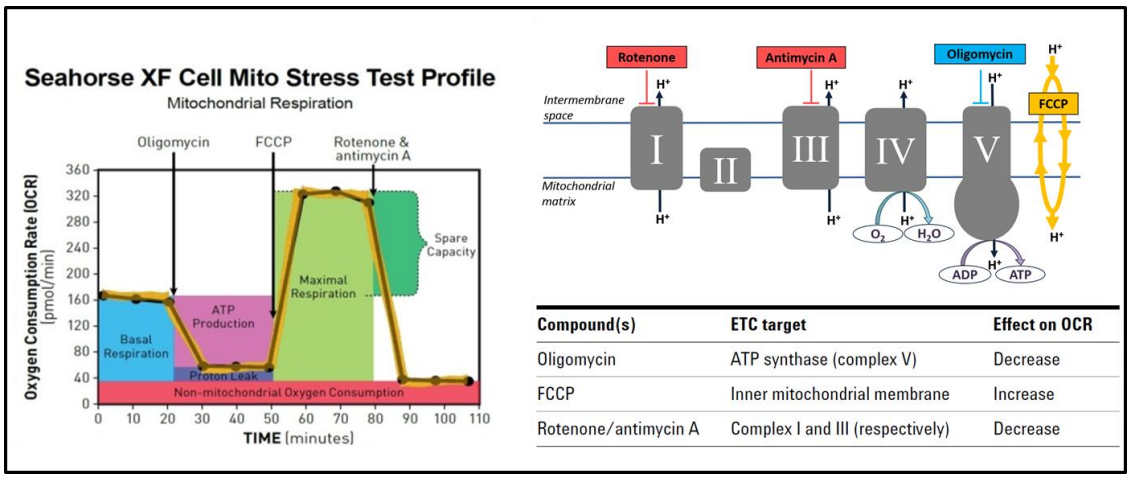

Compound(s)	ETC target	Effect on OCR
Oligomycin	ATP synthase (complex V)	Decrease
FCCP	Inner mitochondrial membrane	Increase
Rotenone/antimycin A	Complex I and III (respectively)	Decrease

Figure 4.9. Cell Mito Stress test profile. This scheme represents the fundamentals of mitochondrial test, modulators, ECT targets, and injection times during test (Agilent Seahorse XFp, Cell Mito Stress Test Kit, User Guide, Kit 103010-100). Oligomycin inhibits ATP synthase (complex V). Carbonyl cyanide-4 (trifluoromethoxy) phenylhydrazone (FCCP) disrupts the mitochondrial membrane potential and inhibits ETC, which produces maximum consumption of oxygen by complex IV. The combination of Rotenone/Antimycin-A shuts down mitochondrial respiration and enables the calculation of non-mitochondrial respiration driven by processes outside the mitochondria.

Parameter Value	Equation
Non-mitochondrial Oxygen Consumption	Minimum rate measurement after Rotenone/antimycin A injection
Basal Respiration	(Last rate measurement before first injection) – (Non-Mitochondrial Respiration Rate)
Maximal Respiration	(Maximum rate measurement after FCCP injection) – (Non-Mitochondrial Respiration)
H+ (Proton) Leak	(Minimum rate measurement after Oligomycin injection) – (Non-Mitochondrial Respiration
ATP Production	(Last rate measurement before Oligomycin injection) – (Minimum rate measurement after Oligomycin injection)
Spare Respiratory Capacity	(Maximal Respiration) – (Basal Respiration)
Spare Respiratory Capacity as a %	(Maximal Respiration) / (Basal Respiration) × 100
Acute Response	(Last rate measurement before oligomycin Injection) – (Last rate measurement before acute injection)
Coupling Efficiency	ATP Production Rate) / (Basal Respiration Rate) × 100

Figure 4.10. Cell Mito Stress Test Kit parameter calculation. This table explains the calculations applied to obtain every parameter (Agilent Seahorse XFp, Cell Mito Stress Test Kit, User Guide, Kit 103010-100).

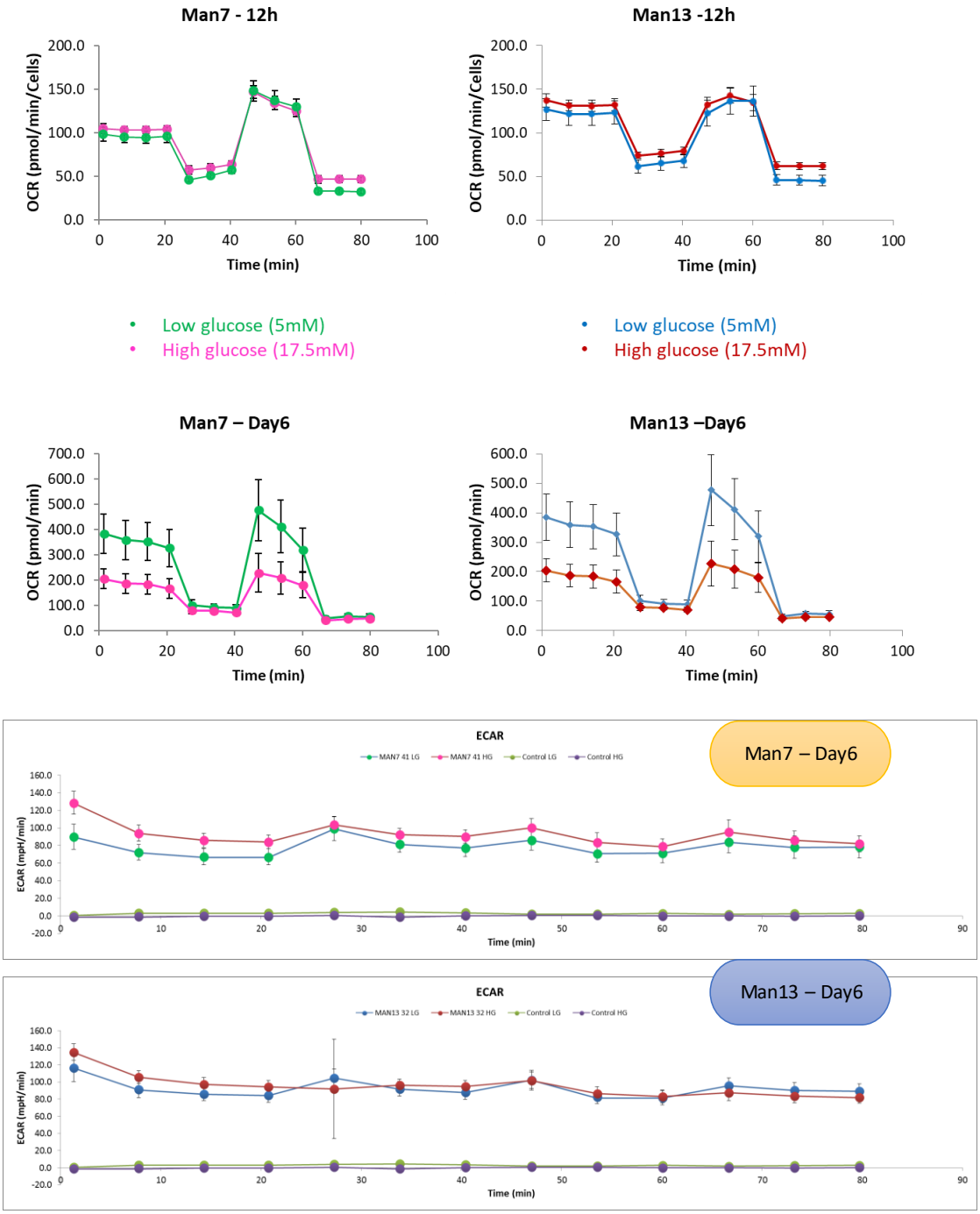

Figure 4.11. Analysis of mitochondrial respiration on HESC (MAN7 and MAN13). MAN7 and MAN13 show similar metabolic profiles. HESC cultured in high glucose have lower mitochondrial respiration activity and higher glycolytic rate than HESC cultured in low glucose. oxygen consumption rate (OCR) and extracellular acidification rate (ECAR) measured in the Seahorse Extracellular Flux assay are shown. To test energetic preference when glucose is present at 17.5mM or 5mM. Results summarized from three independent biological experiments, each consisting of independent cell plating on at least fifteen Seahorse microplate wells for each condition. The error bars represented the standard error of the mean, as calculated by sample standard deviation divided by the square root of the sample size.

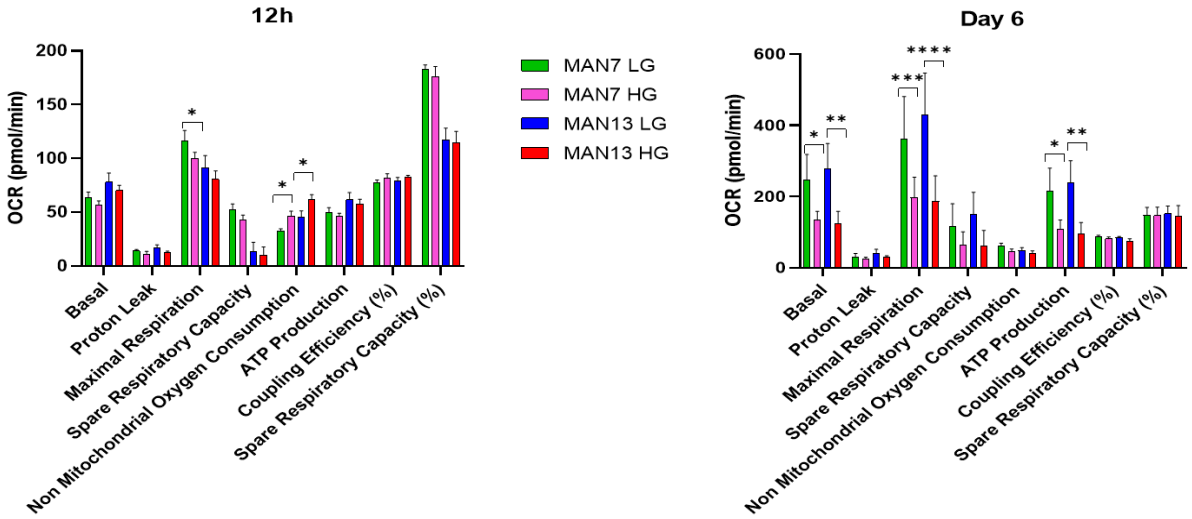

Figure 4.12. Cell Mito Stress Test parameters**.** Parameters calculated from OCR values according to Figure 4.10. Left plot shows comparison between MAN7 and MAN13 cell lines at 12 hours after culture. Right plot shows comparison between MAN7 and MAN13 cell lines at 144 hours after culture (*p<0.05).

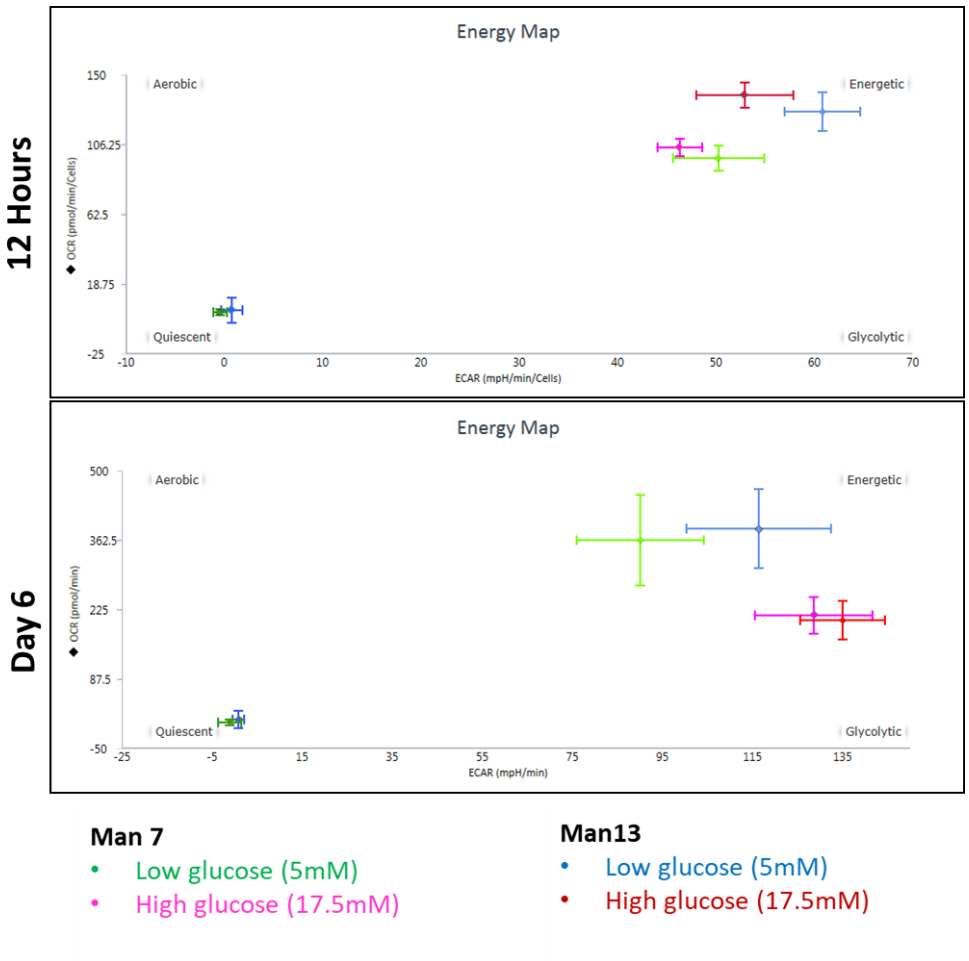

Figure 4.13. Metabolic phenogram contrasting basal OCR and ECAR. MAN7 and MAN13 comparing effect of glucose concentration in atmospheric oxygen. Graphical representation of the energetic shift caused by glucose after six day in culture. Cell lines in high glucose have a higher glycolytic metabolism by day 6 in comparison to their low glucose counterparts.

4.8 Discussion

Human embryonic stem cell research has emerged as an important platform for the understanding and treatment of human diseases. Although there are ethical concerns in regards the usage, and destruction of human embryos, HESCs provide an alternative useful cell source for several potential applications in both basic science and medical treatment. More specifically, they could be a great alternative to replace the use of animal models and human embryos for studying in vitro preimplantation development.

Culture conditions for human embryonic stem cells have been improved during past years with the objective of studding the natural mechanisms of embryonic stem cells. Significant advances have been made over the past decade to understand the metabolic requirements of stem cells and the important role that energy metabolism plays in regulating stem cell function and fate. Metabolic changes are often some of the earliest to occur during cell fate transitions and new evidence supports the idea that metabolic pathways directly contribute to the epigenetic reprograming of the cell. It is extremely important to understanding the microenvironment in which cells are cultured, as according to recent studies, modifying availability of a single metabolic substrate could dramatically impact the stem cell identity [126].

Oxygen and glucose concentration are crucial components during cell culture but their concentration can vary depending on the methodology followed, which is a controversial topic in stem cell research and in assisted reproduction. This study was designed to investigate the impact of oxygen concentration (5% and 20%) in combination with low or high glucose (5 mM or 17.5 mM) on HESCs. Specifically the research was aimed to determine if this impact was similar to that observed on human preimplantation embryos.

Experiments with two HESC lines (MAN7 and MAN13) were carefully carried out with complete control over the atmospheric conditions in which the cells were cultured. Special care was taken to make sure that the low oxygen treated cells were minimally exposed to ambient oxygen during the experimentation. Furthermore, in this study data from two distinct HESC lines in four conditions were compared. This approach was useful to start to identify cell line-specific effects and have a better understanding of the core HESC response to glucose and oxygen concentration.

The maintenance of glycolytic metabolism and high levels of lactate production are crucial to maintain pluripotency in HESCs, and a shift to OXPHOS is indicative of cell differentiation [182] However, there are controversial findings in regards the oxygen role on the metabolic shift. It has been suggested that oxygen levels influence the factors that maintain pluripotency as HESCs replicate well in 1–5% oxygen and resist spontaneous differentiation compared to culture in 21% oxygen [183]. On the other hand, other studies have suggested that a pluripotent stages is relatively insensitive to oxygen levels in chemically defined or undefined culture media [134].

To determine the effect of oxygen on the pluripotency state of the MAN cell lines, characterization of our HESC lines was performed by immunofluorescence and flow cytometry, using some of the most common markers reported by the International Stem Cell Initiative [127]. Interestingly, some recent studies have reported increased expression of pluripotency markers on HESCs in hypoxic conditions (5% oxygen) [184] [185] [186][187]. Other studies have reported non compromised pluripotency due to oxygen level in culture [188]. In this study significant effects were observed due to glucose concentration but not due to oxygen concentration.

Although we also used 5% oxygen, for the low oxygen condition we do not consider this as a hypoxic condition but a physiological oxygen level. In fact, we also evaluated gene expression of hypoxia markers (*HIF1A, HIF2A, ARNT*) without finding differential expression between cultures in 5% and 20% oxygen both cell lines, MAN7 and MAN13. Overall, low oxygen tension has been associated with the promotion of the undifferentiated state in several adult stem cells, but the molecular mechanisms underlying these observations remained obscure until recently. [189]. Moreover, the hypoxic conditions have correlated to the increased expression of pro-survival factors and anti-apoptotic markers. However, I did not find significant differences in MAN7 and MAN13 when evaluating markers of cell survival (*BAX, BCL2, BCL2L1, CBL, DAP3, TP53*) in high and low oxygen. As stated before, some researchers have demonstrated that physiological oxygen levels are beneficial for self-renewal and the in vitro maintenance of the undifferentiated state of HESCs, as well as other stem cells such neural crest stem cells (NSC) and BMSC as there is a decrease in the amount of spontaneous differentiation. There is also some evidence suggesting that ROS production decreases

in low oxygen tension, whereas other studies suggest that acute hypoxia contributes to the generation of ROS [190]. It is clear that the mechanisms underlying stem cell maintenance and their direct association with oxygen are still controversial. In this study, no significant differences were found for genes related to cell growth and differentiation (*CDX2, EGFR, EOMES, EP300, FGF4, ZSCAN4*), oxidative stress (*SOD1, SOD2, SOD3, GPX2*) or transcription factors (EIF1AX, EIF2S2, TRIM28) between cell culture at 5% or 20% oxygen nor 5 mM and 17.5 Mm glucose.

DNA methylation enzymes that can impair stem cell self-renewal and lead to the loss of pluripotency and differentiation were evaluated in this project (*DNMT1*, *DNMT3A*, *DNMT3B*, *TET1*, *TET2*, *TET3*, *MAT2A).* In this study, the expression of *DNMT1* was very low in both embryonic stem cell lines, which was in agreement with the high expression of this enzyme in somatic cells. However, significant differences were identified due to glucose concentration. In MAN7 at physiological oxygen *DNMT1* was upregulated in low glucose ($p=0.0387$) relative to high glucose. In MAN13, *DNMT1* was upregulated in low glucose at atmospheric oxygen ($p=0.0003$) relative to high glucose.

DNMT3A and *DNMT3B* are de novo methyltransferases that function synergistically to methylate the promoters of the Pou5F1/*OCT4* and *NANOG* to reduce pluripotency [191][192]. In this study, at least one of the markers *DNMT3A* or *DNMT3B* showed contrasting expression against *OCT4* and *NANOG*. In MAN7, *DNMT3A* was upregulated when cells were maintained at atmospheric oxygen in low glucose, relative to high glucose ($p=0.0165$). *DNMT3B* in MAN7 at day six of culture (144 h) was upregulated in high glucose at 20% oxygen ($p=0.0085$) compared to the low glucose counterpart and at 5% oxygen, whereas *OCT4* and *NANOG* were downregulated in low glucose. In MAN13, *DNMT3A* was upregulated the high glucose group relative to low glucose ($p<0.0001$), at physiological and atmospheric oxygen. *DNMT3B* was upregulated in high glucose at 20% oxygen compared to the low glucose counterpart ($p=0.0021$) whereas *OCT4* and *NANOG* were downregulated in low glucose. This suggest that these genes were more sensitive to glucose concentration than to oxygen, however there are significant differences between cell lines.

Similarly, MAT2A has been reported downregulated in hPSCs at 5% oxygen when cultured in mTeSR1 medium [193][194]. However Iwe found it upregulated in MAN7

and MAN13 cultured in E8 medium at low glucose ($p<0.0001$) relative to high glucose, in both concentrations 5% and 20% oxygen. These findings suggest that in our culture conditions the synthesis of S-adenosyl methionine (SAM) from ATP and methionine was increased in the presences of high glucose concentration. Which could be indicative of a greater methylation activity.

The DNA demethylation of 5-methylcytosine (5mC) is achieved via successive oxidation reactions catalysed by the TET enzymes. These require oxygen as a co-factor, and hence may link epigenetic processes directly to oxygen gradients during stem cell formation and cell differentiation. TET activity has been compromised at 1% oxygen compared to atmospheric oxygen (20%) [195]. In this study, differential expression was found in relation to the glucose concentration in the medium but not due to oxygen. Nevertheless is important to consider that we have used 5% and 20% oxygen and a completely different culture medium, which suggest that the substrate availability may also be crucial for TET regulation.

We have evaluated the expression of markers for metabolism and mitochondrial activity to help us determine the metabolic state of the cells and to try to identify any altered metabolic pathway. Expression of *SLC2A1* (GLUT1) was found differentially regulated when comparing culture at 20% and 2% oxygen. However, in another study the expression patterns were opposite when comparing H1 and H9 cell lines [196]. Also, *SLC2A1* was found upregulated at 4% oxygen compared to 21% oxygen [184]. In correlation with this study, *SLC2A1* was upregulated in 5% oxygen relative to 20% oxygen in MAN7 and MAN13. This correlates with the reported finding of an increased metabolic flux at physiological oxygen, the upregulation of *SLC2A1* and its association to the promotion of H3K9/H3K27 Acetylation and repression of H3K27 trimethylation. Hence, oxygen controls the direction and magnitude of glucose- derived carbon flux within hPSC; several metabolites that are derived from glucose are epigenetic modifiers [193]. In contrast to the glucose transporter GLUT1, GLUT3 was reported downregulated by physiological oxygen in Hues7 cell line. Silencing GLUT3 caused a reduction in glucose uptake and lactate production as well as *OCT4* expression. GLUT3 and *OCT4* expression were correlated suggesting that HESC self-renewal is regulated by the rate of glucose uptake [186]. In this study with MAN7 and MAN13 cell lines, no

correlation between GLUT3 (*SLC2A3*) and *OCT4* was found. In fact, GLUT3 was found to be regulated by the concentration of glucose in culture media but not by oxygen, and it was inversely correlated with *NANOG*. Core pluripotency factors have been demonstrated to directly regulate glycolysis in PSCs. *OCT4* directly regulates transcription of hexokinase 2 and pyruvate kinase M2. *SOX2*, *OCT4*, and *NANOG* have binding sites at the GLUT1 enhancer to regulate downstream glycolytic flux [197]. Our findings partially correlate with other authors' but suggest that glucose transporters interact closely with pluripotency factors. However, there is not a clear mechanism as there are controversial findings depending on the culture media used and the embryonic stem cell lines. For instance, modified MEM media contains high glucose has been demonstrated to improve the efficiency of ES cell derivation remarkably, compared with Knockout Dulbecco's- Modified Eagle Media [198]. Other studies reported that reduction of glucose stimulated cell proliferation and high glucose enhanced apoptosis in a rat model. Hence, high glucose could be more deleterious to stem cell therapy due to the aggravation of oxidative stress triggered by the hyperglycaemia [199]. Whereas, in a more recent study high glucose was found to inhibit ESC differentiation into cardiomyocytes by suppressing key developmental genes essential for the cardiac program. This was possible due to an anti-oxidative stress mechanism activated due to hyperglycaemia [200].

Furthermore, we have found differences in gene expression of mitochondrial proteins mostly due to glucose concentration but not due to oxygen. Only the mitochondrial transporters *TIMM23* and *TRMT10C* were sensitive to oxygen and glucose. In addition, we could not find any consistent differences in mtDNA as a result of oxygen concentration or glucose. Mitochondrial membrane potential levels were significantly higher in MAN7 relative to MAN13. Significant differences were observed due to glucose only in MAN13, with higher membrane potential in the low glucose group. Other studies reported oxygen levels as the cause of altered mitochondrial gene expression, mtDNA copy number, metabolic flux and carbohydrate use in HESCs. But no alterations were found in glycolytic rate, mitochondrial membrane potential ratio and mitochondrial proteins [188]. Classification of ESCs according to low or high mitochondrial membrane potential also reflects the activation status of the mTOR

pathway (mTORC1), which is correlated with pluripotency and differentiation capacities. The mTORC1 complex is sensitive to amino acids, stress, oxygen, energy, and growth factors. It promotes cell growth and cell cycle progression by inducing anabolic processes, such as the biosynthesis of proteins and lipids and the stimulation of mitochondrial biogenesis and metabolism, while limiting catabolic processes, including autophagy [182]. Decreased pluripotency and increased the differentiation capacities of mESCs have been correlated with high mitochondrial membrane potential [182].

The mitochondrial respiration analysis suggests that high glucose levels in culture media promote glycolytic metabolism as the two cell lines cultured in high glucose showed significant reduced levels or OCR, which correlates to previous reports. A glycolytic metabolic phenotype is crucial in the maintaining stemness while switching to oxidative metabolism is associated with stem cell differentiation [132]. However, this mechanisms may not apply for all types of stem cells.

In another study, undifferentiated mouse TSCs maintained significantly higher oxidative respiration compared to undifferentiated ESCs but oxidative respiration does not significantly alter upon TSC differentiation [201]. Given that stem cells and differentiated cells display different metabolisms and metabolomes, it is not surprising that nutrient and energy-sensing pathways are involved in the regulation of stem cell pluripotency and differentiation. For instance, one study reported that E8 medium supplemented with AlbuMAX significantly increased the basal respiration of HUES 9, H9, and IMR90 iPSCs. These data indicate that chemically defined media induced a profound reliance on biosynthetic fluxes. In turn, metabolic reprogramming influences the respiratory state, gene expression profile, and mitochondrial function. The aforesaid contrast the concept of mitochondrial inactivity as a key requirement for pluripotency-associated metabolic reprogramming and illustrate the confounding effects of nutrient availability in hPSC metabolic studies [133].

Moreover, recent evidence suggests that stem cells may exhibit substantial metabolic diversity, even under routine culture conditions. As we know, stem cells have the capacity to re-enter the cell cycle and proliferate. To proliferate, cells must increase their uptake and catabolism of complex nutrients to support anabolic cell growth. Intermediates of central metabolic pathways are key players that influence cell-

differentiation 'decisions'. Consequently, how cells rewire metabolic pathways to support proliferation can have profound consequences for cellular identity. Glucose for instance, is one of the fundamental substrates for mammalian cells growing in culture. Beyond generating ATP and NAD(P)H, the catabolism of glucose generates precursors to sustain the synthesis of proteins and nucleic acids, such as ribose. Therefore, although the relative dependency on metabolic precursors can vary depending on the cell line, culture conditions and nutrient availability are fundamental for stem cell proliferation as the central role of glucose is supporting anabolic growth [202].

The discrepancy between our study and the literature could be due to significant differences in the experimental settings, as authors reported their finding using different human embryonic stem cell lines cultured in completely different medium formulation.

It is important to recognize the significant progress made in basic and translational research using human embryonic stem cells (HESCs) in the past 20 years. Although the fundamental principle of stem cell research remains the same (i.e. the development of undifferentiated cells into committed cell lineages for the purpose of tissue formation, renewal and repair), the field has evolved and diversify in many new applications, including cell-based therapies, drug screening and study early development.

These new applications are intriguing and promising, however they remain in the early stages and additional research is needed. Especially in regards metabolism, and the regulatory mechanisms involved in cell stemness and cell differentiation. It is important to identify strategies, which human pluripotent stem cells may use to maintain high glycolytic rates depending on the nutrient and oxygen availability. For instance, it would be worth investigating the role of the hexokinase II and pyruvate dehydrogenase (PDH) [131] and other factors such as *ZIC3, ESSRB, LIN28, cMyc, PKM2, LDHA* that have been identified as upstream regulators of OXPHOS, glycolysis and the One carbon metabolic pathway [197]. Also the role of nutrient availability on the regulation of de novo fatty acid synthesis and the methionine pathway should be studied. Finally, it is crucial to understand if mitochondrial differences (structure and activity) are the causes or consequence of cell differentiation, as well as the mechanism that precede this cell decisions [197]. To complement this, further investigation regarding the impact of

nutrient availability on glucose consumption, glucose to lactate flux, DNA methylation, global acetylation and chromatin accessibility would be necessary.

CHAPTER 5

General discussion

Assisted reproduction technologies have been in the spotlight since several studies have reported an increased risk of an adverse perinatal outcome in IVF offspring. Despite numerous pieces of evidence, knowledge about the exact mechanisms affected is still limited. This thesis is primarily focused on studying the impact of glucose and oxygen concentration on the preimplantation human embryo that can have possible long-term consequences in the offspring, and specifically on transcriptomic alterations, mitochondrial function and DNA methylation. `It also studies the impact of the same conditions on human embryonic stem cells with the aim of determining their suitability as a good model for further research on in vitro preimplantation development.

During preimplantation development, embryos are highly sensitive to the environment. Here, transcriptional regulation, epigenetic regulation and metabolism could be easily compromised leading to aberrant long-term health outcomes in the offspring [3] [178]. Previous studies have compared media formulations and culture conditions to demonstrate differential gene expression and DNA methylation [145] [115].

Human embryonic stem cell research has emerged as an important platform for the understanding the development of human diseases. HESCs provide an alternative useful cell source for several applications in basic and applied science. They are suitable candidates to replace the use of animal models for studying human embryo development in vitro [203] [204].

Controversial findings in regards to the impact of oxygen during embryo development have been reported. However, studies tend to agree on the beneficial effect physiological levels of oxygen (~5%) and on the negative effect of atmospheric oxygen tension (~20%). Improvements in human embryo quality and pregnancy rates have been observed with physiological oxygen [148]. Whereas in HESCs, physiological oxygen has been associated with the promotion of the undifferentiated state and to

the increased expression of pro-survival factor and anti-apoptotic markers, although the molecular mechanisms remained unknown until recently [189]. There is also some evidence suggesting that ROS production decreases in low oxygen tension, whereas other studies suggest that acute hypoxia contributes to the generation of ROS [190].

The impact of oxygen and glucose on transcript levels in embryos and in HESCs was evaluated in this thesis. Physiologic (5%) and atmospheric (20%) oxygen was evaluated in both models, and glucose concentrations of 0.9 mM and 3.5 mM in embryos and 5 mM and 17.5 mM in HESCs.

Non-significant effects were found on cell survival and cell differentiation markers in both embryos and HESCs. With the exception of EOMES, which is an important gene for Trophectoderm (TE) differentiation and is affected by ART techniques [152] [153]. In this study, EOMES was upregulated in embryos cultured at 20% oxygen relative to 5% oxygen, which could suggest that trophectoderm cells and placenta formation might benefit from atmospheric oxygen.

Pluripotency markers (*OCT4*, *SOX2* and *NANOG*) were not significantly affected in embryos or in HESCs due to oxygen concentration. These findings are controversial as several studies have reported increased expression of pluripotency markers on HESCs in hypoxic conditions (5%) [184] [185] [186][187]. Other studies have reported non compromised pluripotency due to oxygen level [188]. On the other hand, these markers were found significantly upregulated in high glucose (3.5 mM and 17.5 mM respectively) in both models. *OCT4* has been found upregulated in embryos in ESCM medium relative to KSOM medium [154]. Additionally, these markers have been reported downregulated in fresh embryos, relative to frozen embryos [153].

DNA methyltransferases (DNMTs), which are important epigenetic regulators in embryo and tissue development as well as differentiation [38] were not differentially regulated in this study, when comparing between 5% and 20% oxygen in embryos and in HESCs. In embryos, *DNMT3A* was significantly upregulated in high glucose, whereas expression of *DNMT1* and *DNMT3B* were not significantly different between high glucose and low glucose. Other studies in human embryos reported *DNMT3A* differentially regulated due to the media composition but not due to oxygen

concentration [149]. In HESCs, *DNMT1*, *DNMT3A* and *DNMT3B* were differentially regulated due to oxygen concentration. However, the regulation was different depending on the cell line (MAN7 or MAN13). Similarly, we found MAT2A upregulated in low glucose media. Other studies in HESCs have reported differential regulation when cells are culture in different maintenance medium [193][194].

Despite the requirement of oxygen as a co-factor to oxidase DNA during demethylation catalysed by the TET enzymes [195], oxygen concentration did not affect their expression. Similar to DNA methyltransferases, DNA demethylases (*TET1*, *TET2* and *TET3*) were not affected by oxygen concentration in embryos and in HESCs. *TET1* and *TET2* where upregulated in embryos cultured in high glucose. In HESCs, the regulation was variable for every enzyme but their expression was also significantly affected by glucose concentration. TET enzymes are crucial in the reprogramming of DNA methylation during early embryo development [106]. Their exposure to oxidative stress has been shown to alter their regulation and impact the long-term imprinted gene regulation [104]. This evidence suggests the substrate availability may be crucial to regulate oxidative stress and consequently regulate TET enzymes. To date there are no other studies that provide evidence or direct effect of glucose concentration on the regulation of epigenetic markers.

Mitochondrial enzymes were not significantly affected by oxygen in embryos but *TIMM23* was significantly upregulated in high glucose relative to low glucose. In HESCs, the mitochondrial transporters *TIMM23* and *TRMT10C* were sensitive to both oxygen and glucose in variable levels depending on the cell line. *TIMM23* has been associated with neurological phenotypes and reduced life span in mice, as it has a critical role of the mitochondrial import machinery for maintaining mitochondrial function [205] .It has been reported mis-regulated in embryos when cultured in different media, Whitten's medium and KSOM medium [149].

Glucose transporter 1 (*SLC2A1*) was upregulated in embryos and in HESCs at 5% oxygen relative to 20%. This correlates to other studies [196], [184], [155]. Upregulation of *SLC2A1* is associated with promotion of H3K9/H3K27 acetylation and repression of H3K27 trimethylation. Hence, oxygen controls the direction and

magnitude of glucose- derived carbon flux, and several metabolites of glucose are epigenetic modifiers [193].

Glucose transporter 3 (*SLC2A3*) was not affected by glucose or oxygen in embryos but it was affected by glucose in HESCs. Interestingly, GLUT3 has been reported to be sensitive to oxygen in HESCs [186]. In mouse embryos, hyperglycaemic in vitro culture is associated with downregulation of glucose transporters (*GLUT1, GLUT2, GLUT3*) whereas in equines the effect is opposite [159] [158]. Despite the evidence available in regards the interaction of glucose transporters and pluripotency factors [197] we could not find any correlation in our data. The amino acid transporter (*SLC7A3*) was not affected by oxygen or glucose in HESCs but it was affected by glucose in embryos. *SLC7A3* has been reported differentially regulated when embryos were culture in Whitten's medium or KSOM medium [149] [157]. Additionally, all genes previously mentioned were evaluated in preimplantation blastocysts that were developed in vitro at low or high glucose concentration (0.9 mM or 3.5 mM respectively) to determine differential methylation. Despite the impact of glucose on gene expression, non-significant results were found in terms of differential methylation between the two conditions for these genes.

Mitochondrial function is critical to ensure developmental competence of embryos. Microenvironment changes, nutrient availability have been associated with alterations in blastocyst mitochondrial function [27]. Mitochondrial membrane potential is a key indicator of cellular viability, as it reflects the movement of hydrogen ions across the inner membrane during oxidative phosphorylation for ATP production [32]. Differential mitochondrial allocation in fresh and frozen embryos were observed. In this thesis, frozen embryos presented homogeneous distribution of polarized and depolarized mitochondria through the cytoplasm. On the other hand, fresh embryos presented a clear heterogeneous distribution as polarized mitochondria were preferably allocated in TE with depolarized mitochondria in ICM, which correlates with the functional compartmentalization effect [25]. Although results were not conclusive, the mean ratio of membrane potential was consistently reduced in frozen embryos. This can be an indicator cellular damage or reduced developmental potential [25]. In HESCs mitochondrial membrane potential was significantly different in regards

the cell line. Besides, higher membrane potential levels were observed in low glucose media relative to high glucose. In addition, we could not find any consistent differences in mtDNA as a result of oxygen concentration or glucose. On the other hand, other studies have reported oxygen levels as the cause of altered mitochondrial gene expression, mtDNA copy number, metabolic flux and carbohydrate use in HESCs [188]. Moreover, decreased pluripotency and increased the differentiation capacities in mESCs have been correlated with high mitochondrial membrane potential [182]. This suggest that at least in this study, low glucose could be detrimental for our HESC lines. This correlates with the findings on mitochondrial respiration, as HESCs cultured in high glucose showed significant reduced levels or OCR, which is indicative of a glycolytic phenotype rather than oxidative. A glycolytic phenotype is crucial for maintaining stemness while switching to oxidative metabolism is associated with stem cell differentiation [132]. However, it's important to always carefully consider the cell type, and the metabolic state as naïve and prime cells could respond differently to this principle [206][134].

Although there is clear evidence that ART is associated with a broad range of early life disorders, the exact mechanisms that alter embryo development remain unknown [178]. Numerous evidence suggests that the pathogenesis involves changes in chromatin which can contribute to a persistent dysregulated metabolic phenotype [207]. Children conceived by ART have developed vascular dysfunction [172] altered lipid profile, and cardiovascular dysfunction [171] linked to epigenetic alterations. DNA methylation at genes related to adipogenesis, lipid metabolism and inflammation increase the risk of suffering diabetes, cardiovascular disease and cancer [173]. The embryo culture microenvironment had been found sufficient to induce cardio metabolic disorders in adult offspring including relative hypertension, glucose intolerance and insulin resistance, abnormal hepatic and fat metabolomes and behavioural deficits including memory loss [174].

Here we have confirmed that glucose concentration can alter global DNA methylation in human preimplantation embryos cultured in vitro. Preimplantation blastocyst developed in vitro at low or high glucose concentration (0.9 mM or 3.5 mM respectively) were found differentially methylated, and those differentially

methylated regions resulted into several gene sets that are associated with diverse diseases.

Hypermethylated genes from low glucose embryos are associated wjt Myocardial infarction, Tetralogy of Fallot and Heart malformations. Hypermethylated genes from high glucose embryos were associated with Hypertension, Hypercholesterolemia and Diabetes Mellitus noninsulin-dependent. The influence of epigenetic modifications has also been reported in other neurological disorders, such as epilepsy or intellectual disability disorders where they found a correlation between nutrition and epigenetic modifications [115]. We found Autism, Mental disorders and Epilepsy associated to gene sets hypermethylated in high glucose. Furthermore, get sets related to Craniofacial abnormalities, Embryo development, Brain and Head development, and Neurogenesis were found hypomethylated in high glucose embryos. Hypermethylated genes from high glucose embryos were associated with Mitochondria Complex I deficiency and Leigh syndrome. Mitochondrial Complex I is crucial for mitochondrial respiration and oxidative phosphorylation (OXPHOS) [175]. Complex I deficiency causes Leigh syndrome which is a progressive neurological disorder that affects children [176].

H3K4me3 and H3K27me3 are trimethylation marks that reside in promoters and contribute to the regulation of gene expression [177]. We found H3K27me3 sites hypermethylated in high glucose to be related to neurological disorders, cardiovascular disorders and cancer. H3K27me3 sites hypermethylated in low glucose were related to the Bladder cancer pathway KEGG:05219. Whereas H3K4me3 sites hypermethylated in high glucose resulted enriched for the RNA degradation pathway KEGG:03018.

Methylation of imprinted genes is altered by glucose concentration in embryo culture. Imprinted genes (CDKN1C, KCNQ1, ERLIN2, TRAPPC9, NESP55, and ZFP57) resulted differentially methylated when comparing DNA from high and low glucose embryos. All genes showed different patters of methylation from the gene body to upstream and downstream regions. However, this evidence confirms that altered glucose concentration is enough to generate epigenetic changes in imprinted genes. This is

contrary to other reports, where no evidence was found for ART-associated DNA methylation changes at imprinted genes [114], [178].

Further studies would be required to determine if these epigenetic changes would be maintained in long-term into development or transgenerationally. Moreover, it would now be interesting to evaluate the effect of glucose on chromatin accessibility and histone acetylation. This would provide a better understanding of the epigenetic mechanisms that contribute to the development of diseases.

In summary, this work contributes to the basic knowledge of ART, embryo development and HESCs regulation. This evidence confirms the association of ART techniques with altered transcriptional regulation, metabolism and epigenetic regulation. Minimal variants in embryo culture such as glucose concentration, oxygen tension or cryopreservation treatments can cause significant changes in metabolic or energetic pathways that could lead to aberrant outcomes. The glucose concentration used in culture media caused notable changes in global DNA methylation in human embryos. Glucose concentration also alters mitochondrial function in HESCs, and affect the metabolic state of the cells. Therefore, glucose has a direct impact on maintenance and differentiation of HESCs. HESCs still have a huge potential to be a good model for human preimplantation development. However, an exhaustive optimization of the culture conditions that include an efficient balance of nutrient availability in synergy with oxygen would be first required. This is the first study that evaluates individual culture components, such as glucose to determine significant changes in the preimplantation human development. Further studies are needed to understand the nutrient requirement for human embryo and its response to nutrient availability. This would provide a deeper understanding about embryo metabolism so the microenvironment during embryo culture can be efficiently balanced. Hence, a comprehensive optimization of culture media components and environmental conditions would be critical to minimize aberrant outcomes in assisted reproduction.

CHAPTER 6

General Conclusions

- The effects of oxygen concentration on HESCs and in embryo culture remain controversial, as detrimental effects seem to be directly linked to nutrient availability in the culture media.
- Glucose concentration showed direct effect on the expression of pluripotency markers, DNA methyltransferases, demethylases, glucose transporters and mitochondrial activity markers independently of the oxygen concentration.
- Glucose concentration was found to have direct effect on global DNA methylation in human embryos, and some of the differentially methylated genes are strongly associated with metabolic and neurodegenerative diseases as well as with embryo development signalling pathways.
- Glucose concentration was found to affect methylation levels on several imprinted genes in human embryos.
- Glucose concentration can significantly affect mitochondrial respiration in HESCs under atmospheric oxygen. High glucose concentration (17.5 mM) was found to drive HESCs towards a more glycolytic metabolism than low glucose (5 mM).
- A balance glucose-oxygen seems to be crucial to maintain the pluripotent state of HESC.
- Mitochondrial membrane potential was significantly affected by the glucose concentration in HESCs and it can be used as a good indicator of cell metabolism and viability.
- Mitochondrial DNA abundance was not affected by oxygen nor glucose concentration. However, the expression of genes related to mitochondrial activity was significantly affected by glucose concentration (5 mM vs 17.5 mM).

CHAPTER 7

Future work

- To determine DNA methylation levels of HESCs cultured under physiological and atmospheric oxygen as well as in high and low glucose media.
- To determine the effects of glucose on chromatin accessibility and histone acetylation in human embryos and embryonic stem cells.
- To determine the effect of glucose concentration in global transcriptome in human embryos and HESCs.
- Combine transcriptome and epigenome analysis to elucidate mechanisms affected by glucose and oxygen.
- To evaluate pluripotency of HESCs after kept in culture with high and low glucose media, through germ layer differentiation.
- To determine the effect of physiological oxygen in combination with high and low glucose on the mitochondrial respiration profile of HESCs.
- To determine the effect of glucose and oxygen on mitochondrial respiration in human embryos.
- To determine the effect glucose and oxygen on mitochondrial membrane potential in human embryos.

8. References

[1] M. K. Lee, A. R. Bonneau, and A. J. Giraldez, "Zygotic genome activation during the maternal-to-zygotic transition," vol. 341, no. 1, pp. 459–470, 2014.

[2] Peter Braude, Virginia Bolton, and Stephen Moore, "Human gene expression first occurs between the four- and eight-cell stages of preimplantation development," *Nature*, vol. 332, pp. 459–461, 1988.

[3] R. J. Chason, J. Csokmay, J. H. Segars, A. H. DeCherney, and D. R. Armant, "Environmental and epigenetic effects upon preimplantation embryo metabolism and development," *Trends Endocrinol. Metab.*, vol. 22, no. 10, pp. 412–420, 2011.

[4] R. G. Edwards, J. M. Purdy, P. C. Steptoe, and D. E. Walters, "The growth of human preimplantation embryos in vitro," *Am. J. Obstet. Gynecol.*, vol. 141, no. 4, 1981.

[5] C. Chazaud and Y. Yamanaka, "Lineage specification in the mouse preimplantation embryo," *Development*, vol. 143, no. 7, pp. 1063–1074, 2016.

[6] R. Gualtieri, L. Santella, and B. Dale, "Tight junctions and cavitation in the human pre-embryo," *Mol. Reprod. Dev.*, vol. 32, no. 1, pp. 81–87, 1992.

[7] B. Płusa and A. Piliszek, "Common principles of early mammalian embryo self-organisation," *Dev.*, vol. 147, no. 14, pp. 1–16, 2020.

[8] K. K. Niakan, J. Han, R. A. Pedersen, C. Simon, and R. A. R. Pera, "Human pre-implantation embryo development," *Development*, vol. 139, no. 5, pp. 829–841, 2012.

[9] Y. Zhang, Z. Yang, and J. Wu, "Signaling pathways and preimplantation development of mammalian embryos," *FEBS J.*, vol. 274, no. 17, pp. 4349–4359, 2007.

[10] K. Hardy, M. A. K. Hooper, A. H. Handyside, A. J. Rutherford, R. M. L. Winston, and H. J. Leese, "Non-invasive measurement of glucose and pyruvate uptake by individual human oocytes and preimplantation embryos," *Hum. Reprod.*, vol. 4, no. 2, pp. 188–191, Feb. 1989.

[11] D. R. Brison and H. J. Leese, "Energy metabolism in late preimplantation rat

embryos.," *J. Reprod. Fertil.*, vol. 93, no. 1, pp. 245–51, 1991.

[12] H. J. Leese, "Metabolism of the preimplantation embryo: 40 Years on," *Reproduction*, vol. 143, no. 4, pp. 417–427, 2012.

[13] M. Lane and D. K. Gardner, "Embryo culture medium: which is the best?," *Best Pract. Res. Clin. Obstet. Gynaecol.*, vol. 21, no. 1, pp. 83–100, 2007.

[14] M. Lane and D. K. Gardner, "Amino acids and vitamins prevent culture-induced metabolic perturbations and associated loss of viability of mouse blastocysts.," *Hum. Reprod.*, vol. 13, no. 4, pp. 991–997, Apr. 1998.

[15] D. K. Gardner and H. J. Leese, "Assessment of embryo viability prior to transfer by the noninvasive measurement of glucose uptake.," *J. Exp. Zool.*, vol. 242, no. 1, pp. 103–105, Apr. 1987.

[16] D. K. Gardner, E. Seli, D. Sakkas, and D. Wells, *Human gametes and preimplantation embryos: Assessment and diagnosis*. 2013.

[17] A. L. Gott, K. Hardy, R. M. Winston, and H. J. Leese, "Non-invasive measurement of pyruvate and glucose uptake and lactate production by single human preimplantation embryos.," *Hum. Reprod.*, vol. 5, no. 1, pp. 104–108, Jan. 1990.

[18] K. L. Kind, R. A. Collett, A. J. Harvey, and J. G. Thompson, "Oxygen-regulated expression of GLUT-1, GLUT-3, and VEGF in the mouse blastocyst," *Mol. Reprod. Dev.*, vol. 70, no. 1, pp. 37–44, 2005.

[19] F. D. Houghton, "Energy metabolism of the inner cell mass and trophectoderm of the mouse blastocyst," *Differentiation*, vol. 74, no. 1, pp. 11–18, 2006.

[20] D. K. Gardner and P. L. Wale, "Analysis of metabolism to select viable human embryos for transfer," *Fertil. Steril.*, vol. 99, no. 4, pp. 1062–1072, 2013.

[21] S. Chappel, "The Role of Mitochondria from Mature Oocyte to Viable Blastocyst," *Obstet. Gynecol. Int.*, vol. 2013, pp. 1–10, 2013.

[22] R. Dumollard, M. Duchen, and C. Sardet, "Calcium signals and mitochondria at fertilisation.," *Semin. Cell Dev. Biol.*, vol. 17, no. 2, pp. 314–323, Apr. 2006.

[23] R. Dumollard, M. Duchen, and J. Carroll, "The Role of Mitochondrial Function in the Oocyte and Embryo," *Curr. Top. Dev. Biol.*, vol. 77, no. 06, pp. 21–49, 2007.

[24] J. Van Blerkom, "Mitochondria in early mammalian development," *Semin. Cell Dev. Biol.*, vol. 20, no. 3, pp. 354–364, 2009.

[25] J. Van Blerkom, "Mitochondrial function in the human oocyte and embryo and their role in developmental competence," *Mitochondrion*, vol. 11, no. 5, pp. 797–813, 2011.

[26] R. Dumollard, J. Carroll, M. R. Duchen, K. Campbell, and K. Swann, "Mitochondrial function and redox state in mammalian embryos," *Semin. Cell Dev. Biol.*, vol. 20, no. 3, pp. 346–353, 2009.

[27] M. Wilding, G. Coppola, B. Dale, and L. Di Matteo, "Mitochondria and human preimplantation embryo development," *Reproduction*, vol. 137, no. 4, pp. 619–624, 2009.

[28] A. H. Sathananthan and A. O. Trounson, "Mitochondrial morphology during preimplantational human embryogenesis," *Hum. Reprod.*, vol. 15, no. suppl 2, pp. 148–159, 2000.

[29] S. Anderson, "Sequence and organization of the human mitochondrial genome," *Nat. Vol.*, vol. 290, no. April, pp. 1–18, 1981.

[30] V. K. Mootha *et al.*, "Integrated Analysis of Protein Composition, Tissue Diversity, and Gene Regulation in Mouse Mitochondria ates the majority of cellular reactive oxygen species," *Cell*, vol. 115, pp. 629–640, 2003.

[31] Y. Jiang and X. Wang, "Comparative mitochondrial proteomics: Perspective in human diseases," *J. Hematol. Oncol.*, vol. 5, no. 1, p. 11, 2012.

[32] B. M. Acton, A. Jurisicova, I. Jurisica, and R. F. Casper, "Alterations in mitochondrial membrane potential during preimplantation stages of mouse and human embryo development," *Molecular Human Reproduction*. 2004.

[33] L. D. Zorova *et al.*, "Mitochondrial membrane potential Ljubava," pp. 50–59, 2018.

[34] S. El-Heis and K. Godfrey, "Developmental origins of health and disease," *Obstet.*

Gynaecol. Reprod. Med., vol. 25, no. 8, pp. 236–238, 2015.

[35] A. N. Antonov, "Children born during the siege of Leningrad in 1942.," *The Journal of Pediatrics*, vol. 30. Mosby Publishing Company, US, pp. 250–259, 1947.

[36] Z. Stein, M. Susser, G. Saenger, and F. Marolla, *Famine and human development: The Dutch hunger winter of 1944-1945.* New York, NY, US: Oxford University Press, 1975.

[37] D. J. Barker, "Fetal origins of coronary heart disease," *Evid. Based. Cardiovasc. Med.*, vol. 3, no. 4, pp. 87–88, 1995.

[38] S.-M. Ho *et al.*, "Environmental Factors, Epigenetics, and Developmental Origin of Reproductive Disorders," *Reprod. Toxicol.*, 2016.

[39] S. Canovas, P. J. Ross, G. Kelsey, and P. Coy, "DNA Methylation in Embryo Development: Epigenetic Impact of ART (Assisted Reproductive Technologies)," *BioEssays*, vol. 39, no. 11, pp. 1–11, 2017.

[40] D. K. Gardner and R. L. Kelley, "Impact of the IVF laboratory environment on human preimplantation embryo phenotype," *J. Dev. Orig. Health Dis.*, vol. 8, no. 4, pp. 418–435, 2017.

[41] T. P. Fleming, M. a. Velazquez, and J. J. Eckert, "Embryos, DOHaD and David Barker," *J. Dev. Orig. Health Dis.*, vol. 6, no. 05, pp. 377–383, 2015.

[42] M. A. Hanson and M. K. Skinner, "Developmental origins of epigenetic transgenerational inheritance," *Environ. Epigenetics*, vol. 2, no. 1, p. dvw002, 2016.

[43] S. Feuer and P. Rinaudo, "From Embryos to Adults : A DOHaD Perspective on In Vitro Fertilization and Other Assisted Reproductive Technologies," 2016.

[44] J. C. Dumoulin *et al.*, "Effect of in vitro culture of human embryos on birthweight of newborns," *Hum. Reprod.*, vol. 25, no. 3, pp. 605–612, 2010.

[45] E. C. M. Nelissen *et al.*, "IVF culture medium affects human intrauterine growth as early as the second trimester of pregnancy," *Hum. Reprod.*, vol. 28, no. 8, pp. 2067–2074, 2013.

[46] C. M. Castillo, J. Harper, S. A. Roberts, H. C. O'Neill, E. D. Johnstone, and D. R. Brison,

"The impact of selected embryo culture conditions on ART treatment cycle outcomes: a UK national study," *Hum. Reprod. Open*, vol. 2020, no. 1, pp. 1–13, 2020.

[47] C. G. Vergouw, E. Hanna Kostelijk, E. Doejaaren, P. G. A. Hompes, C. B. Lambalk, and R. Schats, "The influence of the type of embryo culture medium on neonatal birthweight after single embryo transfer in IVF," *Hum. Reprod.*, vol. 27, no. 9, pp. 2619–2626, 2012.

[48] C. Bouillon *et al.*, "Does embryo culture medium influence c born after in vitro fertilization?," *PLoS One*, vol. 11, no. 3, pp. 1–14, 2016.

[49] F. Gu *et al.*, "The effects of embryo culture media on the birthweight of singletons via fresh or frozen-thawed embryo transfer: a large-scale retrospective study.," *BMC Pregnancy Childbirth*, vol. 16, p. 270, 2016.

[50] T. P. Fleming *et al.*, "Origins of lifetime health around the time of conception: causes and consequences," *Lancet*, vol. 391, no. 10132, pp. 1842–1852, 2018.

[51] S. Pandey, A. Shetty, M. Hamilton, S. Bhattacharya, and A. Maheshwari, "Obstetric and perinatal outcomes in singleton pregnancies resulting from ivf/icsi: A systematic review and meta-analysis," *Hum. Reprod. Update*, vol. 18, no. 5, pp. 485–503, 2012.

[52] L. Yamada and S. Chong, "Epigenetic studies in Developmental Origins of Health and Disease: pitfalls and key considerations for study design and interpretation," *J. Dev. Orig. Health Dis.*, vol. 8, no. May, pp. 1–14, 2016.

[53] D. K. Gardner and R. L. Kelley, "Impact of the IVF laboratory environment on human preimplantation embryo phenotype," *J. Dev. Orig. Health Dis.*, pp. 1–18, 2017.

[54] A. Sunde *et al.*, "Time to take human embryo culture," vol. 31, no. 10, pp. 2174–2182, 2016.

[55] P. C. Steptoe and R. G. Edwards, "Birth after the reimplantation of a human embryo," *Arch. Pathol. Lab. Med.*, vol. 116, no. 4, p. 321, 1978.

[56] A. Mandal, "8 million babies born through IVF says study," pp. 2–4, 2018.

[57] Y. C. Cheong, E. S. Ginsburg, and N. S. Macklon, "Ovulation Stimulation and Cycle Management in IVF," 2012.

[58] M. V Sauer, “Assisted reproductive technology.,” *Am. Soc. Reprod. Med.*, vol. 161, no. 2, pp. 164–165, 2015.

[59] I. C. of M. R. S. Sharma, “The Assisted Reproductive Technologies (Regulation) Rules - 2010,” 2010.

[60] C. Audibert and D. Glass, “A global perspective on assisted reproductive technology fertility treatment: an 8-country fertility specialist survey,” *Reprod. Biol. Endocrinol.*, vol. 13, no. 1, p. 133, 2015.

[61] A. Bos-Mikich, F. F. Bressan, R. R. Ruggeri, Y. Watanabe, and F. V. Meirelles, “Parthenogenesis and Human Assisted Reproduction,” *Stem Cells Int.*, vol. 2016, no. January, 2016.

[62] M. Cissen, A. Bensdorp, B. J. Cohlen, S. Repping, J. P. de Bruin, and M. van Wely, “Assisted reproductive technologies for male subfertility,” *Cochrane Database Syst. Rev.*, vol. 2016, no. 2, 2016.

[63] Z. P. Nagy, A. C. Varghese, and A. Agarwal, *Practical Manual of In Vitro Fertilization*, no. January. 2012.

[64] G. Vajta and T. Hardarson, “Real-Time Embryo Monitoring Device for Embryo Selection,” in *Practical Manual of In Vitro Fertilization*, 2012, pp. 483–490.

[65] B. Balaban and D. K. Gardner, “Morphological Assessment of Blastocyst Stage Embryos: Types of Grading Systems and Their Reported Outcomes,” in *Human Gametes and Preimplantation Embryos: Assessment and Diagnosis*, 2013, pp. 1–306.

[66] D. R. Brison, S. A. Roberts, and S. J. Kimber, “How should we assess the safety of IVF technologies?,” *Reprod. Biomed. Online*, vol. 27, no. 6, pp. 710–721, 2013.

[67] E. Van Den Abbeel *et al.*, “Association between blastocyst morphology and outcome of single-blastocyst transfer,” *Reprod. Biomed. Online*, vol. 27, no. 4, pp. 353–361, 2013.

[68] K. Kirkegaard, A. Ahlström, H. J. Ingerslev, and T. Hardarson, “Choosing the best embryo by time lapse versus standard morphology,” *Fertil. Steril.*, vol. 103, no. 2, pp. 323–332, 2015.

[69] E. S. Ginsburg and C. Racowsky, *In Vitro Fertilization*. 2012.

[70] W. B. Schoolcraft, D. K. Gardner, M. Lane, T. Schlenker, F. Hamilton, and D. R. Meldrum, "Blastocyst culture and transfer: Analysis of results and parameters affecting outcome in two in vitro fertilization programs," *Fertil. Steril.*, vol. 72, no. 4, pp. 604–609, 1999.

[71] B. Balaban *et al.*, "Istanbul consensus workshop on embryo assessment: Proceedings of an expert meeting," *Reprod. Biomed. Online*, vol. 22, no. 6, pp. 632–646, 2011.

[72] B. Balaban *et al.*, "Istanbul consensus workshop on embryo assessment: Proceedings of an expert meeting," *Reprod. Biomed. Online*, vol. 22, no. 6, pp. 632–646, 2011.

[73] M. Kasai and T. Mukaida, "Cryopreservation of animal and human embryos by vitrification," *Reprod. Biomed. Online*, vol. 9, no. 2, pp. 164–170, 2004.

[74] T. Mukaida and C. Oka, "Oocyte and embryo cryopreservation," no. April, 2012, pp. 313–325.

[75] L. Nel-Themaat, C.-C. Chang, T. Elliott, P. Bernal, G. Wright, and Z. P. Nagy, "Slow Freezing of Embryos," in *Practical Manual of In Vitro Fertilization*, 2012, pp. 483–490.

[76] A. I. Zhmakin, *Funadamentals of Cryobiology*. 2009.

[77] K. M. Wong, S. Mastenbroek, and S. Repping, "Cryopreservation of human embryos and its contribution to in vitro fertilization success rates," *Fertil. Steril.*, vol. 102, no. 1, pp. 19–26, 2014.

[78] F. Edris, S. Baghdadi, and A. Fares, "Compared to Vitrification , Slow Freezing Technique is Associated With a Higher Post- Thawed Embryos Survival and Clinical Pregnancy Rates . Is This a Myth or a Fact ?," *Med J Obs. Gynecol*, vol. 2, no. 4, p. 1047, 2014.

[79] A. Arav, "Cryopreservation of oocytes and embryos," *Theriogenology*, vol. 81, no. 1, pp. 96–102, 2014.

[80] A. A. Mandawala, S. C. Harvey, T. K. Roy, and K. E. Fowler, "Cryopreservation of animal oocytes and embryos: Current progress and future prospects," *Theriogenology*, vol. 86, no. 7, pp. 1637–1644, 2016.

[81] B. Behr and H. Wang, “Effects of culture conditions on IVF outcome,” *Eur. J. Obstet. Gynecol. Reprod. Biol.*, vol. 115, no. SUPPL., pp. 72–76, 2004.

[82] I. Gruber and M. Klein, “Embryo culture media for human IVF: which possibilities exist?,” *J. Turkish Ger. Gynecol. Assoc.*, vol. 12, no. 2, pp. 110–7, 2011.

[83] J. D. Biggers, D. G. Whittingham, and R. P. Donahue, “The Pattern of Energy Metabolism in the Oocyte and Zygote,” *Proc. Natl. Acad. Sci.*, vol. 58, no. 2, pp. 560–567, 1967.

[84] D. E. Morbeck, R. L. Krisher, J. R. Herrick, N. A. Baumann, D. Matern, and T. Moyer, “Composition of single-step media used for human embryo culture,” *Fertil. Steril.*, vol. 102, no. 3, pp. 1055-1060.e1, 2017.

[85] J. D. Biggers and M. C. Summers, “Choosing a culture medium: making informed choices,” *Fertil. Steril.*, vol. 90, no. 3, pp. 473–483, 2008.

[86] D. E. Morbeck, R. L. Krisher, J. R. Herrick, N. A. Baumann, D. Matern, and T. Moyer, “Composition of commercial media used for human embryo culture,” *Fertil. Steril.*, vol. 102, no. 3, pp. 759-766.e9, 2014.

[87] D. K. Gardner, M. Lane, I. Calderon, and J. Leeton, “Environment of the preimplantation human embryo in vivo: metabolite analysis of oviduct and uterine fluids and metabolism of cumulus cells.,” *Fertil. Steril.*, vol. 65, no. 2, pp. 349–353, 1996.

[88] H. J. Leese *et al.*, “Female reproductive tract fluids: composition, mechanism of formation and potential role in the developmental origins of health and disease.,” *Reprod. Fertil. Dev.*, vol. 20 1, pp. 1–8, 2008.

[89] A. Sunde *et al.*, “Time to take human embryo culture seriously: Table I,” *Hum. Reprod.*, vol. 0, no. 0, p. dew157, 2016.

[90] G. B. McClelland, “TISSUE RESPIRATION | Cellular Respiration,” in *Encyclopedia of Fish Physiology*, A. P. Farrell, Ed. San Diego: Academic Press, 2011, pp. 951–958.

[91] M. S. Nakazawa, B. Keith, and M. C. Simon, “Oxygen Availability and Metabolic Adaptations,” *Physiol. Behav.*, vol. 176, no. 1, pp. 100–106, 2016.

[92] B. Fischer and B. D. Bavister, “Oxygen tension in the oviduct and uterus of rhesus monkeys, hamsters and rabbits,” *J. Reprod. Fertil.*, vol. 99, no. 2, pp. 673–679, 1993.

[93] B. Woodward, “European Society of Human Reproduction and Embryology Revised Guidelines for Good Practice in Eshre Guideline Group,” 2015.

[94] D. B. Gomes Sobrinho *et al.*, “IVF/ICSI outcomes after culture of human embryos at low oxygen tension: a meta-analysis.,” *Reprod. Biol. Endocrinol.*, vol. 9, no. 1, p. 143, 2011.

[95] N. Guo, Y. Li, J. Ai, L. Gu, W. Chen, and Q. Liu, “Two different concentrations of oxygen for culturing precompaction stage embryos on human embryo development competence: A prospective randomized sibling-oocyte study,” *Int. J. Clin. Exp. Pathol.*, vol. 7, no. 9, pp. 6191–6198, 2014.

[96] M. Pantaleon, “The Role of Hexosamine Biosynthesis and Signaling in Early Development,” in *Cell Signaling During Mammalian Early Embryo Development*, H. J. Leese and D. R. Brison, Eds. New York, NY: Springer New York, 2015, pp. 53–76.

[97] K. J. Kaneko, *Metabolism of Preimplantation Embryo Development: A Bystander or an Active Participant?*, 1st ed., vol. 120. Elsevier Inc., 2016.

[98] P. L. Wale and D. K. Gardner, “The effects of chemical and physical factors on mammalian embryo culture and their importance for the practice of assisted human reproduction,” *Hum. Reprod. Update*, vol. 22, no. 1, pp. 2–22, 2016.

[99] J. Ghosh, C. Coutifaris, C. Sapienza, and M. Mainigi, “Global DNA methylation levels are altered by modifiable clinical manipulations in assisted reproductive technologies,” *Clin. Epigenetics*, vol. 9, no. 1, pp. 1–10, 2017.

[100] A. P. A. Van Montfoort *et al.*, “Reduced oxygen concentration during human IVF culture improves embryo utilization and cumulative pregnancy rates per cycle,” *Hum. Reprod. Open*, vol. 2020, no. 1, pp. 1–11, 2020.

[101] A. Pinborg *et al.*, “Epigenetics and assisted reproductive technologies (ART),” *Acta Obstet. Gynecol. Scand.*, vol. 95, p. n/a-n/a, 2015.

[102] E. Ivanova *et al.*, “Erratum: DNA methylation changes during preimplantation

development reveal interspecies differences and reprogramming events at imprinted genes (Clin Epigenet (2020) 12 64 DOI: 10.1186/s13148-020-00857-x)," *Clin. Epigenetics*, vol. 12, no. 1, pp. 1–18, 2020.

[103] B. T. Heijmans *et al.*, "Persistent epigenetic differences associated with prenatal exposure to famine in humans," *Proc. Natl. Acad. Sci. U. S. A.*, vol. 105, no. 44, pp. 17046–17049, 2008.

[104] D. Monk, D. J. G. Mackay, T. Eggermann, E. R. Maher, and A. Riccio, "Genomic imprinting disorders: lessons on how genome, epigenome and environment interact," *Nat. Rev. Genet.*, 2019.

[105] P. J. Ross and S. Canovas, "Mechanisms of epigenetic remodelling during preimplantation development," *Reprod. Fertil. Dev.*, pp. 25–40, 2016.

[106] S. Canovas, P. J. Ross, G. Kelsey, and P. Coy, "DNA Methylation in Embryo Development: Epigenetic Impact of ART (Assisted Reproductive Technologies)," *BioEssays*, vol. 39, no. 11, pp. 1–11, 2017.

[107] M. Iurlaro, F. von Meyenn, and W. Reik, "DNA methylation homeostasis in human and mouse development," *Curr. Opin. Genet. Dev.*, vol. 43, pp. 101–109, 2017.

[108] M. A. H. Surani, S. C. Barton, and M. L. Norris, "Development of reconstituted mouse eggs suggests imprinting of the genome during gametogenesis," *Nature*, vol. 308, no. 5959, pp. 548–550, 1984.

[109] N. Engel, *Genomic Imprinting*, vol. 925. 2012.

[110] L. Hoeijmakers, H. Kempe, and P. J. Verschure, "Epigenetic imprinting during assisted reproductive technologies: The effect of temporal and cumulative fluctuations in methionine cycling on the DNA methylation state," *Mol. Reprod. Dev.*, vol. 83, no. 2, pp. 94–107, 2016.

[111] Z. D. Smith and A. Meissner, "DNA methylation: Roles in mammalian development," *Nat. Rev. Genet.*, vol. 14, no. 3, pp. 204–220, 2013.

[112] L. Li, X. Lu, and J. Dean, "The maternal to zygotic transition in mammals," *Mol. Aspects Med.*, vol. 34, no. 5, pp. 919–938, 2013.

[113] H. Hiura *et al.*, "Characterization of DNA methylation errors in patients with imprinting disorders conceived by assisted reproduction technologies," *Hum. Reprod.*, vol. 27, no. 8, pp. 2541–2548, 2012.

[114] H. Chiba *et al.*, "DNA methylation errors in imprinting disorders and assisted reproductive technology," *Pediatr. Int.*, vol. 55, no. 5, pp. 542–549, 2013.

[115] M. La Rovere, M. Franzago, and L. Stuppia, "Epigenetics and neurological disorders in ART," *Int. J. Mol. Sci.*, vol. 20, no. 17, pp. 1–16, 2019.

[116] W. W. C. Tang, T. Kobayashi, N. Irie, S. Dietmann, and M. A. Surani, "Specification and epigenetic programming of the human germ line," *Nat. Rev. Genet.*, vol. 17, no. 10, pp. 585–600, 2016.

[117] R. Kenneth and T. Dunne, "DNA methylation dynamics of the human preimplantation embryo," *Nature. 2014 July 31; 511(7511) 611–615. doi10.1038/nature13581.*, vol. 511, no. 7511, pp. 611–615, 2014.

[118] D. Grafodatskaya, C. Cytrynbaum, and R. Weksberg, "The health risks of ART," *EMBO Rep.*, vol. 14, no. 2, pp. 129–135, 2013.

[119] J. A. Thomson *et al.*, "Embryonic stem cell lines derived from human blastocysts.," *Science*, vol. 282, no. 5391, pp. 1145–1147, Nov. 1998.

[120] J. Itskovitz-Eldor *et al.*, "Differentiation of human embryonic stem cells into embryoid bodies compromising the three embryonic germ layers.," *Mol. Med.*, vol. 6, no. 2, pp. 88–95, 2000.

[121] L. F. Z. Batista, *Telomere biology in stem cells and reprogramming*, 1st ed., vol. 125. Elsevier Inc., 2014.

[122] G. Chen *et al.*, "Chemically defined conditions for human iPSC derivation and culture," *Nat. Methods*, vol. 8, no. 5, pp. 424–429, 2011.

[123] T. Vazin and W. J. Freed, "Human embryonic stem cells: Derivation, culture, and differentiation: A review," vol. 28, no. 4, pp. 589–603, 2010.

[124] K. Turksen, *Human Embryonic Stem Cells Handbook*, vol. 531, no. 1. 2009.

[125] P. Prajumwongs, O. Weeranantanapan, T. Jaroonwitchawan, and P. Noisa, "Human Embryonic Stem Cells: A Model for the Study of Neural Development and Neurological Diseases," *Stem Cells Int.*, vol. 2016, 2016.

[126] T. Dvash, D. Ben-Yosef, and R. Eiges, "Human embryonic stem cells as a powerful tool for studying human embryogenesis," *Pediatr. Res.*, vol. 60, no. 2, pp. 111–117, 2006.

[127] O. Adewumi *et al.*, "Characterization of human embryonic stem cell lines by the International Stem Cell Initiative," *Nat. Biotechnol.*, vol. 25, no. 7, pp. 803–816, 2007.

[128] J. Hua *et al.*, "Derivation and characterization of human embryonic germ cells: Serum-free culture and differentiation potential," *Reprod. Biomed. Online*, vol. 19, no. 2, pp. 238–249, 2009.

[129] J. Ye *et al.*, "High quality clinical grade human embryonic stem cell lines derived from fresh discarded embryos," pp. 1–13, 2017.

[130] W. Gu *et al.*, "Glycolytic Metabolism Plays a Functional Role in Regulating Human Pluripotent Stem Cell State," *Cell Stem Cell*, vol. 19, no. 4, pp. 476–490, 2016.

[131] S. Varum *et al.*, "Energy metabolism in human pluripotent stem cells and their differentiated counterparts," *PLoS One*, vol. 6, no. 6, 2011.

[132] J. Wu, A. Ocampo, and J. C. I. Belmonte, "Cellular Metabolism and Induced Pluripotency," *Cell*, vol. 166, no. 6, pp. 1371–1385, 2016.

[133] H. Zhang *et al.*, "Distinct Metabolic States Can Support Self-Renewal and Lipogenesis in Human Pluripotent Stem Cells under Different Culture Conditions," *Cell Rep.*, vol. 16, no. 6, pp. 1536–1547, 2016.

[134] T. Teslaa and M. A. Teitell, "Pluripotent stem cell energy metabolism: an update," *EMBO J.*, vol. 34, no. 2, pp. 138–153, 2015.

[135] R. H. Klein and P. S. Knoepfler, *The Molecular Circuitry Underlying Pluripotency in Embryonic and Induced Pluripotent Stem Cells*, vol. 3. Elsevier Inc., 2019.

[136] G. Brady and N. N. Iscove, "Construction of cDNA libraries from single cells," *Methods Enzymol.*, vol. 225, no. 1988, pp. 611–623, 1993.

[137] S. A. Smallwood *et al.*, "Single-cell genome-wide bisulfite sequencing for assessing epigenetic heterogeneity," *Nat. Methods*, vol. 11, no. 8, pp. 817–820, 2014.

[138] G. Chen *et al.*, "Chemically defined conditions for human iPS cell derivation and culture-Supplementary," *Nat. Methods*, vol. 8, no. 5, pp. 424–429, 2011.

[139] K. J. Livak and T. D. Schmittgen, "Analysis of relative gene expression data using real-time quantitative PCR and," *Methods*, vol. 25, pp. 402–408, 2001.

[140] T. D. Schmittgen and K. J. Livak, "Analyzing real-time PCR data by the comparative C(T) method.," *Nat. Protoc.*, vol. 3, no. 6, pp. 1101–8, 2008.

[141] C. M. Rivera and B. Ren, "Mapping human epigenomes," *Cell*, vol. 155, no. 1, pp. 39–55, 2013.

[142] W. Xia *et al.*, "Resetting histone modifications during human parental-to-zygotic transition," *Science (80-.).*, vol. 365, no. 6451, pp. 353–360, 2019.

[143] F. Y. Ideraabdullah, S. Vigneau, and M. S. Bartolomei, "Genomic imprinting mechanisms in mammals," *Mutat. Res. - Fundam. Mol. Mech. Mutagen.*, vol. 647, no. 1–2, pp. 77–85, 2008.

[144] I. M. Morison, C. J. Paton, and S. D. Cleverley, "The imprinted gene and parent-of-origin effect database," *Nucleic Acids Res.*, vol. 29, no. 1, pp. 275–276, 2001.

[145] S. H. M. Kleijkers *et al.*, "Differences in gene expression profiles between human preimplantation embryos cultured in two different IVF culture media," *Hum. Reprod.*, vol. 30, no. 10, pp. 2303–2311, 2015.

[146] C. L. Mulder *et al.*, "Comparison of DNA methylation patterns of parentally imprinted genes in placenta derived from IVF conceptions in two different culture media," *Hum. Reprod.*, vol. 35, no. 3, pp. 516–528, 2020.

[147] B. Kea *et al.*, "Effect of reduced oxygen concentrations on the outcome of in vitro fertilization," *Fertil. Steril.*, vol. 87, no. 1, pp. 213–216, 2007.

[148] M. Meintjes *et al.*, "A controlled randomized trial evaluating the effect of lowered incubator oxygen tension on live births in a predominantly blastocyst transfer program," *Hum. Reprod.*, vol. 24, no. 2, pp. 300–307, 2009.

[149] P. F. Rinaudo, G. Giritharan, S. Talbi, A. T. Dobson, and R. M. Schultz, “Effects of oxygen tension on gene expression in preimplantation mouse embryos,” *Fertil. Steril.*, vol. 86, no. 4 SUPPL., 2006.

[150] E. Mantikou *et al.*, “Factors affecting the gene expression of *in vitro* cultured human preimplantation embryos,” *Hum. Reprod.*, vol. 31, no. 2, p. dev306, 2015.

[151] D. Johnson, J. Jessee, J. Skowronski, and D. Solter, “[35] C o n s t r u c t i o n o f P r i m a r y a n d S u b t r a c t e d c D N A Libraries from Early Embryos Mammalian preimplantation development is characterized by a period following fertilization when the embryo grows , differentiates , and devel- ,” vol. 225, no. 1988, pp. 587–610, 1993.

[152] S. J. Kimber *et al.*, “Expression of genes involved in early cell fate decisions in human embryos and their regulation by growth factors.,” *Reproduction*, vol. 135, pp. 635–647, 2008.

[153] L. Shaw, S. F. Sneddon, D. R. Brison, and S. J. Kimber, “Comparison of gene expression in fresh and frozen-thawed human preimplantation embryos,” *Reproduction*, 2012.

[154] K. Gelber, A. N. Tamura, V. B. Alarcon, and Y. Marikawa, “A potential use of embryonic stem cell medium for the in vitro culture of preimplantation embryos,” *J. Assist. Reprod. Genet.*, vol. 28, no. 8, pp. 659–668, 2011.

[155] T. Kido *et al.*, “Glucose transporter 1 is important for the glycolytic metabolism of human endometrial stromal cells in hypoxic environment,” *Heliyon*, vol. 6, no. 6, p. e03985, 2020.

[156] P. Rinaudo and R. M. Schultz, “Effects of embryo culture on global pattern of gene expression in preimplantation mouse embryos,” *Reproduction*, vol. 128, pp. 301–311, 2004.

[157] G. Giritharan, S. Talbi, A. Donjacour, F. Di Sebastiano, A. T. Dobson, and P. F. Rinaudo, “Effect of ICSI on gene expression and development of mouse preimplantation embryos,” *Reproduction*, vol. 134, no. 1, pp. 63–72, 2007.

[158] M. J. Sánchez-Calabuig *et al.*, “A high glucose concentration during early stages of in

vitro equine embryo development alters expression of genes involved in glucose metabolism," *Equine Vet. J.*, no. September 2019, pp. 1–9, 2020.

[159] K. H. Moley, M. M. Y. Chi, C. M. Knudson, S. J. Korsmeyer, and M. M. Mueckler, "Erratum: Hyperglycemia induces apoptosis in pre-implantation embryos through cell death effector pathways (Nature Medicine (1998) 4 (1421-1424))," *Nat. Med.*, vol. 8, no. 3, p. 303, 2002.

[160] S. K. Feuer, X. Liu, A. Donjacour, R. Simbulan, E. Maltepe, and P. Rinaudo, "Transcriptional signatures throughout development: the effects of mouse embryo manipulation in vitro," *Reproduction*, vol. 153, pp. 107–122, 2017.

[161] S. Bontekoe, E. Mantikou, van W. M, S. Seshadri, S. Repping, and S. Mastenbroek, "Low oxygen concentrations for embryo culture in assisted reproductive technologies.," *Cochrane Database Syst. Rev.*, no. 7, p. N.PAG-N.PAG 1p, 2012.

[162] K. Kirkegaard, J. J. Hindkjaer, and H. J. Ingerslev, "Effect of oxygen concentration on human embryo development evaluated by time-lapse monitoring," *Fertil. Steril.*, vol. 99, no. 3, pp. 738-744.e4, 2013.

[163] U. Waldenström, A. B. Engström, D. Hellberg, and S. Nilsson, "Low-oxygen compared with high-oxygen atmosphere in blastocyst culture, a prospective randomized study," *Fertil. Steril.*, vol. 91, no. 6, pp. 2461–2465, 2009.

[164] E. Mantikou *et al.*, "Factors affecting the gene expression of in vitro cultured human preimplantation embryos," *Hum. Reprod.*, vol. 31, no. 2, pp. 298–311, 2016.

[165] M. Hu *et al.*, "Altered expression of DNA damage repair genes in the brain tissue of mice conceived by in vitro fertilization," *Mol. Hum. Reprod.*, vol. 26, no. 3, pp. 141–153, 2020.

[166] J. W. Catt and M. Henman, "Toxic effects of oxygen on human embryo development," *Hum. Reprod.*, vol. 15, no. SUPPL. 2, pp. 199–206, 2000.

[167] D. E. H. R. C. J. Loscalzo, "Effect of Glucose Concentration During in Vitro Culture of Mouse Embryos on Development to Blastocyst, Success of Embryo Transfer and Litter Sex Ratio," *Bone*, vol. 23, no. 1, pp. 1–7, 2011.

[168] A. Jiménez *et al.*, "Hyperglycemia-induced apoptosis affects sex ratio of bovine and murine preimplantation embryos," *Mol. Reprod. Dev.*, vol. 65, no. 2, pp. 180–187, 2003.

[169] G. L. M. Cagnone, I. Dufort, C. Vigneault, and M. A. Sirard, "Differential gene expression profile in bovine blastocysts resulting from hyperglycemia exposure during early cleavage stages," *Biol. Reprod.*, vol. 86, no. 2, pp. 1–12, 2012.

[170] B. Muller, N. Lewis, T. Adeniyi, H. J. Leese, and D. Brison, "Application of extracellular flux analysis for determining mitochondrial function in mammalian oocytes and early embryos," pp. 1–50, 2019.

[171] M. Ceelen *et al.*, "Growth during infancy and early childhood in relation to blood pressure and body fat measures at age 8-18 years of IVF children and spontaneously conceived controls born to subfertile parents," *Hum. Reprod.*, vol. 24, no. 11, pp. 2788–2795, 2009.

[172] U. Scherrer *et al.*, "Systemic and pulmonary vascular dysfunction in children conceived by assisted reproductive technologies," *Circulation*, vol. 125, no. 15, pp. 1890–1896, 2012.

[173] D. Castellano-Castillo *et al.*, "Altered Adipose Tissue DNA Methylation Status in Metabolic Syndrome: Relationships Between Global DNA Methylation and Specific Methylation at Adipogenic, Lipid Metabolism and Inflammatory Candidate Genes and Metabolic Variables," *J. Clin. Med.*, vol. 8, no. 1, p. 87, 2019.

[174] M. J. Davies *et al.*, "Reproductive Technologies and the Risk of Birth Defects," *N. Engl. J. Med.*, vol. 366, no. 19, pp. 1803–1813, 2012.

[175] E. Fassone and S. Rahman, "Complex I deficiency: Clinical features, biochemistry and molecular genetics," *J. Med. Genet.*, vol. 49, no. 9, pp. 578–590, 2012.

[176] A. H. V Schapira, "Mitochondrial diseases," *Lancet*, vol. 379, no. 9828, pp. 1825–1834, 2012.

[177] M. Bibikova, L. C. Laurent, B. Ren, J. F. Loring, and J. B. Fan, "Unraveling Epigenetic Regulation in Embryonic Stem Cells," *Cell Stem Cell*, vol. 2, no. 2, pp. 123–134, 2008.

[178] B. Novakovic *et al.*, "Assisted reproductive technologies are associated with limited epigenetic variation at birth that largely resolves by adulthood," *Nat. Commun.*, 2019.

[179] P. Lewis, E. Silajdžić, D. R. Brison, and S. J. Kimber, *Embryonic stem cells*, vol. 37. Cell Engineering and Regeneration, Reference Series in Biomedical Engineering, 2018.

[180] S. W. Perry, J. P. Norman, J. Barbieri, E. B. Brown, and A. Harris, "Mitochondrial membrane potential probes and the proton gradient: a practical usage guide," vol. 50, no. 2, pp. 98–115, 2011.

[181] A. A. Memon *et al.*, "Quantification of mitochondrial DNA copy number in suspected cancer patients by a well optimized ddPCR method," *Biomol. Detect. Quantif.*, vol. 13, no. August, pp. 32–39, 2017.

[182] A. Wanet, T. Arnould, M. Najimi, and P. Renard, "Connecting Mitochondria, Metabolism, and Stem Cell Fate," *Stem Cells Dev.*, vol. 24, no. 17, pp. 1957–1971, 2015.

[183] T. Ezashi, P. Das, and R. M. Roberts, "Low O2 tensions and the prevention of differentiation of HES cells," *Nat. Methods*, vol. 2, no. 5, p. 325, 2005.

[184] E. Närvä *et al.*, "Continuous hypoxic culturing of human embryonic stem cells enhances SSEA-3 and MYC levels," *PLoS One*, vol. 8, no. 11, pp. 1–10, 2013.

[185] C. E. Forristal *et al.*, "Environmental Oxygen Tension Regulates the Energy Metabolism and Self-Renewal of Human Embryonic Stem Cells," *PLoS One*, vol. 8, no. 5, pp. 1–9, 2013.

[186] D. R. Christensen, P. C. Calder, and F. D. Houghton, "GLUT3 and PKM2 regulate OCT4 expression and support the hypoxic culture of human embryonic stem cells," *Sci. Rep.*, vol. 5, no. October, pp. 1–14, 2015.

[187] R. Petruzzelli, D. R. Christensen, K. L. Parry, T. Sanchez-Elsner, and F. D. Houghton, "HIF-2α regulates NANOG expression in human embryonic stem cells following hypoxia and reoxygenation through the interaction with an oct-sox cis regulatory element," *PLoS One*, vol. 9, no. 10, pp. 1–11, 2014.

[188] J. G. Lees, J. Rathjen, J. R. Sheedy, D. K. Gardner, and A. J. Harvey, "Distinct profiles of

human embryonic stem cell metabolism and mitochondria identified by oxygen," *Reproduction*, vol. 150, no. 4, pp. 367–382, 2015.

[189] C. Mas-Bargues *et al.*, "Relevance of oxygen concentration in stem cell culture for regenerative medicine," *Int. J. Mol. Sci.*, vol. 20, no. 5, 2019.

[190] P. Chaudhari, Z. Ye, and Y.-Y. Jang, "Roles of Reactive Oxygen Species in the Fate of Stem Cells," *Antioxid. Redox Signal.*, vol. 20, no. 12, pp. 1881–1890, 2014.

[191] J.-Y. Li *et al.*, "Synergistic Function of DNA Methyltransferases Dnmt3a and Dnmt3b in the Methylation of Oct4 and Nanog," *Mol. Cell. Biol.*, vol. 27, no. 24, pp. 8748–8759, 2007.

[192] J. Liao *et al.*, "Targeted disruption of DNMT1, DNMT3A and DNMT3B in human embryonic stem cells," *Nat. Genet.*, vol. 47, no. 5, pp. 469–478, 2015.

[193] J. G. Lees *et al.*, "Oxygen Regulates Human Pluripotent Stem Cell Metabolic Flux," *Stem Cells Int.*, vol. 2019, pp. 1–17, 2019.

[194] S. Ikeda, R. Kawahara-Miki, H. Iwata, M. Sugimoto, and S. Kume, "Role of methionine adenosyltransferase 2A in bovine preimplantation development and its associated genomic regions," *Sci. Rep.*, vol. 7, no. 1, pp. 1–10, 2017.

[195] S. Burr *et al.*, "Oxygen gradients can determine epigenetic asymmetry and cellular differentiation via differential regulation of Tet activity in embryonic stem cells," *Nucleic Acids Res.*, no. January, pp. 1–17, 2017.

[196] N. R. Forsyth, A. Kay, K. Hampson, A. Downing, R. Talbot, and J. McWhir, "Transcriptome alterations due to physiological normoxic (2% O2) culture of human embryonic stem cells.," *Regen. Med.*, vol. 3, pp. 817–833, 2008.

[197] E. Tsogtbaatar, C. Landin, K. Minter-Dykhouse, and C. D. L. Folmes, "Energy Metabolism Regulates Stem Cell Pluripotency," *Front. Cell Dev. Biol.*, vol. 8, no. February, pp. 1–16, 2020.

[198] C. Kim, T. Amano, J. Park, M. G. Carter, X. Tian, and X. Yang, "Improvement of embryonic stem cell line derivation efficiency with novel medium, glucose concentration, and epigenetic modifications," *Cloning Stem Cells*, vol. 11, no. 1, pp.

89–99, 2009.

[199] N. Saki, M. A. Jalalifar, M. Soleimani, S. Hajizamani, and F. Rahim, “Adverse effect of high glucose concentration on stem cell therapy,” *Int. J. Hematol. Stem Cell Res.*, vol. 7, no. 3, pp. 33–39, 2013.

[200] P. Yang, X. Chen, S. Kaushal, E. A. Reece, and P. Yang, “High glucose suppresses embryonic stem cell differentiation into cardiomyocytes: High glucose inhibits ES cell cardiogenesis,” *Stem Cell Res. Ther.*, vol. 7, no. 1, pp. 1–13, 2016.

[201] R. P. Kumar *et al.*, “Regulation of energy metabolism during early mammalian development: TEAD4 controls mitochondrial transcription,” *Development*, no. September, p. dev.162644, 2018.

[202] A. M. Intlekofer and L. W. S. Finley, “Metabolic signatures of cancer cells and stem cells,” *Nat. Metab.*, vol. 1, no. 2, pp. 177–188, 2019.

[203] J. Shand, J. Berg, and C. Bogue, “Human Embryonic Stem Cell (hESC) and Human Embryo Research,” *Pediatrics*, vol. 130, no. 5, pp. 972–7, 2012.

[204] P. Prajumwongs, O. Weeranantanapan, T. Jaroonwitchawan, and P. Noisa, “Human Embryonic Stem Cells : A Model for the Study of Neural Development and Neurological Diseases,” vol. 2016, 2016.

[205] U. Ahting *et al.*, “Neurological phenotype and reduced lifespan in heterozygous Tim23 knockout mice, the first mouse model of defective mitochondrial import,” *Biochim. Biophys. Acta - Bioenerg.*, vol. 1787, no. 5, pp. 371–376, 2009.

[206] T. W. Theunissen *et al.*, “Systematic identification of culture conditions for induction and maintenance of naive human pluripotency,” *Cell Stem Cell*, vol. 15, no. 4, pp. 471–487, 2014.

[207] E. Tzika, T. Dreker, and A. Imhof, “Epigenitics and metabolism in health and disease,” *Front. Genet.*, vol. 9, no. SEP, 2018.